Exploring the developmental functions of Fat cadherins in *Drosophila* and mammals

Inauguraldissertation

zur
Erlangung der Würde eines Doktors der Philosophie
vorgelegt der
Philosophisch-Naturwissenschaftlichen Fakultät
der Universität Basel

von
Leonie Enderle
aus
Lörrach, Deutschland

Basel, 2016

Genehmigt von der Philosophisch-
Naturwissenschaftlichen Fakultät auf Antrag von:

Prof. Dr. Helen McNeill, Dissertationsleiterin
Prof. Dr. Markus Affolter, Fakultätsverantwortlicher
Prof. Dr. Clemens Cabernard, Koreferent

Basel, den 19.04.2016

Prof. Dr. Jörg Schibler
Dekan

0 Table of Contents

1 Acknowledgements

This thesis would not have been possible without my mentors, colleagues and friends, driving research, pushing boundaries, asking questions, lending a helping hand, providing advice or sharing highs and lows:

First and foremost I would like to thank my advisor Dr. Helen McNeill for guiding me through my PhD, her continuous support and motivation. Helen's curiosity and inspiring belief in science, in the value of scientific collaboration and in careful research has significantly shaped the researcher that I am today. Most importantly I will never forget how deeply Helen cares about her students and the advice and support she provided beyond scientific topics!

I am immensely thankful to my Swiss advisor Dr. Markus Affolter for paving the way of my external PhD in Toronto, which I am sure, was a bit of a bureaucratic headache from time to time. I deeply appreciate his time for meetings and scientific input and for inspiring me with his visionary view on research and technology.

I would further like to thank my PhD committee members Dr. Tony Harris and Dr. Ulrich Tepass for providing valuable feedback and scientific advice that has helped developing my projects and stimulated me to view them from entirely different angles. My sincere gratitude also goes to my PhD exam committee members Dr. Clemens Cabernard and Dr. Martin Spiess.

I am incredibly lucky to have experienced working alongside the most amazing team one could hope for! I want to thank my lab members Dr. Caroline Badouel, Dr. Mazdak Bagherie-Lachidan, Dr. Masha Brooun, Ian Hester, Kin Kuok, Nicole Liscio, Dr. Antoine Reginensi, Dr. Robyn Rosenfeld, Pearl Sequeira, Dr. Praveer Sharma, Dr. Anson Sing, Dr. Srdjana Ratkovic, Yonit Tsatskis, Yi Qu, Norman Yau, Kelvin Yeung and Dr. Hongtao Zhang for countless scientific and not-so-scientific discussions and activities! I am still amazed of the lab's spirit and how open, helpful and welcoming my colleagues are, which has made my transition to Canada and a new lab easy and fun and which has helped me through the tough times. I will keep many memories of joint late-night experiments, deep discussions, conference travels, art projects, island trips, crazy Christmas gift exchanges, shared experiences and tons of laughter with exceptional people!

I would further like to thank my collaborators Dr. Brian Raught and Dr. Anne-Claude Gingras and especially Dr. Étienne Coyaud and Dr. James Knight in their labs for help and support with mass spectrometry experiments, reagents and advice.

My gratitude also goes to Dr. Laurence Pelletier and many of his lab members, who have generously shared their reagents, equipment and knowledge on centrosome and cilia biology. I especially thank Dr. Johnny Tkach for advice on establishing CRISPR/Cas9 in my lab and Dr. Monica Hasegan for microscopy help. Most importantly I would like to thank my collaborator and good friend Dr. João Gonçalves for ongoing support and cilia wisdom!

I also want to thank Dr. Mikhail Bashkurov from the LTRI High-Content Screening Facility for providing immense help with imaging and analyzing datasets, for generously developing custom-designed scripts, and for valuable advice.

I highly appreciate the collaborative spirit within the Lunenfeld-Tanenbaum Research Institute, as well as the UofT life science research landscape and am grateful for technical help and many fruitful discussions. I would like to specifically thank the lab of Dr. Jeffrey Wrana, especially Dr. Masahiro Narimatsu, for generously sharing reagents and expertise in numerous situations!

Finally and most importantly, I want to thank my family and friends for their inexhaustible love and support, for believing in me and caring about the emotional wellbeing that is so very important for achieving professional growth and success. It is impossible to put into words what it means to have such amazing people in my life! I am incredibly lucky to have Alex, my partner in crime, by my side, who is my best friend and an exceptional scientist, whose unfailing love and encouragement has kept me going in hard times, and who has helped me immensely while writing this thesis - at times through scientific discussions, at times through heavenly home-cooked dinners!

2 Abstract

The large cadherin Fat has important functions in morphogenetic processes during development of *Drosophila* and mammals. Yet, its molecular partners and signaling pathways are poorly understood. Here I studied a physical link between *Drosophila* Fat and the Hippo pathway regulator Expanded. I found that Expanded interacts with distinct domains of Fat through its FERM domain. This finding offers a possible explanation of how Fat regulates the apical localization of Expanded and its activity in the Hippo pathway. In order to better understand Expanded signaling, I further studied its phosphorylation and determined novel Expanded interactors, including the Yorkie co-factor Mask.

The size and transmembrane nature of the mammalian Fat cadherin Fat4 had previously hindered the use of biochemical approaches to gain insight into its molecular functions. Here I developed several cell culture tools that allowed me to overcome some of these limitations and to study Fat4 localization and function. I performed proximity-dependent biotin identification (BioID) and identified an array of potential novel Fat4 interactors that will serve as a useful resource for future studies. Beside a variety of developmental defects, *Fat4* mutant mice exhibit prenatal renal cysts with regions of abnormal primary cilia. Therefore, to understand if Fat4 regulates primary cilia, as has been suggested for several PCP proteins, I tested the effect of Fat4 depletion on cilia formation and maintenance in cell culture. Dramatic effects on cilia maintenance and centrosome positioning and coherence were found by knockdown with several independent siRNAs. However, CRISPR/Cas9-mediated *Fat4* knockout did not confirm a requirement of Fat4 in these processes and indicated that cilia and centrosome defects were likely RNAi off-target effects. This highlights the potential pitfalls of RNAi and should be regarded as a cautionary tale.

3 List of abbreviations

Δ	deletion
aa	amino acids
AP-MS	Affinity-purification coupled to mass spectrometry
App	Approximated
Atro	Atrophin
BAC	bacterial artificial chromosome
BF	BirA*-Flag
BioID	Biotin Identification
BN PAGE	Blue Native Polyacrylamide Gel Electrophoresis
bp	base pair
Cdh1	Cadherin 1/E-cadherin
Cora	Coracle
CRISPR	Clustered regularly interspaced short palindromic repeats
CP	capping protein
Crb	Crumbs
D	Dachs
Dchs	Dachsous (mammalian)
Dco	Disc overgrown
Dgo	Diego
Dlg	Discs large
Ds	Dachsous
Dsh	Dishevelled
dsRNA	double stranded RNA
Dvl	Dishevelled (mammalian)
EBR	Expanded binding region
ECD	extracellular domain
ERM	ezrin radixin moesin
Ex	Expanded
F-actin	filamentous actin
FAK	focal adhesion kinase

FBM	FERM binding motif (Crb)
FERM	4.1 ezrin radixin moesin
Fj	Four-jointed
FLP	Flipase
Fmi	Flamingo
ft	fat
Fz	Frizzled
Fzd	Frizzled (mammalian)
GA	Golgi apparatus
GFP	green fluorescent protein
gRNA	guide RNA
Hh	Hedgehog
Hpo	Hippo
ICD	intracellular domain
IFT	intraflagellar transport
InDel	Insertion/Deletion
KO	knockout
Kst	Karst
Kug	Kugelei
Lft	Lowfat
Lgl	Lethal giant larvae
MAGUK	membrane-associated guanylate kinase
MASK	multiple ankyrin single KH domain
MEF	mouse embryonic fibroblast
Mer	Merlin
miRNA	micro RNA
MKS	Meckel syndrome
Msn	Misshapen
Mts	microtubule star
Myr	myristoylation signal
NES	nuclear export sequence
Nf2	Neurofibromatosis2
NLS	nuclear localization sequence

NPHP	Nephronophthisis
NT	non-targeting
nt	nucleotides
OCD	oriented cell division
PCNT	Pericentrin
PCP	planar cell polarity
PCR	polymerase chain reaction
Pk	Prickle
PLA	proximity ligation assay
PTM	post-translational modification
RFP	red fluorescent protein
RNAi	RNA interference
SAINT	significance analysis of interactome
Sav	Salvador
Scrib	Scribble
Sd	Scalloped
shRNA	small hairpin RNA
siRNA	short interfering RNA
Slmb	Supernumerary limbs
Tet	Tetracycline
Vang	Van Gogh
Vangl	Van Gogh like
Vil	Villin
WB	Western blot
Wg	Wingless
WRC	WAVE regulatory complex
wt	wildtype
Wts	Warts
YFP	yellow fluorescent protein
Yki	Yorkie
Zyx	Zyxin

4 Materials and Methods

4.1 Chapter A

4.1.1 HEK293T cell maintenance

HEK293T cells were cultured at 37˚C and 5% CO_2 in DMEM (Thermo Fisher Scientific) supplemented with 10% fetal bovine serum (Sigma or Wisent), 1% GlutaMAX (Thermo Fisher Scientific), 100U/ml Penicillin and 100µg/ml Streptomycin.

4.1.2 Transfection and anti-Flag co-IPs in HEK293T

For co-IPs, one 6-well of transfected cells per condition was used. 300'000 HEK293T cells were seeded per 6-well (day 1) and transfected using standard calcium phosphate transfection (day 2, evening). Briefly, a total of 3µg DNA in 75µl ddH_2O was added to 75µl $CaCl_2$ (0.5M). Subsequently, 150µl of 2x HEBS buffer was added quickly and the mixture vortexed immediately. After 30min of incubation at room temperature, the samples were added dropwise to the cells. Medium was replaced the next day (day 3, morning) and cells were harvested and lysed for pulldowns two days after transfection (day 4). The cells were rinsed with PBS and incubated with 0.5ml ice-cold Hepes lysis buffer for 20min at 4˚C on a nutator. To pellet debris, samples were centrifuged in a pre-cooled benchtop centrifuge for 20min at 14000rpm and 4˚C. As "input" sample, 40µl of the supernatant was boiled 3min with 12.5µl 4x SDS sample buffer at 95˚C. Anti-Flag M2 Agarose beads (Sigma) were pre-washed in Hepes lysis buffer 4 times and diluted to a 50% slurry. The remaining supernatant of the samples was incubated with 20µl of bead slurry, at 4˚C for 2-3h while nutating. Beads were pelleted by mild centrifugation and washed with Hepes lysis buffer 4-5 times on ice. After the last washing step, the supernatant was aspirated from the beads and the beads were boiled in 25µl 2x SDS sample buffer for 3min at 95˚C and cooled on ice (= "Flag-IP" samples).

4.1.2.1 2x HEBS buffer

1.5 mM Na_2HPO_4
50 mM Hepes
280 mm NaCl
(pH 7.15)

4.1.3 Hepes lysis buffer

50mM Hepes/NaOH (pH 8)
100mM KCl, 2mM EDTA
0.1% NP40
10% Glycerol
freshly added before use:
1mM PMSF
1x Protease inhibitors (Sigma)
25mM NaF
5mM Na_4PP_i
2mM Na_3VO_4 (heat-inactivated).

4.1.4 S2 cell maintenance and transfection for co-IPs

S2 cells were grown as semi-adherent culture at 25˚C in Schneider's S2 media (Sigma) supplemented with 10% FBS (Sigma or Wisent), 100U/ml Penicillin and 100µg/ml Streptomycin.

4.1.5 Transfection and anti-Flag co-IPs in S2 cells

For co-IPs, one to three 6-wells of transfected cells were combined for each sample. Per 6-well, $3*10^6$ cells were seeded on day 1, transfected with a total of 0.4µg construct DNA using Effectene transfection kit (Qiagen) according to manufacturer's protocol on day 2, medium was replaced on day 3 and cells were harvested and lysed on day 4. Cells were rinsed with PBS and each sample (1-3 6-wells combined) was incubated in 0.5ml ice-cold Hepes lysis buffer for 10min on ice, with occasional inverting or pipetting. To pellet debris, samples were vortexed briefly and centrifuged in a pre-cooled benchtop centrifuge for 20min

at 14000rpm and 4˚C. As “input” sample, 40µl of the supernatant was boiled 3min with 12.5µl 4x SDS sample buffer at 95˚C. Anti-Flag M2 Agarose beads (Sigma) were pre-washed in Hepes lysis buffer 4 times and diluted with Hepes lysis buffer to a 50% slurry. The remaining supernatant of the samples was then incubated with 20µl of bead slurry, at 4˚C for 2-3h while nutating. Beads were pelleted by mild centrifugation and washed with ice-cold Hepes lysis buffer 4-5 times on ice. After the last washing step, the supernatant was aspirated from the beads and the beads were boiled in 25µl 2x SDS sample buffer for 3min at 95˚C and cooled on ice (= “Flag-IP” samples).

4.1.6 Sample preparation of S2 cells for Ex phosphorylation studies

$3*10^6$ cells were seeded per 6-well on day 1, transfected with a total of 0.6-0.9µg construct DNA using Effectene transfection kit (Qiagen) according to manufacturer’s protocol on day 2, medium was replaced on day 3 and cells were harvested and lysed on day 4. For dco RNAi experiments, dco dsRNA complexes (18µg) were added to the medium on day 1. For prolonged dco RNAi (see Fig 16A), dco dsRNA complexes (25µg) were added to the medium on day 1, DNA constructs were transfected on day 4, medium was replaced on day 5 and cells were harvested and lysed on day 5. For lysis, cells were washed with PBS once and each sample was incubated in 0.5ml ice-cold Hepes lysis buffer for 10min on ice, with occasional inverting or pipetting. To pellet debris, samples were vortexed briefly and centrifuged in a pre-cooled benchtop centrifuge for 20min at 14000rpm and 4˚C. 100µl of the supernatant was boiled 3min with 4x SDS sample buffer at 95˚C.

4.1.7 Western blotting

Western blotting was performed under standard conditions. Protein samples were electrophoretically separated by SDS-PAGE on 10% or 12% acrylamide gels and the proteins were transferred to nitrocellulose membranes in transfer buffer containing 10% methanol. Membranes were blocked in 5% skim milk in 0.1% TBS-Tween and probed with appropriate antibodies.

4.1.8 Constructs used in co-IPs in HEK293T and S2 cells

Constructs of N-terminally 3x-HA-tagged Merlin and the Merlin FERM-domain (MerFERM; aa 1-305 of Mer) in pAc5c vectors (pAWH; Gateway #1095; Drosophila Genomics Resource Center) were a gift from Dr. Sarah Hughes. Full-length Kibra and Pez constructs in Gateway pENTR vectors were a gift from Dr. Hugo Stocker and cloned into mammalian expression vectors (Gateway cmv_C-HA) with C-terminal 3x-HA tags using the Gateway technology (Life technologies). p38b-Flag in pAc5c was a gift from Dr. Kyle Belozerov (described in (Belozerov et al., 2012)). Constructs of Expanded and the Expanded FERM domain (ExFERM; aa 1-400 of Ex) in pcmv5 vectors with a C-terminal HA-tag (for mammalian expression under a cmv promoter), and in pAWH (C-terminal HA tag) and pAWF (C-terminal Flag tag) vectors (vectors from: The *Drosophila* Gateway Vector Collection) (for *Drosophila* expression under an actin promoter), had been previously generated by Dr. Caroline Badouel and Dr. Ankush Garg (Badouel et al., 2009). Construct of the BMP receptor 2 (BMPR2-Flag) was a gift from Dr. Masahiro Narimatsu. FatΔECD with a C-terminal 3xFlag in a pcmv5 vector was subcloned by Dr. Richelle Sopko (from FatΔECD described in (Matakatsu and Blair, 2006)) and served as template for all FatΔECD deletion constructs (Sopko et al., 2009). The FatΔECD deletion constructs cΔ55, cΔ245, cΔ255, cΔ310, cΔ444, cΔ492 were generated by Dr. Richelle Sopko (as described in (Sopko et al., 2009)) and cΔ260, cΔ265, cΔ270, cΔ275, cΔ285, cΔ444-154, cΔ310-195, cΔ505-134, cΔ505-124, cΔ505-114, cΔ505-84, cΔ505-64, cΔ505-154;cΔ24, cΔ505-154;cΔ44 were generated by Dr. Ankush Garg. cΔ64 and cΔ444-154;cΔ64 were PCR amplified from FatΔECD and FatΔECD;cΔ444-154, respectively and cloned into pcmv5 using KpnI and BamH1 restriction sites. ΔEBR1, ΔEBR1;cΔ64, ΔEBR1;ΔEBR2 were generated by PCR site directed mutagenesis (ΔEBR1 = cΔ285-245; ΔEBR2 = cΔ64-24). For myristoylated constructs containing the C-terminal 124aa of Fat, Myr-c124 and Myr-c124;ΔEBR2 were generated by site directed mutagenesis with primers containing a myristoylation signal sequence (Myr) (sequence information obtained from pHom-Mem1 vector, Clontech); FatΔECD;cΔ505-134 was used as template. The Fat^{sum} mutation (Ile 4852 to Asn; in C-terminal nomenclature: aa296) was introduced into constructs FatΔECD, FatΔECD;ΔEBR1 and

FatΔECD;ΔEBR1;ΔEBR2 by site directed mutagenesis to generate Fat^{sum}, ΔEBR1;Fat^{sum} and ΔEBR1;ΔEBR2;Fat^{sum}, respectively.

Table 4.1 Cloning primers
The following primers were used for the indicated constructs (restriction sites are underlined; deletion boundaries in quickchange primers are bold; myristoylation signal is in lowercase letter, Fat^{sum} mutation is marked by asterisk):

cΔ64 and cΔ444-154;cΔ64:			
#	Primer Name	Primer Sequence	Notes
L15	ft deltaECD cmv cloning fw	attgatctggtaccacgcgtatggagaggc	KpnI site
L16	ft delta64 flag cmv cloning rev	GCCACCCGGGATCCTTACTTGTCATCGTCATCCTTG TAATCGATGTCATGATCTTTATAATCACCGTCATGG TCTTTGTAGTCTCTAGAcgatggggatgcggctccattggcc	BamH1 site

ΔEBR1 and ΔEBR1;cΔ64			
#	Primer Name	Primer Sequence	Notes
L19	FatdECD_M1 fw	CATTTCCGGAAAGCC**GA**GTGCCAGCAGGCAAAAG	site directed mut.
L20	FatdECD_M1 rev	CTTTTGCCTGCTGGCA**CT**CGGCTTTCCGGAAATG	site directed mut.

ΔEBR1;ΔEBR2:			
#	Primer Name	Primer Sequence	Notes
L21	FatdECD_M2 fw	CCGCATCCCCATC**GC**AGCAAACCCAAGTG	site directed mut.
L22	FatdECD_M2 rev	CACTTGGGTTTGCT**GC**GATGGGGATGCGG	site directed mut.

Myr-c124 and Myr-c124;ΔEBR2			
#	Primer Name	Primer Sequence	Notes
L64	Nmyr-Fat124 cmv5 fw QC	GATCTGGTACCACGCGT**atgatggggagtagcaagagcaagcct aaggaccccagccagcgc**GAGACGAGCAGAAATCCACC	site directed mut.

Fat^{sum}, ΔEBR1;Fat^{sum} and ΔEBR1;ΔEBR2;Fat^{sum}			
#	Primer Name	Primer Sequence	Notes
L74	Fatsum fw	GCAGCCGCGCA**a*** TCTCACTTTGC	site directed mut.
L75	Fatsum rev	GCAAAGTGAGA**t*** TGCGCGGCTGC	site directed mut.

4.1.9 Constructs for Ex phosphorylation studies and AP-MS (S2 cells)

Ex-Flag, ExFERM-Flag (aa1-468), Crb-intra-myc, Crb-intra;ΔFBM-myc and Crb-intra;ΔPBM-myc were gifts from Dr. Nicholas Tapon (described in (Ling et al., 2010; Ribeiro et al., 2014)). Dco^{3}-HA and Dco^{KR}-HA were generated by Dr. Richelle Sopko (described in (Sopko et al., 2009)). Untagged FatΔECD in a pActin vector was generated by Dr. Caroline Badouel (*unpublished*).

4.1.10 Dco dsRNA

To generate Dco double-stranded RNA (dsRNA) (~650bp length), desired DNA fragments were PCR amplified from dco cDNA with primers containing the T7 promoter sequence and transcribed *in vitro* using the MEGAscript T7 kit (Thermo Fisher Scientific). Transcription and purification of dsRNA was performed according to manufacturer's protocol with the following changes: T7 transcription was performed at 37˚C over night and dsRNA LiCl precipitation was carried out for 4h at 4˚C. S2 cells were treated with 7µg dsRNA per 12-well and 18µg or 25µg per 6-well, as described in figure legends.

Table 4.2 Dco dsRNA primers
Primers to amplify DNA sequence coding for dco dsRNA (T7 promoter sequence is bold):

#	Primer Name	Primer Sequence	Notes
L51	DcoRNAi fw	**TAATACGACTCACTATAGGG**CGTTGAATGTATCCAAGCGGCAGG	dsRNA
L52	DcoRNAi rev	**TAATACGACTCACTATAGGG**TAGGTTACAATGTGGGTGCCTTGC	dsRNA

4.1.11 GST pulldown

His-tagged Ex FERM-domain in pEXP1-DEST (His-ExFERM) has been generated by Dr. Caroline Badouel ((Badouel et al., 2009)), His-tagged Atrophin C-terminal domain (His-AtroC) and GST-tagged Fat-ICD have been cloned by Ian Hester (described in (Sing et al., 2014)). GST pulldowns were performed as in (Sambrook and Russell, 2006). Briefly, BL21 bacteria were transformed with the plasmids and protein production was induced by addition of IPTG (Isopropyl β-D-1-thiogalactopyranoside, final concentration 1mM) and induction confirmed by Western blotting. Bacteria were pelleted, resuspended in cold buffer (His-tagged proteins: PBS + Complete protease inhibitor (Roche) + 5mM DTT + Imidazole (10mM final concentration); GST-tagged proteins: PBS + Complete protease inhibitor (Roche) + 5mM DTT + 1mM EDTA), sonicated, supplemented with TritonX-100 and centrifuged to pellet debris. Supernatant was incubated with Ni beads (His-tagged proteins) for 2h or Glutathion Sepharose beads (Amersham, Biosciences) (GST-tagged proteins) over night at 4˚C, rotating. Beads were washed in PBS + 10mM Imidazole (His-tagged proteins on Ni beads) or PBS (GST-tagged proteins on Glutathion beads). His-tagged proteins were

eluted from Ni beads using a high Imidazole buffer (in 50mM Tris pH7.2 + 2% SDS + 10% glycerol + 250mM of Imidazole; 4˚C, 30min, nutating) prior to the GST pulldown and an aliquot of all samples was run on Coomassie gels or Western blots to test if the proteins had been purified.

GST pulldowns were performed by incubating His-tagged protein eluates (His-ExFERM or His-AtroC) with GST-tagged proteins (GST or GST-FatICD) on beads in pulldown buffer (20mM Tris + 1mM EDTA + 1% TritonX-100 + 1mM ß-Mercaptoethanol) for 2h at 4˚C, rotating. Aliquots were taken out to run as "input" samples. For the IP samples, the beads were then washed 3-4 times in pulldown buffer with 10-15min of incubation (room temperature, nutating) in between washes. After the last wash, most supernatant was aspirated and beads were boiled in SDS sample buffer for 3min at 95˚C ("GST-pulldown" samples). Samples were analyzed on Western blots (as described above). Ponceau S stain was used to visualize GST proteins, while anti-His blotting (Sigma 1:5000) was used to visualize His-tagged proteins.

4.1.12 Recombineering to create BACR11D14 *fat*ΔEBR1

A bacterial artificial chromosome (BAC) containing the *fat* gene including upstream regulatory regions, BACR11D14 (BACPAC Resources Center), was used for deletion of the EBR1 coding region in *fat* with Recombineering technology (Copeland et al., 2001). Recombineering was performed using the *galK* selection/counterselection method (Warming et al., 2005). Reagents and protocols were obtained from NCI Frederick (https://ncifrederick.cancer.gov/research/brb/recombineeringInformation.aspx) (Sharan et al., 2009). Recombineering was performed in SW102 bacteria that have been engineered to contain the λ prophage recombineering system and to lack a functional *galactokinase* (*galK*) gene. These bacteria have increased recombination efficiency and cannot grow on galactose as single carbon source, which is used as the basis for selection (Copeland et al., 2001; Warming et al., 2005). In a first step, the EBR1 coding region was replaced by a *galK* cassette through homologous recombination. Successful recombinants (*galK*$^+$) were selected by positive selection on minimal galactose agar plates. To generate a *galK* cassette

containing the *galK* gene flanked by 600bp sequences homologous to the sequences flanking EBR1, sequential PCR was performed with overlapping primers. Primers L27+L28 were used to amplify the left homology arm, primers L31+L32 to amplify the right homology arm and L29+L30 to amplify galK (from pGalK vector; NCI Frederick). To assemble the cassette, all three PCR products were used as template for a PCR with primers L27+L32. The purified PCR product (GalK cassette) was electroporated into SW102 bacteria containing BACR11D14.

As a second step, the *galK* gene was replaced by the EBR1 deletion using homologous recombination. To generate a ΔEBR1 cassette with the same homology arms as used for the *galK* recombination, a PCR with primers L27+L32 was performed using the previously established FatΔECD;ΔEBR1 construct (in pcmv5 vector; see above) as template. The resulting PCR product was purified and electroporated into SW102 bacteria containing BACR11D14-galK. Successful recombinants (*galK*$^-$) were enriched by growing the bacteria on 2-deoxy-galactose (DOG) minimal plates (glycerol as carbon source; counterselection step). DOG is toxic for bacteria with a functional *galK* gene. Individual colonies were further tested for successful *galK* replacement by manual screening (DNA purification, PCR, sequencing). Two clones were found to contain the desired ΔEBR1 modification.

Table 4.3 Recombineering primers
Overlapping primers to generate *galK* and ΔEBR1 cassettes (*galK* sequence is in bold font; overlapping sequences within primers to allow sequential PCRs are highlighted in grey):

#	Primer Name	Primer Sequence	Notes
L27	Ft5' 600bp Rec-1 fw	GGAGATCATATGCGACCGCCAGTGGGTAG	left homology arm
L28	Ft5' 600bp Rec-2 rev	**GATTAATTGTCAACAGG**CGGCTTTCCGGAAATGTCGTGCAAAGTGAG	
L29	GalK5' Rec-3 fw	CATTTCCGGAAAGCCG**CCTGTTGACAATTAATCATCGGCATAGTATATCGG**	*galK*
L30	GalK3' Rec-4 rev	GCTTTTGCCTGCTGGCACT**TCAGCACTGTCCTGCTCCTTGTG**	
L31	Ft3' 600bp Rec-5 fw	**GCAGGACAGTGCTGA**AGTGCCAGCAGGCAAAAGCCCGGAG	right homology arm
L32	Ft3' 600bp Rec-6 rev	CAGATTTTCGTAGCTAGGTCCCCAATTGAGCAGATACTCC	

4.1.13 Generation and staining of ft^{fd}, $ft^{G\text{-}rv}$ and ex^{e1} somatic clones

The following flies were used to generate clones: hsFlp;$ft^{G\text{-}RV}$ FRT40A/Ubi-GFP,FRT40A ; hsFlp;ft^{fd} FRT40A/Ubi-GFP,FRT40A and hsFlp;ex^{e1} FRT40A/Ubi-GFP,FRT40A. Clones were induced by heat-shock (to induce Flp-mediated FRT recombination) at 37˚C for 30-45min (72-84h after egg lay). Wing discs from wandering third instar larvae still attached to cuticle were dissected in cold PBS and fixed with 4% Paraformaldehyde (Electron Microscopy Sciences) in 0.1% PBS-TritonX-100 for 30min at room temperature. Discs were washed 3-5 times 5min with 0.1% PBS-TritonX, permeabilized 30min with 0.3% PBS-TritonX, then blocked for 1h in 10% normal goat serum (NGS) in 0.1% PBS-TritonX. Discs were incubated with primary antibodies in 10% NGS in 0.1% PBS-TritonX over night at 4˚C, washed 3-4 times 5-10min in 0.1% PBS-TritonX and incubated with secondary antibodies in 0.1% PBS-TritonX for 1h at room temperature. Discs were dissected from cuticle in 50% Glycerol and mounted on slides in Vectashield (with or without DAPI; Vector Laboratories). Slides were covered with coverslips and sealed by nail polish. Images were acquired on a Nikon Eclipse 90i confocal microscope using the Nikon EZ-C1 3.80 software.

4.1.14 Ex and ExFERM AP-MS in S2 cells

AP-MS was performed in collaboration with Dr. Anne-Claude Gingras' lab from S2 cells transiently transfected with Ex-Flag or ExFERM-Flag. For AP-MS to identify ExFERM phosphorylation sites, ExFERM-Flag was co-transfected with Crb-intra-myc, Crb-intraΔFBM-myc or Crb-intraΔPBM-myc to induce ExFERM phosphorylation. For each condition, 4 15cm plates of S2 cells (30% confluency) were transfected using standard calcium phosphate transfection (200µg DNA, 400µl 2.5M $CaCl_2$, 4ml 2xHEBS buffer per 4 plates). Cells were harvested 48h after transfection by scraping, pelleted by mild centrifugation (600 x *g*) and lysed in 5times the volume of lysis buffer (over cell pellet mass). Samples were shock-frozen on dry ice and stored at -80˚C before further processing. Dr. Kyle Belozerov in Dr. Anne-Claude Gingras' lab performed Flag-pulldowns, liquid chromatography-tandem mass spectrometry (ThermoFinnigan LTQ mass spectrometer) and data analysis as described in (Belozerov et al., 2012). Spectral

data were interpreted using Mascot software (Matrix Sciences) and analyzed using ProHits software (Liu et al., 2010). Results were compared to control AP-MS runs that had been performed separately with empty Ac5c Flag-vectors (V1-V4) or as part of the Ex AP-MS experiments (GFP). A list of peptide data is shown in Table 7.1. For the analysis, only proteins specific to ExFERM or Ex samples were considered (total peptide number in controls: 0) and proteins detected in at least two AP-MS experiments.

4.1.15 Antibodies used in Chapter A

Ex antibody is a gift from Dr. Richard Fehon, Mask antibody is a gift from Dr. Michael Simon; Crb antibody is a gift from Dr. Ulrich Tepaß. Fat and Dco antibodies have been previously generated in the McNeill lab. The Dco antibody was raised against the Dco C-terminus from a construct kindly provided by Dr. Jeffrey Price.

Table 4.4 Chapter A antibody information
(ms = mouse; rt = rat; gp = guinea pig; x = signal not specific; - = not used)

Antibody	Species	Origin	concentration for WB	concentration for IF
Flag M2	ms	Sigma	1:5000 - 1:10'000	-
HA	rt	Roche	1:2000	-
Fat	rt	H. McNeill	1:1000	1:100
Ex	gp	R. Fehon	x	1:1000
Crb	rt	U. Tepaß	-	1:1000
Dco	rb	H. McNeill	1:1000	x
Arm	ms	DSHB	-	1:400
Myc	gt	Abcam	1:100 – 1:1000	-

4.2 Chapter B

4.2.1 Constructs for BioID

Full-length human FAT4 was cloned into a mammalian pEV expression vector (cmv promoter) with C-terminal BirA*-Flag tag by Keyclone Technologies. This construct was used by Nicole Liscio to generate stably expressing HEK293T cells used for the QEHF BioID. The HEK293 Velos BioID, the HCT116 BioID and the HeLa BioID were performed with cells with a FAT4 construct that had been cloned into the pcDNA5 FRT/TO BirA*-Flag expression vector (gift from Dr. Brian Raught) by Keyclone Technologies (=FAT4-BF). BirA*-Flag (=BF) and GFP-BirA*-Flag (GFP-BF) in Gateway pDEST-CT-BirA*-FLAG-FRT/TO vectors were gifts from Dr. Anne-Claude Gingras. For C-terminal BirA*-Flag tagging, mouse Cdh1 was subcloned using Gateway technology (Life technologies) from a Cdh1 expression vector (gift from Dr. Jeff Wrana) into a Gateway pDEST-CT-BirA*-FLAG-FRT/TO vector (gift from Dr. Anne-Claude Gingras) in collaboration with Dr. Alexander Weiss. In brief, Cdh1 was PCR-amplified using primers containing attB sequences, introduced into a pDONR (BP reaction) and then into pDEST-CT-BirA*-Flag-FRT (LR reaction) (=Cdh1-BF). The Flp-In T-REx system (Thermo Fisher) allowed Flp-recombinase mediated introduction of these constructs into FRT sites in Flp-In T-REx engineered cell lines (see below). In these cells, the Tet repressor system blocks construct expression, unless derepression of the Tet operator (TO) is induced by Tetracycline.

Table 4.5 Cdh1 Gateway primers

Primer name	Primer sequence (attB sequence in lowercase)
Cdh1 GW fwd	ggggacaactttgtacaaaaaagttgccaccATGGGAGCCCGGTGCCGCA
Cdh1 GW rev no Stop	ggggacaactttgtacaagaaagttgggtaGTCGTCCTCACCACCGCCG

4.2.2 Stable cell lines for BioID

The initial QEHF BioID was performed with HEK293T cells constitutively expressing FAT4-BF. These cells had been generated by Nicole Liscio by random integration. Briefly, HEK293T cells were transfected with FAT4-BF and selected with Zeocin. Individual colonies were separated, grown individually and tested for FAT4-BF expression on Western blots. The strongest expressing clone was

selected for FAT4-BF BioID (QEHF). All other stable cell lines were established using the Flp-In system (Invitrogen). HEK293 T-REx Flp-In cells were a gift from Dr. Anne-Claude Gingras and were cultured at 37˚C and 5% CO_2 in DMEM (Thermo Fisher Scientific) supplemented with 10% fetal bovine serum (Wisent), 1% GlutaMAX (Thermo Fisher Scientific), 100U/ml Penicillin and 100µg/ml Streptomycin. HCT116 T-REx Flp-In cells were a gift from Dr. Brian Raught and cultured in RPMI 1640 medium (Sigma) supplemented with 10% fetal bovine serum (Wisent), 100U/ml Penicillin and 100µg/ml Streptomycin. Cells were transfected using Effectene transfection kit (Qiagen) with FAT4-BF, Cdh1-BF, GFP-BF or BF constructs and the Flp-recombinase expression vector pOG44. Per 6-well, 0.4µg construct DNA and 2.4µg pOG44 DNA in 100µl Buffer EC, 22.4µl Enhancer and 20µl Effectene were transfected. Selection with HygromycinB (HEK293: 200µg/ml; HCT116: 50µg/ml) was started 24h after transfection to select stable cells. Stable HeLa T-REx Flp-In cells expressing FAT4-BF and Cdh1-BF were established by Dr. James Knight in Dr. Anne-Claude Gingras' lab (by HygromycinB selection).

4.2.3 Induction and biotinylation tests of stable cell lines

Stable cells were tested for expression after Tetracycline (Tet) induction by supplementing the medium with 1µg/ml Tet over night. Uninduced cells served as controls. For biotinylation tests, cells were incubated over night in medium containing 1µg/ml Tet and 50µM biotin. Cells were either fixed in methanol for immunofluorescence (IF) stainings or crude lysates were made by scraping and dounce-homogenizing the cells in 2x SDS sample buffer (containing 2M Urea) for Western blots. Western blots were performed as described below for FAT4 samples. IF stainings were performed as described below (standard methanol fix immunofluorescence stainings). Biotinylation was probed with Streptavidin conjugated to either a 594 fluorophore or horse radish peroxidase (HRP).

4.2.4 BioID

BioID (Roux et al., 2012) was carried out essentially as described previously (Comartin et al., 2013; Gupta et al., 2015).

4.2.4.1 Cell pellet preparation for BioID

Dr. Etienne Coyaud in Dr. Brian Raught's lab prepared cell pellets from Nicole Liscio's stable HEK293T cells. Per experiment, 5 x 15cm plates of sub-confluent (60%) HEK293 T-REx stable cells were incubated for 24h in complete medium supplemented with 1µg/ml tetracycline (Sigma) and 50µM biotin (BioShop). Cells were collected and pelleted (2'000 rpm, 3 min), the pellet was washed twice with PBS, and dried pellets were snap frozen.

Cell pellets for HEK293 and HCT116 cycling cells and HEK293 starved cells were prepared by me and the subsequent pulldowns and mass spectrometry were performed by Dr. Etienne Coyaud. Per experiment with cycling cells, 5 x 15cm plates of sub-confluent (70-80%) HEK293 T-REx or HCT116 T-REx stable cells were incubated for 24h in complete medium supplemented with 1µg/ml tetracycline (Sigma) and 50µM biotin (BioShop). Cells were collected and pelleted (2'000 rpm, 3 min), the pellet was washed twice with PBS, and dried pellets were snap frozen. Per experiment with starved/ciliated cells, 5 x 15cm plates of HEK293 T-REx stable cells were cultured until confluent (~90%). Medium was changed and cells were incubated in serum-free DMEM supplemented with 1µg/ml tetracycline for 48h and an additional 24h in serum-free medium supplemented with tetracycline and 50µM biotin (BioShop).

4.2.4.2 BioID lysates and pulldowns

Pellets were lysed by Dr. Etienne Coyaud in 10 mL of RIPA lysis buffer (50mM Tris-HCl pH 7.5, 150mM NaCl, 1mM EDTA, 1mM EGTA, 1% TritonX-100, 0.1% SDS, 1:500 protease inhibitor cocktail (Sigma-Aldrich), 250U Turbonuclease (Accelagen)) at 4˚C for 1h, then sonicated (30sec, at 35% power, Sonic Dismembrator 500; Fisher Scientific) to completely disrupt visible aggregates. The lysate was centrifuged at 16'000 rpm (35'000 x *g*) for 30 min. Clarified

supernatants were incubated with 30µl packed, pre-equilibrated Streptavidin-sepharose beads (GE) at 4°C for 3 hr. Beads were collected by centrifugation (2'000 rpm, 2min), washed 6 times with 50mM ammonium bicarbonate pH 8.2, and treated with TPCK-trypsin (Promega, 16h at 37°C). The supernatant containing the tryptic peptides was then collected and lyophilized. Peptides were resuspended in 0.1% formic acid and 1/7th of the sample (representing less than one plate of cells) was analyzed per MS run. Each sample was run in technical duplicates.

4.2.4.3 BioID QEHF mass spectrometry

High performance liquid chromatography was conducted by Dr. Etienne Coyaud using a pre-column (Acclaim PepMap 50mm x 100µm inner diameter (ID) pre-column) and Acclaim PepMap (500mm x 75µm diameter; C18; 2 um;100 Å) RSLC (Rapid Separation Liquid Chromatography) column (Thermo Fisher Scientific), running a 120min reversed-phase buffer gradient at 250nl/min on a Proxeon EASY-nLC 1000 pump in-line with a Thermo Q-Exactive HF quadrupole-Orbitrap mass spectrometer. A parent ion scan was performed using a resolving power of 60'000, then up to the twenty most intense peaks were selected for MS/MS (minimum ion count of 1000 for activation), using higher energy collision induced dissociation (HCD) fragmentation. Dynamic exclusion was activated such that MS/MS of the same m/z (within a range of 10 ppm; exclusion list size = 500) detected twice within 5s were excluded from analysis for 15s. For protein identification, Thermo .RAW files were converted to the .mzXML format using Proteowizard (Kessner et al., 2008), then searched using X!Tandem (Craig and Beavis, 2004) and Comet (Eng et al., 2013) against the human Human RefSeq Version 45 database (containing 36113 entries). Search parameters specified a parent ion mass tolerance of 10ppm, and a MS/MS fragment ion tolerance of 0.4Da, with up to 2 missed cleavages allowed for trypsin. Variable modification +16@M and W, +32@M and W, +42@N-terminus, +1@N and Q were allowed. Proteins identified with a ProteinProphet cut-off of 0.85 (corresponding to ≤1% FDR) were analyzed with SAINT Express v.3.3.

4.2.4.4 BioID Velos mass spectrometry

LC-MS/MS was conducted by Dr. Etienne Coyaud using a 120-min reversed-phase buffer gradient running at 250 nl/min on a Proxeon EASY-nLC pump in-line with a hybrid LTQ-Orbitrap Velos mass spectrometer (Thermo Fisher Scientific). For protein identification, raw files were converted to the mzXML format using Proteowizard open source software (Kessner et al., 2008), then searched using X!Tandem (Craig and Beavis, 2004) against Human RefSeq Version 45. Data were analyzed using the trans-proteomic pipeline (TPP) (Pedrioli, 2010) via the ProHits 2.0.0 software suite (Liu et al., 2010). Proteins identified with a Protein Prophet cut-off of 0.95 were analyzed with SAINT v. 2.3.4 (Choi et al., 2011) with the following settings: nburn 2000, niter 5000, lowMode 1, minFold 1, normalize 0. For BioID, twenty control runs (consisting of 12 Flag-BirA* only runs and eight runs of BioID conducted on untransfected 293 T-REx cells, half with and half without MG132) were collapsed to the highest 4 spectral counts for each hit.

4.2.5 Venn diagrams and GO-term analysis

Area-proportional Venn diagrams were created using BioVenn software (Hulsen et al., 2008). GO-term analysis was performed using the ENRICHR online tool (Chen et al., 2013).

4.2.6 Mammalian cell culture

HEK293T and MCF7 cells stably expressing human FAT4-YFP (Zeocin resistance) or human Dchs1-mCherry (HygromycinB resistance) were a gift from Dr. David Sprinzak and murine Eph4 cells were a gift from Dr. Jeffrey Wrana. Mouse embryonic fibroblasts (MEFs) had been established from $Fat4^{-/-}$ or $Fat4^{+/+}$ (wildtype control) embryos by Ian Hester using standard protocols. MEFs, HeLa, Eph4, HEK293T and MCF7 cells were cultured in DMEM (Thermo Fisher Scientific) supplemented with 10% fetal bovine serum (Wisent), 1% GlutaMAX (Thermo Fisher Scientific), 100U/ml Penicillin and 100µg/ml Streptomycin with appropriate antibiotics (Zeocin: 50-100µg/ml (HEK293T) or 100µg/ml (MCF7); HygromycinB: 100µg/ml (HEK293T) or 50µg/ml (MCF7)). Human hTERT RPE-1

cells (=RPE-1; ATCC) were cultured in DMEM/F12 + GlutaMAX (Thermo Fisher Scientific) supplemented with 10% fetal bovine serum (Wisent), 100U/ml Penicillin and 100µg/ml Streptomycin.

4.2.7 Full-length FAT4 Western blots

Due to the large size of FAT4, special Western blotting conditions are required. For all FAT4 sample preparations Urea was added to the sample to a final concentration of 1M. All FAT4 Western blots were achieved by electrophoretically separating protein samples slowly on 3-8% Tris-Acetate gradient gels (NuPAGE precast system, Life Technologies) (12mAmp per gel; 4h). Gels were transferred slowly to PVDF membranes in a low methanol transfer buffer (0-5% methanol) at 30V over night, 4˚C. Membranes were blocked in 5% skim milk in 0.1% TBS-Tween for at least 1h before primary antibodies were applied in the same blocking solution at 4˚C over night. Membranes were washed at least 3 times 10min, incubated with secondary HRP-conjugated antibodies in 0.1% TBS-Tween for 1-2h at room temperature. Membranes were washed in 0.1% TBS-Tween and developed on a ChemiDoc imager (Bio-Rad).

4.2.8 FAT4 co-immunoprecipitation

FAT4 co-immunoprecipitations were performed from HEK293T cells stably expressing FAT4-YFP and wildtype HEK293T or stable DCHS1-mCherry cells served as controls. Endogenous FAT4 co-immunoprecipitations were performed from Eph4, HeLa and RPE-1 cells. 1-2 confluent 15cm plates per cell line were scrape-harvested and lysed in 1ml TNTE or CHAPS lysis buffer (20min, 4˚C). Cell debris was pelleted by spinning at 14’000rpm for 20min at 4˚C and supernatant was used for pulldowns and as input samples. For FAT4-YFP pulldowns, lysates were incubated with 15µl 50% slurry of GFP-Trap beads (Chromotek) for 2h at 4˚C, nutating. For endogenous FAT4 pulldowns, lysates were first incubated with 6µl FAT4 antibody (TO152AP) or rabbit IgG as controls for 2h, and then 20µl 50% slurry of protein A/G agarose beads (Santa Cruz) was added for 1h. All beads were washed at least 4x with cold lysis buffer before samples were boiled in 2x SDS sample buffer + 2M Urea.

Table 4.5 Lysis buffers

TNTE lysis buffer 50mM Tris pH7.6 150mM NaCl 0.5% TritonX-100 1mM EDTA	**CHAPS lysis buffer** 40mM HEPES (pH 7.5) 120mM NaCl 1mM EDTA 0.3% CHAPS (7% Glycerol)
<u>freshly added before use:</u> 1mM PMSF 1x Protease inhibitors (Sigma) 25mM NaF 5mM Na_4PP_i 2mM Na_3VO_4 (heat-inactivated).	

4.2.9 FAT4 expression in different cell lines (protein lysates)

Different cell lines were cultured using recommended conditions, lysed and probed for FAT4 protein. Confluent 10cm plates were lysed in 1ml TNTE lysis buffer for 10min at 4˚C. Cell debris was pelleted during centrifugation (14'000rpm). Pellet and supernatant were separated and the pellet resuspended in 1ml lysis buffer. Aliquots of both fractions were boiled with SDS sample buffer (with a final concentration of 1M Urea).

4.2.10 Immunofluorescence stainings of cultured cells

Cells were seeded on round glass coverslips (treated by incubation in 1M HCl at 65˚C over night and subsequently ethanol) and fixed in either 4% paraformaldehyde (PFA) or ice-cold methanol. PFA fixation was followed by several washes in PBS, permeabilization in 0.1 – 0.3% PBS-TritonX-100 (+25mM glycine + 25mM NH_4Cl in some cases) and blocking in 0.1% PBS-TritonX with 5% normal goat serum or 0.2% fish skin gelatin or a combination of both. Primary antibodies were applied in blocking solution, cells were washed in 0.1% PBS-TritonX and incubated with secondary antibodies in blocking solution. Methanol fixation was followed by blocking and primary antibodies all in 0.2% fish skin gelatin in PBS and secondary antibodies in PBS. Coverslips were mounted onto glass slides and imaged on a Eclipse 90i confocal microscope (Nikon) or on DeltaVision Elite microscopes (GE Healthcare).

4.2.11 BN PAGE

For each sample cells of a confluent 15cm plate of RPE-1 cells were pelleted, washed and lysed in 200µl digitonin buffer (90µl PBS + 130µl digitonin [4mg/ml] + protease inhibitors) and incubated 10min on ice. Lysates were centrifuged at 10'000 x g for 10min at 4˚C and supernatant was treated with native PAGE sample buffer (Thermo Fisher). Blue native gels (Thermo Fisher) were run and transferred to PVDF membranes according to manufacturer's protocol.

4.2.12 Vil-Cre *Fat4* conditional knockout mice

Mouse handling and husbandry was conducted in compliance with the Canadian council on animal care. Ian Hester and Yi Qu set up mouse breedings, performed PCR-genotyping, sacrificed the mice and helped with dissections. *Fat4* mutant and floxed mice were previously described in (Saburi et al., 2008). Mice containing the Villin-Cre (Vil-Cre) driver were a gift from Dr. Jeffrey Wrana. For conditional *Fat4* knockout in the intestinal tract $Vil^{Cre/+}$; $Fat4^{flox/+}$ mice were established and crossed to $Fat4^{flox/flox}$ or $Fat4^{flox/-}$ mice. $Vil^{Cre/+}$; $Fat4^{flox/flox}$ and $Vil^{Cre/+}$; $Fat4^{flox/-}$ mice were born without obvious defects. Intestines of 2-month old mice were dissected, fixed over night in 4% PFA, dehydrated by serial incubation in ethanol solutions and sent for paraffin-embedding and sectioning service. Intestinal cross-sections were deparaffinized and rehydrated. Antigen retrieval was performed by boiling sections in Antigen Unmasking Solution (Vector Laboratories). Sections were blocked in 3% bovine serum albumine (BSA) and 10% normal goat serum (NGS) in 0.1% PBS-Tween and incubated with primary antibodies in 3% BSA and 3% NGS in 0.1% PBS-Tween. Secondary antibodies were applied in 0.1% PBS-Tween. Dissection, histological stainings and pathological analysis of 6-month old mice was performed by Dr. Steven Gallinger's lab.

4.2.13 siRNA transfection of RPE-1 cells

For siRNA-mediated knockdowns, RPE-1 cells were seeded in 6-wells (on round glass coverslips for immunofluorescence stainings) in complete medium. The next day, medium was changed to OptiMEM (Thermo Fisher) and cells were transfected with approx. 30nM siRNAs using Lipofectamine RNAiMAX kit (Thermo Fisher), according to manufacturer's protocol. For Mock controls, no siRNAs were added. The following day, medium was changed to complete medium for experiments with cycling cells or to starvation medium (serum-free DMEM/F12 + Glutamax) for experiments with starved/ciliated cells. Unless otherwise stated, cells were treated with siRNAs for 3d before fixation or lysis. siRNA target sequences are listed in Table 4.7.

Table 4.7 siRNA information

siRNA name	Target mRNA	Target sequence	Company	Exon
FAT4 #1	Human FAT4	GGAGGGAGCTGTCTACGAA	Dharmacon	9
FAT4 #2	Human FAT4	TAGCAGAACTTCCTATTAT	Dharmacon	9
FAT4 #3	Human FAT4	GCAAAGGGCGCTTGGACTA	Dharmacon	15
FAT4 #4	Human FAT4	GATCATCGGTGGAAACTCT	Dharmacon	8
FAT4 #intra 1	Human FAT4	CTTCCTATAAGGGATGGTA	Sigma	17
FAT4 #intra 2	Human FAT4	CAGATTCCACTGGAATCTT	Sigma	17
FAT4 #intra 3	Human FAT4	GTAATACTTTGGAAATGCA	Sigma	17
FAT4 #3'UTR 1	Human FAT4	GCACTTTAACGCTTTCTTA	Sigma	17
FAT4 #3'UTR 2	Human FAT4	CTTGCTATGCGAATGATGT	Sigma	17

siRNA name	Target mRNA	Target sequence	Company	Exon
FAT1 #1	Human FAT1	CATCGAACAGGCCAATGAA	Sigma	2
FAT1 #2	Human FAT1	CACTTCAGGAGTTCTGTCA	Sigma	10
FAT1 #3	Human FAT1	CAGATTCGAGCTCTAATGA	Sigma	3

siRNA name	Target mRNA	Target sequence	Company
Non-targeting (NT)	Luciferase GL2	CGTACGCGGAATACTTCGA	Dharmacon
Non-targeting (NT)	Scrambled TAZ	GGGCAAGACGAGCGGGAAG	Dharmacon
CCDC41 (pool)	CCDC41	GGAACTAGTTAGAGTCAAG	Dharmacon
		AGGTGAAGTTGGTGACTCA	Dharmacon
		GGAACAACTTGCTCGAGAA	Dharmacon
		GAATCTAGATGAAGAGGTA	Dharmacon
CEP135 (pool)	CEP135	GAATTTGCATGCTGTAGTA	Dharmacon
		GAGAGAACATTCAGACCAA	Dharmacon
		GAAATGTGCACGTGAAACA	Dharmacon
		GCAAATTGATGAACCGGTT	Dharmacon

4.2.14 qRT-PCR RPE-1 cells

qRT-PCR of RPE-1 cells transfected with FAT4 siRNAs was performed with Dr. Alexander Weiss using standard procedures. Briefly, RNA was isolated using RNeasy Mini Kit (Qiagen) and reverse-transcribed using SuperScript III reagents (Thermo Fisher). qRT-PCRs were performed with primers targeting FAT4 or the housekeeping gene HPRT for normalization on a LightCycler 480 (Roche).

Table 4.8 qRT-PCR primers

Primer name	Primer sequence
FAT4 RT fwd	TGTCCCCACATTTGCCAGTA
FAT4 RT rev	GTGAACTGAGAGTTTCCACCG
HPRT RT fwd	TCCAAAGATGGTCAAGGTCGCAAG
HPRT RT rev	TGGCGATGTCAATAGGACTCCAGA

4.2.15 siRNA off-target analysis

Potential off-targets of different siRNAs were assessed using NCBI blast-n function. Targeting sequences of individual siRNAs were entered and blasted to the Human Genomic Plus Transcript (human G+T) database. Blast "hits" are shown in Table 12.1 as defined by blast-n parameters (sequence coverage 63% or higher). To predict off-targets of siRNAs that might act similar to miRNAs, GESS analysis (Yilmazel et al., 2014) was performed as described in the discussion chapter (7-mer homology of guide strands to the full human protein coding transcript library was addressed).

4.2.16 Automated quantification of G-slides

To quantify ciliation, cilia length and centrosome positioning, RPE-1 cells were reverse transfected with FAT4 and control siRNAs and seeded onto 96-well-sized wells on G-slides (Teflon-coated coverslips; gift from Dr. Laurence Pelletier (Gupta et al., 2014)) in complete medium. 24h after transfection, medium was changed to serum-free medium to start starvation. After 48-72h slides were fixed in ice-cold methanol and stained with antibodies against ARL13B and γ-tubulin and the DNA marker Hoechst. Experiments were performed in collaboration with Dr. João Gonçalves. For each experiment technical duplicates were performed (duplicate G-slides transfected and treated

at the same time under the same conditions) and several biological replicates (as annotated in figure legends). Dr. Mikhail Bashkurov performed automated imaging and designed and executed automated image analysis. Z-stack images of cells were taken on an IN Cell Analyzer 6000 (GE Healthcare), equipped with Nikon 20x/0.75 Plan APO objective and 2048x2048 sCMOS camera, followed by custom image analysis routines for Acapella 2.1 Perkin-Elmer.

Ciliation and cilia length analysis was performed as described in (Gupta et al., 2015) and (Shnitsar et al., 2015) by Dr. Mikhail Bashkurov. In brief, 3D image datasets for the γ-tubulin channel were collapsed into a 2D image using pixels with maximum-intensity. Centrosomes were segmented using Spot detection algorithm and 8x8µm regions surrounding each individual centrosome were cropped from the 3D image dataset, acquired for the ARL13B channel. The focal plane was selected within each ARL13B cropped subset. Proximal ciliary domains were segmented based on bright pericentrosomal clusters and final axonemal masks were found using region growing method. The length of each axoneme was measured after ciliary boundaries were detected.
Nucleus-centrosome distance was analyzed by first segmenting nuclear masks based on Hoechst stainings. Each cell's cytosol compartment was detected based on watershed segmentation within the γ-tubulin channel, which has a background cytosolic signal sufficient for robust detection of cellular borders. Centrosomal masks were defined based on the γ-tubulin (or pericentrin) signal. Centrosome-nucleus distance was calculated within each cell, based on step-wise radial dilation of the centrosomal region until non-zero overlap between nuclear and dilated centrosome masks.

4.2.17 Manual cilia quantifications

Cell stainings not performed on G-slides were manually quantified for ciliation. Cells were co-stained with Arl13b and γ-tubulin, GT335 or Pericentrin (or a combination of these) and imaged as sequential panels on DeltaVision Elite microscopes (GE Healthcare) (equipped with Olympus 20x, 40x or 60x objective and 2048x2048 sCMOS camera). Images were processed (deconvolution and maximum projection of z-stacks) and analyzed in Fiji (ImageJ). Ciliation is

defined as the percentage of ciliated cells of a population and was calculated as number of ciliated centrosomes divided by number of all centrosomes.

4.2.18 Quantification of Golgi apparatus area

RPE-1 cells stained with antibodies against the GA marker Gm130, the centrosomal marker Pericentrin and the DNA dye Hoechst were imaged on DeltaVision Elite microscopes (GE Healthcare) (equipped with Olympus 20x/0.75 UPLSAPO objective and 2048x2048 sCMOS camera). Automated analysis was performed by Dr. Mikhail Bashkurov. In brief, nuclear masks were segmented based on Hoechst staining and the cytosol compartment was detected based on watershed segmentation within the Gm130 channel. The GA region was isolated within each cell using Gm130 signal, followed by GA area calculations.

Manual GA area measurements were performed using the free-hand measure tool of Fiji (ImageJ). As seen in Fig. 11.36, automated and manual measurements correlate well.

4.2.19 Wound healing assay

RPE-1 cells were seeded in 12-wells and transfected the next day with siRNAs. 4 12-wells were each transfected with NT siRNA, FAT4 siRNA pool (#1+3+4) or FAT1 siRNA pool (#1+2+3) (approx. 30nM final concentration). Three days after transfection wounds were created by manually scratching the cell monolayer with a 10µl pipette tip. Dr. Mikhail Bashkurov performed automated time-lapse imaging, wound detection and wound area measurements. In brief, brightfield images of wound closure were acquired for up to 16 hours on IN Cell Analyzer 6000 (GE Healthcare) equipped with Nikon 4x/0.2 Plan APO objective and temperature- and CO2-controlled stage. 4-8 images with 5% overlap were captured for each wound every 15 minutes. Upon completion of wound closure acquisition was stopped and images for each well/time-point were stitched using Stitching plugin for ImageJ (Preibisch et al., 2009). The wound region and wound area was obtained using a custom image analysis routine for MATLAB 2015a.

4.2.20 Quantification of centriole splitting and intercentriolar distance

Manual quantification of centriolar splitting was performed on images of RPE-1 cells stained with antibodies against γ-tubulin, Pericentrin, GT335, centrin-GFP or a combination of these (DeltaVision; image z-stacks processed by deconvolution and maximum projection). RPE-1 cells stably expressing centrin-GFP and Arl13b-RFP were a gift from Dr. Laurence Pelletier. Centrioles with a distance larger than 2µm were considered "split". Intercentriolar distance was measured manually in Fiji (ImageJ) on magnified images with centriolar stainings (Centrin-GFP or GT335).

4.2.21 Cilia stainings in embryonic mouse brains

Paraffin-sections of E14 $Fat1^{-/-}$;$Fat4^{-/-}$ double mutant and control brains and E16 or P0 $Fat4^{-/-}$ and control brains were provided by Dr. Caroline Badouel (techniques described in (Badouel et al., 2015)). Stainings were performed as described for intestinal sections (see 4.2.12). For whole-mount preparations of P0 ventricular walls (developing ependyma), lateral ventricles were dissected and fixed in 4% PFA over night. The next day, more detailed dissections were performed, tissues were permeabilized in 0.1% PBS-TritonX-100 and blocked in 0.1% fish skin gelatin + 3% BSA in 0.1% PBS-TritonX-100. Both ventricular walls were stained with different antibodies.

4.2.22 CRISPR/Cas9-mediated GFP tagging of *FAT4* in RPE-1 cells

A guide RNA (gRNA) was designed to span the stop codon of the *FAT4* gene and cloned into BbsI restriction sites of the px330 Cas9 expression vector (pX330-U6-Chimeric_BB-CBh-hSpCas9 (Addgene plasmid #42230; by Dr. Feng Zhang)), creating pX330-gGFP.

A GFP repair plasmid was created by assembling a GFP-Stop-Puromycin cassette with a left homology arm (LA) and a right homology arm (RA) using the 3-way Multisite Gateway system (Invitrogen). In brief, approximately 1kb-long sequences flanking the FAT4 stop codon were PCR-amplified from purified RPE-

1 genomic DNA by nested PCR. Inner primers contained the respective attB sites. Gateway BP reactions were performed with pDONR P2R-P3 (RA) and pDONR P4-P1R (LA). Resulting vectors containing LA and RA and a pENTRY vector containing GFP-Stop-Puro (gift from Dr. Daniel Durocher) were combined in a Multisite-Gateway LR reaction to assemble the final repair cassette in a pDEST vector (= GFP repair vector). RPE-1 cells were transfected with pX330-gGFP and the GFP repair vector using Lipofectamine3000 (Invitrogen) according to manufacturer's protocol. 72h after transfection cells were reseeded in selection medium supplemented with 10µg/ml Puromycin. Drug-resistant colonies were grown individually (FAT4-GFP #3; FAT4-GFP #4) or as pool (FAT4-GFP pool). GFP-tagging of endogenous FAT4 was confirmed by PCR-genotyping and by Western blot.

Table 4.9 gRNA cloning primers for GFP tagging
Oligo sequences containing FAT4 target sequence (spanning stop codon) and BbsI overhangs. Oligos were annealed and cloned into pX330.

Primer name	sequence (BbsI overhang underlined, stop codon in bold)
gFt4_GFP sense	CACCGTATGTG**TGA**AGTTTATGTAC
gFt4_GFP anti	AAACGTACATAAACT**TCA**CACATAC

Table 4.10 Cloning primers for GFP homology arms

Primer name	Primer sequence (attB sites in lowercase)	attB site
Nested LA fw	GGAAGCAGCCTGAAGGGAAC	-
Nested LA rev	GTCTGTTTCAGCAGCATTGTGG	-
Ft4-tag LA fw	GGGGACAACTTTGTATAGAAAAGTTG**cattcaacactacaagcagttccg**	**attB4**
Ft4-tag LA rev	GGGGACTGCTTTTTTGTACAAACTTG**ccacatactgttctgcttcccca**	**attB1r**
Nested RA2 fw	CTTCTCCTCCAGTCGGACTTTC	-
Nested RA2 rev	ACATTTACAAGTAGAAAGCATACAGTATGTTAC	-
Ft4-tag RA rev2	GGGGACAACTTTGTATAATAAAGTTG**cagtatcaaaaacacagcttaggtg**	**attB3**
Ft4-tag RA fw2	GGGGACAGCTTTCTTGTACAAAGTGG**ctcaaaccattgtaaagttgctgac**	**attB2r**

4.2.23 Establishment of CRISPR InDel and full *FAT4* deletion RPE-1 cells

CRISPR/Cas9 technology was employed to introduce small insertions or deletions (InDels) into the *FAT4* gene of RPE-1 cells or to excise the majority of the *FAT4* gene. gRNAs were designed using the CRISPR Design tool (http://crispr.mit.edu/). To create InDels in *FAT4*, two gRNAs targeting exon 1

(gRNA_6; gRNA_7) and two gRNAs targeting exon 9 (gRNA_9; gRNA_10) were chosen. To excise *FAT4*, one gRNA targeting exon1 (gRNA_7) and a second targeting exon17 (gRNA_11; binds after stop codon) were designed. gRNAs were cloned into BbsI sites of the Cas9-expression plasmid px458 (pSpCas9(BB)-2A-GFP; Addgene plasmid # 48138; by Dr. Feng Zhang) using annealed oligos. The resulting px458-gRNA plasmids were transfected into RPE-1 cells (one 6-well per condition) using Lipofectamine3000 (Invitrogen) according to manufacturer's protocol. gRNA_7 and gRNA_11 were co-transfected to achieve *FAT4* gene excision. As an additional condition besides creating InDels with single gRNAs, gRNA_6 and gRNA_7 were also co-transfected to introduce bigger deletions in exon1. Based on the GFP marker within px458, successfully transfected cells (GFP+) were single-cell sorted into 96-well plates by FACS sorting (flow cytometry facility; 2 plates per gRNA) two days after transfection. After 2-3 weeks, colonies that had formed in 96-wells (10-30% of wells had a colony) were trypsinized and replated in 24-well plates. Once confluent, cells in 24-well plates were transferred into 10cm plates. Confluent 10cm plates were trypsinized and ¾ of cells were frozen down (final suspension: ~60% FBS and 8% DMSO), while ¼ of cells were used to make crude cell lysates for Western blot analysis. FAT4 Western blots were performed as described above to identify cell lines that had lost FAT4 (in trypsinized cells loss of a ~200kDa band representing cleaved FAT4 (see Fig. 11.7) can be easily observed).

At the 96-well, 24-well or 10cm stage, a subset of cells was lysed in QuickExtract DNA extraction buffer (Epicentre) and used to PCR-amplify the regions of *FAT4* expected to be modified. To test for *FAT4* excision, a genotyping strategy using primer sets flanking the gRNA_7 target region (to test for wildtype FAT4 alleles) or binding outside of gRNA_7 and gRNA_11 target regions (to test for excised alleles) was developed (see Fig. 11.43). All PCR products were purified (PCR purification kit; Geneaid) and sent for Sanger sequencing. InDel mutations were assessed by analyzing chromatograms with the TIDE web tool (Brinkman et al., 2014).

A total of 94 clones were sequenced of the InDel cell lines (from gRNA_6, gRNA_7, gRNA_9, gRNA_10, gRNA_6+7). 51 of these were selected to test by Western blot, where 22 were found to lose the ~200kDa FAT4 band. Western blots of non-trypsinized cells were performed for a subset of cell lines and confirmed loss of detectable full-length FAT4.

For the FAT4 gene excision CRISPR approach, a total of 57 clones were screened, 6 of which tested positive for the desired deletion (one or two alleles). While 10 clones out of all 57 lost FAT4 protein (trypsinized 200kDa band), only one clone ("NC55") both lost FAT4 protein and showed the large excision by PCR. Loss of FAT4 protein of other clones is likely due to InDels introduced by gRNA_7, resulting in premature stop codons. NC55 gene excision was further confirmed by Sanger sequencing (see also schematic in Fig. 11.43).

Table 4.11 gRNA cloning primers for *FAT4* mutations
BbsI overhang sequences are shown in bold, capital letters

Name	Sense oligo	Antisense oligo	Targeting exon
gRNA_6	**CACCG**aggtgaagccggggcgcgtc	**AAAC**gacgcgccccggcttcacctC	1
gRNA_7	**CACCG**ttggaacacctggcgcggct	**AAAC**agccgcgccaggtgttccaaC	1
gRNA_9	**CACCG**aagaaggtggctacgccact	**AAAC**agtggcgtagccaccttcttC	9
gRNA_10	**CACCG**agggagctgtctacgaagat	**AAAC**atcttcgtagacagctccctC	9
gRNA_11	**CACCG**ttggaacacctggcgcggct	**AAAC**agccgcgccaggtgttccaaC	17

4.2.24 Antibodies used in Chapter B

FAT1 antibody was a gift from Dr. Nicholas Sibinga, p120 antibodies were gifts from Dr. Albert Reynolds, ANKG (ANK3) antibody was a gift from Dr. Vann Bennett, SEPT7 antibody was a gift from Dr. William Trimble, Rootletin antibody was a gift from Dr. Erich Nigg, NPHP1 and IFT88 antibodies were gifts from Dr. Gregory Pazour and a home-made GFP antibody was a gift from Dr. Laurence Pelletier. Giantin and Calreticulin antibodies were provided by Dr. Anne-Claude Gingras. FAT4 TO152AP and FAT4 cys58 antibodies were established in the McNeill lab.

Table 4.12 Chapter B antibody information
(WB = Western blot; IF = immunofluorescence; rb = rabbit; ms = mouse; gt = goat; rt = rat; specific fixation requirements for IF are annotated in square brackets)

Antibody	Species	Origin	Concentration for WB	Concentration for IF
Fat4 TO152AP	rb	H. McNeill	1:500 - 1: 1000	1:100 - 1:200
Fat4 Novus	rb	Novus Biologicals	1:500 - 1: 1000	1:200 - 1:300
Fat4 cys58	rb	H. McNeill	-	1:100 - 1:200
Fat1	rb	N. Sibinga	1:2000	1:500 [PFA]
N-cad	ms	BD Transduction	1:2000	1:300 - 1:500
E-cad	ms	BD Transduction	1:1500 - 1:2000	1:300
SCRIB	gt	Santa Cruz	1:1000 - 1:2000	1:200
NF2	rb	Sigma	1:1000	1:200 - 1:500
p120 F1aSH (human)	rb	A. Reynolds	1:1000	1:200 - 1:800
p120 8D11 (mouse)	ms	A. Reynolds	-	1:300
ANKG	gt	V. Bennett	-	1:200 - 1:800
PAR3	rb	Millipore	1:1000	-
DLG1	ms	Enzo	1:500	-
ERBB2IP	rb	Sigma	1:500	-
Flag	ms	Sigma (M2)	1:5000 - 1:10'000	1:500
Flag	rb	Sigma	-	1:300 - 1:1000
YAP (63.5)	ms	Santa Cruz	1:500	1:100 - 1:200
pYAP (S127)	rb	Cell Signaling	1:500	-
LATS1	rb	Cell Signaling	1:2000	-
pLATS1 (S909)	rb	Cell Signaling	1:1000	-
SEPT7	rb	W. Trimble	1:1000	1:200 - 1:500 [PFA]
ARL13B	rb	Proteintech	-	1:200 - 1:400
γ-tubulin (gamma)	ms	Sigma	-	1:300 – 1:1000
α-tubulin (alpha)	rt	Serotec	1:4000	1:2000
GT335	ms	Adipogen	x	1:300 - 1:1000
acteylated tubulin	ms	Sigma	-	1:1000 [MeOH]
Pericentrin (PCNT)	gt	Santa Cruz (N-20)	-	1:200
CP110	rb	Proteintech	-	1:200
C-NAP1	ms	BD Transduction	x	1:200
Rootletin	rb	E. Nigg	x	1:1000
NPHP1	rb	G. Pazour	-	1:100 [PFA]
IFT88	rb	G. Pazour	-	1:1000 [PFA]
CEP164	rb	Novus Biologicals	-	1:400
GM130	ms	BD Transduction	1:2000	1:500 - 1:1000
Giantin	rb	(A. Gingras)	-	1:5000
Golgin97	ms	Thermo Fisher	1:1000	-
Calnexin	rb	Abcam	1:1000 - 1:2000	1:300
Calreticulin	rb	(A. Gingras)	1:1000	-
GFP	gt	L. Pelletier	1:10'000	1:2000

5 Introduction Chapter A

5.1 Introduction into Fat structure and function

5.1.1 Fat has essential roles during *Drosophila* development

The *fat* (*ft*) locus was first described in early genetic experiments in *Drosophila melanogaster* as causing mutant flies with short and "fat" abdomen (Mohr, 1923; Mohr, 1929). With the establishment and characterization of a genetic null allele, ft^{fd} (*floppy-disc*), *ft* was recognized as a tumor suppressor gene (Bryant et al., 1988); *ft* mutant flies have a prolonged larval period during which imaginal disc epithelia dramatically overgrow, while maintaining single-layered epithelial characteristics and the ability to differentiate into adult structures (Bryant et al., 1988). Overgrown wing discs retain relative anatomical proportions, suggesting that the extra growth is allometric (Bryant et al., 1988; Garoia et al., 2000). Almost twenty years after its first characterization, the overgrowth phenotype of *ft* mutants was found to result from misregulation of the newly identified Hippo tumor suppressor pathway (Bennett and Harvey, 2006; Cho et al., 2006; Silva et al., 2006; Willecke et al., 2006).

ft mutant flies are pupal lethal (Bryant et al., 1988), therefore the analysis of adult structures is limited to animals reaching the pharate-adult stage, hypomorphic alleles or RNAi, and mosaic or tissue-specific mutants. In adult flies, *ft*-mutant tissue shows abnormal polarity of bristles and hairs on legs, notum, abdomen and wings, as well as randomization of photoreceptor clusters in the eye, highlighting a second role of *ft* in planar cell polarity (PCP) (Bryant et al., 1988; Casal et al., 2002; Rawls et al., 2002; Strutt and Strutt, 2002; Yang et al., 2002).

5.1.2 Structure of Fat

Fat is a type-I transmembrane cadherin and with a molecular weight of 560kDa one of the largest members of the cadherin superfamily (Mahoney et al., 1991). Fat contains 34 cadherin repeats, 4 EGF-like domains and 2 Laminin G domains in its extracellular domain (ECD), followed by a single-pass transmembrane

domain and large intracellular domain (ICD) (Mahoney et al., 1991) (Fig. 5.1). These features differ from those of classical cadherins, which typically contain 5 cadherin repeats and have short ICDs with defined catenin binding sites (Ozawa et al., 1990; Yap et al., 1998; Thoreson et al., 2000). In contrast, a motif with only weak similarity to the classical beta-catenin binding sites has been reported in the Fat ICD, and its function and biological significance remain elusive (Clark et al., 1995). Fat is therefore considered an atypical cadherin and founding member of a Fat cadherin subgroup within the cadherin superfamily (Hulpiau and van Roy, 2009).

Cadherin repeats and their calcium-binding linkers form conserved domains that are characteristic of the large cadherin superfamily and are important for protein-protein binding and cell adhesion (Boggon et al., 2002; Hulpiau and van Roy, 2009). Laminin G domains are important for protein binding (Yurchenco et al., 1993) and EGF-like domains have unknown functions but specifically occur in protein domains at the cell surface and are found in many receptors and transmembrane proteins, such as Notch and Crumbs (Wharton et al., 1985; Tepass et al., 1990).

Mature Fat is post-translationally modified through at least two proteolytic cleavage events. One occurs in the Fat ECD, close to the transmembrane domain, resulting in a ~450kDa and a ~110kDa fragment that stay non-covalently attached (Feng and Irvine, 2009; Sopko et al., 2009). Processing appears to happen constitutively as part of receptor maturation (Feng and Irvine, 2009). This could be comparable to the S1 cleavage of Notch or processing of G protein-coupled receptors (GPCRs), such as Flamingo (Fmi) (Logeat et al., 1998; Usui et al., 1999; Krasnoperov et al., 2002). It is unknown which role this cleavage event plays for the activity of Fat but it could be a prerequisite for proper receptor activation or membrane trafficking (such as seen for mammalian Polycystin-1 (Kurbegovic et al., 2014)). A second proteolytic cleavage can occur in the Fat ICD, releasing a Fat fragment that is imported into mitochondria to regulate metabolic processes (Sing et al., 2014).

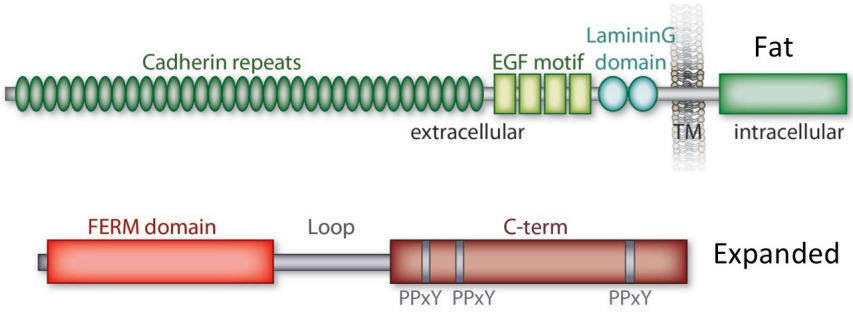

Fig 5.1 Schematics of Fat and Expanded structures
Fat is a type-I transmembrane protein with a molecular weight of 560kDa. The Fat extracellular domain contains 34 cadherin repeats, 4 EGF motifs and 2 Laninin G domains. The intracellular domain does not contain known domains. Expanded (Ex) is a FERM-domain protein with a molecular weight of 160kDa and has a C-terminal domain with PPxY motifs.

5.1.3 Fat and Dachsous form a receptor-ligand pair

Unlike the homophilic interaction typical for most classical cadherins, Fat interacts in a heterophilic way with another large cadherin, Dachsous (Ds) (Clark et al., 1995). *ds* mutant flies have phenotypes in growth and tissue patterning similar to *ft* mutants (Mahoney et al., 1991; Clark et al., 1995; Adler et al., 1998). Ds is distantly related to Fat (52% amino acid similarity) and has 27 cadherin repeats in its ECD and a single-span transmembrane domain. Its ICD is lacking typical motifs except for a weakly conserved beta-catenin binding-like site, similar to Fat. Ds seems to be proteolytically cleaved in its ECD at two alternative sites, indicating it can exist in two different forms at the membrane. In *ft* mutant flies, the distribution between the two Ds forms was found to be slightly shifted, suggesting a possible regulation of Ds by Fat (Ambegaonkar et al., 2012). Fat processing in contrast seems to be independent of Ds (Feng and Irvine, 2009; Sopko et al., 2009).

In epithelial cells, Fat and Ds localize to the subapical membrane apically adjacent to adherens junctions (Strutt and Strutt, 2002; Ma et al., 2003). Experiments in *Drosophila* Schneider 2 (S2) cells suggest that Fat and Ds interact *in trans* on two neighboring cells. S2 cells, which don't express endogenous Fat and Ds, grow in semi-suspension and don't adhere to each other. However,

spontaneous cell aggregation is induced by co-expression of Fat and Ds or by co-culturing Fat expressing cells and Ds expressing cells. Consistent with an interaction *in trans*, aggregation is dependent on the presence of the ECDs but not the ICDs of Fat and Ds. Cells only expressing Ds or Fat don't form aggregates, arguing against an ability to form homophilic interactions (Matakatsu and Blair, 2004; Matakatsu and Blair, 2006). Fat and Ds further seem to recruit and stabilize each other at sites of cell-cell contact. This can be seen in *Drosophila* wing discs, where clonally overexpressed Ds recruits Fat in clone-adjacent cells to the membrane in contact with the clone (Matakatsu and Blair, 2004). Similarly, Fat and Ds proteins in wildtype cells adjacent to a *ft* or *ds* mutant clone relocalize away from the membranes contacting the mutant cell (Strutt and Strutt, 2002; Ma et al., 2003). This interaction has been found to be crucial for Fat and Ds signaling, however it is still unclear whether it plays a role in cell adhesion. While *ft* and *ds* expressing S2 cell aggregates withstand low strain (indicating adhering forces), the effect is weaker than for E-cadherin expressing aggregates and has not been addressed *in vivo*. Interestingly, though, addition of calcium chelators inhibit the S2 cell aggregation assay, suggesting that the Fat-Ds interaction is calcium dependent, similar to classical cadherin-cadherin interactions (Matakatsu and Blair, 2004). Ds is considered the ligand of Fat, as *ds* functions genetically upstream of *ft* in most processes (Yang et al., 2002; Willecke et al., 2008). However, their relationship might be more complicated than that and in some processes both proteins can function independently of each other (Willecke et al., 2008; Degoutin et al., 2013).

5.1.4 The Fat paralog Kugelei has distinct functions from Fat

Besides Fat and Ds, *Drosophila* expresses a third large cadherin with similar characteristics, named Fat-like or Kugelei (Kug) (Gutzeit et al., 1991; Castillejo-Lopez et al., 2004). The ECD of Kug shares similarites with Fat, as it consists of 34 cadherin repeats, 5 EGF-like domains and 1 Laminin G domain, but their ICDs differ significantly (Castillejo-Lopez et al., 2004). *ft* and *kug* seem to have distinct expression patterns. To which extent they are co-expressed and functionally linked is largely unexplored, though. *kug* deletion in the *Drosophila* eye did not cause PCP defects or alter *ft* or *ds* mutant phenotypes (Sharma and McNeill,

2013). Kug is found apically localized in luminal tissues of larvae, such as trachea, hindgut and salivary glands. *kug* knockdown embryos and larvae show malformations of these structures indicative of a role for *kug* in lumen formation or maintenance (Castillejo-Lopez et al., 2004). Interestingly, in *Drosophila* ovaries, Kug localization is planar polarized and involved in regulating actin filament orientation. *kug* mutant females further lay unusually round eggs, due to misaligned F-actin during eggshell formation (Gutzeit et al., 1991; Viktorinova et al., 2009; Viktorinova et al., 2011; Squarr et al., 2016). This suggests that Kug functions in distinct planar polarized processes and in a different manner than Fat. Although the role of *kug* is surprisingly poorly understood in *Drosophila*, its mammalian homologs are the focus of many studies, due to their implications in human genetic disorders and cancers (see below). In concordance with findings in *Drosophila*, the mammalian Kug homologs Fat1 and Fat2 can regulate F-actin, indicating a potential mechanistic conservation (Moeller et al., 2004; Tanoue and Takeichi, 2004; Badouel et al., 2015).

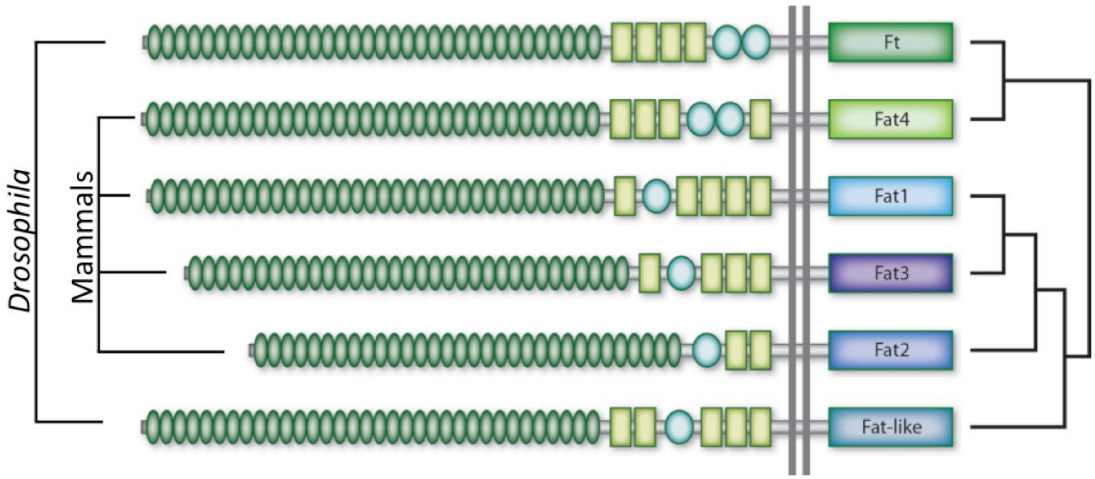

Fig 5.2 Fat cadherins in *Drosophila* and mammals
Drosophila Fat is most closely related to mammalian Fat4, while Fat-like/Kug shares higher homology with mammalian Fat1, Fat2 and Fat3. Cadherin repeats are in dark green, EGF-like motifs are marked by light green rectangles and Laminin G domains by blue circles. Variability of the ICDs is symbolized by different colors.

Mammals have four Fat cadherins, Fat1, Fat2, Fat3 and Fat4 (Dunne et al., 1995; Cox et al., 2000; Mitsui et al., 2002; Nakayama et al., 2002). Sequence analyses indicate that Fat4 is the closest homolog of *Drosophila* Fat, whereas Fat1-3 share higher similarity with Kug (Fig. 5.2) (Dunne et al., 1995; Castillejo-Lopez et al., 2004; Rock et al., 2005; Tanoue and Takeichi, 2005; Saburi et al., 2008). While Fat function is mostly studied and well established in *Drosophila*, functions of mammalian Fat cadherins are still poorly understood (mammalian Fat cadherins are discussed in more detail in Chapter B).

5.2 Fat functions to regulate planar cell polarity

5.2.1 Planar cell polarity in *Drosophila* and mammals

Planar cell polarity (PCP) describes the orientation of cells or cellular processes within the plane of a tissue. It is best understood in *Drosophila* epithelia, where PCP refers to cell orientation in the plane orthogonal to the apical-basal polarity axis. PCP manifests in a multitude of oriented cellular behaviors, such as the distally-pointed bristles of the wing, oriented cell division during wing elongation and the orientation of photoreceptor clusters in the eye of *Drosophila.* In vertebrates, PCP underlies cellular features like the directionality of epidermal hairs, polarized axonal outgrowth, orientation of hair cells in the inner ear (organ of Corti), directional movement and intercalation of cells during gastrulation, neuronal tube closure and convergent extension processes (Djiane et al., 2000; Heisenberg et al., 2000; Tada and Smith, 2000; Wallingford et al., 2000; Darken et al., 2002; Goto and Keller, 2002; Hamblet et al., 2002; Park and Moon, 2002; Wallingford and Harland, 2002; Carreira-Barbosa et al., 2003; Curtin et al., 2003; Takeuchi et al., 2003; Veeman et al., 2003; Gong et al., 2004; Wang et al., 2005; Wang et al., 2006b). PCP is thought to be conveyed mostly through cell-cell adhesion, which allows the cells to communicate long-range vectorial information within a tissue. In *Drosophila*, this cell-cell communication is illustrated by the fact that cells mutant for PCP genes can propagate PCP defects to their wildtype neighbors, resulting in non-autonomous phenotypes. The molecular mechanisms underlying PCP have been studied extensively in flies, as their genetic manipulability allows *in vivo* and mosaic gene ablation experiments needed to understand these complex contextual behaviors.

5.2.2 PCP is established by the Fz/PCP and the Fat/Ds module

Studies in *Drosophila* revealed that PCP is regulated by two modules, the Frizzled (Fz)/PCP pathway, also called the core module, and the Fat/Ds pathway, also referred to as the global module. The Fz/PCP module is based on the transmembrane proteins Fz (Vinson and Adler, 1987; Vinson et al., 1989), Flamingo/Starry night (Fmi) (Chae et al., 1999; Usui et al., 1999) and Van Gogh/Strabismus (Vang) (Taylor et al., 1998; Wolff and Rubin, 1998), as well as the cytoplasmic proteins Disheveled (Dsh) (Klingensmith et al., 1994; Theisen et al., 1994), Prickle/Spiny-legs (Pk) (Gubb et al., 1999) and Diego (Dgo) (Feiguin et al., 2001). Strong interdependences and feedbacks between these molecules result in their asymmetric localization and robust segregation into two distinct complexes on opposite sides of the cells (Bastock et al., 2003; Jenny et al., 2003; Wong et al., 2003; Jenny et al., 2005; Chen et al., 2008; Strutt and Strutt, 2009). Fmi forms homo-dimers across cells and binds a complex of Fz, Dsh and Dgo at one cell membrane, and a complex of Vang and Pk at the adjacent membrane (Tree et al., 2002; Das et al., 2004; Amonlirdviman et al., 2005; Jenny et al., 2005; Strutt and Strutt, 2007). With few exceptions, the asymmetric localization of these complexes is indicative of the orientation of a cell within a tissue; for example in wildtype wings, Fmi/Fz/Dsh/Dgo indicate the distally-oriented cell border (Axelrod, 2001; Strutt, 2001; Tree et al., 2002; Bastock et al., 2003; Das et al., 2004; Chen et al., 2008) and in the *Drosophila* eye the equatorial side of the photoreceptor precursor R3/R4 boundary (Das et al., 2002; Rawls et al., 2002; Strutt et al., 2002; Yang et al., 2002). It is thought that polarity is conveyed by a mechanism where Fmi senses the amount of Fmi-bound Fz in the neighboring cell, and subsequently polarizes the cell in coherence with this neighbor (Strutt and Strutt, 2008; Struhl et al., 2012). However, while this can explain the local orientation of a group of cells, there are still open questions about how the Fz/PCP module senses the global orientation of a tissue in relation to body axes. This likely requires a long-range directional reference signal across the tissue, feeding into Fz/PCP. None of the Fz/PCP module members has been found to be expressed in a gradient or to inherently fulfill this requirement otherwise; therefore other factors likely communicate global vectorial information to Fz/PCP. Diffusible morphogens, especially the Fz ligands Wingless (Wg) and

DWnt4, but also Hedgehog (Hh), have been suggested as global polarizing inputs in different tissues, but whether they can provide directional information remains controversial (Struhl et al., 1997; Wehrli and Tomlinson, 1998; Lawrence et al., 2002; Casal et al., 2006; Lawrence et al., 2007; Strutt, 2009; Sagner et al., 2012; Wu et al., 2013). It has also been studied extensively whether the Fat/Ds global module orients Fz/PCP, but the relationship between the two modules is complex and a field of strong controversy, complicated by limitations of genetic experiments and potential tissue-dependent specificities.

5.2.3 The Fat/Ds module regulates PCP

Both Fat and Ds regulate PCP, as illustrated by the strong planar organization defects in *ft mutant*, *ds* mutant and *ft, ds* double-mutant tissue (Adler et al., 1998; Rawls et al., 2002; Yang et al., 2002). The polarizing activity of the Fat/Ds module is suggested to be based on segregation of Fat and Ds to opposite sides of a cell and their heterotypic interaction across cells (Ambegaonkar et al., 2012; Brittle et al., 2012). While Fat is expressed homogenously, Ds expression forms a gradient across many tissues (Casal et al., 2002; Yang et al., 2002; Ma et al., 2003; Matakatsu and Blair, 2004). This is not only thought to establish Fat-Ds asymmetry but also to transmit information about the global orientation of the tissue to each cell. In line with this model, expression of an inverted Ds gradient in the *Drosophila* eye reverses the normal photoreceptor cluster orientation (Simon, 2004) and artificial Ds gradients in the wing locally reorient bristles (Matakatsu and Blair, 2004).

Four-jointed (Fj), another member of the Fat/Ds module, is expressed in opposite gradients of Ds (Villano and Katz, 1995; Casal et al., 2002; Yang et al., 2002). Fj is a Golgi-localized kinase that phosphorylates both Fat and Ds on cadherin repeats in their ECDs and thereby regulates their adhesion (Strutt et al., 2004; Ishikawa et al., 2008). While Fj-phosphorylated Fat shows an increased affinity for binding Ds, phosphorylated Ds has a reduced capacity to interact with Fat (Brittle et al., 2010; Simon et al., 2010; Hale and Strutt, 2015). This is suggested to further establish Fat-Ds asymmetry at opposite cell borders, adding fidelity to a Ds gradient-based mechanism (Simon, 2004; Brittle et al., 2010;

Simon et al., 2010). This additional level of control is observed in the *Drosophila* eye, where PCP phenotypes of *ds* mutant tissue can be rescued by homogenous (non-gradual) expression of Ds, as long as the Fj gradient is still present (Simon, 2004). A computational model has confirmed that the regulatory interactions between Fj, Fat and Ds are mechanistically sufficient to set up long-range planar cell polarity across the wing (Hale and Strutt, 2015).

Ds and Fj graded expressions are established by morphogens, such as Wg, Hh and Dpp in different tissues, but direct mechanisms are yet to be determined (Casal et al., 2002; Lawrence et al., 2002; Yang et al., 2002; Cho and Irvine, 2004). Interestingly, morphogens are also proposed to scale tissues and could therefore signal information about both global tissue orientation and dimension to Fat/Ds, to link their roles in PCP and growth (Day and Lawrence, 2000; Casal et al., 2002).

5.2.4 Dachs is downstream of Fat but plays a lesser role in PCP

Fat signals at least in part through the unconventional myosin Dachs (D). *d* mutant tissue exhibits phenotypes opposite to *ft* mutants, such as undergrowth and increased apoptosis (Cho et al., 2006; Mao et al., 2006). D localizes asymmetrically at the subapical cell membrane of imaginal disc epithelia, together with Ds at opposite cell membranes of Fat (Mao et al., 2006; Ambegaonkar et al., 2012; Brittle et al., 2012). Although Ds can interact with D (Bosveld et al., 2012), Ds appears to have a minor function in immediate D localization, while asymmetric distribution and levels of D strongly depend on Fat (Brittle et al., 2012). Despite the planar polarization of D protein, it seems to have a lesser role in PCP, as PCP phenotypes of *d* mutant tissues are mild (Mao et al., 2006). *d* functions downstream and in opposition of *ft,* but while overgrowth phenotypes of *ft* mutant tissue are suppressed in a *d* mutant background, PCP phenotypes are alleviated but still present (Mao et al., 2006), suggesting that also other effectors mediate PCP downstream of Fat.

5.2.5 Interactions between Fz/PCP and Fat/Ds

The relationship between the Fz/PCP and Fat/Ds modules remains to be fully explored; while data from the *Drosophila* abdomen suggest that both modules act independently (Casal et al., 2006), data from the *Drosophila* eye is explained best by a model of Fat/Ds signaling upstream of Fz/PCP to regulate photoreceptor precursor R3/R4 fate and subsequent cluster orientation (Yang et al., 2002). For PCP establishment in the wing, Fat/Ds seems to be largely dispensable, with the exception of proximal regions, which rely on a sharp Ds gradient (Matakatsu and Blair, 2004). The observed differences are likely the result of temporal, tissue-specific or context-specific modulations of both pathways or might be explained by additional, yet to be identified upstream or downstream factors, potentially linking or uncoupling both modules.

To answer some of these questions, the molecular mechanisms downstream of Fat/Ds need to be better understood, as there are only few direct Fat and Ds interactors known. One of them is Atrophin (Atro), a transcriptional co-repressor with clear PCP activity, which directly binds to the Fat ICD and therefore might act as a transcriptional mediator of Fat signaling (Fanto et al., 2003). Recently, Fat/Ds/Fj have been also implicated in organizing an apical planar-polarized microtubule network important for vesicular transport of Dsh to distal cell borders, suggesting that both PCP modules are initially linked (at least in the wing) (Harumoto et al., 2010; Matis and Axelrod, 2013).

However, other layers of complexity exist: Fat regulates apical cell membrane tension/constriction and oriented cell division (OCD), which could affect PCP additionally indirectly (Baena-Lopez et al., 2005; Mao et al., 2013). Fat also regulates PCP metabolically, possibly though mitochondrial control of reactive oxygen species gradients in larval tissues (Sing et al., 2014). Furthermore, epistasis experiments in the *Drosophila* eye suggest that at least part of the PCP activity of Fat/Ds depends on their ability to regulate the Hippo pathway (Brittle et al., 2012). While *ft* and *ds* mutant eyes have clear PCP defects, PCP can be largely rescued upon artificial Hippo pathway activation, i.e. blocking of excessive growth caused by loss of Fat and Ds. Inhibition of Hippo signaling in

otherwise wildtype eyes on the other hand causes photoreceptor misorientation (inversions and misrotations), suggesting that *ft* and *ds* might at least partially regulate PCP through the Hippo pathway in the eye (Brittle et al., 2012). Interestingly, both the ECD and ICD of Fat seem to independently function in PCP. Part of the PCP activity of Fat does not require its ICD, as a Fat construct lacking the ICD significantly alleviates PCP phenotypes in *ft* mutant flies (Pan et al., 2013). Fat lacking its ECD also partially rescues PCP defects in *ft* mutant abdomens (Matakatsu and Blair, 2006). Therefore, there might be different signaling branches regulating PCP, one through *in trans* interaction with Ds and one through intracellular interactions of Fat with other factors.

5.3 Fat functions to regulate the Hippo tumor suppressor pathway

5.3.1 The core Hippo pathway

The Hippo pathway (also referred to as Salvador-Warts-Hippo or SWH pathway) is a general controller of growth in *Drosophila* and mammals and is considered a tumor suppressor pathway. Its core consists of a kinase cascade, formed by the Ste20 kinase Hippo (Hpo) (Harvey et al., 2003; Jia et al., 2003; Pantalacci et al., 2003; Udan et al., 2003; Wu et al., 2003) and the NDR family kinase Warts (Wts) (Justice et al., 1995; Xu et al., 1995), as well as their regulatory adaptor proteins Salvador (Sav) (Kango-Singh et al., 2002; Tapon et al., 2002) and Mob as tumor suppressor (Mats) (Lai et al., 2005). The core cascade controls growth mainly by regulating the transcriptional co-activator Yorkie (Yki) through phosphorylation (Huang et al., 2005). In the inactive pathway state, Hpo and Wts are inactive, and unphosphorylated Yki accumulates in the nucleus, where it regulates a wide array of genes, mainly by binding to the transcription factor Scalloped (Sd) (Zhao et al., 2007; Goulev et al., 2008; Wu et al., 2008; Zhang et al., 2008b). Nuclear Yki activates growth-promoting genes, such as *cyclinE* and the microRNA-encoding *bantam*, and anti-apoptotic genes, such as *diap1* (Huang et al., 2005; Hamaratoglu et al., 2006; Nolo et al., 2006; Thompson and Cohen, 2006). In the active pathway state, Hpo is active, binds to Sav and subsequently phosphorylates and activates Wts and Mats (Wu et al., 2003; Wei et al., 2007). Wts in turn phosphorylates Yki at three sites (most critically: Ser168), which creates a binding site for 14-3-3 proteins (Huang et al., 2005; Dong et al., 2007; Zhao et al., 2007; Oh and Irvine, 2008; Oh and Irvine, 2009). 14-3-3 binds and sequesters Yki in the cytoplasm, thereby inhibiting its transcriptional activity (see Fig. 5.3 for Hippo schematic) (Zhao et al., 2007; Oh and Irvine, 2008; Ren et al., 2010). During the *Drosophila* larval period, inactivation of Hippo signaling results in dramatic overproliferation of tissues, especially of imaginal disc epithelia, while hyperactivation leads to undergrowth and apoptosis.

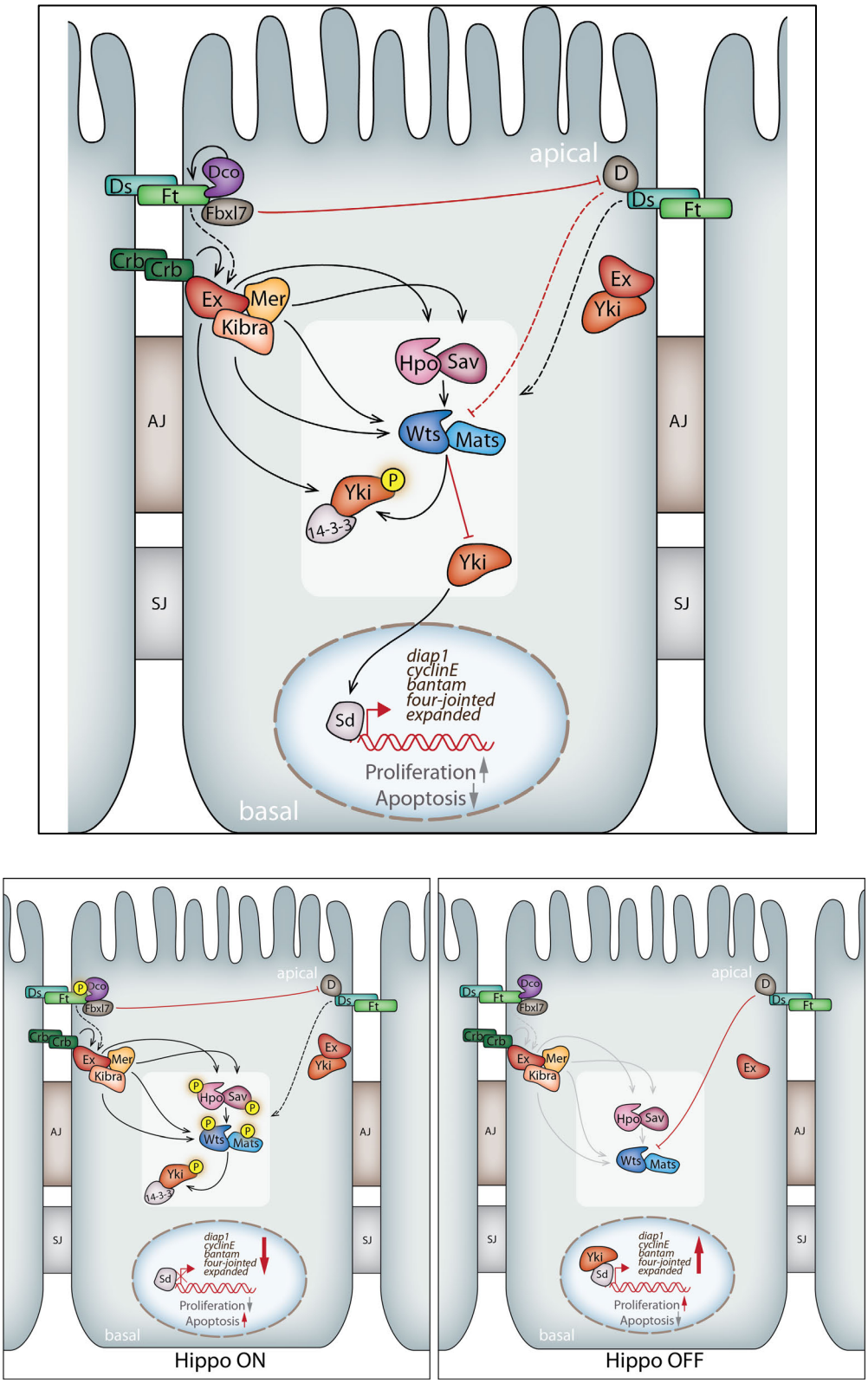

Fig 5.3 The *Drosophila* Hippo pathway
Simplified schematic of regulatory control of the core Hippo pathway. Smaller panels illustrate Hippo signaling in its active (ON) and inactive (OFF) state. AJ = adherens junction; SJ = septate junction.

Upstream regulators of the Hippo pathway include proteins at adherens junctions, regulators of apical-basal polarity, components of the actin cytoskeleton and few transmembrane receptors, such as Fat, Ds and the polarity determinant Crumbs. Especially the subapical domain of cells and adherens junctions have been implicated as domains of active Hippo signaling, and spatial control of Hippo pathway members seems to be crucial for regulating interactions and phosphorylation events (reviewed in (Boggiano and Fehon, 2012; Harvey and Hariharan, 2012; Schroeder and Halder, 2012; Staley and Irvine, 2012; Enderle and McNeill, 2013; Yu and Guan, 2013; Gaspar and Tapon, 2014)).

In epithelial cells, adherens junctions mediate cell-cell contact through classical cadherins linked to the actin cytoskeleton and separate the cell membrane into apical and basolateral compartments. Above adherens junctions lies the subapical domain in invertebrate cells, while in vertebrate cells tight junctions are situated in the equivalent position.

5.3.2 The Expanded-Merlin-Kibra complex regulates the Hippo pathway

At the subapical region of epithelial cells a complex of the 4.1, Ezrin, Radixin, Moesin (FERM)-domain containing proteins Expanded (Ex) and Merlin (Mer) and the WW-domain containing Kibra stimulates the Hippo pathway. Tissue mutant for *ex*, *mer* or *kibra* exhibits overgrowth phenotypes and characteristic induction of Yki target gene expression. Ex, Mer and Kibra can function in a complex, but are not fully redundant and localize independently to the plasma membrane (McCartney et al., 2000). They interact with several Hippo pathway core members, which is thought to be crucial for sequestration of the Hippo core to the subapical membrane and its activation (Sun et al., 2015). In line with this scaffold model, Wts and Hpo are ectopically activated after artificial recruitment to the membrane through a myristoylation signal sequence (Deng et al., 2013; Yin et al., 2013). Simultaneous knockdown of Ex, Mer and Kibra causes a decrease of Hpo membrane localization and activation (Deng et al., 2013). Mer was further shown to directly bind Wts and to regulate its membrane

localization and activity (Yin et al., 2013). Mer can also interact with Sav, which is critical for Hippo pathway activity, possibly by additionally recruiting Hpo to the membrane (Wu et al., 2003; Yin et al., 2013). Ex and Mer bind and stabilize each other and largely regulate growth redundantly, although they seem to differentially regulate other aspects, such as apoptosis (McCartney et al., 2000; Hamaratoglu et al., 2006; Pellock et al., 2007). Ex also interacts with Hpo (Yu et al., 2010), but a potential capacity to recruit Hpo to the membrane has not been fully explored. It is a plausible scenario that at least part of the observed redundancy of Ex and Mer is based on their abilities to bring Hpo and Wts together for activation. Ex can also regulate Yki directly, by binding Yki and retaining it at the subapical membrane independently of Wts-mediated phosphorylation of Yki. Ex directly binds the WW-domain of Yki through PPxY motifs in its C-terminus (Badouel et al., 2009; Oh et al., 2009). This might be a safeguard mechanism or reflect a Hippo-independent Ex signaling branch.

As an additional level of control, many upstream Hippo regulators, including *ex, ft, ds* and *crb*, are transcriptionally controlled by Yki, which is thought to provide a regulatory feedback loop that buffers signaling (Hamaratoglu et al., 2006; Ikmi et al., 2014; Zhu et al., 2015).

5.3.3 Fat is involved in upstream regulation of the Hippo pathway

ft mutant tissue shows overgrowth phenotypes due to a function of *ft* upstream of the Hippo pathway. Fat promotes Hippo signaling and hence Yki inhibition, and *ft* mutant clones exhibit characteristic upregulation of Yki target genes (Bennett and Harvey, 2006; Cho et al., 2006; Silva et al., 2006; Willecke et al., 2006). While direct molecular links are still missing, Fat seems to regulate the Hippo pathway at least in part through regulation of Wts stability. *ft* mutant tissue shows reduced Wts protein levels, an effect that is dependent on the Fat effector D. D interacts with Wts in cell culture and promotes Wts turnover, suggesting that Fat regulates Wts levels by inhibiting D (Cho et al., 2006). *d* mutant tissue has opposite phenotypes to *ft* mutant tissue and loss of *d* strongly suppresses the growth aspects of *ft* mutants (Mao et al., 2006). Furthermore, Fat

and Dachs have recently been implicated in regulating the conformational state of Wts, which appears tightly linked to its activity (Vrabioiu and Struhl, 2015).

Genetic experiments suggest that *ft* negatively regulates *d* at least in part by binding to the F-box protein Fbxl7 (Bosch et al., 2014; Rodrigues-Campos and Thompson, 2014). Strongly resembling loss of *ft*, loss of *fbxl7* results in overgrowth and patterning defects and in loss of D asymmetry. Fbxl7 co-localizes with Fat in a polarized fashion, but whether Fbxl7 regulates D asymmetry through degradation, endocytosis or a different mechanism is controversial (Bosch et al., 2014; Rodrigues-Campos and Thompson, 2014). Additionally, the palmitoyltransferase Approximated (App) is involved in regulation of D localization and activity by unknown mechanisms. *app* mutant flies are phenotypically similar to *d* mutants, displaying mild PCP defects and undergrowth, likely due to the function of App on D and finally Fat signaling (Matakatsu and Blair, 2008).

5.3.4 Fat genetically interacts with Ex

Fat might also signal through Ex. *ft* and *ex* mutant tissues are phenotypically similar. Besides similar overgrowth behavior, both *ft* and *ex* (but not *mer*) mutant tissue shows delayed cell cycle exit, manifesting as ectopic S-phase entry in *Drosophila* eye disc clones in normally postmitotic regions and increased CyclinE levels (Bennett and Harvey, 2006; Silva et al., 2006; Willecke et al., 2006; Pellock et al., 2007). Interestingly, loss of *ex* also causes PCP phenotypes in the eye, but a role of *ex* in PCP and a potential relationship with the Fat/Ds module is completely unexplored (Blaumueller and Mlodzik, 2000; Pellock et al., 2007). *ft* and *ex* further show similarities in the regulation of apoptosis: in the pupal retina, where a dramatic increase in interommatidial cells is seen in several Hippo pathway mutants, both loss of *ft* and loss of *ex* result in an only mild increase (Hamaratoglu et al., 2006). And while *ex* and *mer* are strongly genetically interacting in this tissue, *ft;ex* double mutants don't show obvious additive effects (Bennett and Harvey, 2006; Hamaratoglu et al., 2006). Interommatidial cell number is mainly regulated through apoptosis of supernumerary cells (Baker, 2001), which is strongly suppressed in *mer*, *hpo* or

wts mutants, likely caused by elevated expression of *diap1* (Hamaratoglu et al., 2006). Yet, specifically loss of *ft* or *ex*, despite their ability to regulate the Hippo pathway and *diap1* expression, don't dramatically affect interommatidial cell apoptosis, further suggesting they might function within the same pathway (Bennett and Harvey, 2006). Several studies have shown that Fat also regulates subcellular Ex localization. *ft* mutant clones exhibit a reduction of apical Ex, apparently caused by a shift to more basal regions. However, reduced Ex protein was reported by one group, suggesting that Ex might be destabilized without Fat (Bennett and Harvey, 2006; Cho et al., 2006; Silva et al., 2006; Willecke et al., 2006). Therefore, the regulation of Ex localization was proposed as a mechanistic link of Fat to Hippo signaling. However, Fat and Ex can also function in parallel pathways, as additive growth phenotypes were found in some double mutant tissues and *d* mutants suppressed the effect of loss of *ft* on Ex (Feng and Irvine, 2007). Possibly, these controversies can be explained by either tissue specific differences or the existence of distinct signaling sub-branches of Fat.

5.3.5 Ds regulates Hippo signaling independently and through Fat

Ds also regulates the Hippo pathway, both through its interaction with and regulation of Fat and through directly interacting with Hippo pathway regulators (Degoutin et al., 2013). Fat has been shown to read the steepness of the Ds gradient (thought to reflect the size of the tissue) and accordingly regulate growth, and sharp Ds boundaries result in ectopic growth (Rogulja et al., 2008; Willecke et al., 2008). This mechanism may explain why Fj also regulates Hippo signaling (Willecke et al., 2006). However, Ds gradient information does not seem to be critical for a function of Fat in Hippo signaling, as overexpression of a truncated Fat that lacks the extracellular domain (FatΔECD) and is unable to interact with Ds can rescue the overgrowth phenotypes of *ft* mutant discs almost entirely (Matakatsu and Blair, 2006). It has therefore been suggested that Ds induces Fat receptor clustering to promote its activation, which is mimicked by FatΔECD overexpression through increasing Fat abundance in the entire cell (Feng and Irvine, 2009). *ft* mutants also have a stronger overgrowth phenotype than *ds* mutants, and *ft*, *ds* double mutants have partially additive effects on growth, indicating that they both can also function independently from each

other. Accordingly, Ds was found to regulate the Hippo pathway through its intracellular domain (Matakatsu and Blair, 2006; Willecke et al., 2008). Ds can also interact with the WD40 protein Riquiqui, which associates with the kinase Minibrain that phosphorylates and inhibits Wts (Degoutin et al., 2013).

5.3.6 Fat is phosphorylated by the casein kinase Dco

The activity of Fat is further regulated by the casein kinase I Disc overgrown (Dco), which phosphorylates the Fat intracellular domain at several sites and leads to Fat activation (Feng and Irvine, 2009; Sopko et al., 2009; Pan et al., 2013). Phosphorylation of Fat is promoted upon interaction with Ds, while a specific *dco* mutant with dominant-negative properties, dco^{3}, exhibits reduced Fat phosphorylation and increased Yki-dependent growth (Cho et al., 2006; Feng and Irvine, 2009; Sopko et al., 2009). However, the molecular function of Fat phosphorylation and how phosphorylation influences Fat activity remains to be investigated. Dco is involved in multiple processes, such as the regulation of Wnt and Hedgehog pathways and in circadian rhythm (Price and Kalderon, 2002; Jia et al., 2005; Klein et al., 2006). This could explain why complete loss of function *dco* alleles fail to grow instead of showing overgrowth phenotypes (Zilian et al., 1999). Loss of *dco* also results in PCP phenotypes, but as Dsh is another target of Dco and its asymmetric localization depends on Dco phosphorylation, PCP phenotypes in *dco* mutants are thought to primarily result from Dsh deregulation, possibly in combination with reduced Fat activity (Klein et al., 2006; Strutt et al., 2006).

5.3.7 Lowfat, Ds and Fat reciprocally regulate their stability and localization

A common interactor of Fat and Ds is Lowfat (Lft), a conserved protein of unknown function. Lft was found to regulate Fat and Ds post-transcriptionally and stabilize both proteins at the subapical domain. Similarly, Fat and Ds promote Lft localization to the subapical region. *lft* mutants have very mild phenotypes qualitatively resembling those of *ft* and *ds* mutants in some aspects, including rounding of the adult wing. Only in the sensitized background of a

weak *ft* allele does additional loss of *lft* result in stronger phenotypes, including PCP defects (Mao et al., 2009). This suggests that Lft fine-tunes Fat/Ds signaling.

5.3.8 Functional domains of Fat

As Fat is involved in regulation of both PCP and Hippo signaling, structure-function approaches have aimed to distinguish which regions of Fat are responsible for its activity in growth and PCP (see also Fig. 5.4). As described above, both the Fat ICD and the Fat ECD contain the ability to regulate PCP independently from each other (Matakatsu and Blair, 2006; Pan et al., 2013). Fat lacking its ICD (FatΔICD) induces strong overgrowth phenotypes in both wildtype and *ft* mutant flies when overexpressed (Matakatsu and Blair, 2006). This suggests that FatΔICD acts in a dominant-negative fashion, potentially by inhibiting Ds *in trans*. Strikingly, overexpression of Fat lacking its ECD (FatΔECD) is able to rescue the lethality of *ft* mutants and the overgrowth phenotypes of *ft* mutant tissues to almost wildtype sizes (Matakatsu and Blair, 2006). Therefore, all or most Hippo pathway activity lies in the Fat ICD, which was further dissected in several follow-up studies. One structure-function approach was based on Fat ICD conservation between species. When compared to the ICD of the closest mammalian Fat homolog, Fat4, very limited homology is found, which occurs in form of six conserved clusters (region A-F). Regions A, B and C do not show obvious roles in Hippo or PCP signaling (Pan et al., 2013), however region B seems to be important for a function of Fat in mitochondria and regulation of larval metabolism (Sing et al., 2014). Deletion of region D shows wing overgrowth, indicating a role in Hippo signaling (Pan et al., 2013), likely due to its ability to interact with Fbxl7 (Bosch et al., 2014). It should be noted, however, that most of these experiments were performed in flies with a $ft^{fd}/ft^{G\text{-}rv}$ trans-heterozygous background. However, while $ft^{G\text{-}rv}$ is widely considered a null allele of *ft*, its molecular nature is based on complex rearrangements within the *ft* locus, and it is unclear if the disruption of the gene causes a true null allele. Indeed, $ft^{G\text{-}rv}$ behaves slightly differently than ft^{fd} in some contexts, such as establishing PCP in the eye (Sharma and McNeill, 2013) and regulating global metabolism through mitochondria (Yonit Tsatskis, *unpublished data*). Therefore, the establishment of novel *ft* null alleles, for example using the CRISPR/Cas9

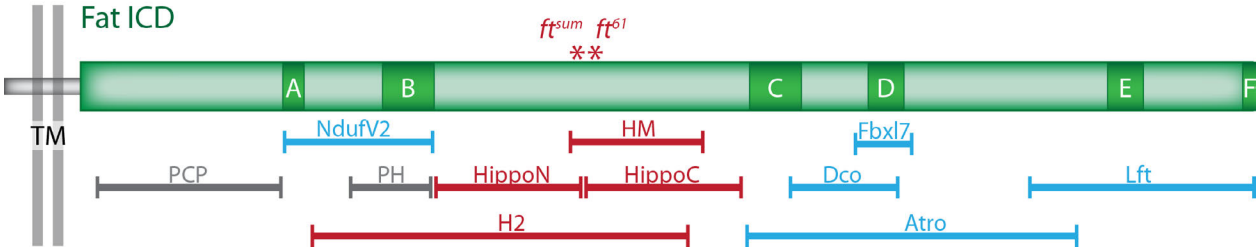

Fig 5.4 Functional domains of the Fat intracellular domain
Conserved regions A-F of Fat are shown as dark green boxes (as defined by (Pan et al., 2013)). Red regions were found to be important for Hippo signaling/growth control in different studies (HM: (Bossuyt et al., 2014); HippoN+HippoC: (Matakatsu and Blair, 2012); H2: (Zhao et al., 2013)). Point mutations ft^{sum} (Bossuyt et al., 2014) and ft^{61} (Bosch et al., 2014) specifically disrupt Hippo signaling. Blue regions indicate where Fat interactors have been mapped to interact with Fat. A juxtamembrane region important for PCP and a small region with PCP and Hippo activity (PH) are shown in grey.

system, might be required to fully explore the ability of different regions within Fat to rescue *ft* mutant phenotypes.

Three other studies that assessed different regions of the Fat ICD irrespective of conservation independently found overlapping regions to contain strong Hippo activity (domains HippoN, HippoC, HM and H2, see Fig. 5.4). Their consensus region lies between conserved regions B and C (Matakatsu and Blair, 2012; Zhao et al., 2013; Bossuyt et al., 2014). Two distinct point mutations within HippoC, ft^{sum} *and* ft^{61}, cause strong Hippo pathway defects but no PCP phenotypes, further emphasizing the importance of this region for growth control. Interestingly, none of the known Fat interactors were mapped to interact with this part of Fat, suggesting that the molecular partners relaying Fat signaling through this domain are yet to be identified (see also Fig. 4). A juxtamembrane-positioned region in the Fat ICD, as well as the C-terminal region "F", were found to exert PCP activity (Matakatsu and Blair, 2012; Pan et al., 2013). In summary, distinct separable domains within the Fat protein are responsible for its function in growth and PCP. The fact that some of these regions are conserved to mammalian Fat4 suggests that they might function similarly in other species.

5.4 Functions of Expanded

5.4.1 Ex links Crumbs to the Hippo pathway

Besides Fat, the apical polarity determinant Crumbs (Crb) can also regulate Ex localization (Chen et al., 2010; Grzeschik et al., 2010; Ling et al., 2010; Robinson et al., 2010). Crb is a homophilic cell adhesion molecule with critical roles in the establishment of apical-basal cell polarity (Tepass et al., 1990; Knust et al., 1993; Roper, 2012; Zou et al., 2012). Crb was also found to control growth through the Hippo pathway by regulating the apical localization of Ex. *crb* mutant tissue overgrows and exhibits increased Yki target gene expression (Chen et al., 2010; Grzeschik et al., 2010; Ling et al., 2010; Robinson et al., 2010). Crb directly interacts with Ex through a FERM binding motif (FBM) in its short intracellular domain (Chen et al., 2010; Grzeschik et al., 2010; Ling et al., 2010; Robinson et al., 2010). In cell culture studies, Crb recruits Ex to the plasma membrane where Ex is phosphorylated by an unknown kinase. The cause and exact function of Ex phosphorylation remains to be determined, but phosphorylation correlates with Ex degradation through the E3 ligase supernumerary limbs (Slmb), suggesting a tight regulation of Ex function and levels (Ling et al., 2010; Ribeiro et al., 2014; Zhang et al., 2015). In *Drosophila* larvae, *crb* mutant tissue shows loss of apically localized Ex and accumulation of basolateral (and apparently inactive) Ex, reminiscent of the Ex mislocalization observed in *ft* clones (Bennett and Harvey, 2006; Silva et al., 2006; Willecke et al., 2006; Chen et al., 2010; Grzeschik et al., 2010; Ling et al., 2010; Robinson et al., 2010). However, the relationship between Crb and Fat in Ex regulation remains unexplored.

5.4.2 Ex is involved in photoreceptor differentiation, endocytosis and F-actin regulation

Fully *ex* mutant eye discs show a strong defect in photoreceptor differentiation. Additional loss of *mer* enhances this phenotype, although loss of *mer* alone does not cause eye differentiation defects (Maitra et al., 2006; Pellock et al., 2007). This indicates that *ex* and *mer* have distinct functions but genetically interact in photoreceptor differentiation and eye field development. Other Hippo pathway

members don't exhibit similar eye development defects and also the fact that *ex* and *mer* mutants have different eye phenotypes cannot easily be explained by distinct signaling branches converging in Yki regulation. Therefore, *ex* and *mer* probably regulate other processes than Hippo signaling. In one study, a cooperative role of Ex and Mer in surface receptor endocytosis has been proposed, where Ex and Mer function to limit the abundance and signaling capacity of various receptors at the plasma membrane (Maitra et al., 2006). Ex and Mer were found associated with endocytic vesicle markers, and simultaneous loss of *ex* and *mer* resulted in reduced endocytosis of Notch from the cell surface and therefore increased Notch activity (McCartney and Fehon, 1996; Maitra et al., 2006). *ex, mer* double mutants were further found to have increased surface levels of Fat, EGFR, Smoothened and DE-Cadherin, which might explain the dramatic defects of *ex, mer* double mutant eyes (Maitra et al., 2006). However, a complicating matter in interpreting these data is the fact that the Hippo pathway through Yki regulates levels of apical membrane proteins, including Fat and EGFR (Hamaratoglu et al., 2009). Therefore, some of the observed effects in *ex, mer* double mutants are likely due to their function in canonical Hippo signaling. However, whether or how Yki regulates endocytosis has not been investigated and *ex, mer* double mutants have different phenotypes in the eye than mutants for other Hippo pathway members. Therefore, future studies will have to elucidate which functions of Ex and Mer require the core Hippo pathway and how they regulate receptor endocytosis.

Ex has also been shown to regulate apical filamentous actin (F-actin) levels. F-actin levels influence Hippo signaling and correlate with growth. Accordingly, loss of negative regulators of F-actin, such as capping proteins (CP), promotes Yki activity, while loss of positive regulators or chemical destabilization of F-actin inhibits Yki. In turn, the Hippo pathway, including Ex, was found to negatively affect apical F-actin levels (Fang and Adler, 2010; Fernandez et al., 2011; Sansores-Garcia et al., 2011). As different reports have shown that Yki is not always required for F-actin level regulation by Hippo pathway members, it is unclear if the relationship between Hippo/Yki and F-actin forms a feedback loop (Fang and Adler, 2010; Fernandez et al., 2011; Sansores-Garcia et al., 2011).

Finally, a recent report suggests that Ex functions to regulate F-actin and Yki regulation in a way that is independent of core Hippo signaling and Wts-mediated phosphorylation (Gaspar et al., 2015). In this study, the LIM-domain protein Zyxin (Zyx), which promotes actin polymerization through Ena/VASP proteins, was found to strongly antagonize Ex function. *zyx* mutants have undergrowth phenotypes and *zyx ,ex* double mutants significantly rescue *ex* mutant phenotypes, such as interommatidial cell number, growth and photoreceptor differentiation. As loss of *zyx* only has minor effects on *ft*, *hpo* and *wts* mutant phenotypes, Zyx was proposed to function in a parallel Ex signaling path, largely independent of the core Hippo pathway. As a model, the authors suggest that Zyx and Ex have reciprocal effects on F-actin, which ultimately results in Yki regulation (Gaspar et al., 2015). Additional research is required to answer how these findings can be integrated into a cohesive model of how the actin cytoskeleton and the Hippo pathway interact. It will also be important to reconcile these data with previously established roles of Ex.

6 Abstract Chapter A

Although many facets of Hippo signaling have been elucidated in recent years, its upstream regulators remain at best partially understood. Fat is one of the few cell surface proteins known to regulate the Hippo pathway, but exactly how it connects to and which kind of signal it conveys to the core kinase cascade remain open questions. Ex is a possible direct link between Fat and Hpo and could further interconnect Fat and Crb signaling with regards to growth control. Yet, as summarized here, the function of Ex in the Hippo pathway is complicated and its roles in other processes are poorly studied. In the following chapter, I have therefore further analyzed the relationship between Fat and Ex to answer if they interact to relay Fat signaling. I have also addressed if Fat signaling is involved in Ex phosphorylation and I have identified putative novel Ex interactors to better understand Ex signaling in the future.

7 Results Chapter A

7.1 Analysis of an interaction between Fat and Ex

7.1.1 Expanded as a potential mediator of Fat signaling

While it has been well established that *Drosophila* Fat functions in regulation of the Hippo pathway, the direct mediators relaying Fat signaling from the cell surface to the core Hippo pathway are unknown. The findings that *expanded* (*ex*) is epistatic to *fat* (*ft*) in the *Drosophila* pupal retina (Willecke et al., 2006) and that Ex subcellular localization is regulated by Fat in larval epithelia (Bennett and Harvey, 2006; Silva et al., 2006; Willecke et al., 2006) prompted us to test for physical interactions between Fat and Ex.

Fat is an extremely large protein with a molecular weight of 560kDa, but a Fat construct lacking the majority of the extracellular domain (ECD), FatΔECD, is able to rescue growth defects of *fat* mutant fly tissue to almost wild-type levels. This indicates that the intracellular domain (ICD) of Fat is crucial for growth control (Matakatsu and Blair, 2006). Interestingly, the ICD of Fat needs to be membrane tethered to function, since the ICD alone is not able to rescue (Matakatsu and Blair, 2012). Accordingly, I have used FatΔECD for most biochemical experiments due to its more manageable size.

I based my studies on preliminary results from a former postdoc, Dr. Ankush Garg, who had shown co-immunoprecipitation of Fat and Ex in cell culture. When overexpressed in HEK293 cells, full-length Ex, as well as the Ex FERM-domain (ExFERM) strongly bound FatΔECD. In contrast, the Ex C-terminal and linker domains were unable to interact with FatΔECD (Dr. Ankush Garg, *unpublished results*).

Dr. Garg had tested the Fat intracellular domain broadly for its ability to co-immunoprecipitate ExFERM. He had found that deleting the last 245 amino acids (aa) of FatΔECD did not affect the ExFERM binding, however deletion of bigger C-terminal regions resulted in a loss of the ExFERM interaction. He had also

generated a few FatΔECD constructs with substantial internal deletions, lacking the region around aa 245. Surprisingly, these constructs were still able to co-immunoprecipitate ExFERM, suggesting that more than one site within FatΔECD was important for the interaction with Ex.

I adopted an unambiguous nomenclature to name FatΔECD constructs, counted from the C-terminus of Fat (noted by a "c" in front of each construct). C-terminal deletions were named "cΔ" followed by the amino acid marking the start of the deletion. Internal deletions were denoted by the positions of the deleted amino acids, counted from the C-terminus (e.g. cΔ24-64 representing a deletion ranging from C-terminal residue 24 to C-terminal residue 64). A graphical illustration of deletion constructs is shown in Fig. 7.6.

I confirmed Dr. Garg's initial findings and observed a very robust interaction between FatΔECD and full-length Ex or ExFERM, both in HEK293T cells and *Drosophila* S2 cells (see Fig. 7.1; Fig. 7.7). I found that cΔ245 still bound Ex with full strength but that constructs shorter than cΔ245 by only 10aa (cΔ255) or all bigger C-terminal deletions (cΔ260, cΔ265, cΔ270, cΔ275, cΔ285, cΔ310, cΔ444, cΔ492) were unable to interact with ExFERM (Fig. 7.1; Fig. 7.2; Fig. 7.6). This suggested that the N-terminal half of FatΔECD is not important for Ex binding and that a domain required for Ex interaction (referred to as Ex binding region or EBR) exists in the region of aa 245 and aa 265.

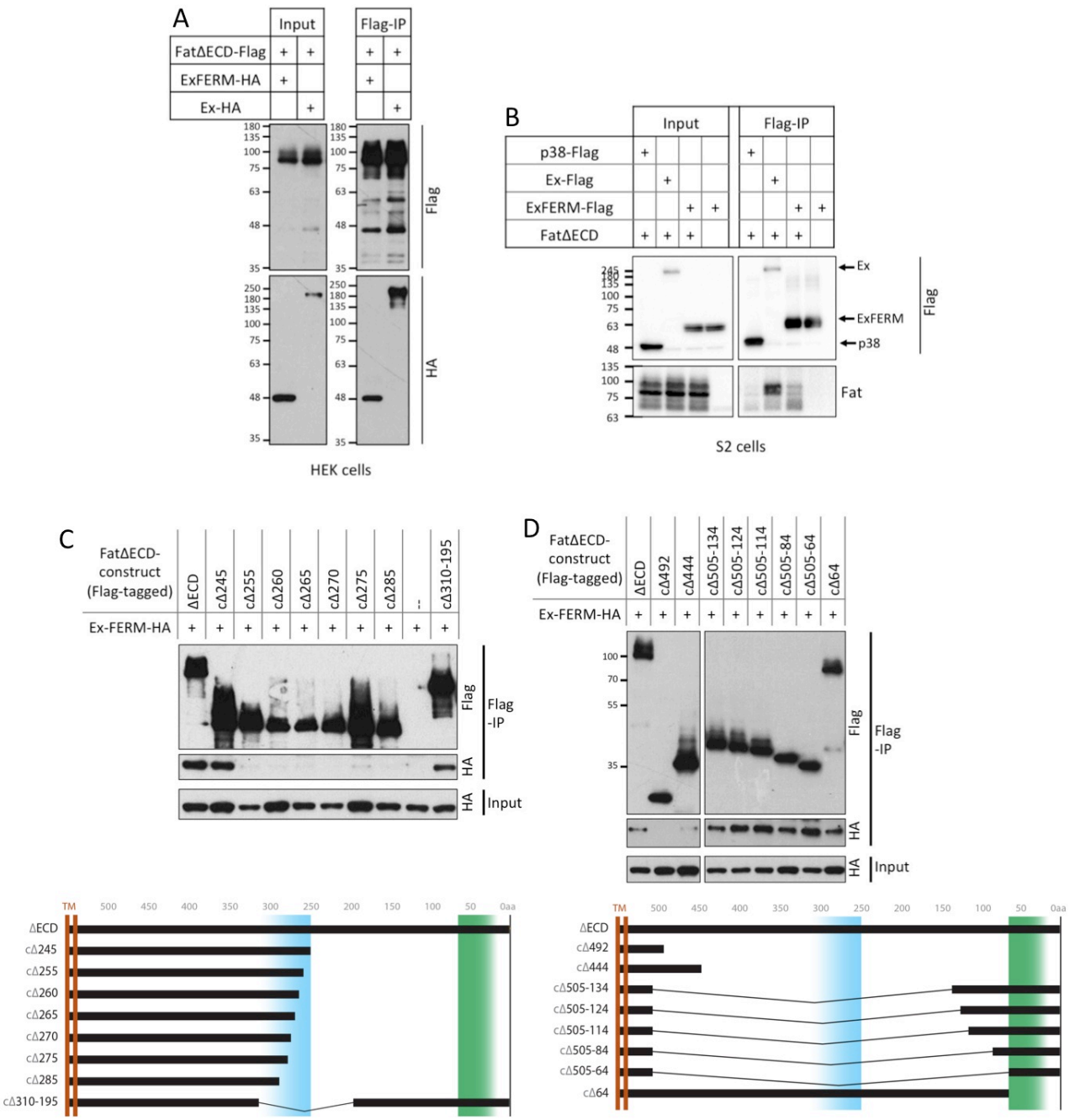

Fig 7.1 FatΔECD interacts with Ex

FatΔECD co-immunoprecipitates with full-length Ex and the Ex FERM-domain, but not with p38 (unrelated control) in HEK293T (A) and S2 cells (B). (C), (D): Co-IPs (HEK293T cells) of FatΔECD deletion constructs with ExFERM indicate two distinct ExFERM binding regions, one in the medial Fat ICD (C) and a second within the last 64aa (D). Schematics of FatΔECD deletion constructs are depicted, with EBR1 in blue and EBR2 in green.

7.1.2 Defining Expanded binding regions within the Fat intracellular domain

Interestingly, FatΔECD deletion constructs containing the transmembrane region as well as different parts of the far C-terminus still strongly pulled down ExFERM in all experiments (e.g. internal deletion constructs cΔ310-195; cΔ505-134), confirming initial findings of two independent EBRs (Fig. 7.1C,D; Fig. 7.6). These internal deletion constructs could contain as little as the last 64 aa of the Fat C-terminus and had equal binding strength as full-length FatΔECD (Fig. 7.1D). Deleting the last 64 aa in a wildtype FatΔECD did not affect the interaction with ExFERM, emphasizing that remaining binding regions are sufficient to mediate Ex binding (Fig. 7.1D).

I then tried to narrow down the C-terminal EBR further, in the background of a construct lacking the other EBR, cΔ444-154. Deleting the last 24 aa within construct cΔ444-154 (= construct cΔ444-154;cΔ24) did not affect its ExFERM binding strength, however deleting the last 44aa (= construct cΔ444-154;cΔ44) reduced binding (Fig. 7.2A). This suggested that the second EBR (EBR2) lies between C-terminal residue 24 and 64.

I also deleted the last 64aa in cΔ444-154 (= construct cΔ444-154;cΔ64), which showed variably reduced binding to ExFERM, ranging from weak to undetectable co-immunoprecipitation (Fig. 7.2B; Fig. 7.3B,C). This further strengthened that the last 64 aa comprise the second EBR, and that ExFERM binding is only lost when both EBRs are deleted. Yet, due to the remaining weak ExFERM interaction of this construct, it could not be fully excluded that other regions of FatΔECD were involved in Ex binding. It should be noted, that cΔ444-154;cΔ64 and full-length Ex repeatedly failed to co-immunoprecipitate (Fig. 7.3B). This could indicate that in this assay, full-length Ex is more sensitive to the loss of EBRs, further suggesting that these are indeed major regions required for interaction.

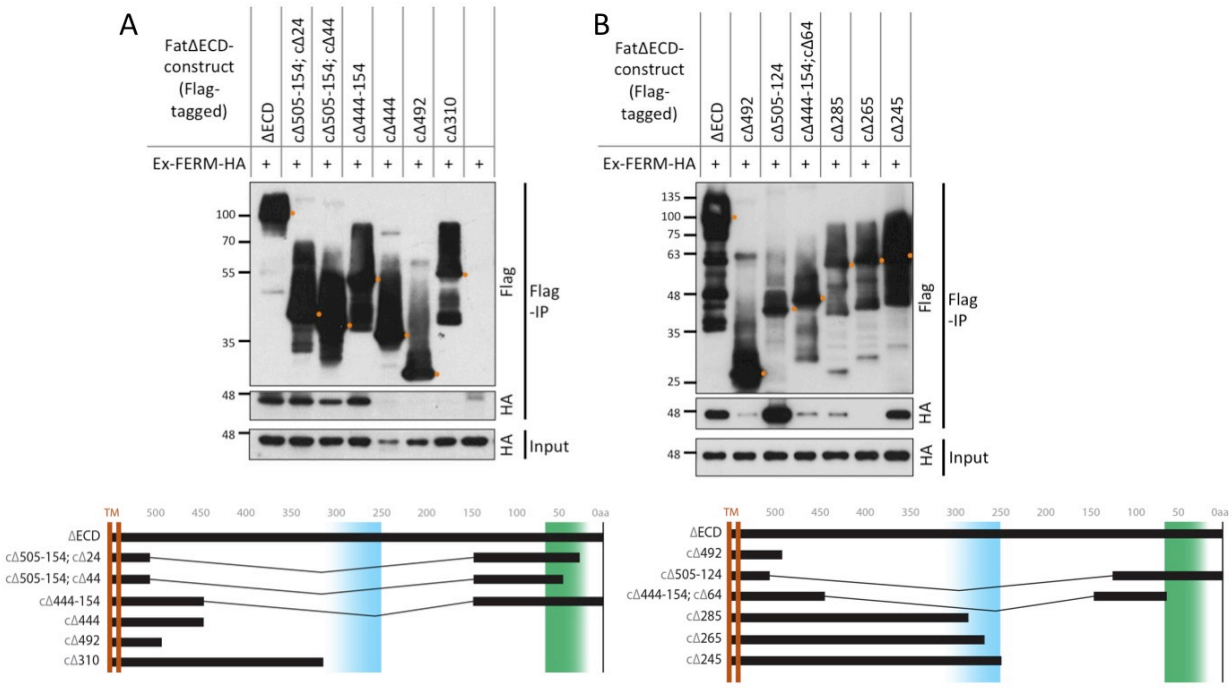

Fig 7.2 Fat contains two distinct EBRs
(A) Deletion of the C-terminal 24aa of FatΔECD doesn't affect ExFERM binding. (B) A large internal deletion combined with loss of the C-terminal 64aa of FatΔECD (cΔ444-154;cΔ64) loses ExFERM binding (HEK239T cells). Schematics of FatΔECD deletion constructs are depicted, with EBR1 in blue and EBR2 in green.

A complicating matter in systematically testing different regions of the Fat intracellular domain was that Fat-ICD, a Fat construct containing the ICD without the transmembrane domain, showed much weaker binding of Ex than FatΔECD (data not shown). A similar observation was made for the interaction between Fat and Dco, which relied on membrane-tethered Fat constructs such as FatΔECD (Sopko et al., 2009). A possible explanation is a difference in sub-cellular localization between FatΔECD and Fat-ICD, as Fat-ICD shows a cytoplasmic and nuclear localization (Yonit Tsatskis, *unpublished data*). This highlighted the necessity to membrane-tether Fat constructs to assess their Ex binding capacity.

Therefore, to further test the requirement of EBR2 in the Fat C-terminus, I generated a construct spanning the last 124aa of Fat and tagged it N-terminally with a myristoylation signal sequence for membrane tethering (construct Myr-

c124). Myr-c124 was sufficient to co-immunoprecipitate Ex and ExFERM, although the interactions were weaker than with FatΔECD (Fig. 7.3A,B). To test if the observed binding capacity was due to EBR2, I then deleted 40 amino acids containing the putative EBR2 (= aa24-64) within Myr-c124, creating Myr-c124;ΔEBR2. Indeed, Myr-c124;ΔEBR2 lost the ability to bind Ex and ExFERM, illustrating that EBR2 is necessary for Ex binding in this context (Fig. 7.3A,B).

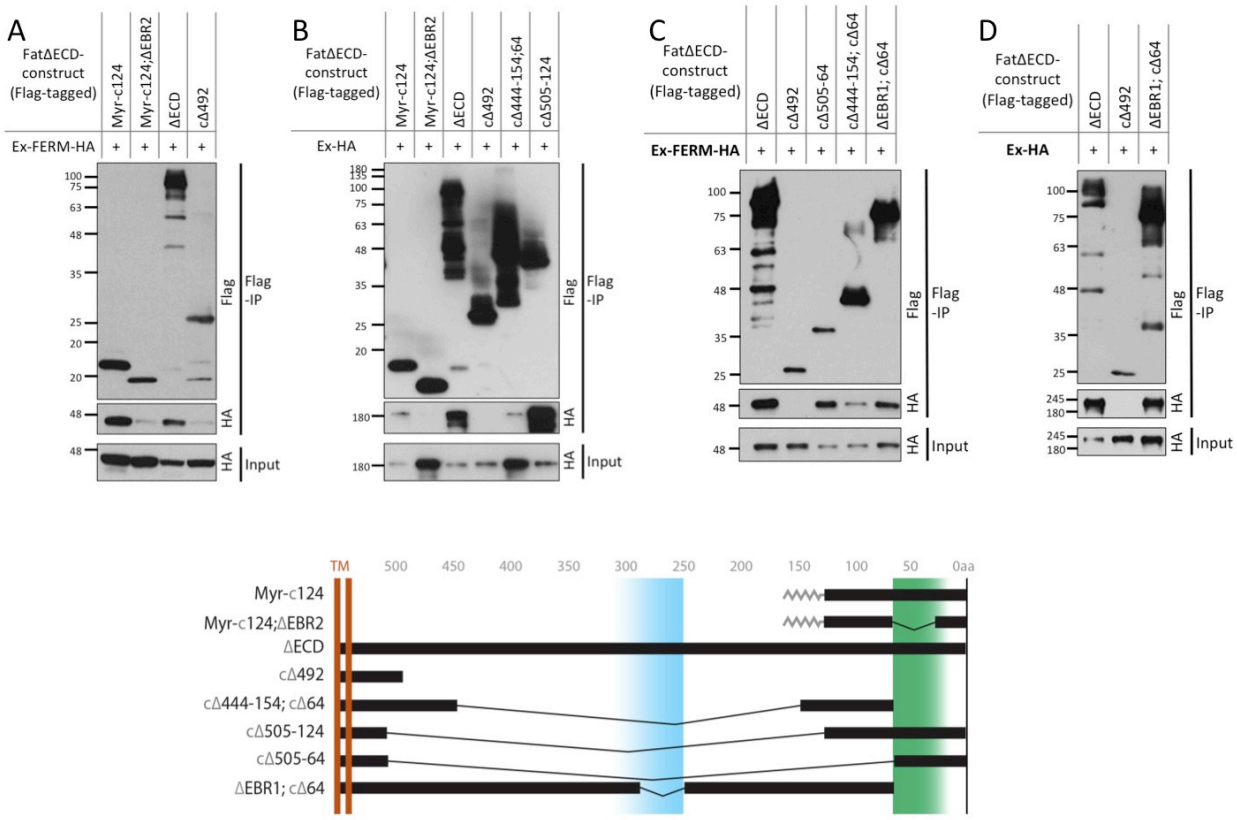

Fig 7.3 Deletion constructs to test requirements of EBRs
The short C-terminal Fat-ICD construct Myr-c124 co-immunoprecipitates ExFERM (A) and Ex (B), unless EBR2 is deleted. While the large Fat4ΔECD deletion construct cΔ444-154;cΔ64 loses most ExFERM (C) and Ex (B) binding capacity, deleting EBR1 and the EBR2 region does not abolish ExFERM (C) or Ex (D) interaction. All co-IPs performed in HEK293T cells.

In order to test if co-ablation of both EBRs would result in loss of the interaction with Ex, I generated FatΔECD constructs with clean double deletions of the EBRs. I defined EBR1 generously as aa245-285 and EBR2 as aa24-64. Surprisingly, neither construct ΔEBR1;ΔEBR2 nor ΔEBR1;cΔ64 showed a loss or reduction of

Ex binding (Fig. 7.3C,D; Fig. 7.5), suggesting that not all regions with Ex binding capacity had been deleted.

At this point I can only speculate about potential reasons. There could be a third EBR that I have not discovered or the EBR1 boundaries were defined too narrowly. Indeed, none of the tested deletion constructs unambiguously addressed the region between aa 154 and aa 245 of FatΔECD. The detection of a third EBR in this region would have been obscured by the fact that all the constructs used to screen for Ex binding sites and which affected this region, still contained one of the other EBRs as well (Fig. 7.5). A Fat construct containing aa 154-245 with a myristoylation signal sequence for membrane tethering could help exploring this option and remains to be tested in the future. A similar strategy could address if the EBR1 boundaries need to be repositioned.

7.1.3 EBR1 and EBR2 coincide with known functional and conserved regions of Fat

The Fat intracellular domain lacks typical domains, which makes it challenging to perform classical structure-function-type analyses. However, from sequence alignments of *Drosophila* Fat with its insect and vertebrate orthologs, several conserved regions become apparent, suggesting that these could harbor functional relevance across species (Pan et al., 2013; Bossuyt et al., 2014)(Fig. 7.4A). In the last few years, it was further established that distinct regions in the Fat intracellular domain are required for Hippo and PCP signaling (Matakatsu and Blair, 2012; Pan et al., 2013; Zhao et al., 2013; Bossuyt et al., 2014). Two adjacent regions were found harboring Hippo activity, HippoN and HippoC. While these are poorly conserved to mammalian Fat homologs, they are highly conserved within insect species (Matakatsu and Blair, 2012).

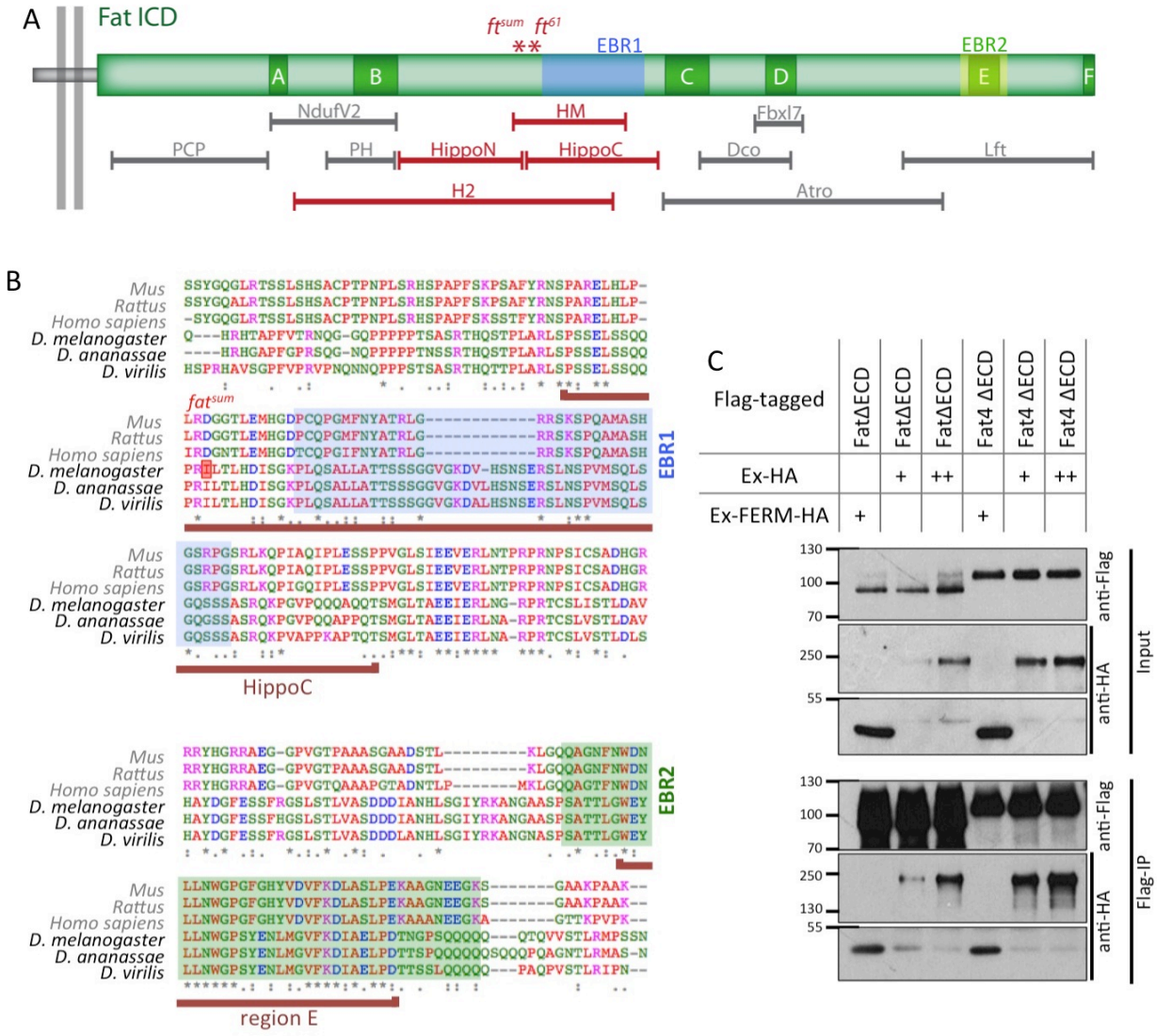

Fig 7.4 EBRs in relation to Fat functional domains and conserved regions
(A) Overview of Fat functional domains. Dark green boxes mark regions conserved to mammals. EBR1 co-incides with the HM, H2 and HippoC domains, which were independently reported to be important for Hippo pathway regulation. EBR2 co-incides with the conserved region E. (B) Clustal Omega alignment of Fat cadherins of the *Drosophila* species *melanogaster*, *ananassae* and *virilis* and the mammals *Mus musculus (Mus), Rattus norvegicus (Rattus)* and *Homo sapiens*. Conserved residues are marked with an asterisk, the residue mutated in *fat*^{sum} flies is marked in red. (C) Fat4ΔECD (*Mus musculus*) co-immunoprecipitates Ex and ExFERM with similar strength as FatΔECD in HEK293T cells.

Intriguingly, EBR1 lies within and covers a large part of HippoC. If HippoC indeed comprises a criticial binding site important for Ex regulation, this could explain the Hippo pathway activity of the HippoC region. EBR2 further encompasses homology region E (as defined in (Pan et al., 2013)), suggesting potential conservation of Fat-Ex binding to mammals (Fig. 7.4B).

I therefore tested if the Fat homolog Fat4 retained the ability to bind Ex, by performing pulldowns of mouse Fat4ΔECD in HEK293T cells transfected with either *Drosophila* Ex or ExFERM. Indeed, Fat4ΔECD strongly interacted with Ex and ExFERM, suggesting functional conservation of at least one EBR in Fat4 (Fig 7.4C).

Within HippoC, a single point mutation, Fat^{sum} ("Fat super-size me"), can completely disrupt the Hippo signaling capacity of Fat without affecting PCP (Bossuyt et al., 2014). This point mutation lies around 10aa N-terminally of EBR1, prompting me to test if it affected the interaction with Ex. I introduced the Fat^{sum} mutation into the background of full-length FatΔECD and the ΔEBR1 and ΔEBR1;ΔEBR2 constructs, but found no significant changes in ExFERM binding strengths (Fig. 7.5). This indicates that the effect of the Fat^{sum} mutation on Hippo signaling is not due to loss of Ex binding.

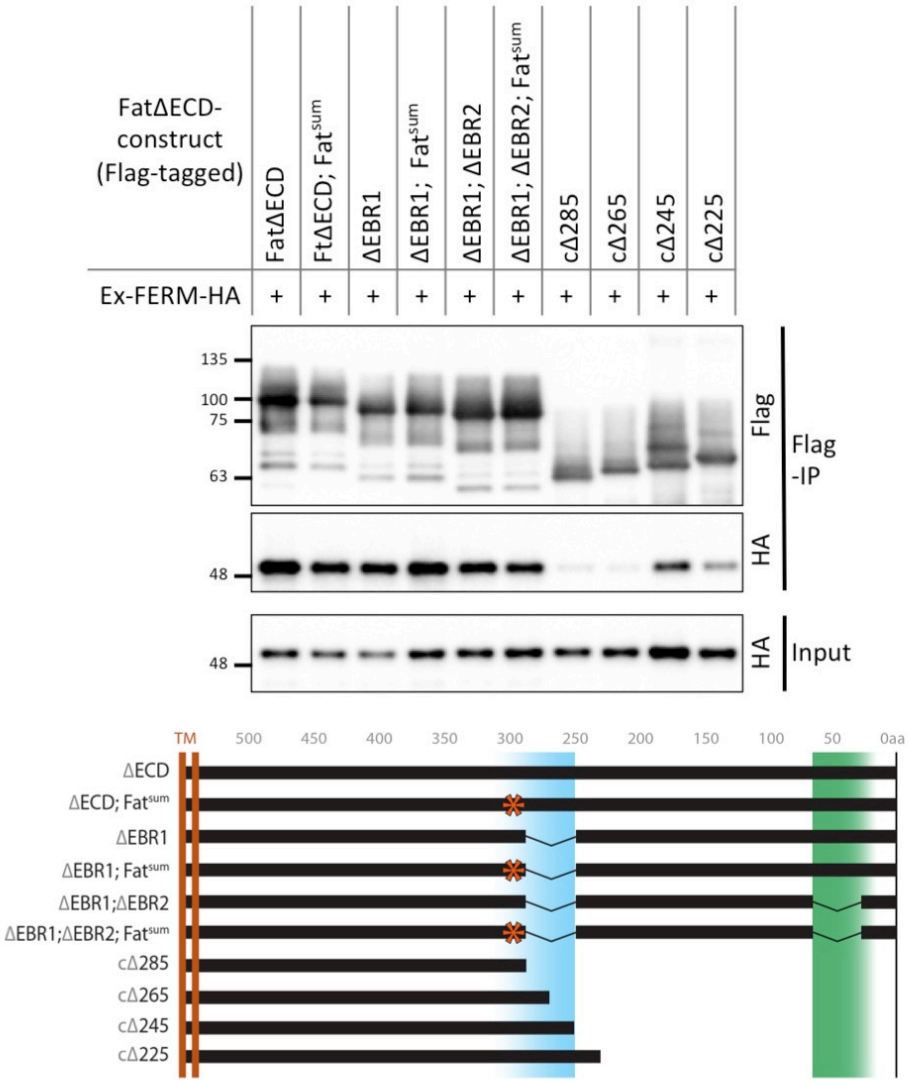

Fig 7.5 The Fat^{sum} mutation does not affect the interaction of FatΔECD and ExFERM
The Fat^{sum} mutation (Ile 4852 to Asn) is marked by an asterisk in the Fat deletion construct schematic. Binding of FatΔECD to ExFERM is not affected by Fat^{sum} mutation and individual or simultaneous deletion of EBR1 and EBR2, indicating other regions can also mediate the interaction with Ex (HEK293T cells).

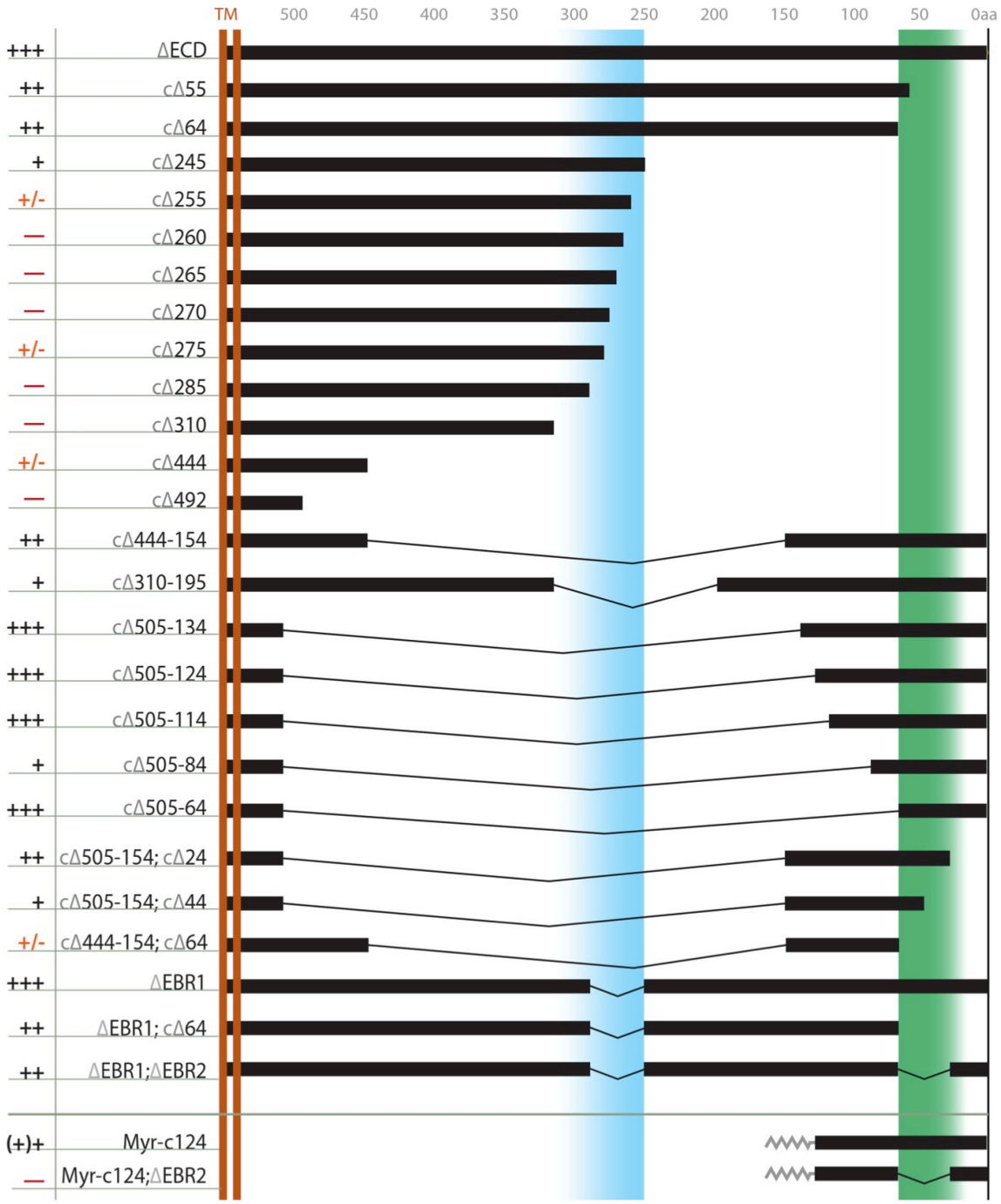

Fig 7.6 Summary of Fat-ExFERM co-IP experiments
Schematic illustration of FatΔECD deletion constructs (transmembrane domain on the left, C-terminus on the right) and their ability to bind the FERM-domain of Ex in HEK293T cells. Rating of binding strength averaged over all experiments: +++ wildtype binding; ++ strong binding; + weak binding; +/- weak inconsistent binding; - no binding. Blue shaded region indicates EBR1, green shaded region indicates EBR2. Scale on top indicates amino acids counted from the C-terminus.

7.1.4 FatΔECD binds several FERM-domain proteins

I next asked how specific the Fat-Ex interaction was and whether other FERM-domain proteins could interact with Fat. Merlin (Mer) is a related FERM-domain protein found in complex with Ex, but unlike *ex*, *mer* was not found to genetically interact with *ft* (Hamaratoglu et al., 2006). Surprisingly, I found both the Mer FERM-domain (MerFERM) as well as the full-length protein strongly interacting with FatΔECD in co-immunoprecipiation experiments, both in HEK293T and S2 cells (Fig. 7.7). MerFERM interacted with Fat deletion constructs in a similar pattern as ExFERM, suggesting they bind similar regions of Fat (Fig. 7.7C,D). I also tested if Ex and Mer compete for FatΔECD binding, but co-expression of Ex and Mer or ExFERM and MerFERM resulted in strong, potentially even enhanced binding to FatΔECD (Fig. 7.8A). As Ex and Mer also interact with each other (Fig. 7.7D)(McCartney et al., 2000), it is possible that Fat, Ex and Mer form a complex.

Lastly, to address if Fat was a more general FERM-domain interactor, I further tested for an interaction with the FERM-domain protein Pez, a protein involved in Hippo pathway regulation in the *Drosophila* midgut (Poernbacher et al., 2012). I also tested the WW-domain protein Kibra, an interactor of Ex, Mer and Pez (Genevet et al., 2010; Yu et al., 2010; Poernbacher et al., 2012). Preliminary results showed both Pez and Kibra co-immunoprecipitating with FatΔECD, however the interaction with Kibra was weaker than with Pez, Ex or Mer, suggesting preferential binding of FERM-domain proteins (Fig. 7.8A).

While these results hint at a broader function of Fat, possibly recruiting or concentrating several Hippo regulating factors in a cell, I would suggest to include more controls and test unrelated proteins before confidently stating such a hypothesis. There is evidence that Fat and Ex genetically interact *in vivo*, therefore a physical interaction of the two is a plausible scenario. However, while overexpression and cell culture systems can be useful tools to study protein interactions, they bear a high risk of generating artifacts.

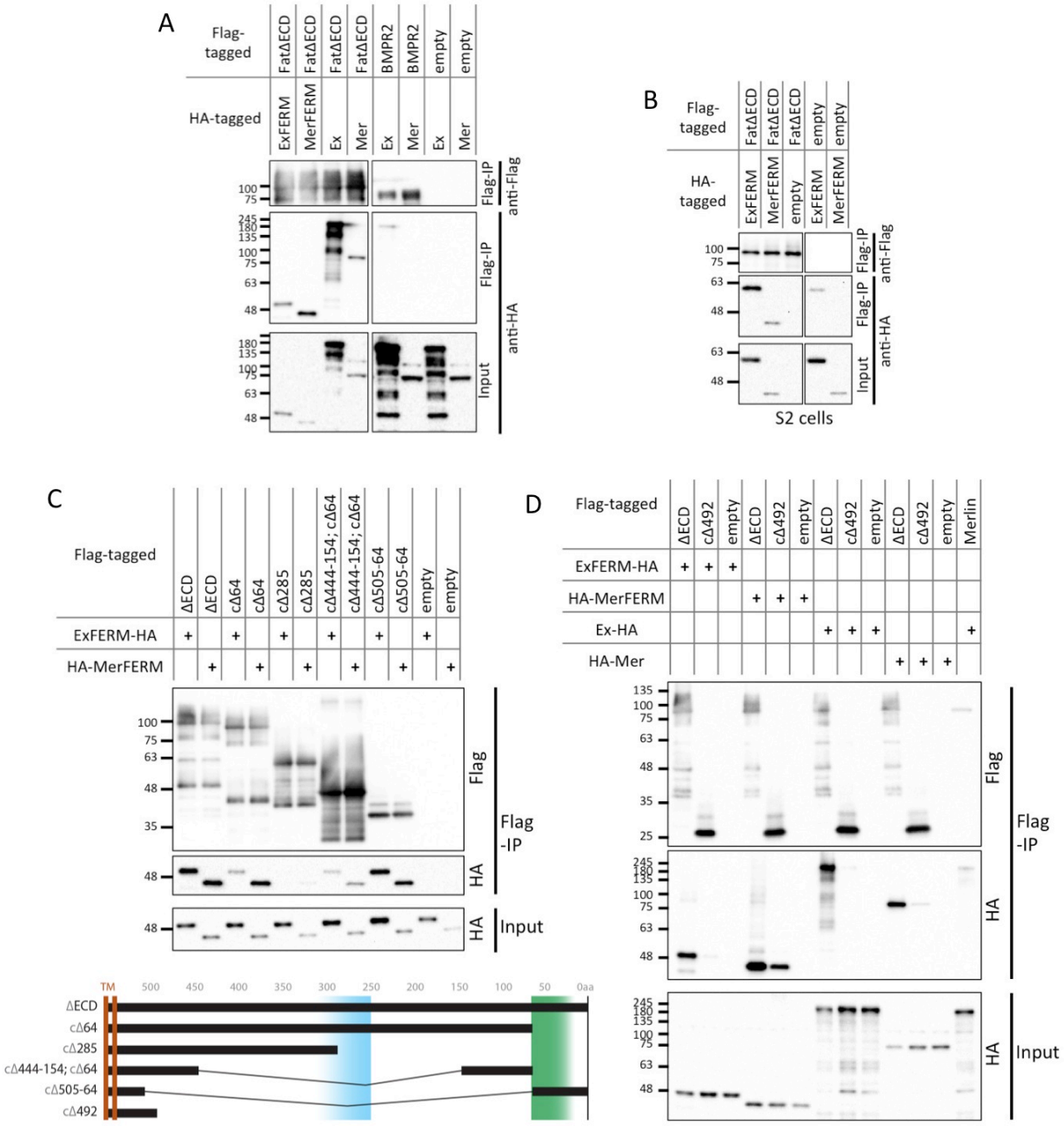

Fig 7.7 Fat interacts with Ex and Mer through similar regions
FatΔECD co-immunoprecipitates Ex and Mer in HEK293T cells (A) and S2 cells (B). Fat deletion analysis (HEK293T cells) indicates that Ex and Mer interact with the same regions of FatΔECD through their FERM domains (C, D).

As interactions detected in co-IPs provide no information about whether two proteins bind directly or indirectly (meaning through other common interactors), I tested the Fat-Ex interaction *in vitro*. I purified His-tagged ExFERM and GST-tagged FatICD on resin. However, while the positive control Atrophin-His strongly bound to FatICD-GST but not GST alone, ExFERM non-specifically bound to both (Fig. 7.8B). Increase of salt concentrations during the pulldown resulted in complete loss of ExFERM binding but might have interfered with binding in general. Therefore, it remains unknown if Fat and Ex bind directly.

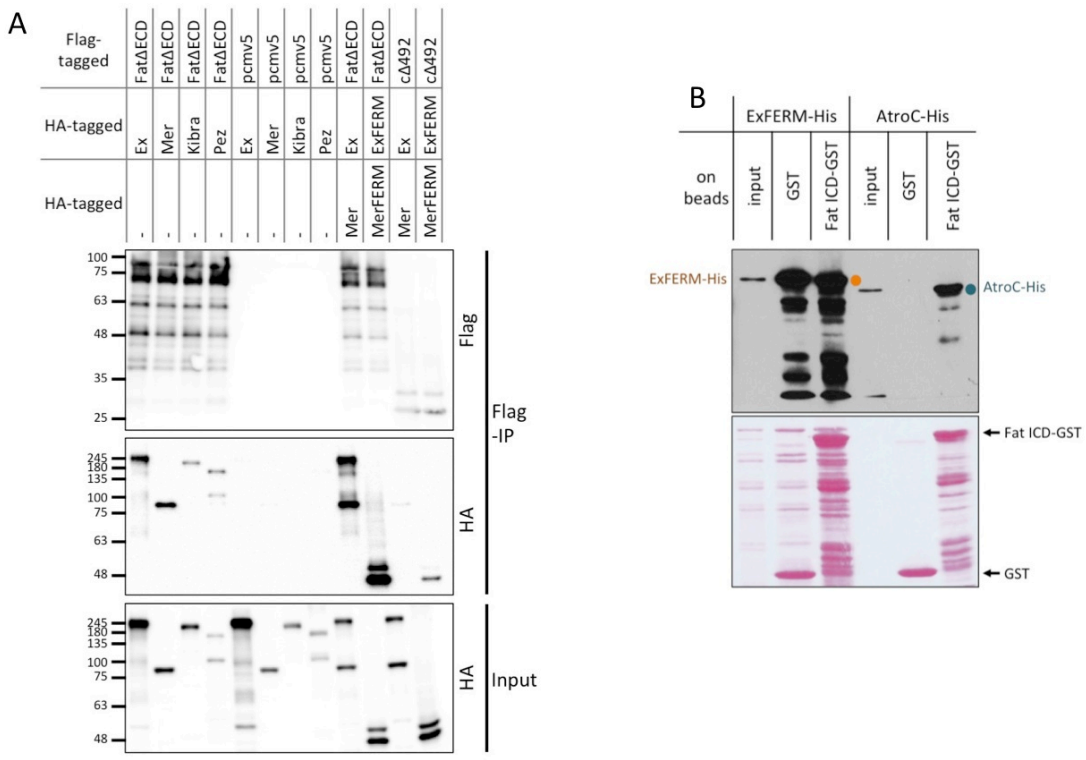

Fig 7.8 Ex and Mer do not compete for Fat interaction
(A) The FERM-domain proteins Ex, Mer and Pez and the WW-domain protein Kibra (weaker) bind FatΔECD. When co-expressed, similar levels of Mer and Ex are co-immunoprecipitated with FatΔECD, indicating they are not competing for binding. The same is found with both FERM domains. (B) *In vitro* GST-pulldown of bacterially purified Fat ICD and ExFERM. While the positive control AtroC (C-terminal domain) interacts with FatICD-GST but not with plain GST, ExFERM non-specifically binds to the GST beads. Whether ExFERM interacts directly with Fat remains unknown.

7.1.5 Characterization of the Fat-Expanded interaction *in vivo*

To switch to a less artificial system, I attempted to verify the Fat-Ex interaction in semi-endogenous and endogenous co-IP experiments in S2 cells and *Drosophila* larval tissue. Unfortunately the available Ex antibodies showed poor sensitivity to endogenous protein on Western blots and it remained inconclusive if endogenous Fat and Ex can interact.

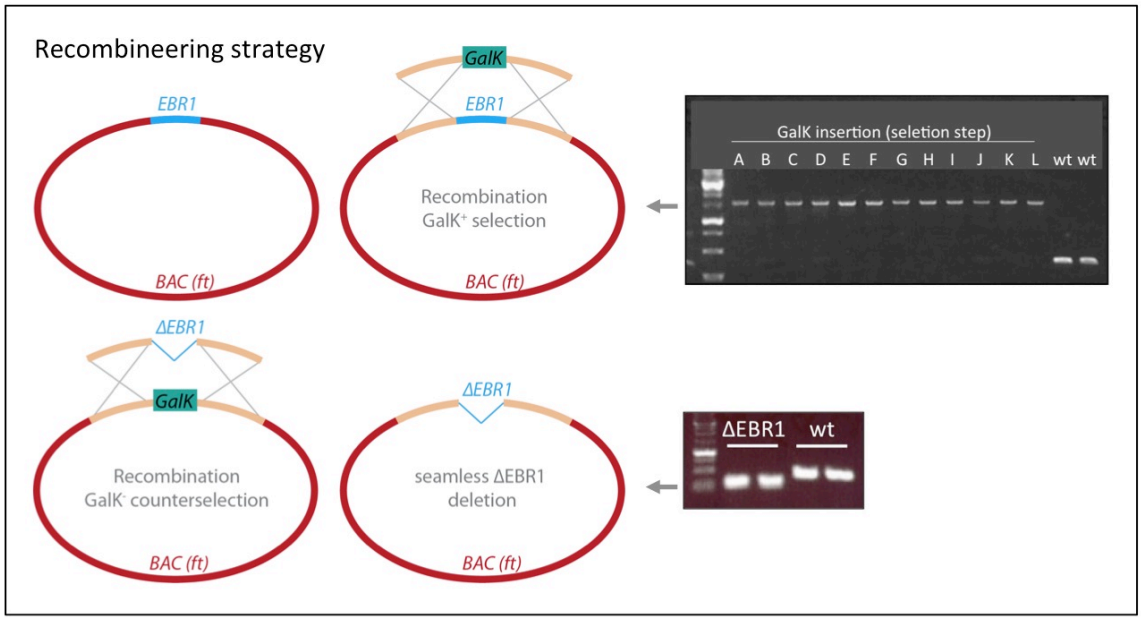

Fig 7.9 Recombineering-mediated deletion of EBR1
Recombineering strategy involves two consecutive recombination steps to seamlessly delete the EBR1-coding region within the *ft* gene in aBAC (bacterial artificial chromosome). In a first step, the EBR1-coding region is replaced with a GalK cassette by homologous recombination. PCR-screening after GalK-selection shows several positive bacterial colonies. In a second step, the GalK cassette is replaced by a EBR1-deletion construct by homologous recombination. After GalK counterselection, two ΔEBR1-positive colonies were found by PCR screening and confirmed by Sanger sequencing.

The critical test of the proposed Fat-Ex interaction through distinct regions is to create flies expressing Fat lacking all EBRs. Therefore, while I was characterizing EBRs, I used recombineering to introduce a deletion of the EBR1-coding region into the *ft*-containing BAC BACR11D14 as a first step toward creating a FatΔEBR1;ΔEBR2 expressing fly (Fig. 7.9). However, because the FatΔECD ΔEBR1;ΔEBR2 double deletion construct failed to abolish Ex binding, I paused

the recombineering approach at that point. For a meaningful *in vivo* investigation, a better understanding of the regions of Fat essential for Ex interaction is required. In the future, deletions of the EBRs in the endogenous *ft* locus should be generated and tested, which became possible with the discovery and wide implementation of the CRISPR/Cas9 genome editing technique.

In case that deletion of one or two EBRs would only result in a partial loss of Ex binding strength, I wondered if a partial defect of Ex localization would be detectable in imaginal discs. I therefore evaluated the phenotypic range of Ex mislocalization that is caused by loss of *ft* in somatic clones induced by heat-shock-controlled Flipase recombination (FLP/FRT). In found that in ft^{fd} and $ft^{G\text{-rv}}$ clones in wing and eye discs the Ex mislocalization is extremely subtle and not always detectable. More pronounced examples are shown in Fig 7.10. Interestingly, Ex shifting coincided with a slight increase and similar basal shift of Crb. Therefore, I cannot exclude that a change in cell morphology or junctional position causes the visual difference of Ex inside *ft* clones. *ft* clones have been shown to be apically constricted (Jaiswal et al., 2006), which might affect spatial organization of proteins at the apical and subapical membrane. However, as other reports have shown dramatic changes in Ex localization (for example (Bennett and Harvey, 2006)), possibly technical differences or a different genetic background are responsible for the discrepancy. A more robust testing system will be required to address whether loss of EBRs in Fat causes subtle changes in Ex localization *in vivo*.

In summary, Fat and Ex are able to interact directly or indirectly in cell culture through distinct domains in the Fat ICD. The overlap of one of the EBRs with a functional region that contains Hippo signaling activity is in agreement with a role for Ex in transducing Fat signaling to the Hippo pathway. However, a more in-depth analysis of the requirement of Ex for Fat signaling in cells and flies is needed to draw final conclusions. Also the functional relationship between Fat and Mer or Kibra is currently unclear, but it is conceivable that a large Hippo regulatory complex formed by these factors exists at the subapical domain of epithelial cells.

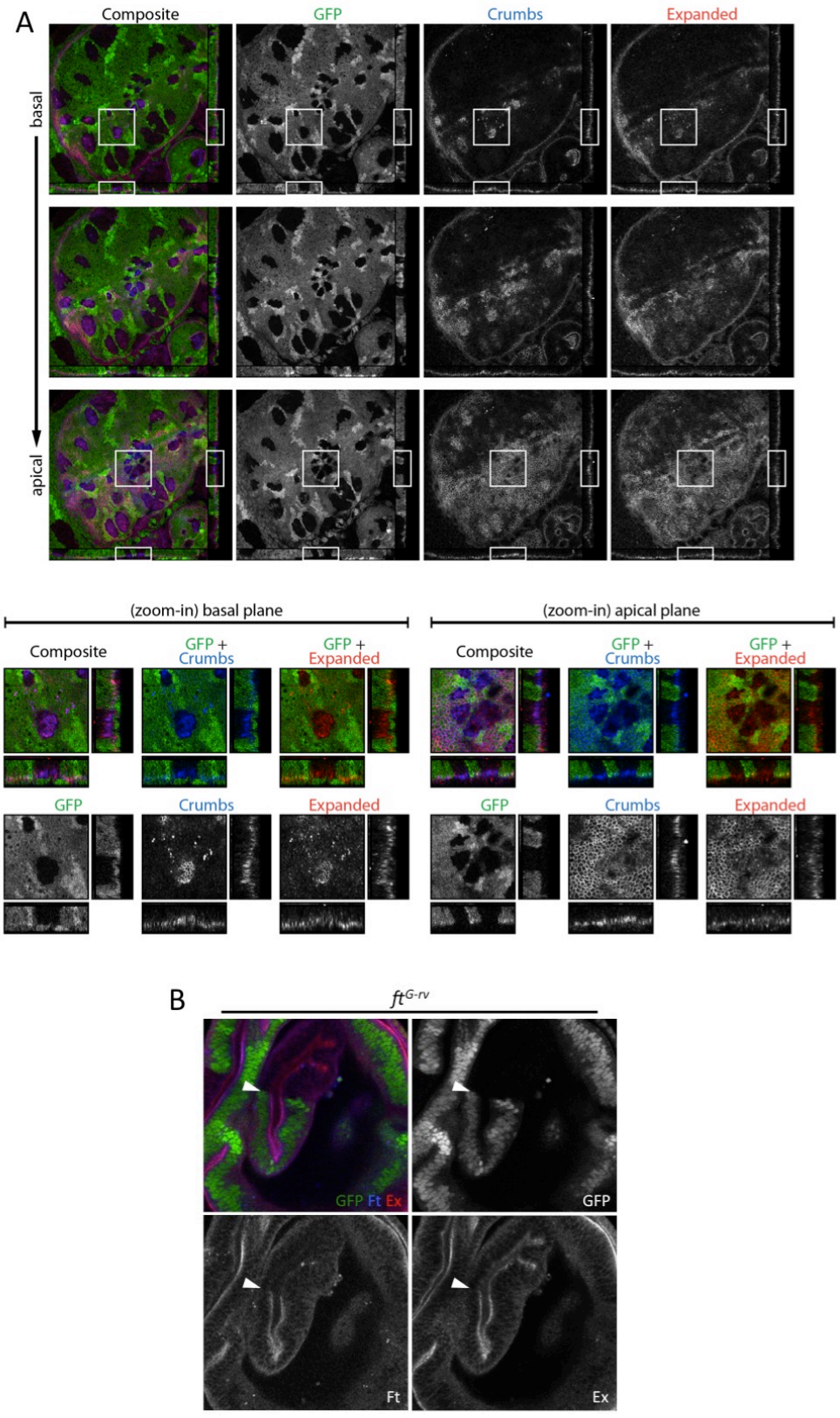

Fig 7.10 *ft* clones affect Ex localization in larval wing discs
ft^{fd} (A) and $ft^{G\text{-}rv}$ (B) clones are induced using the heat-shock FLP-FRT system. Clones are marked by absence of GFP. (A) Z-stacks of Ex staining shows apical loss and more basal enrichment of Ex in clones close to the dorso-ventral boundary. Wing disc is co-stained for Crb. (B) Shown is the wing pouch region, which is visibly overgrown due to larger $ft^{G\text{-}rv}$ clones. Apical surfaces are visible in folds. Fat staining confirms loss of *ft* and Ex staining (red) is reduced apically in *ft* clones. Arrow marks clone borders.

7.2 Analysis of Ex phosphorylation and novel Ex candidate interactors

7.2.1 Phosphorylation of Ex by Dco

Another question that I wanted to address was if Fat is involved in posttranscriptional regulation of Ex. Previous studies had not only found a genetic link between *ex* and *ft* but also between *ex* and *crb*. Crb can interact directly with Ex through a FERM binding motif (FBM) in its short intracellular domain (Chen et al., 2010; Grzeschik et al., 2010; Ling et al., 2010; Robinson et al., 2010). In cell culture studies, Crb recruits Ex to the membrane, where Ex gets hyperphosphorylated by an unknown kinase and is subsequently degraded, suggesting a tight regulation of Ex function and levels (Ling et al., 2010; Ribeiro et al., 2014). In *Drosophila* larvae, *crb* mutant tissue shows loss of apically localized Ex and accumulation of basolateral (and apparently inactive) Ex, reminiscent of the Ex mislocalization observed in *ft* clones (Bennett and Harvey, 2006; Silva et al., 2006; Willecke et al., 2006; Chen et al., 2010; Grzeschik et al., 2010; Ling et al., 2010; Robinson et al., 2010). However, the relationship between Crb and Fat and whether they have distinct or synergistic roles in regulating Ex is unknown.

In cell culture, a clear phospho-shift of Ex can be observed upon Crb overexpression, which is reverted by phosphatase treatment and is not seen upon overexpression of a Crb construct lacking the FBM (Ling et al., 2010) (see also Fig. 7.11). The cause and exact function of Ex phosphorylation remains to be determined, but phosphorylation correlates with Ex degradation through the E3 ligase Slimb (Ribeiro et al., 2014; Zhang et al., 2015) and might regulate the pool of active Ex at the subapical membrane. The question arises which kinase phosphorylates Ex and if this phosphorylation is regulating Ex activity in growth control.

Unpublished results from a former postdoc in our lab indicated that purified CK1ε, the mammalian homolog of the kinase Dco, phosphorylates not only Fat (Sopko et al., 2009) but also the N-terminal half of Ex *in vitro* (Richelle Sopko,

unpublished data). This posed the question whether Dco is the kinase responsible for Ex phosphorylation upon membrane tethering. An appealing model would be that Ex is recruited to the membrane by Crb and/or Fat, where it comes into close proximity to the Fat interactor Dco and gets phosphorylated in its FERM domain.

To test this hypothesis, I modulated Dco levels in experiments based on the published cell culture studies co-expressing Ex and Crb constructs (Ling et al., 2010). A slightly longer ExFERM construct including a region just C-terminal of the FERM domain was used for these experiments (courtesy of Dr. Nicholas Tapon (Ribeiro et al., 2014)). As expected, co-expression of ExFERM and the Crb intracellular domain (Crb-intra) in S2 cells led to a strong phospho-shift of ExFERM. Similarly, Crb-intraΔPBM, which contains a deletion of the Crb PDZ binding motif (PBM), was able to cause ExFERM hyperphosphorylation. In contrast, Crb-intraΔFBM, which lacks the FERM binding motif (FBM) did not lead to an electrophoretic shift of ExFERM, emphasizing the importance of the FBM for recruitment and regulation of Ex (Fig. 7.11) (Ling et al., 2010; Ribeiro et al., 2014).

To test if Dco plays a role in Ex phosphorylation, I treated S2 cells with shRNA targeting Dco. Transfection of shRNA resulted in a strong reduction of endogenous Dco levels but did not visibly affect hyperphosphorylation of ExFERM. Additional expression of FatΔECD did not have an effect either (Fig. 7.11 and 7.12). Phosphorylated ExFERM was still able to interact with FatΔECD, possibly with even enhanced capacity (Fig 7.12C; preliminary data). Neither overexpression of Dco^{3}, a mutant form of Dco thought to act in a dominant negative fashion (Cho et al., 2006), nor the kinase-dead mutant Dco^{KR} (Strutt et al., 2006) visibly affected the Ex phospho-shift (Fig. 7.12). Lastly, treatment with the CK1ε inhibitor PF670462 had no effect (Fig. 7.12).

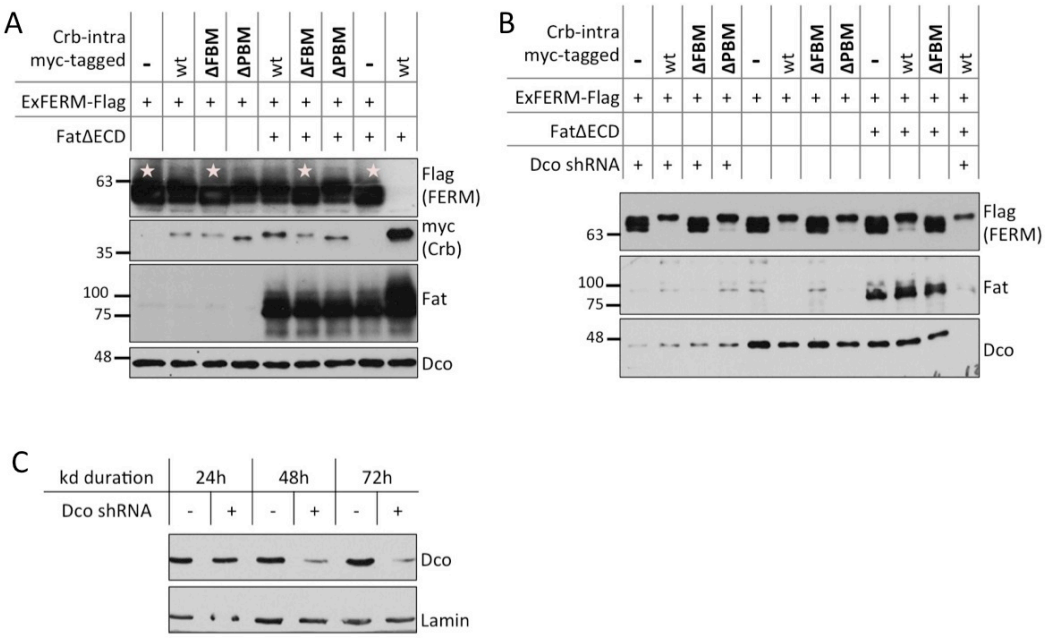

Fig 7.11 Ex hyperphosphorylation is not affected by Dco knockdown or FatΔECD expression

Western blots of S2 cells transiently transfected as indicated. Crb-intraΔFBM lacks the FERM-binding motif and does not cause ExFERM electrophoretic delay, similar to absence of Crb-intra expression (marked by stars in (A)). Crb-intraΔPBM lacks the PDZ-binding motif which does not affect ExFERM gel shift . (B) Dco knockdown by shRNA treatment for 96h or co-expression of FatΔECD does not reverse the ExFERM shift. (C) Time course of Dco shRNA treatment indicates highest efficiency after 72h of knockdown.

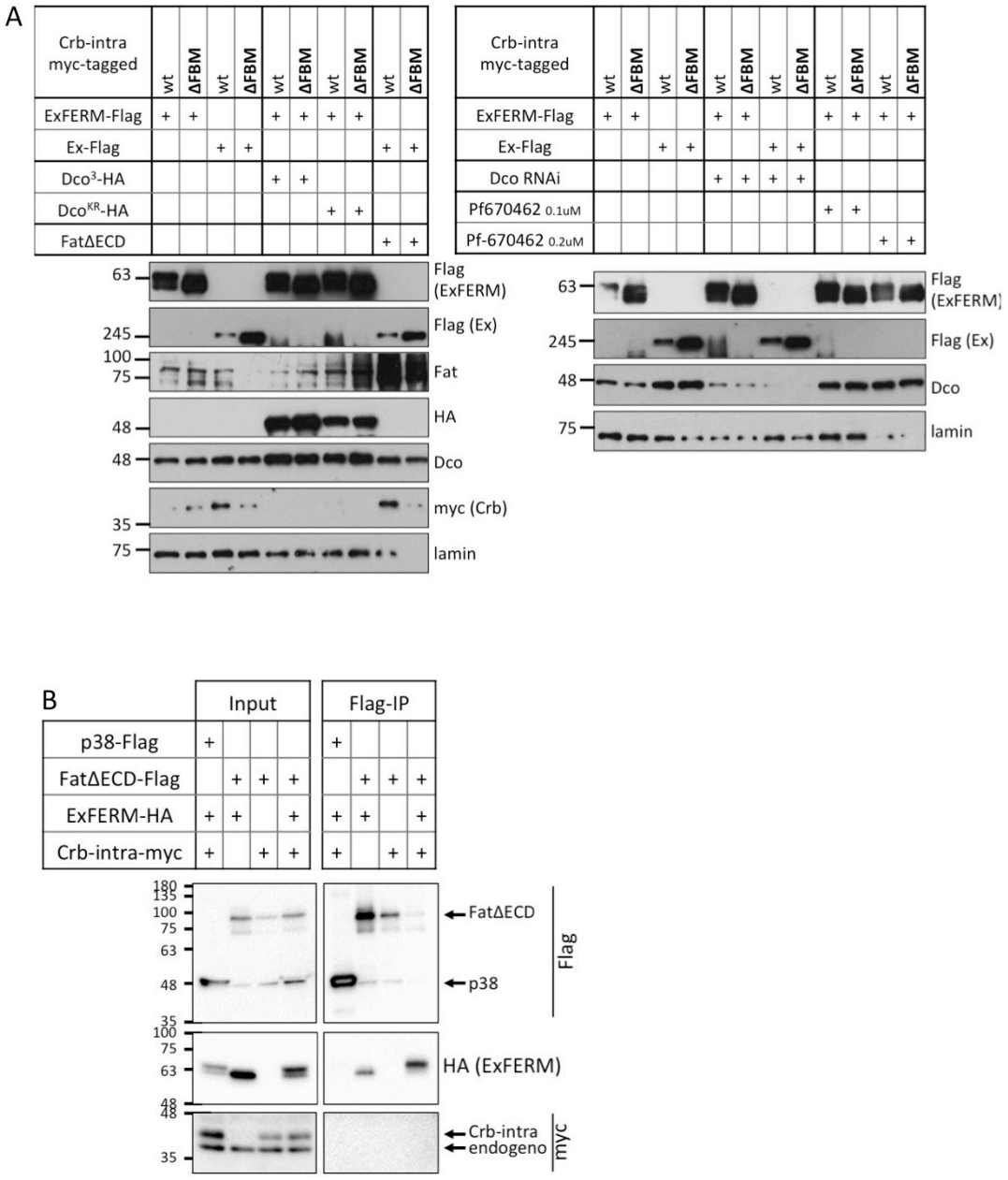

Fig 7.12 Ex phosphorylation in reponse to Dco modulations
(A) S2 cells are treated with Dco shRNA or with Casein kinase inhibitor Pf670462 and transiently transfected as indicated. Full-length Ex and Ex-FERM show a size shift if the Crb-intracellular domain is present. Dco RNAi and two concentrations of Pf670462 don't visibly affect the Ex shift. No effect is seen with co-expression of FatΔECD. (B) Flag-IP in S2 cells. Electrophoretically shifted (phosphorylated) and unshifted ExFERM co-immunoprecipitates with FatΔECD. p38-Flag serves as negative control. No interaction between FatΔECD and Crb-intra is detected.

At this point I concluded that Dco either has no critical function for Ex hyperphosphorylation or low levels of Dco are sufficient to fulfill its kinase function. A subsequent mass spectrometry approach in S2 cells to identify phosphorylated residues within ExFERM after Crb-intra co-expression was unsuccessful, most likely due to an unfavorable trypsin digestion pattern causing incomplete sequence coverage of ExFERM (Fig. 7.13) (similar observations were made by (Ribeiro et al., 2014)). This precluded a deeper investigation of the Ex phosphorylation mechanism through mutational or motif analysis.

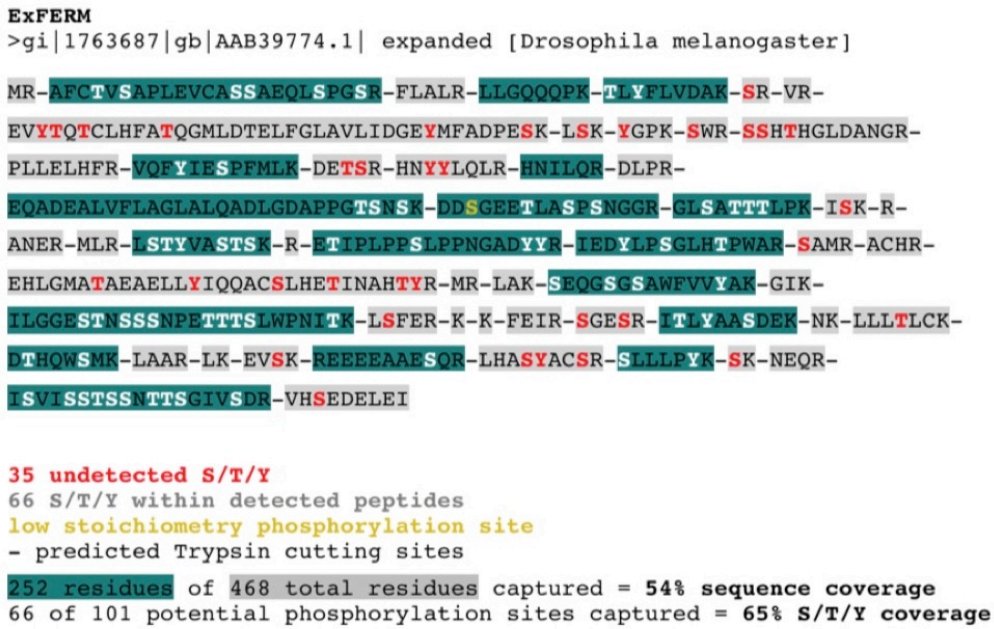

Fig 7.13 Trypsin digestion pattern of ExFERM identified in AP-MS
ExFERM trypsin digestion cut sites are symbolized by hyphens. Peptides detected by mass spectrometry are in green. Phosphorylatable residues (S/T/Y) in white were recovered by mass spectrometry (65%). S/T/Y in red were not detected (35%). After co-expression of Crb-intra, only a low stoichiometry phosphorylated residue was discovered (marked in yellow; Ser189).

7.2.2 Mask as a novel Expanded interactor

While no Ex phosphorylation sites were identified with this approach, the AP-MS data revealed an informative set of Ex interactors (Table 7.1). Both full-length Ex-Flag and ExFERM-Flag were used as baits and were paired with and without co-expression of Crb-intra. Although peptide counts were generally low due to the nature of the transient transfection method used, the interactor lists contained several known Ex interactors.

One of the known interactors validating our AP-MS approach was Yki. Ex interacts with Yki through its C-terminal PPxY motifs, which allows it to regulate Yki activity independently of Yki phosphorylation by Wts (Badouel et al., 2009; Oh et al., 2009). In agreement with these findings, we detected Yki peptides in the full-length Ex AP-MS but not in the ExFERM AP-MS (ExFERM lacks the C-terminal PPxY motifs).

Strikingly, the most abundant interactor in all AP-MS experiments was Mask (multiple ankyrin repeats single KH domain), which was mainly found in ExFERM runs. At the time, *mask* was poorly studied, but *mask* mutant clones were shown to be smaller than their twin spots and had increased apoptotic markers (Smith et al., 2002). This is reminiscent of negative regulators of Hippo signaling and similar to the phenotypes of *yki* mutant clones (Huang et al., 2005). Therefore, Mask seemed like a promising candidate to test for functions in Hippo signaling.

I confirmed the AP-MS data in co-immunoprecipitation experiments, where endogenous Mask co-purified with Flag-tagged ExFERM in S2 cells (Fig. 7.14). Full-length Mask (predicted size: 420kDa) and a lower 170kDa band co-immunoprecipitated with ExFERM-Flag (see Fig. 7.14A, 3-8% gradient gel). On regular 10% SDS-PAGE, the 420kDa band cannot be resolved but the 170kDa band was repeatedly detected in ExFERM pulldowns. Preliminary results indicated that Mask does not interact with Mer, at least not in a similar strength as with ExFERM (Fig. 7.14). Whether an interaction of Mask with full-length Ex can be detected remains to be fully expored.

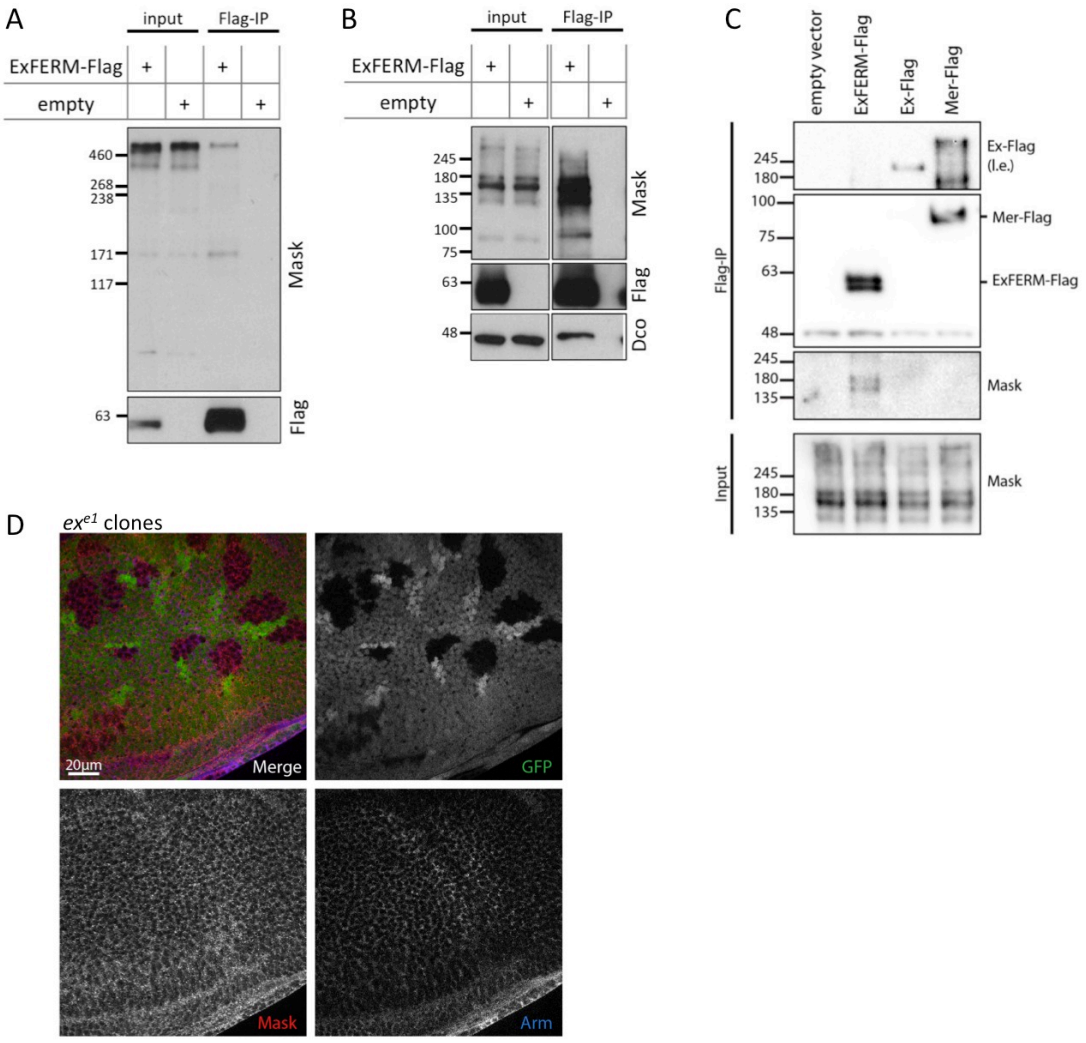

Fig 7.14 Expanded interacts with Mask
(A-C) Co-immunoprecipitation of Flag-tagged ExFERM with endogenous Mask in transiently transfected S2 cells by anti-Flag IP. (A) Full-length Mask (predicted size: > 400kDa) and a smaller band (170kDa) in ExFERM-Flag pulldowns are shown on a 3-8% gradient gel to resolve large proteins. (B,C) Anti-Flag co-IP samples on 10% SDS PAGE show the Mask-positive 170kDa band in cells transfected with ExFERM-Flag but not Mer-Flag. (D) *ex*^{e1} clones are induced using the heat-shock FLP-FRT system. Clones are marked by the absence of GFP. Arm = Armadillo. Loss of *ex* in 3rd instar wing disc clones does not visibly affect Mask staining.

Mask levels and localization were not obviously altered in *ex*^{e1} mutant clones in wing discs (Fig. 7.14D). However, before I could investigate their relationship further, two groups simultaneously published Mask as a novel Hippo pathway regulator (Sansores-Garcia et al., 2013; Sidor et al., 2013). Both groups

discovered Mask independently of Ex in an RNAi screen and a Yki activity modifier screen, respectively. They found Mask to physically interact with Yki and regulate Yki activity in the nucleus, likely acting independently of the phosphorylation-based regulation by Wts (Sansores-Garcia et al., 2013; Sidor et al., 2013). A direct link between Mask and Ex was not explored in both publications. However, especially since Ex has been shown to also directly bind and regulate Yki in a Wts-independent manner (Badouel et al., 2009; Oh et al., 2009), it would be interesting to better understand what the molecular and functional relationships of Ex, Mask and Yki are.

7.2.3 Information from the Ex and ExFERM interactomes

The Ex and ExFERM AP-MS identified several other putative novel interactors and gave additional information about the requirement of the Ex FERM-domain for interactions with known partners. One example is Hpo, whose interaction with Ex has been validated in S2 cells (Yu et al., 2010). Hpo was a strong hit in the ExFERM AP-MS runs, suggesting that it is the FERM-domain, which mediates Hpo binding.

Interestingly, we also found Rassf peptides in our runs. Rassf is known to compete with Sav for binding to the Hpo SARAH domain, thereby negatively regulating Hpo activity (Polesello et al., 2006; Ribeiro et al., 2010). While it is possible that Rassf co-immunoprecipitated with Hpo in the AP-MS, the fact that we see Rassf peptides in one full-length Ex run where no Hpo peptides were detected, argues for a Hpo independent interaction with Ex/ExFERM. Rassf peptides were also found in an independent ExFERM mass spectrometry in Dr. Nicholas Tapon's lab (*personal communication*), which increases the confidence that Rassf is a real interactor of Ex.

Another AP-MS hit was Karst (Kst), the *Drosophila* beta-heavy-spectrin. At the time of the experiment, no link between Ex and Kst was known, but recently Kst has been implicated in Hippo pathway regulation (Deng et al., 2015; Fletcher et al., 2015). Kst was shown to interact with Ex in co-IPs from S2 cells, and Ex is likely the molecular link between spectrin-transmitted cytoskeletal tension and

Hippo pathway-dependent growth control (Fletcher et al., 2015). Several other links between Kst and the Hippo pathway might exist, as Kst was detected as an AP-MS interactor of Dachs (Kwon et al., 2013), and *kst* expression is modulated in *wts* mutant tissue, possibly through a direct regulation by Yki, which binds the *kst* locus (Oh et al., 2013). In our AP-MS, Kst was only found in the full-length Ex interactome but not in the ExFERM interactome, despite the apparent lower efficiency of full-length Ex affinity purification. This suggests that the C-terminal half of Ex mediates the interaction with Kst. Kst has been shown to interact with Crb, and as the FBM of Crb is important for this interaction, a FERM-protein mediator has been suspected. Therefore, it is possible that Ex functions as a connector between Crb and Kst (Medina et al., 2002; Pellikka et al., 2002).

Other interactors with lower peptide numbers have been linked to Hippo pathway signaling or members and are therefore interesting candidate interactors. These include the Ste20 kinase Misshapen (Msn) (Li et al., 2014a; Meng et al., 2015), the actin regulator Hem (Kwon et al., 2013) and the STRIPAK member Microtubule star (Mts) (Ribeiro et al., 2010). The relative enrichment of ribosomal proteins in contrast likely represents common contaminants, which in mammalian AP-MS experiments are usually filtered out by algorithms used for data interpretation.

In summary, Ex is strongly phosphorylated upon recruitment to the plasma membrane by Crb. Modulation of Dco levels or expression of FatΔECD have no visible effect on Ex hyperphosphorylation, suggesting that other mechanisms are likely responsible for this event. Mass spectrometry of ExFERM and full-length Ex failed to identify stochiometric phospho-residues but revealed potential novel interactors of Ex, such as the Yki regulator Mask

Table 7.1 Expanded AP-MS (anti-Flag)

ExFERM-3F			Ex-3F			sum	Gene symbol	Full name	Molecular Functions
BR1	BR2	BR3	BR1	BR2	BR3				
177	119	99	26	17	11	449	ex	expanded	Bait
26	25	18				69	mask	multiple ankyrin repeats single KH domain	cytoskeletal anchoring at plasma membrane // cell proliferation // centrosome duplication // Yki interactor
15	14	10				39	hpo	hippo	Germinal center/Ste20 kinase // Ser/Thr kinase // cell proliferation // tissue morphogenesis // Ex interactor
4	5	4		3	9	25	RpL4	Ribosomal protein L4	large ribosomal protein // structural constituent of ribosome // Mer interactor
	2	2		7	8	19	CG4887	Dmel_CG4887	Zinc finger protein // unknown function
3	2	3	3		3	14	Nop56	Dmel_CG13849	unknown function // pit interactor
5	3		2	3		13	RpS18	Ribosomal protein S18	small ribosomal protein // structural constituent of ribosome // Mer interactor // Hpo interactor
		3	1	4	4	12	Prp8	Dmel_CG8877	pre-mRNA processing factor // deubiquitinase // splicing
	4			4	4	12	CG18428	Dmel_CG18428	Nuclear RNA-splicing-associated protein // unknown function
			4	4	3	11	yki	yorkie	transcription coactivator activity // Hippo pathway effector
	2	2	1	1	5	11	l(3)72Ab	Putative U5 small nuclear ribonucleoprotein 200 kDa helicase	RNA helicase // mRNA splicing (putative)
		2		4	4	10	Elp1	Putative elongator complex protein 1	phosphorylase kinase regulator activity (putative)
7	1	2				10	Nop60B	Nucleolar protein at 60B	ribosomal RNA processing // pseudouridine synthase activity
		3		2	4	9	CG11266	Dmel_CG11266	= Caper // mRNA splicing
	2	2		4	1	9	CG9372	Dmel_CG9372	Serine protease/endopeptidase // CG1092 interactor
	2	5			2	9	ncd	non-claret disjunctional	kinesin // mysoin-kinesin ATPase superfamily // required for chromosomal segregation meiosis/mitosis
4			4			8	Oat	Ornithine aminotransferase precursor	ornithine-oxo-acid transaminase activity (putative) // unknown function
	5			3		8	Cul-2	Dmel_CG1512	ubiquitin protein ligase binding // E3 ligase binding protein (CRL complex)
2	4			2		8	Rassf	Ras association family member	dSTRIPAK interactor // zinc ion binding // Hpo interactor
		2		2	3	7	Prp19	GTP-binding-protein	U-box ubiquitin ligase // mRNA splicing // Fat interactor
4			3			7	CRIF	CR6-interacting factor // CG7172	Growth arrest/DNA-damage-inducible protein-interacting protein 1
2		2	1	1	1	7	RpL14	Ribosomal protein L14	large ribosomal protein // structural constituent of ribosome
		4			3	7	Nup75	Dmel_CG5733	nuclear pore complex // nucleoporin Nup85-like
			4	2		6	Slu7	Pre-mRNA-splicing factor Slu7	zinc finger protein // mRNA splicing // mitotic spindle orientation
	2			2	2	6	RpL24	Ribosomal protein L24	large ribosomal protein // structural constituent of ribosome
3				3		6	zormin	Dmel_CG33484	spectrin repeats // actin binding // unknown function
3		1		2		6	RpL8	Ribosomal protein L8	large ribosomal protein // structural constituent of ribosome
				3	2	5	kst	karst / beta-heavy-spectrin	PH domain // actin binding // microtubule binding // Dachs interactor // Crb interactor // Ex interactor
				2	3	5	fws	four way stop	= COG5 // spermatid meiosis // Golgi function
				2	3	5	RhoGAP92B	Rho GTPase-activating protein 92B	GTPase activator // phospholipid binding

ExFERM-3F			Ex-3F			sum	Gene symbol	Full name	Molecular Functions
BR1	BR2	BR3	BR1	BR2	BR3				
	1			2	2	5	mRpL44	mitochondrial ribosomal protein L44	mitochondrial large ribosomal protein
2			2		1	5	His2A:CG31618	Histone H2A	Histone 2A family // nucleosome core component
		2		3		5	Cp190	Centrosomal protein 190kD	gypsy chromatin insulator complex component // DNA binding // microtubule binding // chromatin silencing
3			2			5	NHP2	H/ACA ribonucleoprotein complex subunit 2-like protein	ribosomal protein L7Ae family // ribosome biogenesis
	2	2			1	5	hoip	hoi-polloi	ribosomal protein L7Ae family // mRNA splicing
4		1				5	IntS1	Dmel_CG3173	Integrator 1 // snRNA processing //
			2	2		4	CG17931	#N/A	SERF family member // unknown function
				2	2	4	UbcD10	Ubiquitin conjugating enzyme 10	Ubiquitin-conjugating enzyme E2
		1		3		4	**Hem**	**HEM-protein**	**Nck-associated protein 1 // oocyte growth // Fat interactor**
2			2			4	chb	chromosome bows	CLASP family member // microtubule plus end tracking // microtubule stabilization // mitotic spindle formation
2			2			4	l(2)06496	Dynactin 3, p24 subunit	microtubule-based movement (putative) // unknown function // GI interactor
	2			2		4	Cpsf160	cleavage and polyadenylation specificity factor	myosin binding // mRNA binding // mRNA poly-adenylation
	2			1	1	4	mRpS10	mitochondrial ribosomal protein S10	mitochondrial small ribosomal protein
	2				2	4	CG11030	Dmel_CG11030	unknown function
		3		1		4	RpLP2	Ribosomal protein LP2	large ribosomal protein // structural constituent of ribosome
				2	1	3	SF1	Splicing factor 1	zinc finger // mRNA splicing // wing morphogenesis
				1	2	3	cdc16	Dmel_CG6759	anaphase promoting complex member // ubiquitin-protein transferase activity // mitotic cell cycle
				1	2	3	sec15	Exocyst complex component 6	Exocyst complex member // intracellular trafficking // vesicle-membrane tethering
				1	2	3	CstF-64	Cleavage stimulation factor 64 kilodalton subunit	mRNA cleaving (putative)
				1	2	3	exo84	Dmel_CG6095	Exocyst complex member // intracellular trafficking // vesicle-membrane tethering // PH domain
				1	2	3	**CG11505**	**La-related protein CG11505**	**RNA-binding domain // unknown function // Fat interactor**
				1	2	3	Srp14	Signal recognition particle protein 14	SRP9/SRP14 subunit // ER signal peptide binding
1			2			3	Patronin	short spindle 4	Calmodulin-regulated spectrin-associated protein // microtubule minus-end binding // mitotic spindle elongation
	1			1	1	3	CG1092	Dmel_CG1092	unknown function // binds CG9372
	1			2		3	Clc	Clathrin light chain	Clathrin complex member // vesicle formation // protein trafficking
		1			2	3	pit	pitchoune	DEAD box helicase family // RNA helicase // cell growth/proliferation // Nop56 interactor
	2				1	3	CG10286	Dmel_CG10286	unknown function
	2			1		3	**msn**	**misshapen**	**Germinal center/Ste20 kinase // Ser/Thr kinase // MAP4K activity // tissue morphogenesis // Fat interactor**

ExFERM-3F			Ex-3F			sum	Gene symbol	Full name	Molecular Functions
BR1	BR2	BR3	BR1	BR2	BR3				
		2			1	3	Gl	Glued / Dynactin 1, p150 subunit	dynein binding // microtubule motor activity // mitosis // cell fate // l(2)06496 interactor
			1		1	2	CG18528	Dmel_CG18528	tRNA modification (putative)
				1	1	2	Nup107	Nucleoporin 107kD	Nuclear pore complex // SMAD nuclear import
	1			1		2	mRpS31	mitochondrial ribosomal protein S31	mitochondrial small ribosomal protein
	1				1	2	dgt3	dim gamma-tubulin 3	mitotic splinde organization // mitotic nuclear division
	1	1				2	mbo	members only / Nup88	Nucleoporin 88 // nuclear pore complex
	1	1				2	CG1316	Dmel_CG1316	mRNA binding // unknown function

protein trafficking	nuclear pore complex	germinal center kinases	unknown function
ribosomal proteins	microtubule and cytokinesis	chromatin regulation	**Hippo pathway interactors (bold)**
mRNA processing	ubiquitination	cytoskleton-associated proteins	

8 Discussion Chapter A

8.1 The relationship of Fat and Expanded

How Fat regulates the Hippo pathway in *Drosophila* has not been fully elucidated and molecular links of Fat are largely unknown. Particularly, no factors have been identified yet that interact with a Fat region which confers strong Hippo activity. However, Ex has been proposed as a candidate mediator of Fat signal transduction, since *ex* and *ft* appear to function in the same genetic pathway (Bennett and Harvey, 2006; Cho et al., 2006; Silva et al., 2006; Willecke et al., 2006). Initial data in our lab further pointed to a physical interaction between Fat and Ex, as both proteins could be co-immunoprecipitated in cell culture. From these premises, I characterized the Fat-Ex interaction further.

8.1.1 Fat and Expanded interact directly or indirectly in cell culture

Based on genetic interactions of Fat and Ex in *Drosophila* and initial data in the lab showing an interaction between the FERM-domain of Ex and Fat in cell culture, I further characterized the Fat-Ex interaction. I confirmed that Fat and ExFERM interact differentially dependent on the Fat regions available, indicating that defined domains mediate the interaction. I could narrow down two distinct regions involved in Ex binding: EBR1 lies in the middle of the Fat ICD, while EBR2 lies in its C-terminus within the last 64 amino acids. Deletion constructs lacking one of the two EBRs are still able to bind to Ex, indicating that each of them is sufficient for Ex binding (see Fig 7.6 for overview).

However, a clean double deletion construct (FatΔECD;ΔEBR1;ΔEBR2) could still interact with Ex with significant strength, suggesting that other regions of the Fat ICD can mediate Ex binding as well. Indeed, none of the deletion constructs fully addresses if the region between amino acid 124 and 245 of FatΔECD has Ex binding activity, which should be tested individually. As a myristoylated C-terminal Fat construct loses Ex binding upon deletion of EBR2, this region seems appropriately defined. Therefore, testing the requirement of EBR1 in a similar manner, using short myristoylated deletion constructs, can address if the EBR1

boundaries need to be repositioned and should be considered for future investigation.

Despite these remaining questions, the two identified EBRs are in intriguing positions of FatΔECD: EBR1 overlaps entirely with the so-called "HippoC" region of Fat, which harbors Hippo-pathway activity (Matakatsu and Blair, 2012). If HippoC is critical for Ex binding *in vivo*, this could explain its Hippo-regulating function. However, this needs to be addressed in more detail and *in vivo*, as a Fat construct harboring the Fat^{sum} mutation did not affect the interaction with Ex, although Fat^{sum} is considered disruptive specifically of the Hippo-activity in this region (Bossuyt et al., 2014). More recently, a second point mutation, Fat^{61} with similar effects was found in close proximity to Fat^{sum} (Bosch et al., 2014), which could be tested for effects on Ex for completion, both in terms of Fat-Ex interaction in cell culture and Ex localization in imaginal discs. Elucidating the molecular consequences of these point mutations will greatly increase our understanding of the role of Fat in the Hippo pathway.

EBR2 is located within one of the few highly conserved regions between Fat and its mammalian homologs, which prompted me to test if Fat4 retained the ability to bind Ex. Indeed, Fat4ΔECD interacted with Ex in comparable strength as FatΔECD, suggesting functional conservation of at least one of the EBRs. It would be interesting to further investigate if this interaction of Fat4 relies solely on EBR2, considering that EBR1 does not appear to be conserved. Interestingly, although the mammalian homologs of Ex, Frmd1 and Frdm6, do not contain a C-terminal domain equivalent to Ex, the FERM domain is conserved (Hamaratoglu et al., 2006). It is therefore possible that Fat4 and Frmd1/Frmd6 interact in mammals through their FERM domains, similar to *Drosophila*.

8.1.2 Fat interacts with Mer

Surprisingly, Fat co-immunoprecipitated also the Ex interactor Mer. The interaction between Fat and Mer appears to occur mainly through the Mer FERM-domain and relies on the same regions of the Fat ICD. However, while *ft* and *ex* interact genetically, *ft* and *mer* do not, and Fat and Mer are generally

considered to constitute different signaling branches upstream of the Hippo pathway. Mer localization is also not visibly affected by loss of *ft*. However, recent insight into the importance of subapical recruitment of Hippo pathway members indicates that several upstream regulators form scaffolds and are part of a large Hippo pathway complex required for activation and transduction of signaling. Therefore, Ex, Mer and Kibra, which have previously been found to form a complex, might further interact with Fat (or Crb). It is conceivable that their ability to form a complex even promotes their interaction with Fat (as indicated in Fig. 7.8) through reciprocal stabilization. As most of these experiments were performed in HEK293 cells with overexpressed proteins, it is unlikely that endogenous Ex/Frmd1/Frmd6 "bridges" Mer and Fat through interacting with both, but cannot be fully excluded either. Testing the ability of Fat to interact with FERM-domain proteins with no (known) functions in Hippo signaling, such as Moesin or Yurt, could address if Fat generally interacts with FERM-domain proteins or more specifically with Hippo regulators.

8.1.3 Functional implications for a Fat-Ex interaction

Our understanding of Hippo signaling is evolving, as more studies describe intricate fine-tuning and cross-talk between many upstream Hippo regulators. Even in the Fat ICD alone, different regions have been reported to play distinct roles in the regulation of the Hippo pathway (Bosch et al., 2014). Considering the genetic behavior of *ft* and *ex*, Ex may have an important function in Fat signal transduction (Bennett and Harvey, 2006; Cho et al., 2006; Silva et al., 2006; Willecke et al., 2006). However, it is also possible that the interaction between Fat and Ex is part of a smaller branch of Fat signaling while most of the Fat signaling capacity is dependent on D (Feng and Irvine, 2007). Finally, it cannot be fully excluded that Fat and Ex interact only in cell culture models but not significantly so in *Drosophila*. Considering the rather subtle changes of Ex localization in *ft* mutant clones that I have seen, it will be challenging to distinguish between these options *in vivo*. However, the CRISPR/Cas9 toolbox enables new and more sensitive approaches to these questions, such as deletion of EBRs within the endogenous Fat protein and tagging endogenous Ex or Mer to study their subcellular localizations. Dr. Hongtao Zhang and Yi Qu in our lab have

recently established a *Drosophila* strain where the HippoC-coding domain has been deleted in the endogenous *ft* locus using CRISPR/Cas9 (ΔHippoC). It will be interesting to test if a reduction or basolateral shift of Ex is visible in somatic ΔHippoC clones. Although deletion of EBR1 in cell culture did not disrupt the Fat-Ex interaction, it is possible that *in vivo* this relationship is more sensitive and more easily disturbed.

8.1.4 How does the Fat-Ex interaction integrate with Crb and D?

Additionally, an important question is whether crosstalk between Fat and Crb exists in the regulation of Ex. If Crb and Fat cooperate in the spatial regulation of Ex, this might explain why a wide phenotypic range of Ex mislocalization for both loss of *ft* and loss of *crb* have been reported in different studies (Bennett and Harvey, 2006; Cho et al., 2006; Silva et al., 2006; Willecke et al., 2006; Chen et al., 2010; Grzeschik et al., 2010; Ling et al., 2010; Robinson et al., 2010). An attempt to generate somatic *ft* clones expressing *crb* RNAi in wing discs was unsuccessful, likely because the mutant cells were outcompeted, suggesting that a genetic interaction between *ft* and *crb* might exist (Dr. Srdjana Ratkovic, *unpublished data*). A different way to address this question would be to generate *ft* clones in a background sensitized by *crb* haploinsufficiency. If Fat and Crb regulate Ex localization partially redundantly, this might cause a stronger effect on Ex localization or levels. A similar strategy could also be employed to test ΔHippoC flies.

It should further be addressed what the relationship between Ex and D downstream of Fat is, as a previous study suggested that loss of D suppresses the ability of Fat to regulate Ex localization (Feng and Irvine, 2007). However, as mentioned before, subtle differences in Ex localization might not be easy to detect in every context. And as it is still unclear how Fat regulates D and where D is placed in the Hippo pathway hierarchy, further studies will be required before the relationship between Ex and D can be addressed confidently.

8.1.5 Ex might mediate growth-independent aspects of Fat signaling

There is also a possibility that an interaction of Ex and Fat has significance in a different signaling branch than growth regulation. Interestingly, *ex* mutant eye discs were found to exhibit PCP defects (Blaumueller and Mlodzik, 2000; Pellock et al., 2007) and the PCP defects of *ft* mutant eyes can be largely suppressed if the Hippo pathway is activated to compensate for loss of *ft* (Brittle et al., 2012). Therefore, there is a possibility that at least part of the PCP activity of Fat requires the Hippo pathway and that Fat might signal to it through Ex. Apart from the original observations of photoreceptor misorientations in *ex* mutant eyes, a potential role of Ex in PCP has not been studied. However, it would be exciting to understand the involvement of Ex in this process and how it links to Fat/PCP.

Another intriguing finding is that *ex* and *mer* might cooperatively regulate surface concentrations of different receptors. Maitra and colleagues have reported increased levels of Fat and other transmembrane proteins in *ex, mer* double mutant discs (Maitra et al., 2006). Later, the Hippo pathway has been shown to regulate the abundance of several apical/subapical proteins through Yki by unknown mechanisms (Hamaratoglu et al., 2009) and to control transcription of several upstream Hippo regulators, presumably as a feedback strategy (Hamaratoglu et al., 2006; Ikmi et al., 2014; Zhu et al., 2015). Therefore, some of the observed effects in *ex, mer* mutant eye discs might be explained by their activity in canonical Hippo signaling. However, pulse-chase experiments in *ex, mer* double clones have shown a clear decrease of Notch receptor surface clearance, suggesting that at least endocytosis of Notch is cooperatively regulated by Ex and Mer, which also colocalize with vesicular markers (Maitra et al., 2006). It is conceivable that this might also apply to Fat, and that interactions with Ex and Mer target Fat to sites of active endocytosis. In eye discs, single mutants of *ex* or *mer* had very subtle effects on receptor endocytosis (Maitra et al., 2006); therefore it might only be possible to observe this phenotype in double mutant tissue. The observation that both Ex and Mer bind to FatΔECD in a

non-competitive fashion and possibly with enhanced strength (Fig. 7.8), could hint towards a synergistic regulation of both proteins.

Interestingly, the F-box protein Fbxl7 was recently found to interact with the intracellular domain of Fat (Bosch et al., 2014). Fbxl7 appears to constitute one of the signaling branches that regulate the Hippo pathway and D asymmetry downstream of Fat (Bosch et al., 2014; Rodrigues-Campos and Thompson, 2014). Fat and Fbxl7 have a similar relationship as Fat and Ex with respect to regulation of subcellular localization. Fbxl7 and Fat colocalize at the subapical membrane and in intracellular vesicles. In *ft* mutant clones, Fbxl7 no longer localizes to the subapical membrane but is found more cytoplasmic and basal (Bosch et al., 2014).

Reciprocally, Fbxl7 seems to partially regulate the membrane localization of Fat. Although Fbxl7 is a F-box protein, it does not appear to regulate the stability of Fat, as *fbxl7* mutant clones only show a mild subapical increase of Fat (possibly a feedback from increased Yki activity), and *fbxl7* overexpression results in strong subapical enrichment of Fat (Bosch et al., 2014). As these changes are not associated with changes of Fat protein levels (Bosch et al., 2014), they could represent differential membrane stability of Fat through altered recycling rates, similar as proposed for Fat regulation by Ex and Mer (Maitra et al., 2006). Indeed, Fbxl7 also interacts with and regulates the membrane to vesicle translocation of the Fat interactor Cindr (Bosch et al., 2014).

Taken together, Fat appears to recruit or stabilize Fbxl7 at the subapical membrane, while Fbxl7 seems to regulate the recycling or membrane-to-vesicle ratio of Fat, as well as that of the Fat signaling members D, Cindr and possibly Ds (Bosch et al., 2014; Rodrigues-Campos and Thompson, 2014). Considering the similarities of subcellular localization control by Fat and their implications in receptor recycling, it would be interesting to look at the relationship between Ex and Fbxl7.

Bosch and colleagues suggest a model where two different regions in the Fat ICD regulate growth in form of parallel signaling branches, before converging on a common substrate upstream or at the level of Wts (Bosch et al., 2014). It is an appealing model that partially redundant signaling branches of Fat have evolved to control the Hippo pathway or other functions of Fat, which would also explain why different structure-function approaches have found distinct and non-overlapping regions of Fat to be important for growth control and PCP. Ex might represent one such signaling branch.

8.1.6 Ex phosphorylation at the plasma membrane

In response to its interaction with Crb or by membrane-tethering, Ex is phosphorylated by an unknown kinase. Although *in vitro* data had pointed to a potential function of the Fat kinase Dco in Ex phosphorylation, I could not find further evidence for such a relationship (Fig. 7.11-12). It is unknown if Ex phosphorylation changes Ex signaling activity or specificity, but it has recently been shown that it regulates Ex levels, as phosphorylation primes Ex for ubiquitination by the SCF-Slimb ubiquitin ligase and subsequent proteasome-dependent degradation (Robinson et al., 2010; Ribeiro et al., 2014; Zhang et al., 2015). Presence of Fat (in form of FatΔECD) did not seem to affect Crb-mediated Ex phosphorylation, but preliminary results might indicate a preferential interaction of FatΔECD with phosphorylated ExFERM, which offers a potential mechanism for Fat-Crb crosstalk (Fig. 7.12). It is appealing to speculate that Fat might interact with phosphorylated Ex and stabilize it at the membrane by (partially) preventing Ex degradation. This could explain why loss of *ft* results in reduced apical Ex levels and should be investigated further.

In preliminary experiments I could not detect an interaction between FatΔECD and Crb-intra (Fig. 7.12), however it would be interesting to elucidate if Ex interacts with Fat and Crb simultaneously as part of a bigger complex, or if different Ex populations bind to Fat and Crb.

8.2 Ex AP-MS

8.2.1 Proteomics reveal novel candidate interactors of Ex

With the generation of Ex interactomes, potential novel binding and signaling partners of Ex were revealed. The fact that several known Ex interactors are found amongst the high-confidence hit list (Yki, Hpo, Kst) shows that the data have a strong potential to be valid and significant.

One of the major problems with using transient transfection for the AP-MS approach is that only a subset of cells expresses the bait protein. Therefore, spectral counts are often lower than from stably expressing cells. In the case of Ex, the smaller and more robustly expressed Ex FERM-domain is represented with 5-10 times higher peptide numbers than the much larger full-length Ex. This could explain why several interactors of ExFERM are not found in full-length Ex runs. The more bait protein is affinity-purified from the cells, the higher are the chances that low-abundance or weak interactors are captured as well. This might also account for the fact that the ExFERM mass spectrometry run with the highest Ex peptide numbers shows several interactors with low numbers that are not shared with the other runs (see Table 7.1). Indeed, comparison with an unpublished ExFERM mass spectrometry data set provided by Dr. Nicholas Tapon's lab shows that some of these proteins are repeatedly recovered as ExFERM interactors. Amongst these are Bruce, an E2 ubiquitin conjugating enzyme functioning in apoptotic control through regulating the Yki target dIAP1 (Domingues and Ryoo, 2012), and Sulf1, an endosulfatase shown to regulate the Wg gradient in *Drosophila* wing discs (Kleinschmit et al., 2010). Dr. Tapon's and our data sets don't fully overlap and technical differences exist in the experimental setups. However, besides Bruce and Sulf1, also Hpo, Yki, Mask, Rassf, CG11266 and pit are shared between our data sets, adding additional weight to the potential validity of these interactors (Dr. Nicholas Tapon, *personal communication*).

Another interesting hit despite its low peptide numbers was Misshapen (Msn). Msn is a Ste20 kinase and was recently shown to function in a partially

redundant manner with Hpo to regulate Yki in *Drosophila* wing discs (Meng et al., 2015). In *Drosophila* enteroblasts, Msn apparently replaces Hpo entirely in the regulation of Wts and Yki (Li et al., 2014a). In human cells, the Msn homologs MAP4K4/6/7 are able to phosphorylate LATS1/2 together with MST1/2 (Meng et al., 2015). Msn was also identified as a Fat interactor in an AP-MS screen (Kwon et al., 2013). Considering that Ex binds and regulates Hpo, it is plausible that it can also bind and regulate Msn.

Candidates such as Msn that are recovered in the mass spectrometry with low peptide numbers could still be valid interactors. To address this and to create a more robust data set, AP-MS from S2 stably expressing full-length Ex and ExFERM would be an informative starting point. Further, co-immunoprecipitation experiments in S2 cells and genetic interaction studies in flies can address if some of these candidates are real Ex interactors involved in Ex function.

8.2.2 ExFERM interacts with the Yki regulator Mask

Surprisingly, we found a novel interactor of ExFERM to be the strongest hit in our AP-MS. At the time Mask was only vaguely characterized as involved in RTK signaling and by the fact that *mask* mutant tissue shows significant undergrowth phenotypes (Smith et al., 2002). Shortly after we performed the AP-MS, two studies were published placing *mask* genetically downstream of *wts* as a critical co-factor for Yki (Sansores-Garcia et al., 2013; Sidor et al., 2013). Mask knockdown and *mask* mutant tissues show strong undergrowth and reduction of Yki target gene expression (such as *fj*, *DIAP1* and *ex*). Interestingly, the transcriptional activity but not the subcellular localization of Yki depends on Mask. Mask seems to bind to Yki through its Ankyrin repeats and to regulate Yki directly, independent of the phospho-regulation by Wts. Mask is conserved to humans, where the two Mask homologs (ANKHD1 and ANKRD17) bind the Yorkie homolog YAP and are critical for YAP target gene expression. YAP and ANKHD1 are frequently co-expressed in cancers and low *ANKHD1* expression correlates with better relapse-free survival of breast cancer patients (Sansores-Garcia et al., 2013; Sidor et al., 2013). These studies suggest that Mask acts on the

level of Yki rather than within or upstream of the core Hippo pathway and it poses the question why we find Mask as an interactor of Ex.

Ex was shown to regulate Yki through the Hippo pathway in cooperation with Mer (Hamaratoglu et al., 2006), possibly through interaction with Hpo (Yu et al., 2010). However, Ex can also regulate Yki independently of the core Hippo cassette and Wts phosphorylation by directly binding and sequestering Yki away from the nucleus (Badouel et al., 2009; Oh et al., 2009). It is therefore possible that Ex co-regulates both Yki and Mask through direct interactions to sequester them simultaneously in the cytoplasm. It is not clear if the specificity of the Mask antibody (Smith et al., 2002) would allow membrane recruitment assays of Mask in cell culture, which could further clarify the relationship between Ex and Mask. Genetic studies are more difficult to design, as one needs to distinguish between the direct and the indirect regulation (through Wts) of Yki and Mask by Ex; also, as Yki and Mask interact, unraveling whether Ex effects Mask directly or through its interaction with Yki is challenging. A first experiment should be to test if a tripartite complex of Ex, Yki and Mask can be detected.

Intriguingly, other FERM-domain proteins have been found to localize both to the plasma membrane and the nucleus and contain putative nuclear localization and export sequences (NLS and NES, respectively) (Frame et al., 2010). The FERM-domain protein Focal adhesion kinase (FAK) for example is thought to shuttle between the cell cortex, where it regulates cell adhesion and extracellular matrix interactions, and the nucleus, where it promotes proliferation and survival (Lim, 2013). Also the mammalian homolog of Merlin, NF2, was reported to translocate to the nucleus, where it forms specific interactions important for its tumor-suppressive potential (Li et al., 2010; Li et al., 2014b). The human Ex homolog FRMD6 has a putative NES (Frame et al., 2010). It would be interesting to test if Ex can form a complex with Yki and Mask either at the cell cortex or in the nucleus.

While Mask is the strongest interactor in our ExFERM AP-MS, it is not found in the runs with full-length Ex. A possible explanation is the lower efficiency of the

Ex AP-MS, where between 5 to 10 times fewer bait peptides were recovered compared to the ExFERM runs. However, AP-MS of full-length Ex in S2 cells, which was performed as part of a large-scale Hippo interactome project, did not identify Mask as a hit either (Kwon et al., 2013), suggesting that Mask is more likely to be identified with the isolated Ex FERM domain than in context of the full-length protein.

An explanation for this could be that ExFERM represents an activated or more accessible form of Ex, possibly mimicking an "open" conformation of the protein. Such a conformational regulation of activity has been established for other FERM-domain family members, such as the ERM group (ezrin, radixin, moesin) and Merlin/NF2, where the N- and C-termini of the proteins interact to adapt a closed confirmation (Bretscher et al., 1995; Sherman et al., 1997; Reczek and Bretscher, 1998; Ishikawa et al., 2001). Interestingly, based on its tumor-suppressive function, NF2 seems to be active in its "closed" confirmation and inactivated by phosphorylation events that hinder the interaction between its N- and C-terminus (Sherman et al., 1997; Shaw et al., 2001). However, some controversy exists on this topic (Sher et al., 2012; Yin et al., 2013), which probably can be explained by multiple regulatory inputs and conformational states of Mer/NF2, that result in different activities based on the accessibility of binding domains.

Whether Ex is undergoing similar activity-coupled conformational changes is unknown. However, if this was the case, one would expect that the full-length protein and the isolated FERM domain show different efficiencies of certain protein-protein interactions. Conformational regulation of Ex would implicate an interesting additional layer in Ex signaling control.

9 Introduction Chapter B

9.1 Fat cadherins in mammals

While Fat function is well established in *Drosophila*, the roles of Fat cadherins in mammals are much less understood. A particular problem is the large size of Fat cadherins, which limits the use of many standard molecular tools for their study. In Chapter B, I present my approaches to elucidate functions of mammalian FAT4, the closest homolog of *Drosophila* Fat. In the first part, I generated tools to identify novel FAT4 interactors, to study FAT4 localization and to deplete FAT4 in cell culture. In the second part I investigated a role of FAT4 in primary cilium structure, as a putative mechanism underlying kidney cyst development in *Fat4* mutant mice.

9.1.1 Conservation of Fat cadherins in mammals

In mammals, four Fat cadherins are present, Fat1-4 (Dunne et al., 1995; Cox et al., 2000; Mitsui et al., 2002; Nakayama et al., 2002). Sequence analysis shows that Fat4 is the true ortholog of Fat, while Fat1, Fat2 and Fat3 share higher similarity with Kug (Dunne et al., 1995; Castillejo-Lopez et al., 2004; Rock et al., 2005; Tanoue and Takeichi, 2005; Saburi et al., 2008). In fact, Fat1, Fat2, Fat3 and Kug cluster into a different phylogenetic subgroup of the cadherin superfamily than Fat and Fat4 (Hulpiau and van Roy, 2011). Mammals further express two Dachsous cadherins, Dchs1 and Dchs2 (Rock et al., 2005). In analogy to the *Drosophila* Fat-Ds relationship, Fat4 and Dchs1 interact *in trans*, and their depletion in mice causes similar developmental phenotypes, which are not significantly enhanced in *Fat4, Dchs1* double knockout animals, indicating that they share a common pathway (Saburi et al., 2008; Mao et al., 2011a; Bagherie-Lachidan et al., 2015; Mao et al., 2015). In contrast, mouse models with deletions of *Fat1*, *Fat2* and *Fat3* have largely distinct phenotypes (Ciani et al., 2003; Barlow et al., 2010; Deans et al., 2011; Saburi et al., 2012), in accordance with their separate phylogenetic origins. A schematic of the Fat-Dachsous family in *Drosophila* and mammals is shown in Fig. 5.2.

9.1.2 Fat1 has diverse developmental roles

Fat1 is expressed almost ubiquitously in the developing embryo, with strong expression in brain, kidney, lung and neural tube (Cox et al., 2000; Ciani et al., 2003; Rock et al., 2005). *Fat1* knockout mice die shortly after birth and exhibit aberrant glomerular slit junctions in their kidneys, as well as less penetrant forebrain and eye development defects that in severe cases lead to holoprosencephaly (forrain underdevelopment) and cyclopia (Ciani et al., 2003; Sugiyama et al., 2015). Fat1 is also involved in cortical development, and *Fat1* knockout mice can exhibit neural tube closure defects and exencephaly accompanied by increased proliferation of cortex neuronal stem cells (Saburi et al., 2012; Badouel et al., 2015). In cell culture, FAT1 binds the F-actin regulating Ena/VASP proteins Mena and VASP through EVH1 domain-binding motifs in its ICD and can recruit additional actin polymerization factors, including ARP3 and N-WASP, to control actin dynamics. FAT1 localizes to filopodia, lamellipodia and cell-cell junctions and is involved in regulation of actin cytoskeleton polarity in migrating cells (Moeller et al., 2004; Tanoue and Takeichi, 2004). Fat1 also interacts with the polarity protein Scribble (Scrib) (Skouloudaki et al., 2009). In zebrafish, *Fat1* depletion results in a cystic kidney phenotype, which is ameliorated by additional depletion of the *Yki* homolog *Yap*, while *Yap* overexpression causes cysts on its own. Scrib antagonizes Yap-induced cysts and likely provides a link between Fat1 and the Hippo pathway in this system (Skouloudaki et al., 2009). Therefore, although loss of *Fat1* does not cause obvious overgrowth, Fat1 might signal to the Hippo pathway for other processes. It is also possible that other morphogenesis defects caused by loss of *Fat1* mask typical Hippo-like phenotypes. In smooth muscle cells, FAT1 interacts with human Atrophin homologs, suggesting that the *Drosophila* Fat-Atro interaction is conserved to mammals (Hou and Sibinga, 2009). Similar to *Drosophila* Fat, FAT1 is processed in its extracellular domain, resulting in a ~430kDa and a ~85kDa fragment. This cleavage event was found to be dependent on the protease Furin, although FAT1 can also be cleaved at a different site in a Furin-independent way, depending on the cell line (Sadeqzadeh et al., 2011). In summary, vertebrate Fat1 functions in various tissues throughout development and has potential roles in regulating the actin cytoskeleton and the Hippo pathway *in vivo*.

9.1.3 Fat2 and Fat3 are not critically required for embryonic development

Fat2 is specifically expressed in the adult cerebellum and therefore much more restricted in expression than Fat1, Fat3 and Fat4 (Nakayama et al., 2002; Rock et al., 2005). The function of Fat2 is elusive, as *Fat2* knockout mice are viable and do not exhibit obvious phenotypes (Barlow et al., 2010). However, *FAT2* is mutated in several cancers, indicating a function as a tumor suppressor in humans (Gao et al., 2014; Lin et al., 2014). Fat3 is mostly expressed in the developing central nervous system, spinal cord, olfactory bulb and retina, as well as in adult lungs (Mitsui et al., 2002; Rock et al., 2005; Nagae et al., 2007). *Fat3* knockout mice are viable, but have defects in retinal interneurons that cause structural defects in retina layering (Deans et al., 2011). How Fat3 acts mechanistically is largely unknown, but an EVH1 domain similar to Fat1 has been identified in the Fat3 ICD, indicating direct roles in actin regulation (Deans et al., 2011).

9.1.4 Fat4 has critical functions in the developing embryo

Fat4 is expressed widely in the developing mouse embryo, with enrichment in the central nervous system (Rock et al., 2005). In analogy to *Drosophila* Fat and Ds, mammalian Fat4 and Dchs1 colocalize at apical junctions of neuronal precursors and interact *in trans* in a calcium-dependent manner in cell culture (Ishiuchi et al., 2009). *Fat4* and *Dchs1* mutant mice are phenotypically very similar, and double mutant mice do not exhibit obvious additive phenotypes, suggesting that Fat4 and Dchs1 are functioning together (Saburi et al., 2008; Mao et al., 2011a; Bagherie-Lachidan et al., 2015; Mao et al., 2015). Loss of *Fat4* in the murine embryonic cortex affects apical junction morphology, likely mediated through the Pals complex: Fat4 was found to interact with Mupp1/Mpdz and its interactor Pals1/Mpp5, a membrane-associated guanylate kinase (MAGUK) (Ishiuchi et al., 2009). Mupp1 and Pals1 are homologs of *Drosophila* Stardust and Patj, respectively, which are involved in regulating apical-basal polarity and junction establishment with Crb/CRB1 (Bachmann et al., 2001; Roh et al., 2002). Loss of *Fat4* also leads to neuronal migration defects in the murine developing

cortex, and point mutations in FAT4 and DCHS1 are associated with van Maldergem syndrome in humans, which is characterized by migration and differentiation defects of cortical neurons and skeletal abnormalities (Cappello et al., 2013; Zakaria et al., 2014; Badouel et al., 2015). Apart from Mupp1 and Pals1, only the Lowfat homologs LIX1 and LIX1L have been validated as interactors of FAT4 in cell culture (Mao et al., 2009). However, the function of LIX1/LIX1L is unstudied. Therefore, most molecular mechanisms underlying Fat4 function are still largely unknown.

9.1.5 Fat4 plays a role in PCP signaling

In contrast to *Fat1*, loss of *Fat4* causes phenotypes that are considered typical PCP defects. In *Fat4* knockout mice these manifest in shortened body axes due to skeletal malformations, curly tails, as well as typical cochlea shortening and hair cell polarity defects in the organ of Corti (Saburi et al., 2008; Mao et al., 2011a; Saburi et al., 2012). Cochlea shortening often results from a defect in the normal convergent extension process (Yamamoto et al., 2009). *Fat4* knockout mice die perinatally exhibiting cystic kidney defects, which correlate with a loss of spindle orientation alignment in kidney tubules (Saburi et al., 2008). Randomized cell division axes are thought to cause kidney tubule dilation instead of proper elongation, ultimately causing cysts (Fischer et al., 2006). Some of the observed *Fat4* mutant kidney cysts also exhibit abnormal primary cilia, which might add to the phenotype (Saburi et al., 2008). Primary cilia defects are functionally associated with diverse cystic kidney defects (Yoder et al., 2002; Yoder, 2007). The function of Fat4 in oriented cell division (OCD) is reminiscent of a similar role for *Drosophila* Fat, which regulates OCD in the wing and eye (Baena-Lopez et al., 2005). Interestingly, this function was suggested to depend on proper D asymmetry, as D localization influences the division axis by regulating membrane tension and cell shape (Mao et al., 2011b). As no clear ortholog of D is found in mammals, Fat4 regulates OCD likely through other pathways.

Fat4 genetically interacts with the Fj homolog Fjx1 in kidney cyst formation and negatively regulates Fjx1 expression in kidneys (Saburi et al., 2008), which is similar to the relationship between Fat and Fj in *Drosophila*. This suggests that

Fat4/Dchs1/Fjx1 have functionally conserved roles in regulating PCP. There also seem to exist tissue-specific genetic interactions between different Fat cadherins: Fat1 is partially redundant to Fat4 in kidney tubule elongation and cochlea extension, while Fat3 and Fat4 synergistically regulate vertebral arch formation (Saburi et al., 2012). Therefore, at least in some tissues, different Fat cadherins can function in the same processes and possibly pathways, but the molecular mechanisms are unknown.

Fat4 also genetically interacts with the core PCP pathway. The core molecules of the Fz/PCP module are conserved in vertebrates and function in diverse planar polarized processes: Fz (FZD1-10 in humans) (Deardorff et al., 1998; Djiane et al., 2000; Wallingford et al., 2001; Wang et al., 2006b), Dsh (DVL1-3 in humans) (Sokol, 1996; Heisenberg et al., 2000; Tada and Smith, 2000; Wallingford et al., 2000; Hamblet et al., 2002), Vang (VANGL1-2 in humans) (Kibar et al., 2001; Murdoch et al., 2001; Darken et al., 2002; Goto and Keller, 2002; Jessen et al., 2002; Park and Moon, 2002), Fmi (CELSR1-3 in humans) (Curtin et al., 2003), Pk (PK1-2 in humans) (Carreira-Barbosa et al., 2003; Takeuchi et al., 2003; Veeman et al., 2003) and Dgo (Inversin/Diversin in humans) (Simons et al., 2005). Regulation of PCP in vertebrates is less understood than in *Drosophila*, but seems to similarly involve asymmetric distribution of Fz/PCP proteins, such as observed in the inner ear (Wang et al., 2005; Montcouquiol et al., 2006; Wang et al., 2006a; Wang et al., 2006b; Deans et al., 2007; Song et al., 2010). It is unclear if vertebrate Fz/PCP and Fat4/Dchs1 signaling is linked. However, loss of one copy of *Vangl2* in *Fat4* mutant mice causes more severe kidney cysts and shortened cochlea, suggesting that Fat4 and Vangl2 function in parallel pathways in these organs (Saburi et al., 2008; Saburi et al., 2012).

9.1.6 Fat4 and Hippo signaling

In contrast to its conservation in PCP signaling, it is not clear whether Fat4 is involved in mammalian Hippo signaling. The core of the Hippo pathway is highly conserved to vertebrates and consists of mammalian MST1/2 (homologs of Hpo) (Creasy and Chernoff, 1995b; Creasy and Chernoff, 1995a), Sav1 (homolog of Sav) (Tapon et al., 2002), LATS1/2 (homologs of Wts) (Tao et al., 1999; Yabuta et

al., 2000) and MOB1A/B (homologs of Mats) (Stavridi et al., 2003; Bichsel et al., 2004; Chow et al., 2010). MST1/2 and LATS1/2 form a kinase cascade to negatively regulate YAP/TAZ (homologs of Yki) through phosphorylation (Chan et al., 2005; Zhao et al., 2007; Hao et al., 2008; Lei et al., 2008; Oka et al., 2008; Zhang et al., 2008a). Active YAP/TAZ enters the nucleus and promotes expression of various genes by binding to TEAD transcription factors (homologs of Sd) (Vassilev et al., 2001; Sawada et al., 2008). Phosphorylation of YAP/TAZ by LATS1/2 creates a binding site for 14-3-3 proteins and results in cytoplasmic retention and subsequent proteasomal degradation (Kanai et al., 2000; Vassilev et al., 2001; Zhao et al., 2007; Zhao et al., 2008).

Developmental loss of core Hippo pathway proteins can also result in overgrowth, which occurs most severely in the mouse liver (Camargo et al., 2007; Dong et al., 2007). Many upstream regulators of Hippo signaling are conserved from *Drosophila* to mammals. For example, the mammalian Mer ortholog NF2 (Neurofibromatosis2), the Crb homolog CRB3 and the Kibra ortholog KIBRA/WWC1 have been shown to regulate YAP/TAZ (Varelas et al., 2010; Zhang et al., 2010; Xiao et al., 2011). It is a topic of controversy whether the mammalian Ex homologs Frmd1 and Frmd6/Willin have a conserved role in Hippo signaling. Ex and Frmd1/6 show only limited similarity, which is restricted to the FERM domain (Hamaratoglu et al., 2006). Frmd1 and Frmd6 lack an equivalent C-terminal domain and with it PPxY motifs, which in Ex are required for direct interaction with Yki (Badouel et al., 2009; Oh et al., 2009). However, as Ex also interacts with Hpo in *Drosophila* (Yu et al., 2010), the ability to interact with Mst1/2 might be conserved. Frmd1 has not been investigated, but two studies reported that human FRMD6 exhibits clear tumor suppressor properties in cultured cells. However, they found contradictory results about the ability of FRMD6 to activate the core Hippo pathway (as assessed by MST and LATS phosphorylation) and the requirement of intact Hippo signaling for FRMD6 function (Angus et al., 2012; Visser-Grieve et al., 2012). Further studies will be required to answer whether cell-type specific differences can explain this discrepancy. Interestingly, Bossuyt and colleagues suggest that the function of Ex and Fat in Hippo signaling is a novel evolutionary acquisition only in the

arthropod lineage, as this is where both proteins gained domains crucial for growth control (such as the C-terminus in Ex and the HippoN/HippoC domains in Fat) (Bossuyt et al., 2014).

Similar to Frmd6, whether Fat4 functions in vertebrate Hippo signaling is a field of controversy and active research. While a fusion protein of the Fat ECD and the Fat4 ICD rescues PCP defects in *ft* mutant flies almost entirely, it fails to rescue overgrowth and lethality (Pan et al., 2013). This suggests that PCP activity but not Hippo activity is conserved between *Drosophila* Fat and mammalian Fat4. However, initial studies of Fat4 knockdown in the chick neural tube reported increased neural progenitor proliferation and Yap activation (Van Hateren et al., 2011). In human breast cancer cell lines knockdown of FAT4 causes YAP activation and increased YAP target gene expression (Ito et al., 2015). Also in cortical development, neural proliferation and migration phenotypes caused by knockdown of Fat4 are dependent on Yap levels (Cappello et al., 2013). In contrast, *Fat4* knockout mice don't exhibit clear phenotypes that resemble Hippo signaling defects (Saburi et al., 2008; Bossuyt et al., 2014). Especially, loss of *Fat4* does not result in typical liver hyperplasia, even in a sensitized background where additionally one allele of *Nf2* is deleted (Bossuyt et al., 2014). Rather, *Fat4* knockout kidneys are smaller than wildtype kidneys (Saburi et al., 2008; Saburi et al., 2012). And although a role of Fat4 in the development of kidney tubular structures was initially suggested to depend on Yap (Das et al., 2013), the requirement of Yap in this process was later genetically tested and refuted (Bagherie-Lachidan et al., 2015). Therefore, it is still unclear if a function for Fat4 in the Hippo pathway is conserved between flies and vertebrates.

However, increasing correlative data points towards a role of FAT4 as a tumor suppressor. Missense and nonsense mutations and reduced expression of *FAT4* have been associated with multiple types of cancers. For example, recurrent *FAT4* mutations were found in pancreatic tumors (Furukawa et al., 2015), gastric cancer (Zang et al., 2012), melanoma (Nikolaev et al., 2012), ovarian tumors (Crobach et al., 2015), esophageal squamous cell carcinoma (Gao et al., 2014), colorectal cancer (Yu et al., 2015) and splenic lymphoma (Parry et al., 2013).

Also, FAT4 expression is frequently reduced in gastric cancer (Cai et al., 2015; Jung et al., 2015). In a breast cancer mouse model that exhibited decreased Fat4 expression, tumorigenesis was reduced upon re-expression of Fat4. Furthermore, *FAT4* promoter methylation is frequently found in breast cancer cell lines (Qi et al., 2009) and lung adenocarcinomas (Rauch et al., 2012). While it is unclear if a causal relationship exists between these events and tumor formation or progression, it is possible that the tumor suppressor function of Fat is conserved across species.

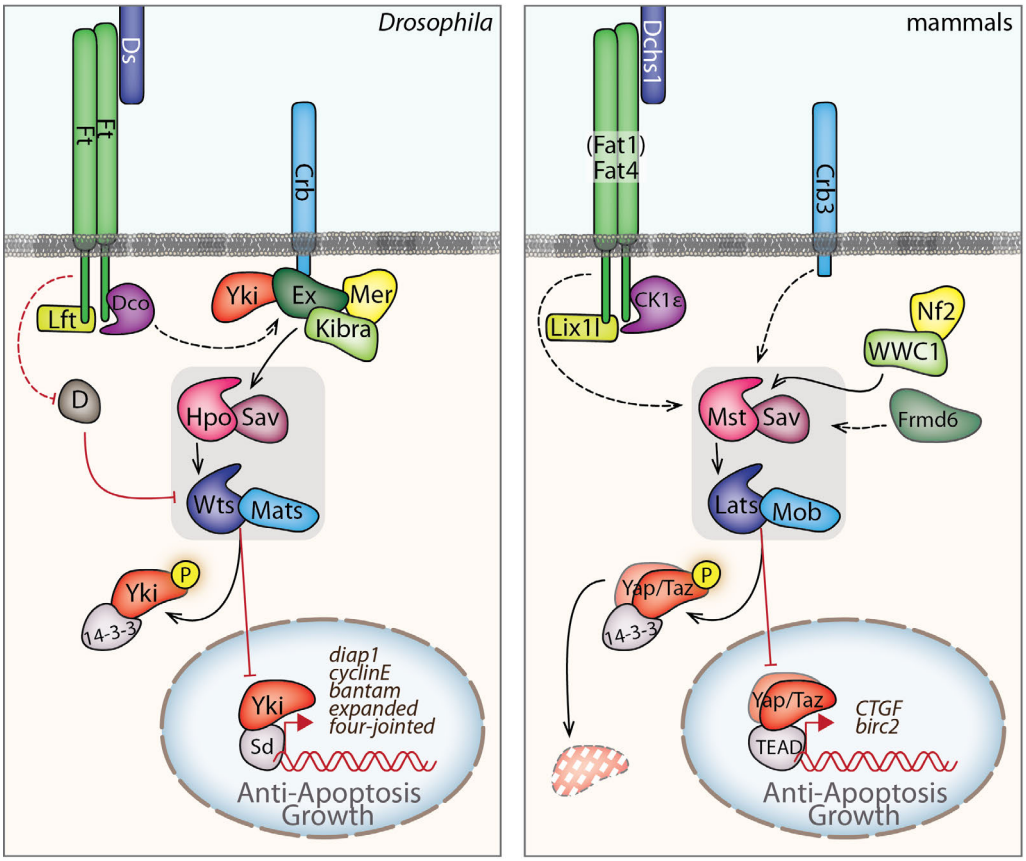

Fig 9.1 Schematic of Hippo signaling in *Drosophila* and mammals
The core Hippo pathway (grey box) is highly conserved across species, whereas the roles of many proteins functioning as upstream regulators in *Drosophila* are poorly understood in mammals. Direct molecular links between Fat/FAT4 and Hippo signaling are unknown. *Drosophila* full names/abbreviations (mammalian) shown are: Fat/Ft (FAT1-4); Dachsous/Ds (Dchs1/2); Discs-overgrown/Dco (CK1ε); Lowfat/Lft (Lix1l); Crumbs/Crb (Crb1-3); Expanded/Ex (Frmd1/6); Merlin/Mer (Nf2); Kibra (WWC1); Hippo/Hpo (Mst1/2); Salvador/Sav (Sav); Warts/Wts (Lats1/2); Mats (Mob); Yorkie/Yki (Yap/Taz); Scalloped/Sd (TEAD1-4).

9.2 Role and functions of primary cilia

In the second part of this chapter, I investigated a potential link of FAT4 and primary cilia. *Fat4* mutant mice exhibit kidney cysts, and primary cilia defects have been observed in cystic kidney tubules. I present findings of cilia and centrosome abnormalities in FAT4 knockdown cell culture systems. The following part of the introduction provides a general overview over primary cilia and the centrosome cycle.

9.2.1 Centrosome cycle

The centrosome functions as a major microtubule organizing center in animal cells and can thereby influence cell shape, polarity, motility and division (Andersen, 1999; Piel et al., 2001; Bornens, 2002; Luders and Stearns, 2007). Microtubules are nucleated at γ-tubulin ring complexes that surround the centrosome as part of the pericentriolar matrix (Zheng et al., 1995; Wiese and Zheng, 1999; Moritz et al., 2000). Cells in G1 phase have one centrosome, which consists of two centrioles. The mother centriole, marked by distal and subdistal appendages, is older and originates from before the previous cell cycle. The daughter centriole stems from the centrosome duplication step of the previous cell cycle (Chretien et al., 1997). In G1 phase, mother and daughter centrioles are loosely tethered by a proteinaceous linker composed of structural and fibrous proteins attached to the proximal end of both centrioles, which keeps them in close proximity (Paintrand et al., 1992; Fuller et al., 1995; Fry et al., 1998). Cells in G1 phase or in cell cycle arrest (G0) can initiate ciliogenesis, which requires the mother centriole to form the basal body as a structural platform for cilium assembly (Cohen et al., 1988). As cells proceed to S phase, a new centriole forms adjacent to each existing centriole, thereby duplicating the centrosome (Cohen et al., 1988). Initially, a short procentriole orthogonal to each centriole is synthesized, which elongates during S and G2 phase and is tightly linked to the cell cycle (Hinchcliffe et al., 1999; Meraldi et al., 1999). Procentrioles remain tightly linked (“engaged”) to the centrioles until their disengagement during cytokinesis (Piel et al., 2001). This is thought to be crucial for limiting centrosome duplication to once per cell cycle and providing a licensing mechanism for a new round of centriole duplication after mitosis (Tsou and

Stearns, 2006). The original daughter centriole fully matures previous to mitosis, which includes acquisition of distal and subdistal appendages that are important for microtubule anchoring and ciliogenesis (Paintrand et al., 1992). In G2 phase, the centriolar linker (also called centrosomal linker, as it connects the duplicated centrosome in the late cell cycle) is disassembled to allow the two centrosomes to separate and prepare mitotic spindle assembly. Linker disassembly is regulated by NEK2, a NIMA-family kinase localizing to centrioles only in S/G2 phase that directly phosphorylates several linker components (Fry et al., 1998; Helps et al., 2000; Bahe et al., 2005; Yin et al., 2013). Centrosome-nucleated microtubules are involved in mitotic spindle formation and chromosome segregation during M-phase. During cytokinesis, each daughter cell inherits one centrosome consisting of a mature mother and a new daughter centriole.

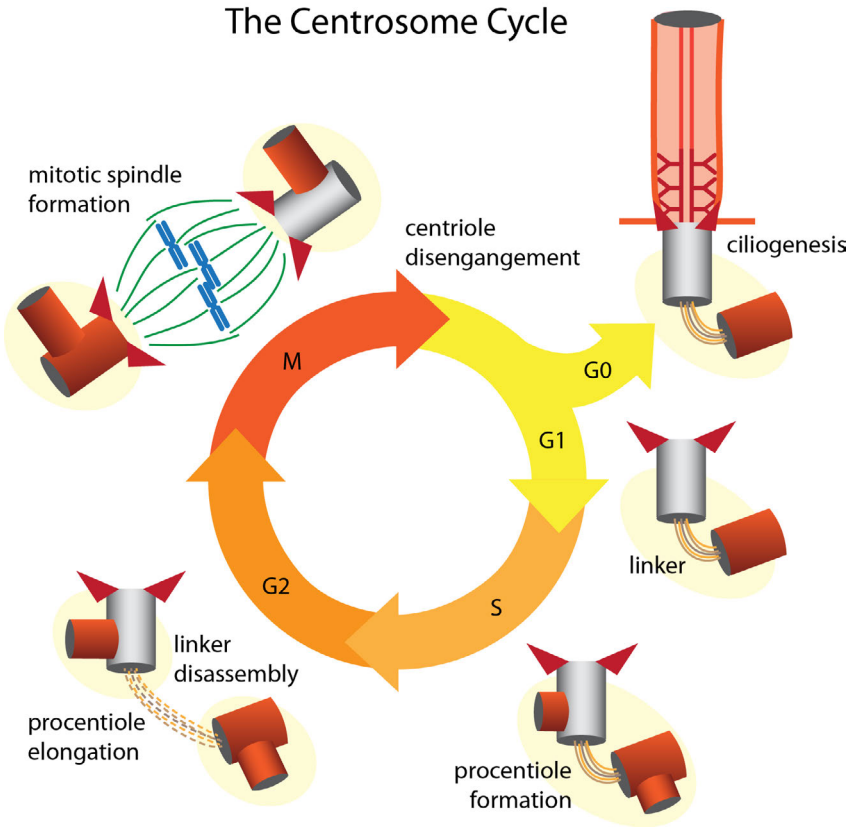

Fig 9.2 The centrosome cycle
Schematic of centrosome changes throughout the cell cycle. Mother centriole shown in grey, daughter centriole and developing procentrioles (S, G2, M phase) are in orange. Centrosome appendages mark the mother centriole and the fully matured daughter centriole (shown as red triangles).

9.2.2 Cilia are highly organized microtubule-based structures

Cilia are found in specialized cell types in invertebrates (in *Drosophila* only in sperm and sensory neurons) and in almost all vertebrate cell types. Cilia perform a wide variety of crucial functions during development and adult homeostasis and cilia malfunctions can cause diverse disorders collectively named ciliopathies (reviewed in (Hildebrandt et al., 2011)). Cilia can be grouped into motile and non-motile or primary cilia. Motile cilia are important for generating surface flow in different organs (such as airway epithelia and brain ventricles) and for the motility of sperm. Crucially, specialized cilia in the node of early embryos create directional flow that initiates left-right asymmetry (Nonaka et al., 1998; Nonaka et al., 2002; McGrath et al., 2003). This explains why some ciliopathies cause *situs inversus*, a condition where the position of visceral organs in the body is left-right reversed (Afzelius, 1976; Nonaka et al., 2002). Primary cilia are non-motile and primarily perform sensory and signaling functions.

Cilia are highly specialized microtubule-based organelles protruding from the cell surface. The ciliary skeletal structure, the axoneme, consists of nine microtubule doublets organized in a ring. Most motile cilia have an additional microtubule doublet in the center (9+2 formation) important for ciliary beating, which is absent in primary cilia (9+0 formation). The axonemal microtubules emerge from the nine microtubule triplets of the mother centriole, which docks to the plasma membrane during ciliogenesis and forms the basal body (Cohen et al., 1988). The basal body connects to the periciliary membrane through transition fibers, likely the equivalent of centriolar distal appendages (Anderson, 1972). Distal appendage/transition fiber composition is not fully elucidated but contains Cep164, Cep89 and CCDC41, which are all crucial for basal body docking to the membrane and the early steps of ciliogenesis (Graser et al., 2007a; Sillibourne et al., 2013; Tanos et al., 2013). Transition fibers are part of the junction between the basal body and ciliary axoneme referred to as the transition zone. In a poorly understood manner, the transition zone serves as a gate to regulate passage of proteins trafficking in and out of the cilium (Garcia-Gonzalo et al., 2011; Williams et al., 2011; Chih et al., 2012).

Several proteins associated with multiple ciliopathies are part of the transition zone (reviewed in (van Reeuwijk et al., 2011)). Based on interprotein-interactions, they can be grouped into two modules: The NPHP module contains proteins of the NPHP family, including NPHP1, 2, 4 and 8, which are encoded by genes frequently mutated in the ciliopathy nephronophthisis (Winkelbauer et al., 2005; Fliegauf et al., 2006; Sang et al., 2011). The MKS/JBTS module similarly contains products of genes linked to Meckel syndrome and Joubert syndrome, such as the transmembrane proteins Meckelin/TMEM67, MKS1 and the tectonic complex (Dowdle et al., 2011; Garcia-Gonzalo et al., 2011; Sang et al., 2011; Chih et al., 2012). Both modules appear to cooperatively regulate transition zone formation, ciliogenesis and cilium function (Williams et al., 2008; Williams et al., 2010; Garcia-Gonzalo et al., 2011; Williams et al., 2011). Nephronophthisis primarily manifests in kidney cyst formation, and Meckel syndrome and Joubert syndrome are associated with kidney, brain and limb defects, which emphasizes that cilia in different organs exhibit differential sensitivities to functional loss of transition zone components (Tobin and Beales, 2009; Hildebrandt et al., 2011).

No proteins can be synthesized within the cilium, therefore all necessary components must be transported to the cilium. Active ciliary import and export is mediated by the intraflagellar transport (IFT) system, which plays important roles in cilium formation and maintenance (Kozminski et al., 1993; Pazour et al., 1998; Marshall and Rosenbaum, 2001; Qin et al., 2004). IFT is microtubule-based and is executed by several IFT proteins that associate with kinesin-2 for anterograde (microtubule plus-end directed) transport of cargo into the cilium, and dynein-2 for retrograde (microtubule minus-end directed) transport out of the cilium (Kozminski et al., 1995; Pazour et al., 1999; Porter et al., 1999; Signor et al., 1999).

9.2.3 Cilia as signaling centers

Cilia also serve important functions as signaling centers. Best understood is a crucial function in Hedgehog (Hh) signaling, which occurs mainly at the cilium. In the absence of Hh, the Hh receptor Patched-1 (Ptch1) localizes to the ciliary membrane and is thought to block entry of the transmembrane protein

Smoothened (Smo) and Gli transcription factors (Gli2/3) into the cilium. Suppressor of Fused (SuFu), a negative regulator of Glis, also localizes to the cilium. Glis are thought to accumulate at the ciliary base and be cleaved into their repressor form. Upon binding of Hh, Ptch1 no longer inhibits Smo, which accumulates in the cilium and in turn inhibits Sufu. Glis are enriched at the ciliary tip and activated into their transcriptional activator form. Retrograde IFT transports activated Glis out of the cilium to allow them to translocate into the nucleus (Huangfu et al., 2003; Corbit et al., 2005; Liu et al., 2005; May et al., 2005; Rohatgi et al., 2007; Ocbina and Anderson, 2008).

Cilia and cilia-associated proteins have also been implicated in canonical and non-canonical (PCP) Wnt signaling and vice versa. However this remains a controversial topic. Canonical Wnt signaling refers to the regulation of stability and transcriptional activity of ß-catenin through Fz and Dvl. Wnt activates Fz and Dvl, which results in inhibition of the ß-catenin destruction complex and allows ß-catenin to enter the nucleus and function as a transcriptional coactivator (MacDonald et al., 2009). Several studies indicate that cilia or components of cilia restrict canonical Wnt signaling, and that Wnt signaling is frequently hyperactive when cilia are disturbed (Gerdes et al., 2007; Corbit et al., 2008; Jonassen et al., 2008; Voronina et al., 2009; McDermott et al., 2010). However, this was not found consistently, indicating tissue or protein specific requirements (Ocbina et al., 2009; Wallingford and Mitchell, 2011). PCP components (such as Dvl and Vangl2) are important for basal body positioning and orientation and directional ciliary beating (Park et al., 2008; Mitchell et al., 2009; Guirao et al., 2010; Hashimoto et al., 2010; Song et al., 2010; Tissir et al., 2010; Boutin et al., 2014). Also, loss of Fz, Dvl, Celrs2/3 and Prickle causes cilia defects in different model systems, apparently due to defective docking of the basal body to the membrane (Oishi et al., 2006; Park et al., 2008; Oteiza et al., 2010; Tissir et al., 2010). Several PCP-associated proteins have been reported to localize to the cilium or basal body, such as NPHP2/Inversin, Dvl, Vangl2 and the PCP effector WD40/Fritz (Otto et al., 2003; Ross et al., 2005; Simons et al., 2005; Kim et al., 2010). Further, loss of the ciliopathy proteins BBS1/4/6 or Ofd1 causes PCP-like phenotypes such as convergent extension defects in different

systems (Ross et al., 2005; Ferrante et al., 2009). However, the underlying mechanisms are unknown and as the PCP modules are thought to mainly function by asymmetric membrane association, it is still unclear how cilia fit in as PCP signaling platforms.

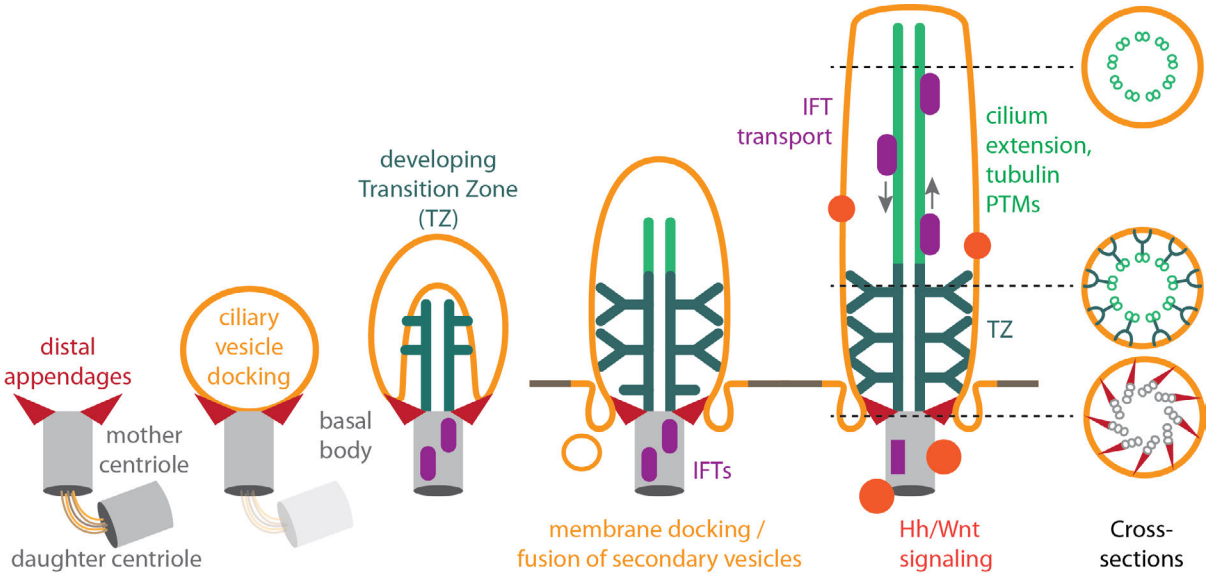

Fig 9.3 Overview of ciliogenesis and mature primary cilium
Simplified schematic illustrates the formation of a primary cilium (from left to right). IFT = intraflagellar transport; TZ = transition zone; PTMs = post-translational modifications.

9.2.4 Ciliogenesis

Ciliogenesis starts with the interaction of the mother centriole with the Golgi-derived ciliary vesicle through distal appendages (Sorokin, 1962; Sorokin, 1968). Subsequently, microtubules anchored at the mother centriole grow out into the ciliary vesicle, which invaginates and envelopes the growing axoneme in form of a double sheath. Secondary vesicles are thought to expand the sheath through fusion (Sorokin, 1962). Depending on the cell type, the mother centriole docks at the plasma membrane during early or late ciliogenesis, where the ciliary membrane fuses with the plasma membrane (Sorokin, 1962; Sorokin, 1968; Cohen et al., 1988). The outer sheath membrane which originated from the ciliary vesicle gives rise to the periciliary membrane at the intersection of plasma membrane and ciliary membrane and continues to serve as a vesicular docking site (Peters et al., 1983; Papermaster et al., 1985). Vesicle trafficking is therefore

an important requirement for different steps of ciliogenesis, from early onset to ciliary elongation and cilium maintenance. Accordingly, several molecules involved in vesicle formation, targeting and fusion have been identified to be critically required for ciliogenesis, such as the Rab GTPases Rab8 and Rab11, the membrane shaping proteins EHD1 and EHD3, components of the exocyst, as well as budding and fusion proteins AP-1, Clathrin and SNAREs (Nachury et al., 2007; Yoshimura et al., 2007; Mazelova et al., 2009; Zuo et al., 2009; Kaplan et al., 2010; Knodler et al., 2010; Westlake et al., 2011; Lu et al., 2015). Most cargo vesicles stem from the Golgi apparatus (GA), and some proteins involved in ciliary transport localize to both GA and cilium, such as IFT20 (Follit et al., 2006; Nachury et al., 2007; Kim et al., 2014b).

The base of the axoneme is structurally distinct and develops into the transition zone, which marks the transition of mother centriole triplet microtubules to axonemal doublets (Rosenbaum and Child, 1967; Boisvieux-Ulrich et al., 1989). It is characterized by Y-shaped linker structures (as observed in electron microscopy), which connect the microtubule doublets to the enveloping membrane (Gilula and Satir, 1972). In *Chlamydomonas* and *Caenorhabditis elegans* IFT is crucial for cilium elongation but not formation of the transition zone, suggesting that the earliest stages of ciliogenesis do not critically depend on IFT (Perkins et al., 1986; Brazelton et al., 2001; Williams et al., 2011). Interestingly, some transition zone proteins are required for successful migration and docking of the basal body and ciliary vesicle to the membrane, indicating that these proteins are recruited and functioning at very early stages of ciliogenesis (Dawe et al., 2007; Dawe et al., 2009). Besides IFT, also the biochemical properties of the axoneme are involved in cilium elongation and length regulation. Post-translational tubulin modifications commonly found in cilia are acetylation, glutamylation, detyrosination and glycylation, which stabilize microtubules and influence kinesin-mediated transport (Westermann and Weber, 2003; Pathak et al., 2007; Verhey and Gaertig, 2007; Sirajuddin et al., 2014). Cilia are highly dynamic structures, which seem to achieve a steady-state by incorporating new proteins at the same rate as disassembly occurs (Stephens, 1997; Marshall and Rosenbaum, 2001). Altering this equilibrium, such as by

blocking anterograde transport or increasing the available pool of soluble tubulin, subsequently shortens or lengthens cilia, respectively (Stephens, 1997; Sharma et al., 2011; Wang et al., 2013). Interestingly, ciliary length control can also occur through regulation of the IFT cargo load capacity (Pan and Snell, 2014).

9.2.5 Cilium disassembly

Cilium disassembly is much less understood than cilium formation. The resorption of cilia is coordinated with the cell cycle and occurs prior to mitosis, which allows the mother centriole to participate in mitotic spindle formation. In cell culture, re-entry into the cell cycle from G0 by serum treatment causes activation of Human Enhancer of Filamentation 1 (HEF1) and Aurora A kinase, which in turn activates the histone deacetylase HDAC6 (Pugacheva et al., 2007). Activation of HDAC6 by Aurora A or other signaling branches leads to deacetylation of acetylated ciliary microtubules and ultimately cilium disassembly (Pugacheva et al., 2007; Kinzel et al., 2010; Lee et al., 2012). An HDAC6-independent mechanism of cilium resorption has also been identified, which depends on shifting the balance of cilium assembly/disassembly towards disassembly (Kobayashi et al., 2011; Spalluto et al., 2012; Kim et al., 2015). An open question remains whether cilia have regulatory roles in cell cycle progression. Interestingly, Nde1 depletion causes longer cilia and a concomitant delay in cell cycle re-entry. As this delay seems to correlate with the length of the cilium, an appealing hypothesis is that cilia disassembly is a limiting checkpoint for cell cycle re-entry (Kim et al., 2011).

9.2.6 Ciliary gating and control of composition

Fluorescence recovery after photobleaching (FRAP) studies in cell culture indicate that ciliary membrane composition is regulated, as several proteins were found to neither enter nor exit the cilium despite being mobile within the ciliary membrane (Hu et al., 2010). Additionally, free diffusion into the cilium of soluble proteins appears to be size-dependent, with limited or inhibited entry for large molecules (Kee et al., 2012; Breslow et al., 2013; Lin et al., 2013). This

indicates that a diffusion barrier at the base of the cilium controls the content of the ciliary membrane and lumen. Different mechanisms that might promote compartmentalization of the cilium have been suggested, such as a physical barrier of transition fibers and the ciliary necklace, a structure characterized by intramembraneous particles visible in freeze-fracture electron microscopy (Gilula and Satir, 1972; Menco, 1980; Fisch and Dupuis-Williams, 2011). Loss of transition zone proteins can result in enrichment or loss of ciliary proteins, indicating that the transition zone normally restricts these molecules from entry or exit of the cilium (Garcia-Gonzalo et al., 2011; Chih et al., 2012). Furthermore, the base of the ciliary membrane has a distinct lipid composition, possibly controlling diffusion of membrane proteins (Vieira et al., 2006). Interestingly, the ciliary import machinery is reminiscent of nuclear import and cilia contain Importin-beta proteins, which are known regulators of nucleo-cytoplasmic trafficking (Fan et al., 2007; Hurd et al., 2011). Importin-beta is required for ciliary import of certain proteins, such as the kinesin KIF17, which contain a motif similar to nuclear localization sequences (Dishinger et al., 2010; Hurd et al., 2011). Additionally, some nuclear pore components have been reported to localize at the ciliary base (Kee et al., 2012). These findings suggest that selective transport into cilia might occur by similar means and in analogy to nuclear import.

Another barrier structure at the ciliary base was proposed to be composed of Septins. Septins are GTPases that can assemble into macromolecules and form filaments and rings, well known to mediate compartmentalization processes in yeast (Barral et al., 2000; Takizawa et al., 2000). In mammalian cells, Septins are implicated in creating barriers at the midbody, dendritic spines or the sperm flagellum (Cesario and Bartles, 1994; Schmidt and Nichols, 2004; Ihara et al., 2005; Xie et al., 2007; Estey et al., 2010). In the sperm flagellum, which is a specialized cilium, loss of Septins causes mislocalization of flagellar proteins and motility defects that result in infertility in mice (Ihara et al., 2005; Kissel et al., 2005; Steels et al., 2007; Kwitny et al., 2010). In *Xenopus*, Septin2 and Septin7 are required for cilia of the embryonic epidermis and are regulated by the cilia-localized PCP effector Wdpcp/Fritz (Kim et al., 2010). In *Xenopus* embryos and

different mammalian cell cultures, Septins localize to the base of the cilium in a ring-like structure (Hu et al., 2010; Kim et al., 2010) or along the ciliary axoneme (Ghossoub et al., 2013). Knockdown of Septin2 results in reduction of overall ciliation, where remaining cilia are short and show increased diffusion of membrane components between ciliary and periciliary membrane (Hu et al., 2010). Part of this barrier function of Septin2 seems to be due to its function in localizing the B9 transition zone complex (Chih et al., 2012). Therefore, it remains to be investigated whether Septins form a ring-like structure that itself restricts ciliary membrane diffusion or if Septins serve as scaffolds for other factors. In summary, ciliary gating is based on several, potentially independent, mechanisms that ensure a highly regulated composition of the ciliary membrane and lumen, with critical implications for the ciliary structure and cilium-based signaling.

10 Abstract Chapter B

In the past, several approaches have been performed in our lab to understand the role of mammalian Fat4 during development. While *Fat4* mutant mice show phenotypes attributed to defective PCP, these mice have no obvious growth defects and it is unclear if Fat4 plays a role in Hippo signaling (Saburi et al., 2008; Mao et al., 2011a; Saburi et al., 2012; Zakaria et al., 2014). *Fat4* mutant mice die at birth, emphasizing important developmental functions of Fat4 (Saburi et al., 2008). Frequently, these mice exhibit kidney cysts, craniofacial and brain abnormalities and cochlea defects (Saburi et al., 2008; Mao et al., 2011a; Saburi et al., 2012). However, we understand little about the molecular mechanisms underlying these phenotypes. A major problem is our lack of knowledge of Fat4 interactors that could provide links to the physiological processes in which Fat4 is involved. Another issue is that Fat4 is an extremely large protein (540kDa), which poses a challenge for biochemical studies, and few molecular and cell culture tools have been established to study Fat4. To tackle this problem, we decided to define novel FAT4 interactors using proteomic approaches, establish cell culture systems for FAT4 overexpression or depletion and optimize FAT4 detection and immunoprecipitation, which I will summarize in this chapter.

11 Results Chapter B

11.1 Establishment of FAT4 interactomes and cell culture tools

11.1.1 BioID reveals novel candidate interactors of FAT4

In an effort to identify interactors of human FAT4, a former student, Nicole Liscio, performed proximity-dependent biotin identification (BioID) (Roux et al., 2012) in collaboration with Dr. Brian Raught's lab. BioID is a mass spectrometry-based approach especially suitable for investigating less soluble proteins (such as transmembrane proteins) and weak interactions. The modified *Escherichia Coli* promiscuous biotin ligase BirA* (BirA 118G mutation) fused to the bait of interest serves to biotin-label direct interactors and proteins in close vicinity (~10nm radius (Kim et al., 2014a)), here referred to as "proximity interactors". High-affinity Streptavidin pulldowns allow the retrieval of biotinylated prey under harsher conditions than conventional AP-MS, where protein-protein interactions need to be preserved (see Fig. 11.1 for a BioID schematic).

BioID was performed from HEK293T cells stably expressing full-length human FAT4 C-terminally tagged with BirA*-Flag and processed on a high-sensitivity Q Exactive HF hybrid quadrupole-Orbitrap (QEHF) mass spectrometer. The BioID revealed a list of FAT4 proximity interactors that include many transmembrane and membrane-associated proteins, junctional and cytoskeleton-associated proteins, members of major signaling pathways, regulators of apical-basal polarity, as well as PCP associated proteins (Table 11.1). GO-term analysis of all hits (SAINT scores ≥ 0.85) indicates significant enrichment of biological processes related to cellular junctions, polarity and adhesion (Fig. 11.2).

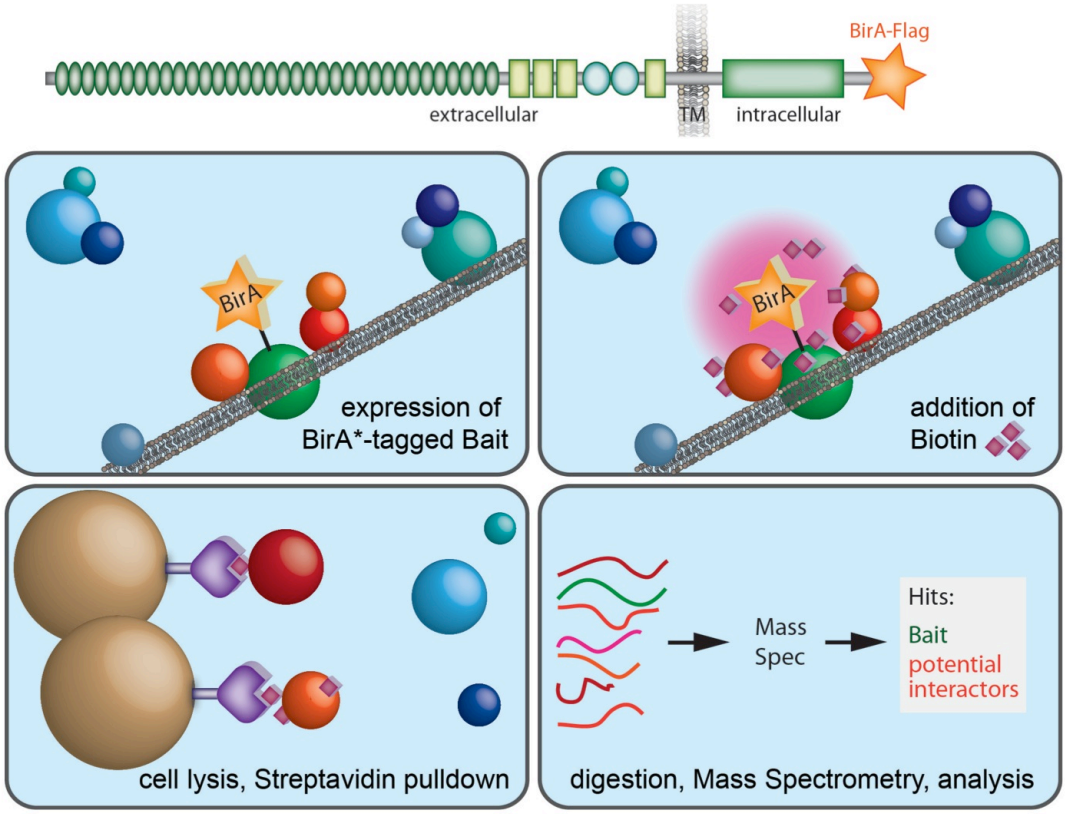

Fig 11.1 Schematic of FAT4 BioID.
The modified promiscuous biotin ligase BirA* is fused to full-length FAT4 at its C-terminus (intracellular domain), and the fusion protein is expressed in HEK293 cells. Upon treatment with biotin in the cell culture medium, BirA* promotes biotinylation of direct interactors and proteins in close proximity. Biotinylated proteins (representing the close molecular environment of the bait) are purified using a high-affinity streptavidin pulldown, trypsin-digested and subjected to mass spectrometry.

Amongst the top six molecular functions in GO terms of FAT4 proximity interactors are cell adhesion molecule binding, cadherin binding, receptor tyrosine kinase (RTK) binding and structural constituent of cytoskeleton. An enrichment of solute carrier proteins (leading to the significant GO-term enrichment "amino acid transmembrane transporter activity") is likely not specific to FAT4, as solute carriers are integral membrane proteins frequently found with transmembrane baits (see also Discussion). To summarize, FAT4 proximity interactors are frequently involved in cell junctions and adhesion, in agreement with the putative roles of FAT4 itself. Links to signaling molecules and receptors, such as RTKs, could explain some of the fundamental roles of FAT4 in morphogenetic processes during development.

Table 11.1 FAT4 BioID (QEHF) in HEK293 cells
(Hits (SAINT > 0.83) with average peptide numbers > 4.5 are shown; full list is shown in Appendix Table 13.1). Known FAT4 interactors LIX1L and MPDZ are highlighted.

FAT4 BioID (QEHF) HEK293 cells					
Gene Name	Full name	Top 2 negative controls		FAT4: Average over 4 replicates	SAINT
FAT4	*FAT atypical cadherin 4*			1154	NA
birA	*E.Coli biotin ligase*	1919	1748	768.25	NA
UTRN	*utrophin*	36	36	159.75	1.00
DLG1	*discs large homolog 1*	31	28	137	1.00
ERBB2IP	*erbb2 interacting protein*	32	30	136.5	1.00
SCRIB	*scribbled planar cell polarity protein*	24	21	133.5	1.00
DSG2	*desmoglein 2*	20	15	126.5	1.00
SEPT7	*septin 7*	28	25	103.25	1.00
GPRIN1	*G protein regulated inducer of neurite outgrowth 1*	5	4	93	1.00
ANK3	*ankyrin 3, node of Ranvier (ankyrin G)*	21	21	90	1.00
ACTB	*actin, beta*			56.25	1.00
CTNND1	*catenin delta 1*	10	9	55.75	1.00
AHCTF1	*AT-hook containing transcription factor 1*	18	14	55.25	1.00
NUMB	*numb homolog (Drosophila)*	9	8	54.5	1.00
EPB41L1	*erythrocyte membrane protein band 4.1-like 1*	5	4	46.25	1.00
JUP	*junction plakoglobin*	10	9	45.75	1.00
VANGL1	*VANGL planar cell polarity protein 1*	2	2	43.75	1.00
NEFM	*neurofilament, medium polypeptide*			43.25	1.00
JPH1	*junctophilin 1*	3		38.5	1.00
MYO1B	*myosin IB*	7	6	38.5	1.00
HMGN2	*high mobility group nucleosomal binding domain 2*			38	1.00
EEF1A2	*eukaryotic translation elongation factor 1 alpha 2*	8	7	36	1.00
ZDHHC5	*zinc finger, DHHC-type containing 5*			34.25	1.00
MARK2	*microtubule affinity regulating kinase 2*	3		31.75	1.00
SPTAN1	*spectrin alpha, non-erythrocytic 1*	6	5	29.25	1.00
VANGL2	*VANGL planar cell polarity protein 2*			26.5	1.00
MAP4K4	*mitogen-activated protein kinase kinase kinase kinase 4*			26.25	1.00
PALM	*paralemmin*	8	5	25.75	1.00
BAIAP2	*BAI1 associated protein 2*	6	4	24.25	1.00
BAIAP2L1	*BAI1 associated protein 2 like 1*	4	4	24	1.00
PPFIBP1	*PPFIA binding protein 1*	2		23.75	1.00
MARK3	*microtubule affinity regulating kinase 3*	5		22.75	0.98
WDR6	*WD repeat domain 6*	5	2	22.25	1.00
SLC25A4	*solute carrier family 25 (mitochondrial carrier; adenine nucleotide translocator), member 4*	6	4	22	0.96
EPB41L5	*erythrocyte membrane protein band 4.1 like 5*	4	3	21.75	1.00
SNAP23	*synaptosome associated protein 23kDa*	7	7	21.75	0.97
SEPT8	*septin 8*	4	3	20.25	1.00
FLNC	*filamin C*			19.5	1.00
DLG5	*discs large homolog 5*			19	1.00
PEAK1	*pseudopodium enriched atypical kinase 1*	6	5	18.75	0.95
USP6NL	*USP6 N-terminal like*			18.5	1.00
NEFL	*neurofilament, light polypeptide*			17.75	1.00
SLC3A2	*solute carrier family 3 (amino acid transporter heavy chain), member 2*			17	1.00
HSPB1	*heat shock protein family B (small) member 1*			16	1.00
NOTCH2	*notch 2*	3		16	0.99
PLEKHA5	*pleckstrin homology domain containing A5*	4	4	15.75	0.97
LIX1L	*limb and CNS expressed 1 like*			15.5	1.00
KIDINS220	*kinase D-interacting substrate 220kDa*			15.25	1.00
LSR	*lipolysis stimulated lipoprotein receptor*	2		15.25	1.00
GORASP2	*golgi reassembly stacking protein 2*	4	3	14.75	0.99
DTNA	*dystrobrevin alpha*	4	3	14.25	0.98

FAT4 BioID (QEHF) HEK293 cells				FAT4:	
Gene Name	Full name	Top 2 negative controls		Average over 4 replicates	SAINT
SLITRK5	*SLIT and NTRK like family member 5*			14	**1.00**
SNTB2	*syntrophin beta 2*	5	3	14	**0.94**
NF2	*neurofibromin 2 (merlin)*	2		13	**1.00**
MPP7	*membrane protein, palmitoylated 7*	2		12.75	**0.99**
KIAA1522	*KIAA1522*			12.5	**1.00**
IDH2	*isocitrate dehydrogenase 2 (NADP+), mitochondrial*			12.25	**1.00**
CC2D1A	*coiled-coil and C2 domain containing 1A*	4	3	12.25	**0.85**
DSC2	*desmocollin 2*			11	**1.00**
FAM171B	*family with sequence similarity 171 member B*			11	**1.00**
CXADR	*coxsackie virus and adenovirus receptor*			10.75	**1.00**
EIF3CL	*eukaryotic translation initiation factor 3 subunit C-like*			10.75	**1.00**
STEAP3	*STEAP3 metalloreductase*			10.75	**1.00**
TOR1AIP1	*torsin 1A interacting protein 1*	2		10.75	**0.99**
TRIP6	*thyroid hormone receptor interactor 6*	3		10.75	**0.89**
PVRL2	*nectin cell adhesion molecule 2*			10.5	**1.00**
SEPT10	*septin 10*			10.25	**1.00**
TECR	*trans-2,3-enoyl-CoA reductase*	2		10	**0.98**
BRIX1	*BRX1, biogenesis of ribosomes*	2	2	10	**0.96**
ATP2B4	*ATPase plasma membrane Ca2+ transporting 4*			9.75	**1.00**
NISCH	*nischarin*			9.75	**1.00**
PTPN14	*protein tyrosine phosphatase, non-receptor type 14*			9.75	**1.00**
RAB10	*RAB10, member RAS oncogene family*			9.75	**1.00**
STX5	*syntaxin 5*	3		9.75	**0.89**
MINK1	*misshapen-like kinase 1*			9.5	**1.00**
PVRL3	*nectin cell adhesion molecule 3*			9.5	**1.00**
TP53	*tumor protein p53*	3		9.5	**0.87**
LOC100505818	*LOC100505818*			9.25	**1.00**
PDLIM4	*PDZ and LIM domain 4*			9.25	**1.00**
EGFR	*epidermal growth factor receptor*			9	**1.00**
LRRC1	*leucine rich repeat containing 1*			9	**1.00**
SLC12A2	*solute carrier family 12 (sodium/potassium/chloride transporter), member 2*			8.75	**1.00**
CTNNB1	*catenin beta 1*	2		8.75	**0.96**
LLGL1	*lethal giant larvae homolog 1 (Drosophila)*	2	2	8.75	**0.85**
CTNNAL1	*catenin alpha-like 1*			8.25	**1.00**
EHD1	*EH domain containing 1*			8.25	**1.00**
OCLN	*occludin*	2		8.25	**0.95**
PPFIA1	*PTPRF interacting protein alpha 1*			8	**1.00**
RASAL2	*RAS protein activator like 2*			8	**1.00**
APC	*adenomatous polyposis coli*			7.75	**1.00**
PIK3R2	*phosphoinositide-3-kinase regulatory subunit 2*			7.75	**1.00**
PKP4	*plakophilin 4*			7.75	**1.00**
CDCA3	*cell division cycle associated 3*			7.5	**1.00**
SEPT5	*septin 5*			7.5	**1.00**
PYCR1	*pyrroline-5-carboxylate reductase 1*			7.25	**1.00**
RAB35	*RAB35, member RAS oncogene family*			7.25	**1.00**
ADCY9	*adenylate cyclase 9*			7	**1.00**
ALDH1B1	*aldehyde dehydrogenase 1 family member B1*			6.75	**1.00**
CDC42EP4	*CDC42 effector protein 4*			6.5	**1.00**
FAM171A2	*family with sequence similarity 171 member A2*			6.5	**1.00**
PTMA	*prothymosin, alpha*			6.5	**1.00**
UNC13B	*unc-13 homolog B (C. elegans)*			6.25	**1.00**
KDELR1	*KDEL endoplasmic reticulum protein retention receptor 1*	2		6.25	**0.84**
GPRIN3	*GPRIN family member 3*			6	**1.00**
GSK3B	*glycogen synthase kinase 3 beta*			6	**1.00**
SLC38A2	*solute carrier family 38 member 2*			6	**1.00**
SMPD4	*sphingomyelin phosphodiesterase 4*			6	**1.00**

FAT4 BioID (QEHF) HEK293 cells				
Gene Name	**Full name**	**Top 2 negative controls**	**FAT4: Average over 4 replicates**	**SAINT**
LPHN2	*adhesion G protein-coupled receptor L2*		5.75	**1.00**
PAG1	*phosphoprotein membrane anchor with glycosphingolipid microdomains 1*		5.75	**1.00**
PSD3	*pleckstrin and Sec7 domain containing 3*		5.75	**1.00**
SLC7A5	*solute carrier family 7 (amino acid transporter light chain, L system), member 5*		5.75	**1.00**
NHSL1	*NHS like 1*		5.5	**1.00**
PLCH1	*phospholipase C eta 1*		5.5	**1.00**
RAP1A	*RAP1A, member of RAS oncogene family*		5.5	**1.00**
ARL6IP5	*ADP ribosylation factor like GTPase 6 interacting protein 5*		5.25	**1.00**
ZDHHC8	*zinc finger, DHHC-type containing 8*		5.25	**1.00**
NOS1AP	*nitric oxide synthase 1 adaptor protein*		5	**1.00**
PIK3R1	*phosphoinositide-3-kinase regulatory subunit 1*		5	**1.00**
CDKAL1	*CDK5 regulatory subunit associated protein 1 like 1*		4.75	**1.00**
FAF2	*Fas associated factor family member 2*		4.75	**1.00**
OAT	*ornithine aminotransferase*		4.75	**1.00**
RAB3D	*RAB3D, member RAS oncogene family*		4.75	**1.00**
SEPT3	*septin 3*		4.75	**1.00**
MPDZ	*multiple PDZ domain protein*		4.75	**0.98**

FAT4 BioID (QEHF) – ENRICHR GO term analysis (molecular function)

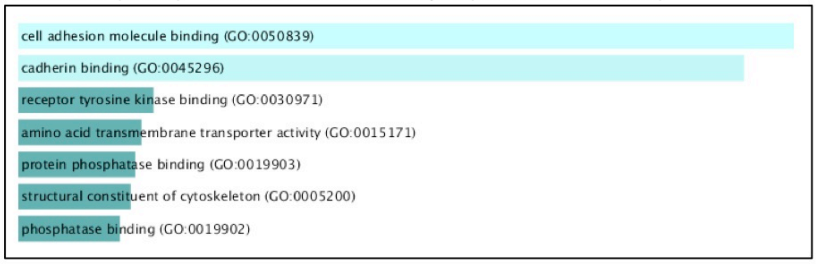

GO Term	GO Overlap	P-value	Combined Score	Genes
cell adhesion molecule binding (GO:0050839)	15/168	6.07E-09	30.56	GSK3B;CXADR;JUP;CTNND1;ANK3;EGFR;NISCH;ERBB2IP;APC;NUMB;CTNNB1;UTRN;PVRL3;CTNNAL1;PVRL2
cadherin binding (GO:0045296)	7/27	1.40E-07	28.93	JUP;APC;CTNND1;NUMB;CTNNB1;ANK3;CTNNAL1
receptor tyrosine kinase binding (GO:0030971)	5/42	2.54E-04	9.63	PIK3R2;FRS2;PIK3R1;TP53;PTPN14
amino acid transmembrane transporter activity (GO:0015171)	6/66	2.37E-04	9.24	SLC25A15;SLC7A5;SLC38A1;SLC6A8;SLC3A2;SLC38A2
protein phosphatase binding (GO:0019903)	7/94	2.27E-04	9.03	JUP;ERBB2;ATP2B4;CTNNB1;PIK3R1;TP53;EGFR
structural constituent of cytoskeleton (GO:0005200)	7/100	3.24E-04	8.88	ERBB2IP;NEFL;NEFM;TLN2;ANK3;SPTAN1;ACTB
phosphatase binding (GO:0019902)	8/136	3.72E-04	8.53	DLG1;JUP;ERBB2;ATP2B4;CTNNB1;PIK3R1;TP53;EGFR

FAT4 BioID (QEHF) – ENRICHR GO term analysis (biological process)

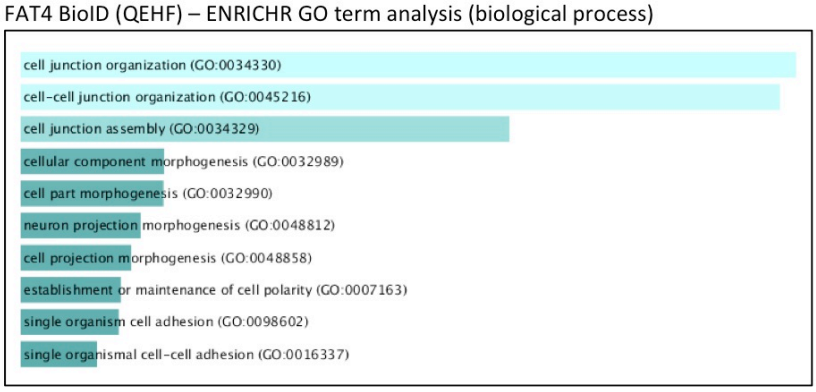

GO Term	GO Overlap	P-value	Combined Score	Genes
cell junction organization (GO:0034330)	19/189	8.59E-12	42.17	CXADR;JUP;CTNND1;INADL;MPP7;ACTB;DLG1;OCLN;APC;DLG5;TRIP6;NUMB;CTNNB1;PKP4;NF2;FLNC;TLN2;PVRL3;PVRL2
cell-cell junction organization (GO:0045216)	18/161	6.17E-12	41.69	CXADR;JUP;CTNND1;INADL;MPP7;ACTB;DLG1;OCLN;APC;DLG5;TRIP6;NUMB;CTNNB1;PKP4;NF2;TLN2;PVRL3;PVRL2
cell junction assembly (GO:0034329)	16/160	4.42E-10	33.73	JUP;CTNND1;INADL;MPP7;ACTB;DLG1;OCLN;APC;DLG5;TRIP6;CTNNB1;PKP4;FLNC;TLN2;PVRL3;PVRL2
cellular component morphogenesis (GO:0032989)	21/437	1.84E-07	23.56	GSK3B;JUP;KIDINS220;MINK1;ANK3;BAIAP2;EGFR;ACTB;RAB10;EPB41L5;SEPT7;APC;PEAK1;FLOT1;NUMB;SLITRK5;CTNNB1;NEFL;UTRN;PVRL2;LLGL1
cell part morphogenesis (GO:0032990)	16/248	1.46E-07	23.54	KIDINS220;MINK1;ANK3;BAIAP2;EGFR;ACTB;RAB10;SEPT7;APC;FLOT1;NUMB;SLITRK5;NEFL;UTRN;PVRL2;LLGL1
neuron projection morphogenesis (GO:0048812)	14/175	7.75E-08	22.88	KIDINS220;MINK1;ANK3;BAIAP2;ACTB;EGFR;RAB10;APC;NUMB;FLOT1;SLITRK5;NEFL;UTRN;LLGL1
cell projection morphogenesis (GO:0048858)	15/228	2.87E-07	22.60	KIDINS220;MINK1;ANK3;BAIAP2;EGFR;ACTB;RAB10;SEPT7;APC;FLOT1;NUMB;SLITRK5;NEFL;UTRN;LLGL1
establishment or maintenance of cell polarity (GO:0007163)	11/100	1.06E-07	22.29	ERBB2IP;RAB10;GSK3B;DLG1;VANGL2;DLG5;SCRIB;CDC42BPB;MPP7;LLGL1;MARK2
single organism cell adhesion (GO:0098602)	16/259	2.54E-07	22.23	KIRREL;CXADR;JUP;STXBP3;CTNND1;HSPB1;SCRIB;EGFR;ACTB;DLG1;PEAK1;DLG5;CTNNB1;PKP4;PVRL3;DSC2
single organismal cell-cell adhesion (GO:0016337)	15/235	4.13E-07	21.59	KIRREL;CXADR;JUP;STXBP3;CTNND1;HSPB1;SCRIB;EGFR;ACTB;DLG1;DLG5;CTNNB1;PKP4;PVRL3;DSC2
establishment or maintenance of bipolar cell polarity (GO:0061245)	6/25	1.72E-06	20.95	ERBB2IP;VANGL2;DLG5;SCRIB;LLGL1;MARK2

Fig 11.2 GO term analysis of FAT4 BioID hits (QEHF)

GO term analysis for molecular functions and biological processes are shown as bar graphs and matching tables containing information about significance and gene names. Analysis was performed using ENRICHR. GO terms sorted by combined scores. Only top GO terms are shown.

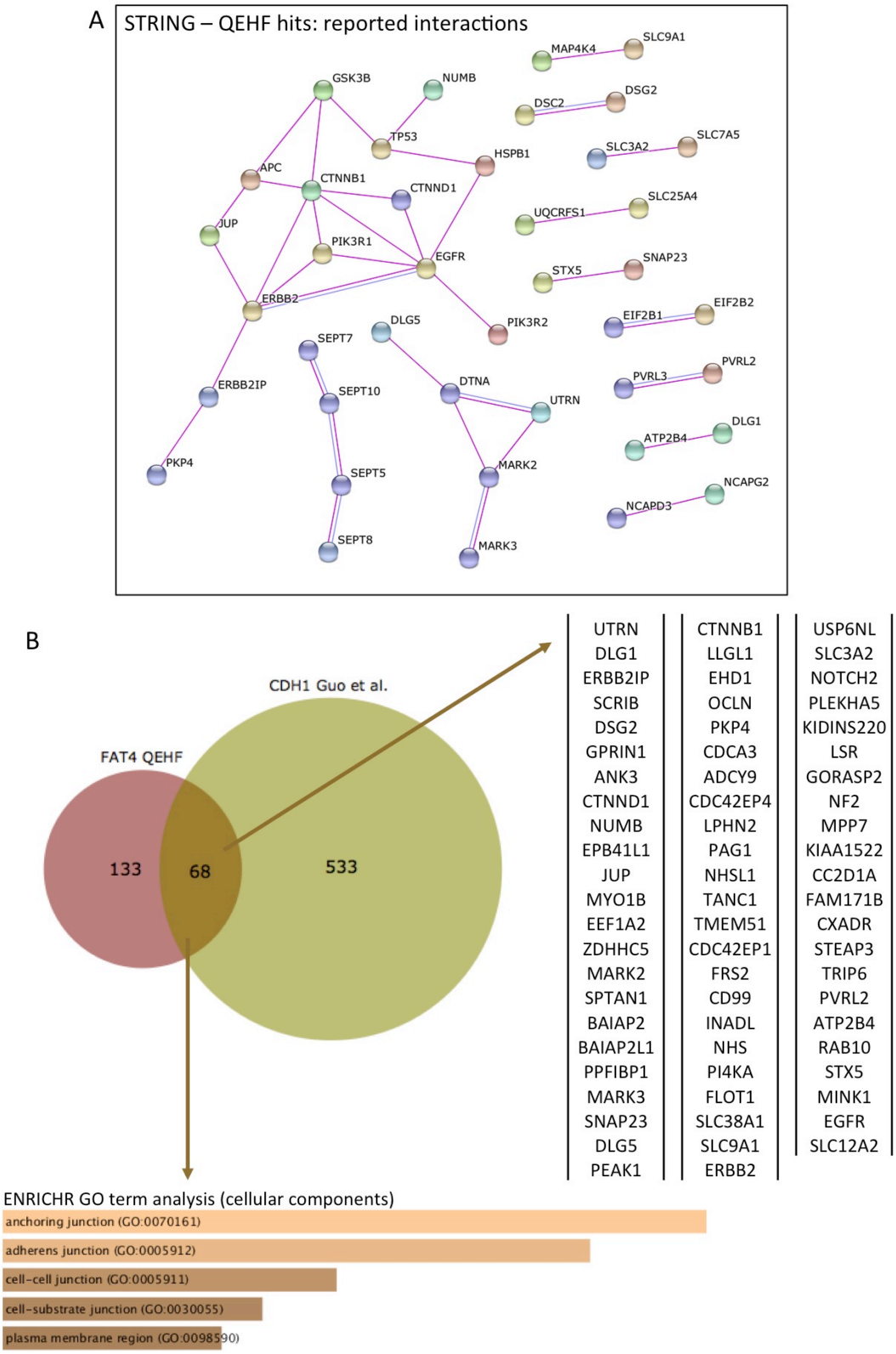

Fig 11.3 FAT4 BioID hits (QEHF) analysis

(A) STRING analysis (prediction method: experiments; high confidence) shows reported interactions between FAT4 proximity interactors. (B) Venn diagram shows comparison of FAT4 BioID hits with a published CDH1 BioID dataset (Guo et al., 2014). 68 shared proximity interactors are listed on the right. GO term analysis of cellular components of shared FAT4-CDH1 proximity interactors indicate a strong overlap of junctional proteins. Top 5 GO terms are shown (sorted by combined score).

11.1.2 A potential role for CTNND1/p120-catenin in FAT4 signaling

As BioID detects the molecular surroundings of a protein, identified BioID hits do not necessarily represent immediate interactors of the bait. I therefore attempted to validate some of the BioID hits in FAT4 co-immunoprecipitation (co-IP) experiments, to address if they are physically associated with FAT4. I selected some of the most abundant high-fidelity interactors, DLG1, ERBB2IP, SCRIB, CTNND1 and NUMB, as well as the Hippo pathway regulator NF2 to test by co-IP. I also tested the PCP regulator VANGL2, but found that the available VANGL2 antibody showed high unspecific background and could not be used for detection in co-IPs.

Unfortunately, the original FAT4-BirA*-Flag (FAT4-BF) cells used for BioID had been lost shortly after completion of the BioID. Instead, I performed pulldowns in HEK293T cells stably expressing full-length human FAT4 with a C-terminal yellow fluorescent protein (YFP) tag (FAT4-YFP). I used GFP-Trap agarose beads to efficiently capture FAT4-YFP from cell lysates. As a negative control served wildtype HEK293T cells and HEK293T cells stably expressing Ds1-mCherry. However, probing against SCRIB, DLG1, NUMB, ERBB2IP, CTNND1 and NF2 did not show any specific interactions with FAT4, despite strong enrichment of FAT4 protein in the pulldown fractions (Fig. 11.5A-D).

In parallel, I tested different cell lines, preferentially of epithelial origin, for FAT4 protein expression by Western blot. Similar to HEK293T cells, HaCaT (human immortalized keratinocyte cells) and MCF7 (human breast adenocarcinoma cells) cells did not express detectable levels of FAT4. Others, such as HeLa (human cervical cancer cells), Eph4 (murine immortalized mammary gland epithelial cells) and MCF10A (human immortalized mammary gland epithelial cells) cells expressed FAT4 at varying levels. The highest FAT4 expression was found in RPE-1 cells, human hTERT immortalized retinal pigment epithelium cells (Fig. 11.4).

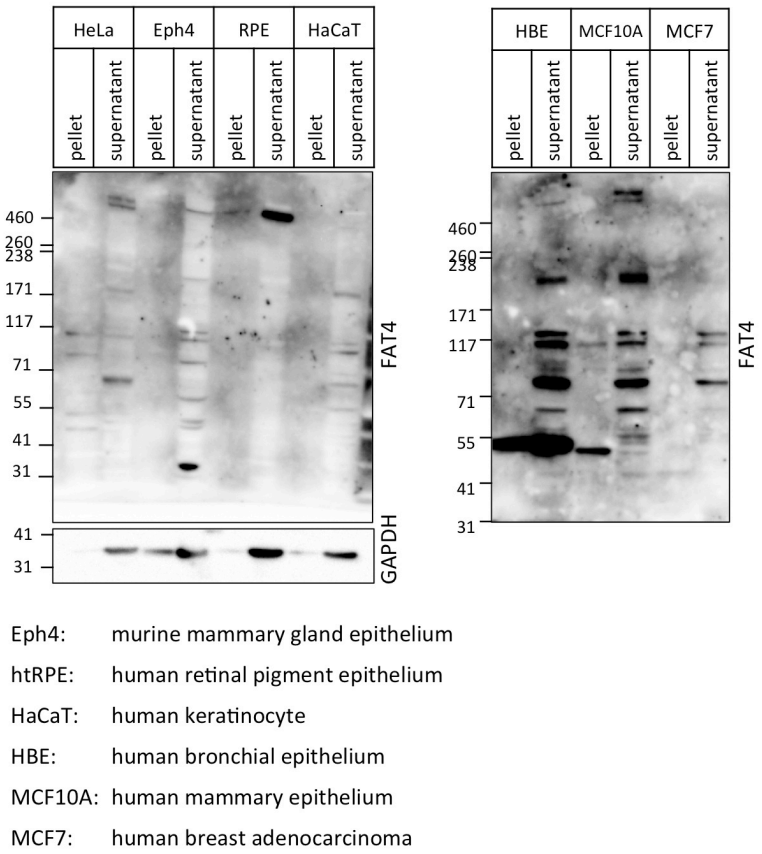

Fig 11.4 FAT4 expression in different epithelial cell lines
Test for endogenous *FAT4* expression in different cell lines by Western blot. Full-length FAT4 (540kDa) is expressed at different levels, with highest expression in RPE-1 cells. Specificity of lower bands is uncertain. Cells were lysed and insoluble fraction (pellet) separated from lysates (supernatant) by centrifugation. Low/absent FAT4 in cell pellet fraction indicates efficient solubilization of FAT4 during lysis. GAPDH levels serve as loading control.

I next tested if I could pull down endogenous FAT4 using an affinity-purified rabbit antibody generated in our lab (TO152AP). While the TO152AP pulldowns from HeLa, Eph4 and RPE-1 cells showed a clear full-length FAT4 band, the levels were generally low (Fig. 11.5E-H). I next probed these IP samples with antibodies against some of the BioID hits. Interestingly, CTNND1/p120 catenin was co-immunoprecipitated with TO152AP in Eph4 cells in two independent experiments, suggesting that p120 is a direct or indirect interactor of Fat4 (Fig. 11.5G,H).

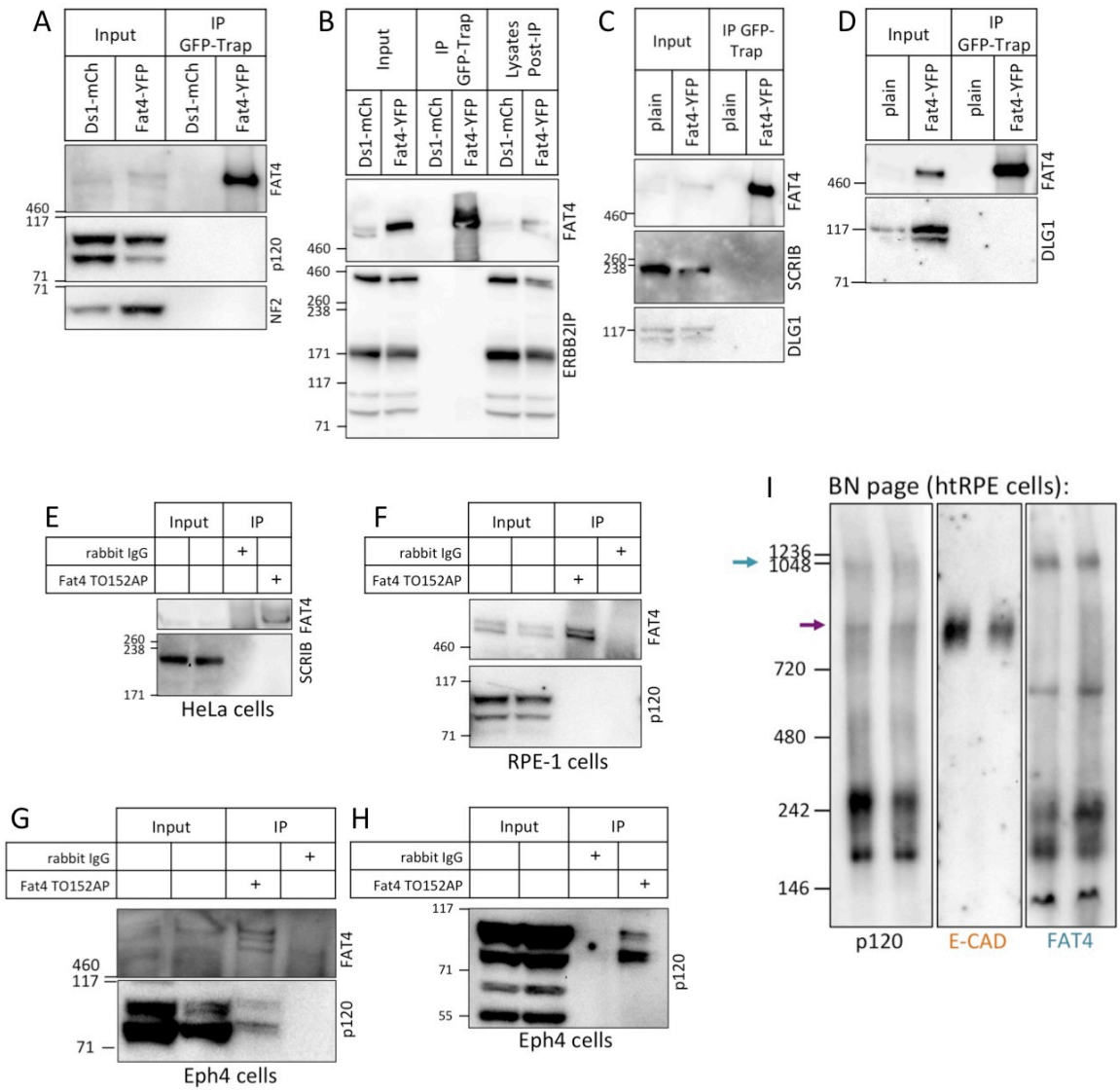

Fig 11.5 FAT4 co-immunoprecipitation experiments for BioID hit validation
(A – D) FAT4-YFP stably expressed in HEK293T cells was immunoprecipitated with GFP-trap beads. Despite enrichment of FAT4-YFP in IP samples (also compare IP and post-IP lane in (B)), no interactions with the BioID hits NF2, p120, ERBB2IP, SCRIB or DLG1 were detected. (E-H) Immunoprecipitation of endogenous Fat4/FAT4 from HeLa, RPE-1 and Eph4 cells using anti-FAT4 antibody (TO152AP) is weaker than from overexpression (rabbit IgG serves as IP control). Interaction of endogenous p120 is found in Eph4 cells (G, H). (I) Blue-Native PAGE from RPE-1 cells shows p120 present in two high-molecular complexes, one co-labelled with the established p120 interactor E-cad (purple arrow) and a second co-labelled by FAT4 antibody (blue arrow), suggesting that p120 can form a distinct complexes with FAT4 and E-cad.

However, Eph4 cells proved to be a difficult cell culture system to study Fat4, as their Fat4 expression levels are very low and at the detection limit of qRT-PCR. Accordingly, unless the amount of cells was scaled up or Fat4 levels were enriched in pulldowns, the full-length Fat4 protein was hardly detectable on Western blots. Additionally, I was unable to generate Eph4 cells stably expressing human FAT4, likely due to a combination of low transfection efficiency, low plasmid integration frequency and a high selection antibiotics tolerance of Eph4 cells.

I also tried to confirm the Fat4-p120 interaction in RPE-1 and HeLa cells, but could not see an interaction of endogenous FAT4 and p120 (Fig. 11.5F). However, preliminary tests of crude plasma membrane preps from RPE-1 cells assessed by Blue Native PAGE (BN-PAGE), a non-denaturing electrophoresis technique based on separation of Coomassie Blue-labeled protein complexes, suggested that FAT4 and p120 could form a complex. A high-molecular weight protein band (~1000kDa) was recognized by both p120 and FAT4 antibodies and was distinct from lower-running bands that have been previously identified as p120/E-cadherin complexes (Kiss et al., 2008) (see purple arrow in Fig. 11.5I). This suggests that FAT4 and p120 can interact and form a complex in mouse and human cells. However, in order to confirm the specificity of the FAT4 antibody signal, the BN-PAGE experiment should be repeated using FAT4 depleted cells.

11.1.3 Fat4 function in the intestinal tract

p120 catenin is an armadillo-repeat containing protein that interacts with various classical cadherins (Daniel and Reynolds, 1995; Yap et al., 1998; Thoreson et al., 2000) (reviewed in (Reynolds, 2007)). In contrast to alpha and beta catenins that convey cadherin signalling and link to the cytoskeleton, the major role of p120 is the regulation of cadherin levels and stability at the plasma membrane (Ireton et al., 2002; Davis et al., 2003; Xiao et al., 2003). Epithelial integrity in the mouse intestine has been shown to be highly sensitive to loss of *p120*, which leads to loss of epithelial barrier function (Smalley-Freed et al., 2010; Smalley-Freed et al., 2011). Mosaic intestinal *p120* deletion using an inducible Villin-Cre (Vil-Cre) driver causes chronic focal inflammation and

tumour formation (Smalley-Freed et al., 2011), while ubiquitous intestinal *p120* deletion driven by constitutively expressed Vil-Cre leads to a rapid death of mice from intestinal bleeding (Smalley-Freed et al., 2010).

In collaboration with Dr. Albert Reynolds, whose research centers on p120, we reasoned that the intestinal system is a good organ to study if p120 and Fat4 are molecularly dependent on each other. We decided to test if conditional intestinal *Fat4* knockout mice developed intestinal pathologies similar to *p120* loss or exhibited changes in p120 protein. Conversely, we wanted to address if Fat4 levels or localization are changed in *p120* knockout mice. Ian Hester in our lab established Vil-Cre$^{+/Cre}$;Fat4$^{flox/flox}$ mice and Vil-Cre$^{+/Cre}$; Fat4$^{flox/-}$ (containing a floxed *Fat4* allele over a *Fat4* mutation (Saburi et al., 2008)), which were viable and showed no apparent phenotype. I dissected and stained small and large intestinal tissue of two-month old mice with antibodies against p120 and Fat4 (TO152AP), but found no major structural defects in mutant intestines, and p120 levels and localization were unchanged compared to littermate controls (controls: Vil-Cre$^{+/Cre}$;Fat4$^{flox/+}$ n=2; knockouts: Vil-Cre$^{+/Cre}$;Fat4$^{flox/\Delta}$ n=2) (Fig. 11.6). The TO152AP staining appeared to be non-specific, as no difference between mutant and control tissue was found, similar to previous observations in mouse brains and kidneys (Dr. Caroline Badouel, Dr. Mazdak Bagherie-Lachidan, *unpublished results*). Unfortunately, this finding precluded the use of TO152AP to assess Fat4 in *p120* mutant tissue from Dr. Reynolds' lab.

Lastly, with the help of Dr. Steven Gallinger's lab, we histologically evaluated the intestinal tract of 6-month-old Vil-Cre *Fat4* knockout mice (control mice: Vil-Cre$^{+/Cre}$;Fat4$^{flox/+}$ n=3; knockout mice: Vil-Cre$^{+/Cre}$;Fat4$^{flox/flox}$ n=2 and Vil-Cre$^{+/Cre}$;Fat4$^{flox/\Delta}$ n=1). However, no pathological changes in the *Fat4* knockout intestines were detected, suggesting that loss of *Fat4* does not lead to similar defects as loss of *p120*. However, as we could not determine the efficiency of the Vil-Cre driven *Fat4* knockout system, we were not confident that *Fat4* was sufficiently depleted in these mice.

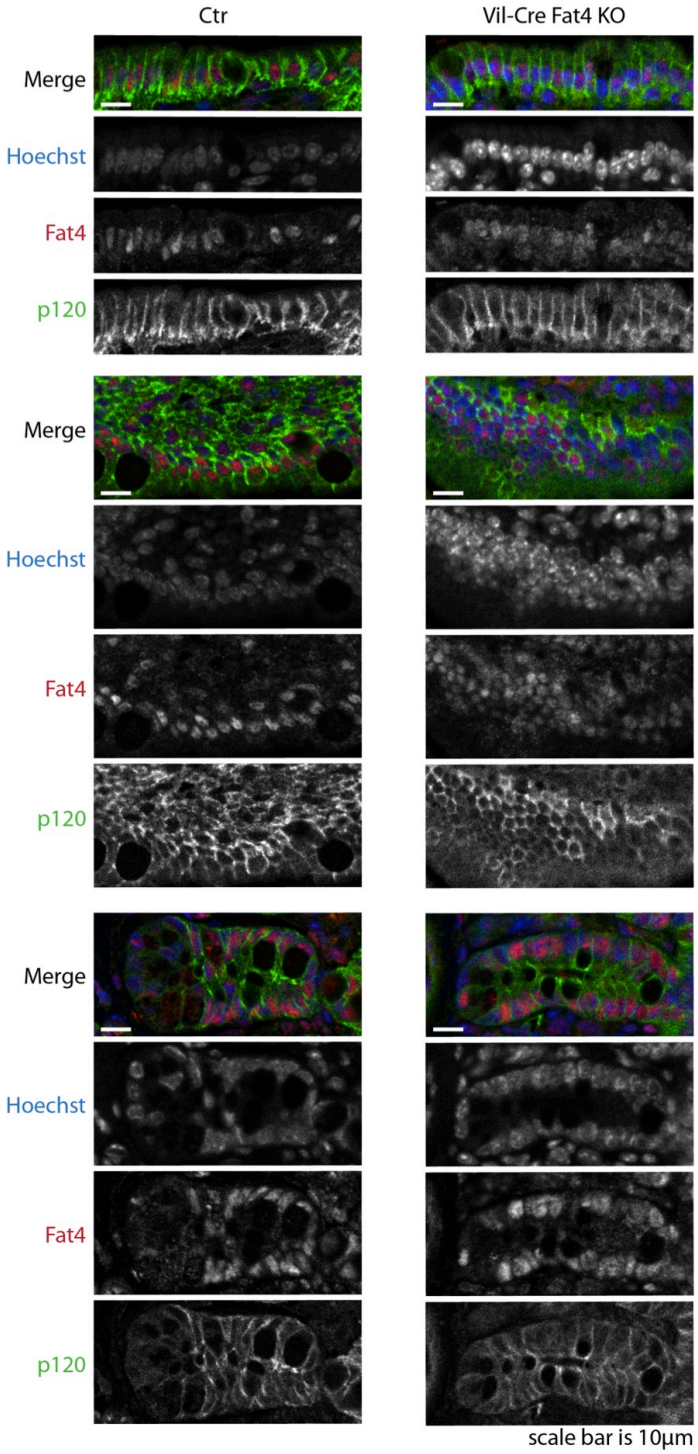

Fig 11.6 Vil-Cre driven *Fat4* knockout does not affect p120
Representative stainings of small intestinal sections from Vil-Cre$^{+/Cre}$; Fat4$^{flox/+}$ (ctr) or Vil-Cre$^{+/Cre}$; Fat4$^{flox/-}$ (Vil-Cre Fat4 KO) mice. Fat4 (TO152AP) staining is likely non-specific, as no reduction in signal is seen in Fat4 KO mice. No difference in p120 staining was observed. Ctr n = 2; KO n = 2

11.1.4 Establishing a cell culture system to study FAT4

To investigate if loss of FAT4 affected distribution or levels of some of the other BioID hits, I tested FAT4 knockdown by RNA interference (RNAi) in RPE-1 cells. Four independent siRNAs (Dharmacon), as well as their pool, resulted in a strong knockdown of FAT4 expression within 3 days, as judged by Western blot analysis and quantitative PCR (qPCR) (Fig. 11.7).

On Western blots, the FAT4 antibody TO152AP (which is raised against the FAT4 ICD) recognized a protein doublet above the 460kDa mark, as well as several lower bands. However, only the upper band of the high-molecular weight doublet was affected by the different siRNAs, suggesting it reflects full-length FAT4 protein (560kDa) while lower bands are likely non-specific (Fig. 11.7A). Furthermore, prolonged siRNA treatment (up to 8 days) did not enhance the knockdown or visibly reduce any of the lower bands. Trypsin treatment of live RPE-1 cells similarly only resulted in loss of the upper doublet band (and appearance of a 200kDa and 70kDa band), suggesting that the lower doublet band represents a protein that is not accessible to Trypsin (possibly it is not spanning the plasma membrane) (Fig. 11.7B). While *Drosophila* Fat and mammalian FAT1 are processed and the resulting protein fragments can be detected on Western blot (Magg et al., 2005; Feng and Irvine, 2009; Sopko et al., 2009; Sadeqzadeh et al., 2011), I could only verify the existence of a full-length form of FAT4. I also generated RPE-1 cells expressing endogenous FAT4 with a C-terminal GFP tag through genomic insertion of a GFP-coding cassette using the CRISPR/Cas9 strategy. Western blot analysis of these cells similarly only confirmed the presence of a presumably full-length FAT4-GFP protein (Fig. 11.7D). This doesn't fully exclude that FAT4 is processed, as the extreme C-terminus with the GFP tag could be cleaved off; however, from these findings it seems more likely that no major processing of FAT4 happens in RPE-1 cells, at least not as observed for *Drosophila* Fat or mammalian FAT1.

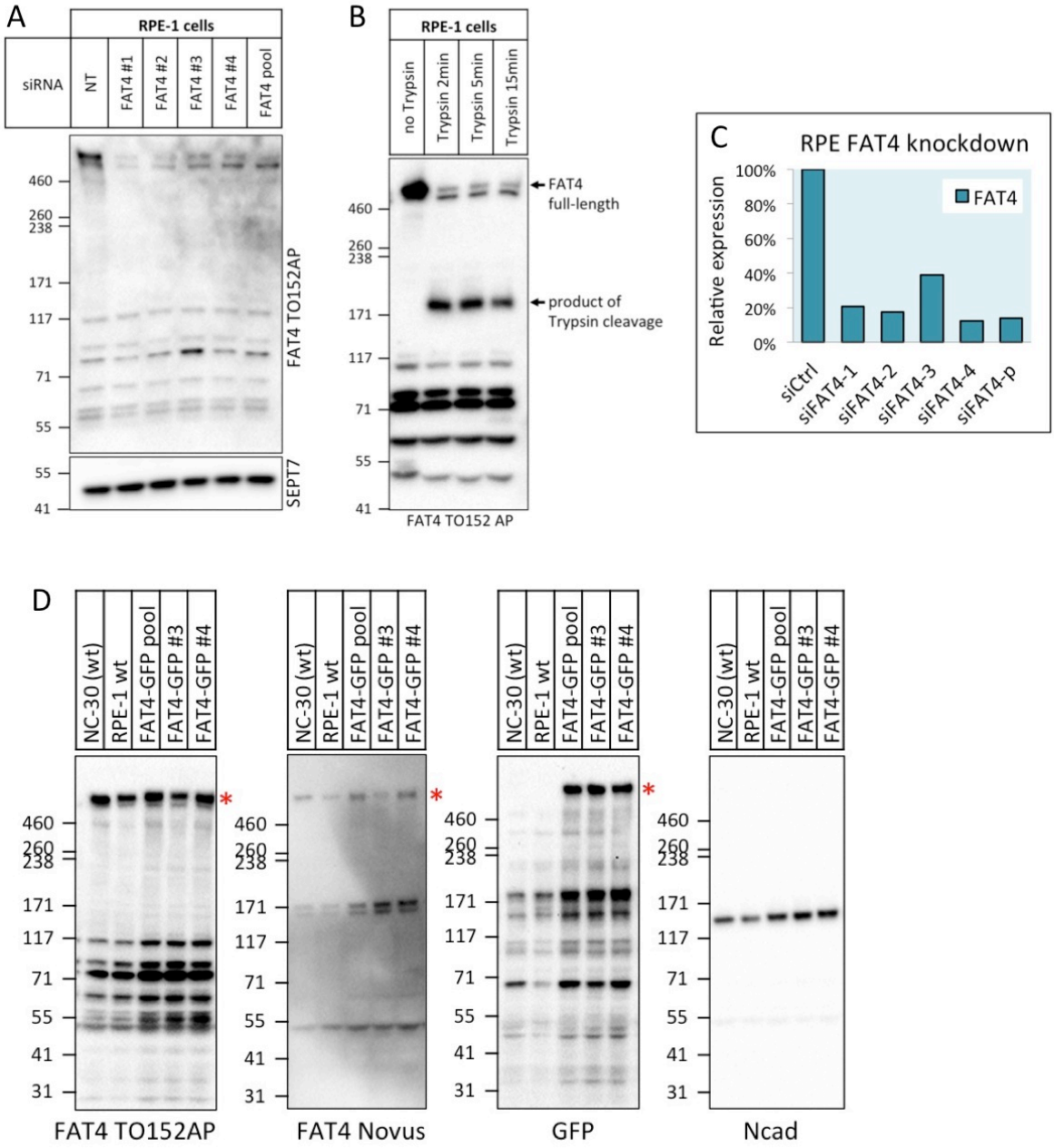

Fig 11.7 FAT4 knockdown by RNAi
(A) siRNA-mediated knockdown (3 days) of FAT4 with 4 different siRNAs and their pool results in clear reduction of FAT4, which runs as a high-molecular weight band on Western blot, likely representing full-length FAT4 (540kDa). (B) Trypsination of live cells as indicated results in cleavage of full-length FAT4 (but not of the slightly lower-migrating band recognized by TO152AP). (C) Quantitative PCR confirms that FAT4 mRNA levels are strongly reduced after 3-day siRNA treatment of RPE-1 cells. (D) GFP-tagging of endogenous FAT4 by CRISPR/Cas9 in RPE-1 cells indicates that FAT4 mainly exists as full-length protein. FAT4-GFP #3 and #4 are clonally grown cell lines, while FAT4-GFP pool cells were pooled after selection for successful GFP integration. NC-30 is a clonally grown cell line used as clonal wildtype control.

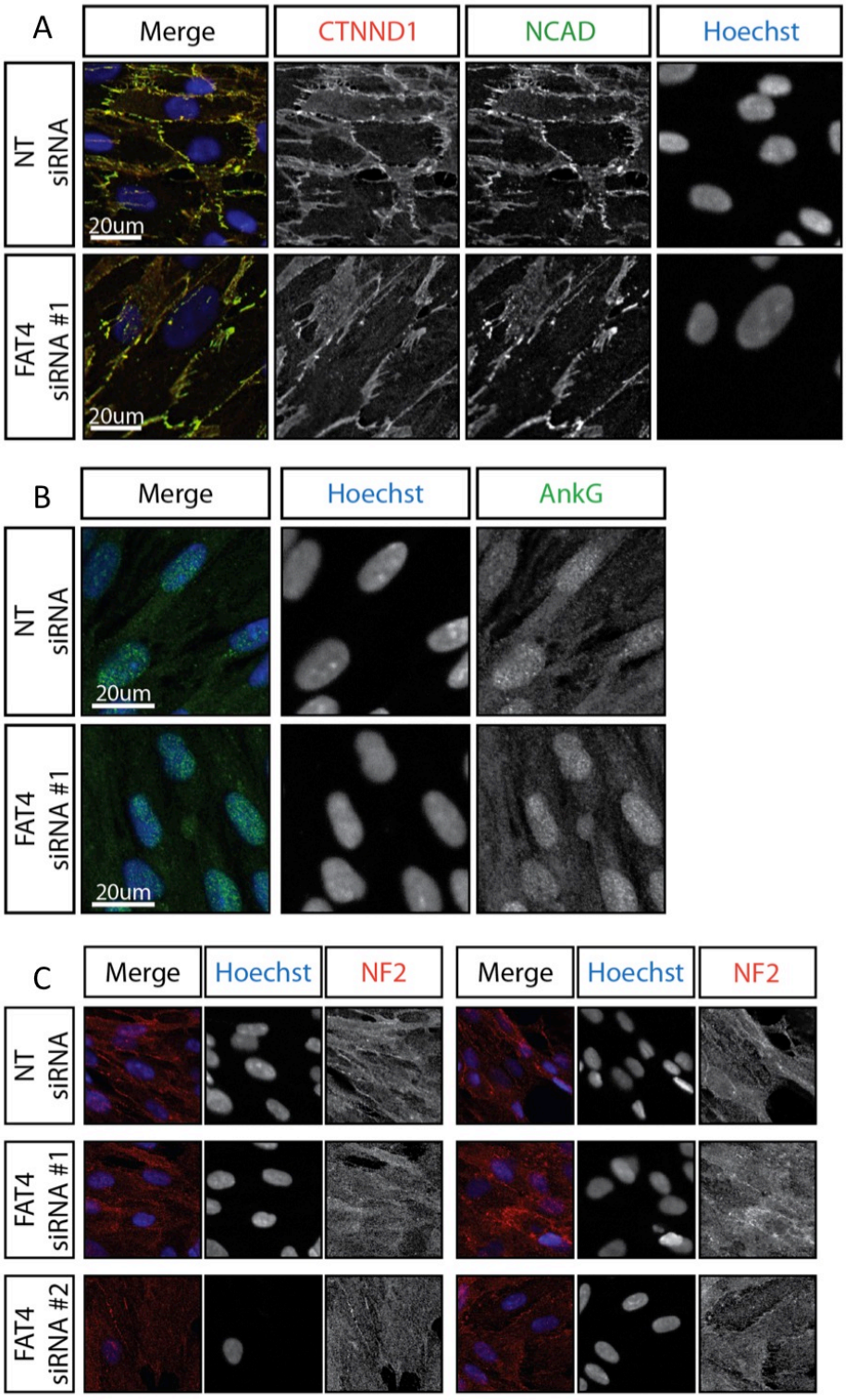

Fig 11.8 FAT4 proximity interactors in response to FAT4 knockdown
(A-C) Immunofluorescence stainings of RPE-1 cells transfected with siRNAs for 72h and labeled with antibodies as indicated. No significant changes in levels and localization of p120, ANKG/ANK3 or NF2 were found.

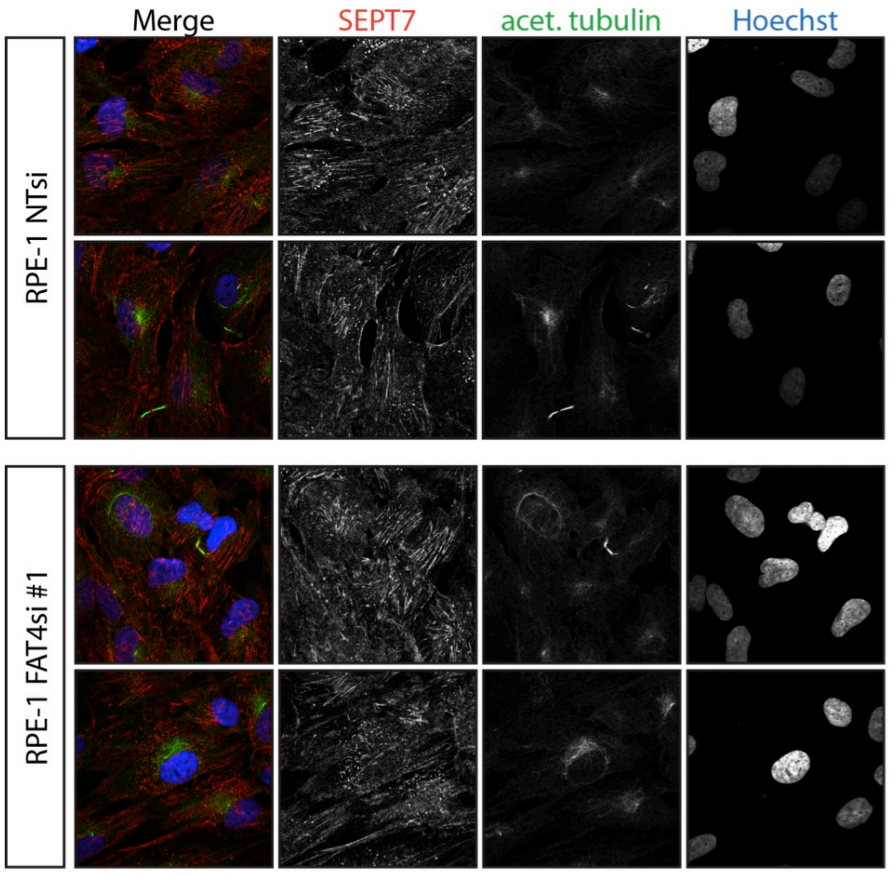

Fig 11.9 SEPT7 localization is unchanged after FAT4 knockdown
Immunofluorescence stainings of RPE-1 cells transfected with siRNAs for 72h and labeled with antibodies as indicated.

I next asked if FAT4 knockdown affects localization or levels of potential interactors identified by BioID. I used siRNA-transfected RPE-1 cells to address potential p120 dependence on FAT4, but in accordance with our observations in *Fat4* mutant intestines, I did not see changes in p120 protein levels or in localization in Western blots and IF (Fig. 11.8; 11.10). I also tested if FAT4 knockdown affects the polarity regulator SCRIB, the Hippo pathway regulator NF2, the cilium and cytokinesis regulator SEPT7 and the cytoskeletal linker protein ANK3/AnkG. None of these were changed as assessed by Western blots or immunofluorescence stainings of FAT4 depleted cells (Fig. 11.8; 11.9; 11.10).

In previous affinity-based mass spectrometry experiments of truncated FAT4, Nicole Liscio had found Partitioning Defective 3 Homolog (PARD3/PAR3) as a high-confidence interactor (Badouel et al., 2015). She further showed that truncated FAT4 co-immunoprecipitated endogenous PAR3 in HEK293 cells (Nicole Liscio, *unpublished*). In the FAT4 BioID, PAR3 peptides were not increased over controls, which illustrates that AP-MS and BioID can detect different subsets of interactors (Lambert et al., 2015). I found that the 180kDa and 150kDa isoforms of PAR3 are expressed in RPE-1 cells and repeatedly saw a mild reduction of both after knockdown of FAT4 by two different siRNAs (Fig. 11.10). A functional link between FAT4 and PAR3 is a tempting hypothesis, since FAT4 knockout mice show defects in oriented cell division, and should be a subject for future studies.

11.1.5 FAT4 knockdown affects Hippo pathway members

To test if FAT4 knockdown would affect the Hippo pathway, I probed lysates of RPE-1 cells treated with FAT4 siRNAs for YAP and saw a reduction of YAP levels (Fig. 11.10). To further test if this reduction of YAP reflected a function for FAT4 in mammalian Hippo pathway regulation, I also probed for pYAP, LATS1 and pLATS1. If FAT4 functioned in analogy to *Drosophila* Fat, FAT4 reduction should result in a decrease of LATS phosphorylation and potentially protein levels, as well as a decrease in YAP phosphorylation and concomitant increase of YAP stability (see also Fig. 9.1 for a schematic). While I observed a reduction of LATS1 levels upon FAT4 knockdown, pLATS1 was not reduced consistently. Phosphorylated YAP (S127) seemed repeatedly reduced (stronger with siRNA #2) but since total YAP levels decreased as well, it was unclear if total YAP activity changed in these cells (Fig. 11.10).

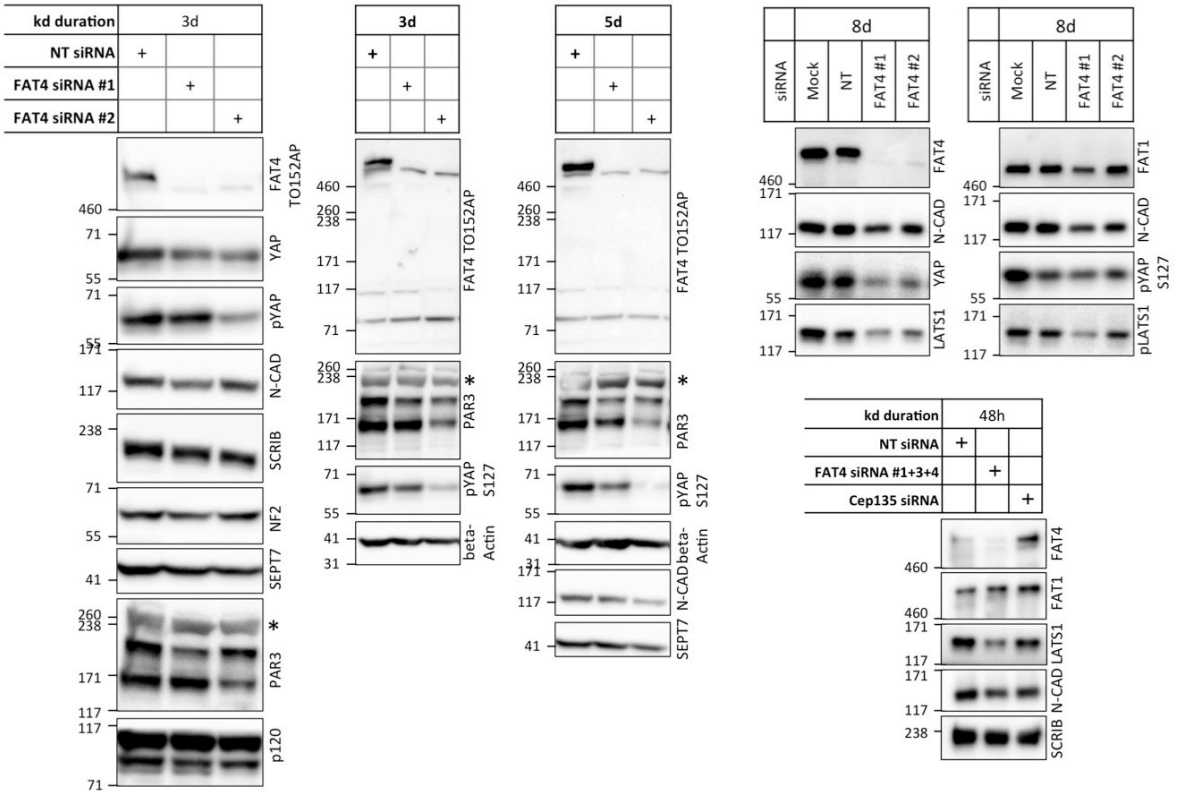

Fig 11.10 Protein responses to FAT4 knockdown
Western blot analysis of RPE-1 cells transfected with siRNAs as indicated. Changes in YAP, pYAP (Ser127), LATS, pLATS (Ser909) and PAR3 levels are shown (band marked with * is likely unspecific).

11.1.6 Follow-up FAT4 BioID experiments

The initial FAT4 BioID was performed on a high-sensitive Q Exactive HF hybrid quadrupole-Orbitrap (QEHF) mass spectrometer and resulted in a large number of high-fidelity proximity interactors (Table 11.1). Interestingly, I noticed that many hits, especially most of the hits with the highest peptide numbers, are known E-cadherin (CDH1) interactors. When FAT4 hits (identified proximity interactor hits: 201) are compared to published CDH1 BioID results from the gastric cancer cell line MKN28E (identified proximity interactor hits: 601) (Guo et al., 2014), 34% of FAT4 hits are shared with the CDH1 BioID (68 common interactors) (Fig. 11.3). No functional links are known between FAT4 and CDH1 and their respective localizations in epithelial cells are not expected to overlap

significantly, as CDH1 primarily localizes to adherens junctions and FAT4 is thought to localize apically of adherens junctions.

In order to directly compare proximity proteomes of FAT4 and CDH1, I established HEK293 cells expressing FAT4-BirA*-Flag (FAT4-BF) and Cdh1-BirA*-Flag (Cdh1-BF), as well as GFP-BirA*-Flag (GFP-BF) and BirA*-Flag (BF) as controls, to perform follow-up BioID runs. Since the original FAT4-BirA*-Flag (FAT4-BF) stable HEK293 cells had been lost, I chose to generate the new lines with the Flp-In T-REx system (Invitrogen). The Flp-In system can increase efficiency of DNA integration into the genome, which proved to be extremely low with standard transfection of the FAT4-BF plasmid. This system also has several advantages: first, cells can be selected as polyclonal cultures, which reduces the risk of artifactual clonal behaviors. Second, every transgene introduced into a specific Flp-In T-REx HEK293 line is integrated into the same landing site in the genome, making different transgenic lines more comparable. This is of advantage when performing comparative proteomics with different baits. Third, transgene expression is inducible by addition of tetracycline to the cell culture medium, which reduces the chance of adverse effects of prolonged gene overexpressions.

I confirmed that the stable cell lines could be induced by tetracycline and that the expressed BirA* fusion proteins biotinylated other proteins upon addition of biotin by Western blot (Fig. 11.11A-D). Immunofluorescence stainings of fixed cells highlighted that FAT4-BF was expressed and mostly localized to the plasma membrane, where also the strongest biotinylation signal was observed (Fig. 11.12).

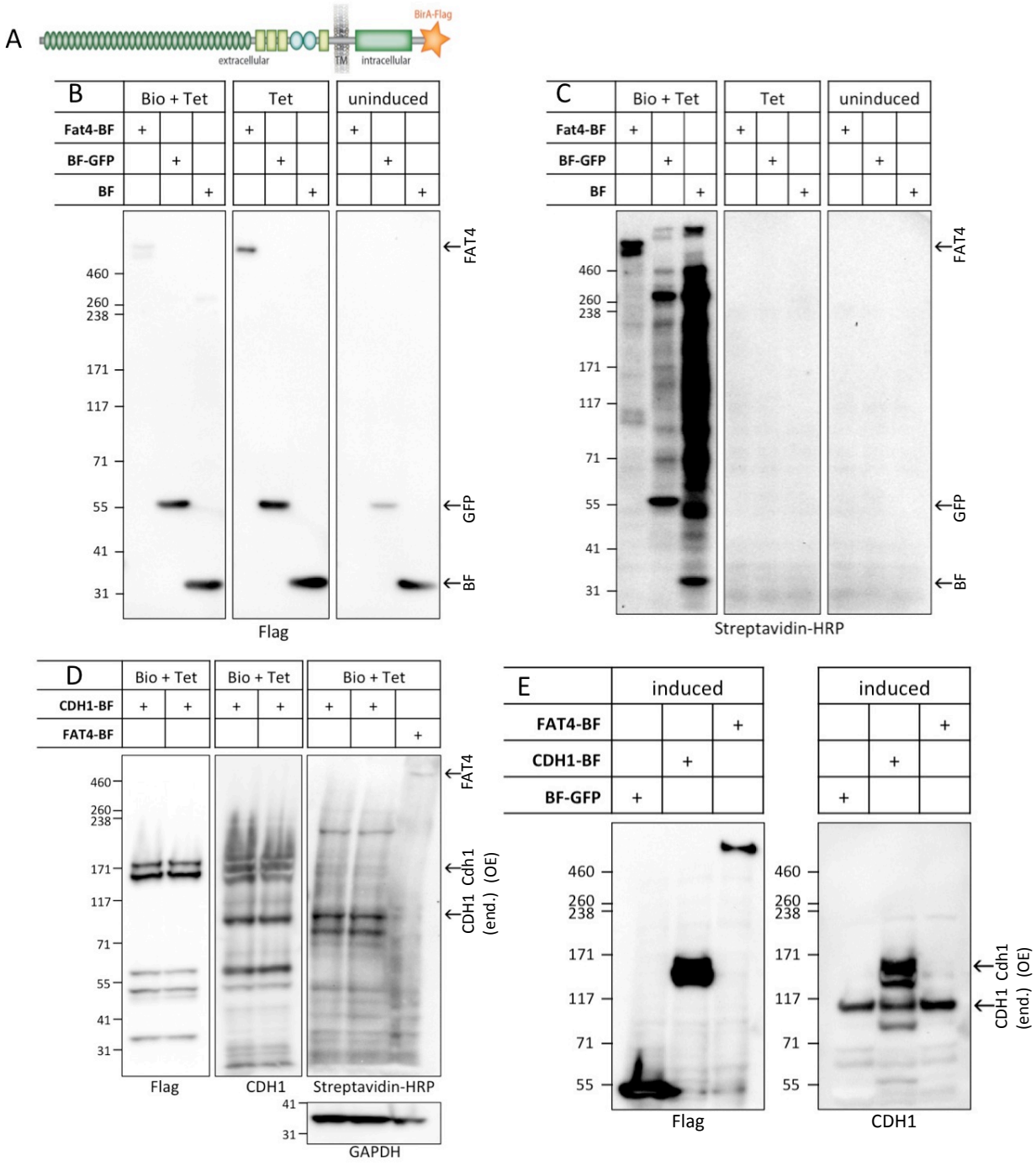

Fig 11.11 Expression and biotinylation tests of new cell lines for BioID
(A) Schematic of BirA*-Flag tagged FAT4 (FAT4-BF). (B-D) HEK T-REx cells expressing Fat4-BF (570kDa), Cdh1-BirA*-Flag (Cdh1-BF; 170kDa), GFP-BirA*-Flag (GFP-BF; 55kDa) or BirA*-Flag (30kDa; BF) tested for their response to Biotin treatment and Tetracyclin (Tet) induction. FAT4-BF expression is lower compared to control cell lines and does not leak in the absence of Tet (B). (C, D) Biotinylation is addressed by Streptavidin labeling and shows both self-biotinylation of the baits as well as biotinylation of other proteins. It appears that strong biotinylation of endogenous CDH1 is seen in Cdh1-BF erexpressing cells, indicating Cdh1-BF is properly localized at sites of endogenous CDH1 (D, lowest arrow). (E) HCT116 cells tested for Tet-induced expression of FAT4-BF, Cdh1-BF and GFP-BF. OE = overexpression; end = endogenous.

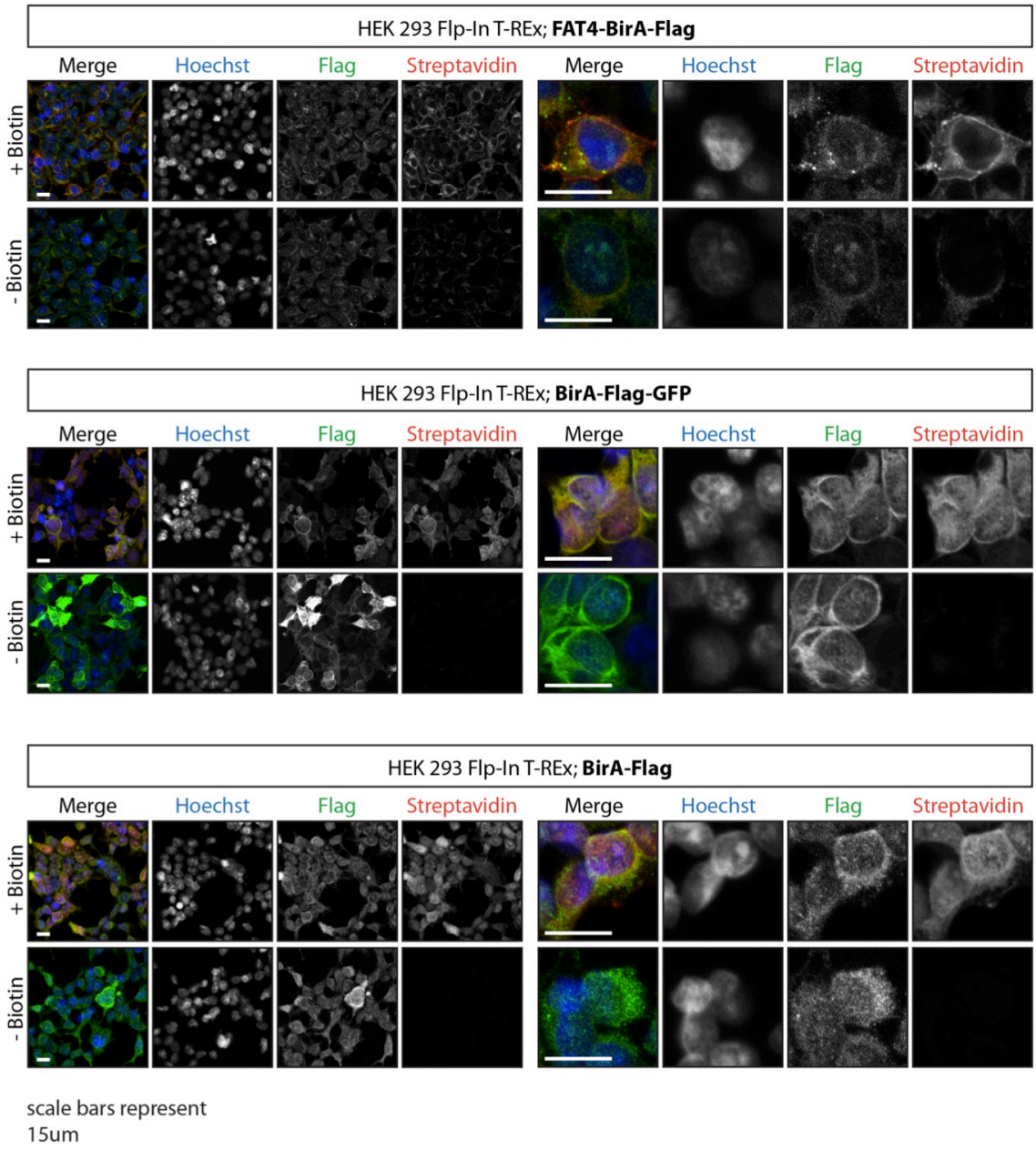

Fig 11.12 Biotinylation test of HEK293 stable cell lines for BioID
Stable HEK293 lines are induced by Tetracycline and either cultured with or without biotin for 24h. Streptavidin labeling shows successful biotinylation, largely colocalizing with BirA*-Flag-tagged proteins.

BioID of FAT4-BF and Cdh1-BF was performed on a LTQ Orbitrap Velos Hybrid ("Velos") mass spectrometer, which achieves a lower sensitivity than the QEHF hybrid Orbitrap. As a consequence, less signal depth and retrieved interactors were obtained than in QEHF runs (Table 11.2). Nevertheless, we found that 28 (=38%) high-confidence hits of the Velos runs had been previously identified in the QEHF FAT4 BioID, indicating that these are robust proximity interactions that should be prioritized for future studies (Fig. 11.14). Several of the hits that were tested in FAT4 co-IPs are included in this list, namely p120, SCRIB, DLG1, ERBB2IP and NUMB.

Additionally, we found a large overlap of proximity interactors of FAT4 and Cdh1. A total of 48 shared interactions were detected, which represent 66% of all Velos FAT4 BioID hits and 24% of all Cdh1 BioID hits. As expected, most adherens junction-associated proteins are shared between FAT4 and Cdh1, while LIX1L is a specific interactor of FAT4 (Fig. 11.14).

The most abundant GO-terms for molecular functions of BioID hits were similar to the previous BioID, such as cell adhesion molecule binding, cadherin binding and kinase binding. Additionally, molecules involved in actin binding were significantly enriched (Fig. 11.13). GO-term analysis of biological processes revealed almost identical terms for both Velos and QEHF BioIDs (compare Fig. 11.13 with Fig. 11.2), indicating a significant enrichment of proximity interactors involved in cell junction and polarity regulation.

Table 11.2 FAT4 and Cdh1 BioID (Velos) in HEK293 cells
(Hits with SAINT scores > 0.75 for FAT4 as bait are shown; full list is shown in Appendix Table 13.2)

Gene Name	Full name	Top 2 controls		FAT4 (cycling)		FAT4 (starved)		Cdh1 (cycling)		Cdh1 (starved)	
				Average over 4 replicates	SAINT	Average over 4 replicates	SAINT	Average over 4 replicates	SAINT	Average over 4 replicates	SAINT
FAT4	*FAT atypical cadherin 4*			1269	NA	1115	NA				
CDH1	*cadherin 1*							66	NA	63	NA
MLLT4	*myeloid/lymphoid or mixed-lineage leukemia; translocated to, 4*	42	34	184	1.00	235	1.00	385	1.00	418	1.00
DST	*dystonin*	6	5	97	1.00	71	1.00	15	0.97	7	
IRS4	*insulin receptor substrate 4*	27	25	93	1.00	54		141	1.00	37	
ERBB2IP	*erbb2 interacting protein*	11	4	87	1.00	96	1.00	134	1.00	172	1.00
ESYT1	*extended synaptotagmin like protein 1*	10	8	46	1.00	64	1.00	43	1.00	35	1.00
SCRIB	*scribbled planar cell polarity protein*			44	1.00	79	1.00	85	1.00	79	1.00
UTRN	*utrophin*	15	11	37	1.00	64	1.00	16		17	
EPHA2	*EPH receptor A2*	4	4	34	1.00	43	1.00	52	1.00	58	1.00
DSG2	*desmoglein 2*	4		32	1.00	53	1.00	91	1.00	73	1.00
JUP	*junction plakoglobin*	5	4	31	1.00	29	1.00	173	1.00	161	1.00
SSRP1	*structure specific recognition protein 1*	5	3	26	1.00						
DLG1	*discs large homolog 1*			21	1.00	54	1.00	61	1.00	66	1.00
VANGL1	*VANGL planar cell polarity protein 1*			21	1.00	22	1.00	58	1.00	43	1.00
CYFIP2	*cytoplasmic FMR1 interacting protein 2*	4	4	20	1.00	49	1.00	17		19	0.99
PTPN13	*protein tyrosine phosphatase, non-receptor type 13*	3		19	1.00	9	0.95	10	0.98		
NUMB	*numb homolog (Drosophila)*			18	1.00	18	1.00	51	1.00	38	1.00
ANK3	*ankyrin 3, node of Ranvier (ankyrin G)*			14	1.00	47	1.00	110	1.00	129	1.00
MARK2	*microtubule affinity regulating kinase 2*			11	1.00	7	1.00	67	1.00	45	1.00
BAIAP2L1	*BAI1 associated protein 2 like 1*			7	1.00	12	1.00	1			
MARK3	*microtubule affinity regulating kinase 3*			7	1.00	5	1.00	41	1.00	33	1.00
VANGL2	*VANGL planar cell polarity protein 2*			7	1.00	13	1.00	27	1.00	13	1.00
DLG5	*discs large homolog 5*			5	1.00	4	0.98	3	0.97		
SSR4	*signal sequence receptor, delta*			5	1.00	11	1.00			1	
ESYT2	*extended synaptotagmin like protein 2*			4	1.00	13	1.00	6	1.00	3	
FLOT2	*flotillin 2*			4	1.00	8	1.00	31	1.00	21	1.00
SUPT16H	*SPT16 homolog, facilitates chromatin remodeling subunit*	6	5	24	0.99						
PHACTR4	*phosphatase and actin regulator 4*	2		9	0.99	22	1.00	17	1.00	31	1.00
NCKAP1	*NCK associated protein 1*	2		8	0.99	45	1.00	9	0.99	12	1.00
CEP89	*centrosomal protein 89kDa*			5	0.99	6	1.00	3			
LIX1L	*limb and CNS expressed 1 like*			5	0.99	7	1.00				
OCLN	*occludin*			4	0.99	1		16	1.00	16	1.00
NUP155	*nucleoporin 155kDa*			4	0.98	1		6	1.00	4	1.00
DDRGK1	*DDRGK domain containing 1*			2	0.95	1		2		2	
MYO1B	*myosin IB*	2		9	0.93	12	1.00	14	1.00	6	0.96
YKT6	*YKT6 v-SNARE homolog (S. cerevisiae)*	5	4	13	0.89	13	0.90	36	1.00	41	1.00
NUMBL	*numb homolog (Drosophila)-like*	3		13	0.88	8		39	1.00	23	1.00
PFKL	*phosphofructokinase, liver type*	3		7	0.86	7	0.85				
TOP2B	*topoisomerase (DNA) II beta*	5	4	18	0.85						
ACBD3	*acyl-CoA binding domain containing 3*	4	2	8	0.81	4		52	1.00	46	1.00
SULT1A1	*sulfotransferase family 1A member 1*	4	3	8	0.79						
ZNF326	*zinc finger protein 326*	4		5	0.76						
RAI14	*retinoic acid induced 14*	16	12	38		63	1.00	33	0.77	26	
ADD3	*adducin 3*	7	7	18		41	1.00	46	1.00	29	1.00
ADD1	*adducin 1*	11	8	22		32	1.00	58	1.00	34	1.00
SEPT8	*septin 8*					15	1.00	24	1.00	18	1.00
CDIPT	*CDP-diacylglycerol--inositol 3-phosphatidyltransferase*			4		12	1.00			5	

ECH1	*enoyl-CoA hydratase 1, peroxisomal*	2		**3**	**11**	1.00				
LLGL1	*lethal giant larvae homolog 1 (Drosophila)*			**2**	**11**	1.00	**11**	1.00	**8**	1.00
OSBPL8	*oxysterol binding protein like 8*			**2**	**11**	1.00	**2**		**11**	1.00
STIM1	*stromal interaction molecule 1*			**4**	**9**	1.00	**2**		**3**	
ABI1	*abl interactor 1*			**2**	**8**	1.00	**6**	1.00	**9**	1.00
HSPA12A	*heat shock protein family A (Hsp70) member 12A*				**7**	1.00				
LSR	*lipolysis stimulated lipoprotein receptor*				**6**	1.00	**1**		**4**	
KANK2	*KN motif and ankyrin repeat domains 2*			**2**	**5**	1.00				
ROR2	*receptor tyrosine kinase-like orphan receptor 2*				**5**	1.00	**14**	1.00	**10**	1.00
BAIAP2	*BAI1 associated protein 2*			**2**	**5**	1.00	**1**			
PALM	*paralemmin*				**5**	1.00	**3**		**4**	
CXADR	*coxsackie virus and adenovirus receptor*				**4**	1.00				
CYFIP1	*cytoplasmic FMR1 interacting protein 1*	12		**14**	**43**	0.99	**17**		**10**	
PTPN1	*protein tyrosine phosphatase, non-receptor type 1*	4		**5**	**13**	0.98	**18**	0.99	**26**	1.00
TACC1	*transforming acidic coiled-coil containing protein 1*	4	2	**5**	**13**	0.98	**2**		**5**	
CLNS1A	*chloride nucleotide-sensitive channel 1A*	5	4	**13**	**16**	0.97	**27**	1.00	**19**	1.00
CKAP4	*cytoskeleton-associated protein 4*	4	4	**6**	**12**	0.97	**6**		**19**	1.00
LEMD3	*LEM domain containing 3*	4	4	**6**	**13**	0.95	**72**	1.00	**58**	1.00
SNTB2	*syntrophin beta 2*	3		**1**	**8**	0.95	**3**		**2**	
GPRIN1	*G protein regulated inducer of neurite outgrowth 1*	7		**6**	**20**	0.94	**23**	0.98	**35**	1.00
VAPB	*VAMP (vesicle-associated membrane protein)-associated protein B and C*	6	6	**6**	**19**	0.94	**30**	1.00	**45**	1.00
SRPR	*SRP receptor alpha subunit*	2		**2**	**6**	0.94	**8**	0.98	**11**	0.98
CTNND1	*catenin delta 1*	3		**1**	**9**	0.93	**251**	1.00	**334**	1.00
HSD17B12	*hydroxysteroid (17-beta) dehydrogenase 12*	3		**1**	**8**	0.91	**1**		**5**	0.83
MTDH	*metadherin*	10	5	**5**	**21**	0.78	**5**		**14**	
EPB41L2	*erythrocyte membrane protein band 4.1-like 2*	39	39	**91**	**116**	0.76	**170**	1.00	**154**	1.00
EPB41L1	*erythrocyte membrane protein band 4.1-like 1*			**3**	**14**	0.75	**16**	0.75	**24**	1.00

FAT4 BioID (Velos) – ENRICHR GO term analysis (molecular function)

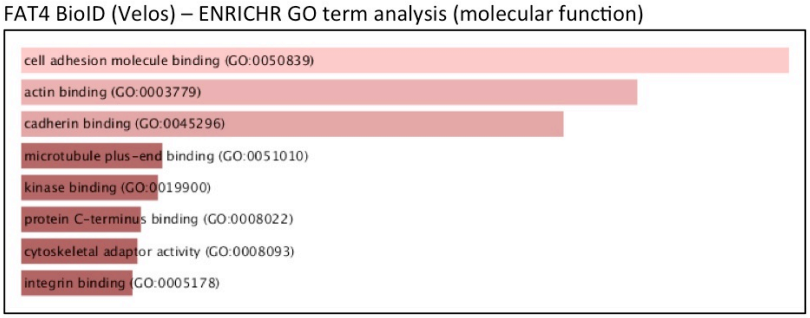

GO Term	GO Overlap	P-value	Combined Score	Genes
cell adhesion molecule binding (GO:0050839)	9/168	5.52E-08	27.37	ERBB2IP;CXADR;JUP;DST;CTNND1;NUMB;ANK3;UTRN;MLLT4
actin binding (GO:0003779)	11/386	7.75E-07	22.92	CYFIP1;MYO1B;BAIAP2L1;DST;EPB41L1;EPB41L2;UTRN;ADD3;ADD 1;SNTB2;PHACTR4
cadherin binding (GO:0045296)	4/27	8.79E-06	20.75	JUP;CTNND1;NUMB;ANK3
microtubule plus-end binding (GO:0051010)	2/11	1.37E-03	8.99	STIM1;DST
kinase binding (GO:0019900)	8/487	1.16E-03	8.86	PTPN1;TOP2B;DLG1;PFKL;JUP;CTNND1;UTRN;LLGL1
protein C-terminus binding (GO:0008022)	5/162	7.3E-04	8.36	TOP2B;DLG1;DST;BAIAP2;MLLT4
cytoskeletal adaptor activity (GO:0008093)	2/18	3.27E-03	8.26	BAIAP2L1;BAIAP2
integrin binding (GO:0005178)	4/102	1.09E-03	8.11	ERBB2IP;CXADR;DST;UTRN

FAT4 BioID (Velos) – ENRICHR GO term analysis (biological process)

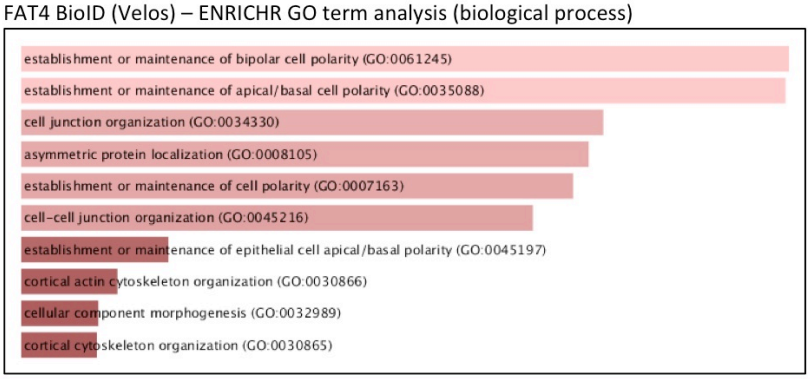

GO Term	GO Overlap	P-value	Combined Score	Genes
establishment or maintenance of bipolar cell polarity (GO:0061245)	6/25	3.83E-09	36.77	ERBB2IP;VANGL2;DLG5;SCRIB;LLGL1;MARK2
establishment or maintenance of apical/ basal cell polarity (GO:0035088)	6/25	3.83E-09	36.69	ERBB2IP;VANGL2;DLG5;SCRIB;MARK2;LLGL1
cell junction organization (GO:0034330)	11/189	9.74E-10	33.09	DLG1;OCLN;NUMBL;CXADR;JUP;DST;DLG5;CTNND1;NUMB; MLLT4;MTDH
asymmetric protein localization (GO: 0008105)	5/18	4.43E-08	32.81	ERBB2IP;NCKAP1;VANGL2;DLG5;SCRIB
establishment or maintenance of cell polarity (GO:0007163)	9/100	1.03E-09	32.50	ERBB2IP;NCKAP1;DLG1;VANGL2;DST;DLG5;SCRIB;LLGL1;MARK2
cell-cell junction organization (GO:0045216)	10/161	3.34E-09	31.70	DLG1;OCLN;NUMBL;CXADR;JUP;DLG5;CTNND1;NUMB;MLLT4; MTDH
establishment or maintenance of epithelial cell apical/basal polarity (GO:0045197)	4/17	1.92E-06	24.50	ERBB2IP;VANGL2;DLG5;MARK2
cortical actin cytoskeleton organization (GO: 0030866)	4/19	2.82E-06	23.49	DLG1;EPB41L1;EPB41L2;LLGL1
cellular component morphogenesis (GO: 0032989)	12/437	4.85E-07	23.12	TOP2B;NUMBL;JUP;DST;ABI1;NUMB;ANK3;UTRN;BAIAP2;ADD1; LLGL1;EPHA2
cortical cytoskeleton organization (GO: 0030865)	4/21	4.01E-06	23.09	DLG1;EPB41L1;EPB41L2;LLGL1
cell projection morphogenesis (GO:0048858)	9/228	8.67E-07	22.21	TOP2B;NUMBL;DST;ABI1;NUMB;ANK3;UTRN;BAIAP2;LLGL1
actin filament-based process (GO:0030029)	10/303	9.84E-07	21.68	PTPN1;NCKAP1;DLG1;MYO1B;CXADR;EPB41L1;EPB41L2;ADD1; LLGL1;PHACTR4
cell part morphogenesis (GO:0032990)	9/248	1.70E-06	21.39	TOP2B;NUMBL;DST;ABI1;NUMB;ANK3;UTRN;BAIAP2;LLGL1
axonogenesis (GO:0007409)	7/109	7.23E-07	21.19	TOP2B;NUMBL;DST;NUMB;ANK3;BAIAP2;LLGL1
cell junction assembly (GO:0034329)	8/160	6.77E-07	21.16	DLG1;OCLN;JUP;DST;DLG5;CTNND1;MLLT4;MTDH
neuron projection morphogenesis (GO: 0048812)	8/175	1.29E-06	20.74	TOP2B;NUMBL;DST;NUMB;ANK3;UTRN;BAIAP2;LLGL1
actin cytoskeleton organization (GO: 0030036)	9/253	1.99E-06	20.60	PTPN1;NCKAP1;DLG1;CXADR;EPB41L1;EPB41L2;ADD1;LLGL1; PHACTR4

Fig 11.13 GO term analysis of FAT4 BioID hits (Velos)

GO term analysis for molecular functions and biological processes are shown as bar graphs and matching tables containing information about significance and gene names. Analysis was performed using the ENRICHR tool. GO terms were rated by combined scores. Only top GO terms are shown.

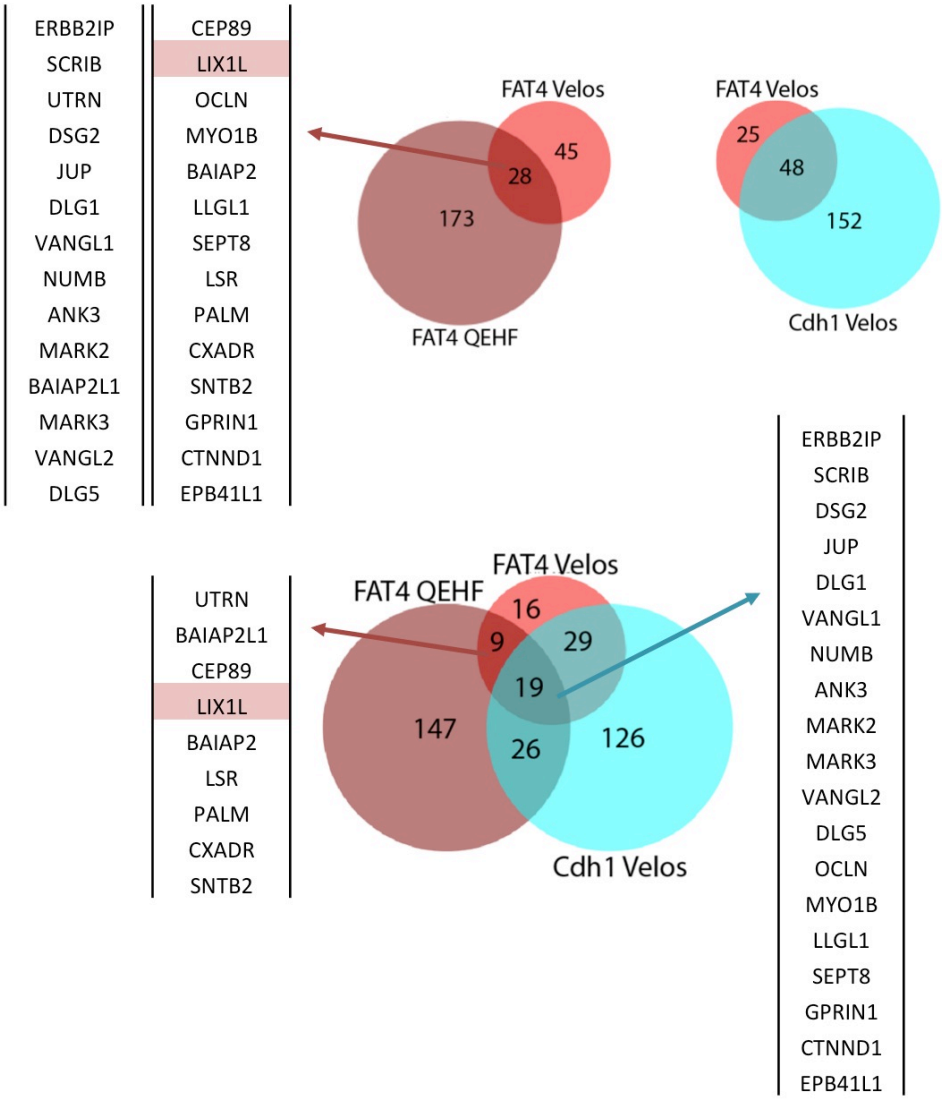

Fig 11.14 Comparison of FAT4 and Cdh1 BioID hits
Venn diagrams illustrate overlaps between FAT4 (Velos and QEHF) and Cdh1 (Velos) BioIDs in HEK293 cells. Gene lists show shared interactors between both FAT4 BioIDs (top left), unique FAT4 interactors (bottom left) and shared interactors between all three BioIDs (bottom right).

11.1.7 FAT4 BioID in other cell lines

We also performed FAT4 (and Cdh1) BioIDs in other cell lines in order to better evaluate general proximity interactors, as well as the level of proteome overlap. We first decided to use a cell line with polarized characteristics, which better simulates the physiological situation of FAT4 and Cdh1 in polarized epithelia. Cultured HEK293T cells are not polarized, which could bring proteins from

different membrane domains into non-physiological contact. We chose HCT116 cells, a human colorectal carcinoma cell line that exhibits characteristics of polarized epithelial cells (Reinacher-Schick and Gumbiner, 2001).

In a similar fashion as for HEK293 T-REx cells, I generated HCT116 T-REx cells with stably integrated FAT4-BF, Cdh1-BF or GFP-BF constructs (Fig. 11.11E). Unlike in HEK293 cells, immunofluorescence stainings revealed that only a subset of cells expressed significant levels of FAT4-BF, which was mainly found in vesicle-like structures in the cytoplasm and at the cell membrane in F-actin rich protrusions. Cdh1-BF showed higher and more uniform expression and similarly localized to cell protrusions and strongly to sites of cell-cell contact, as expected (Fig. 11.15).

BioID in HCT116 cells was performed as for HEK293 cells. However, although we retrieved numerous FAT4 peptides in this BioID, we identified few specific FAT4-BF proximity interactors. This did not seem to be a technical issue, as the parallel runs with Cdh1-BF as bait resulted in a list of proximity interactors, including known binding partners (Table 11.4). I also performed FAT4 and Cdh1 BioIDs in HeLa cells, which gave very similar results (Table 11.3; Fig 11.17). Interestingly, in HeLa cells FAT1 was amongst the few hits, which further indicates that FAT4 and FAT1 can form heterodimers (Badouel et al., 2015). Most cell lines (including HEK293T) don't express FAT cadherins, therefore such interaction has not been discovered in previous mass spectrometry approaches. The known FAT4 interactor LIX1L was recovered in HCT116 and HeLa BioIDs, suggesting that the experimental conditions allowed detection of specific interactors, but for unknown reasons with severely lower sensitivity and prey retrieval efficiency than in HEK293 cells. High abundance of the heat-shock protein HSPA5 as a proximity interactor of FAT4 in HeLa cells (Fig. 11.17) could indicate that overexpression of FAT4-BF in these cells triggers a stress response and possibly problems in protein folding. This might also explain why FAT4-BF expression in HCT116 and HeLa cells was low and not observed robustly in the entire cell population (see Fig. 11.15; Fig. 11.16).

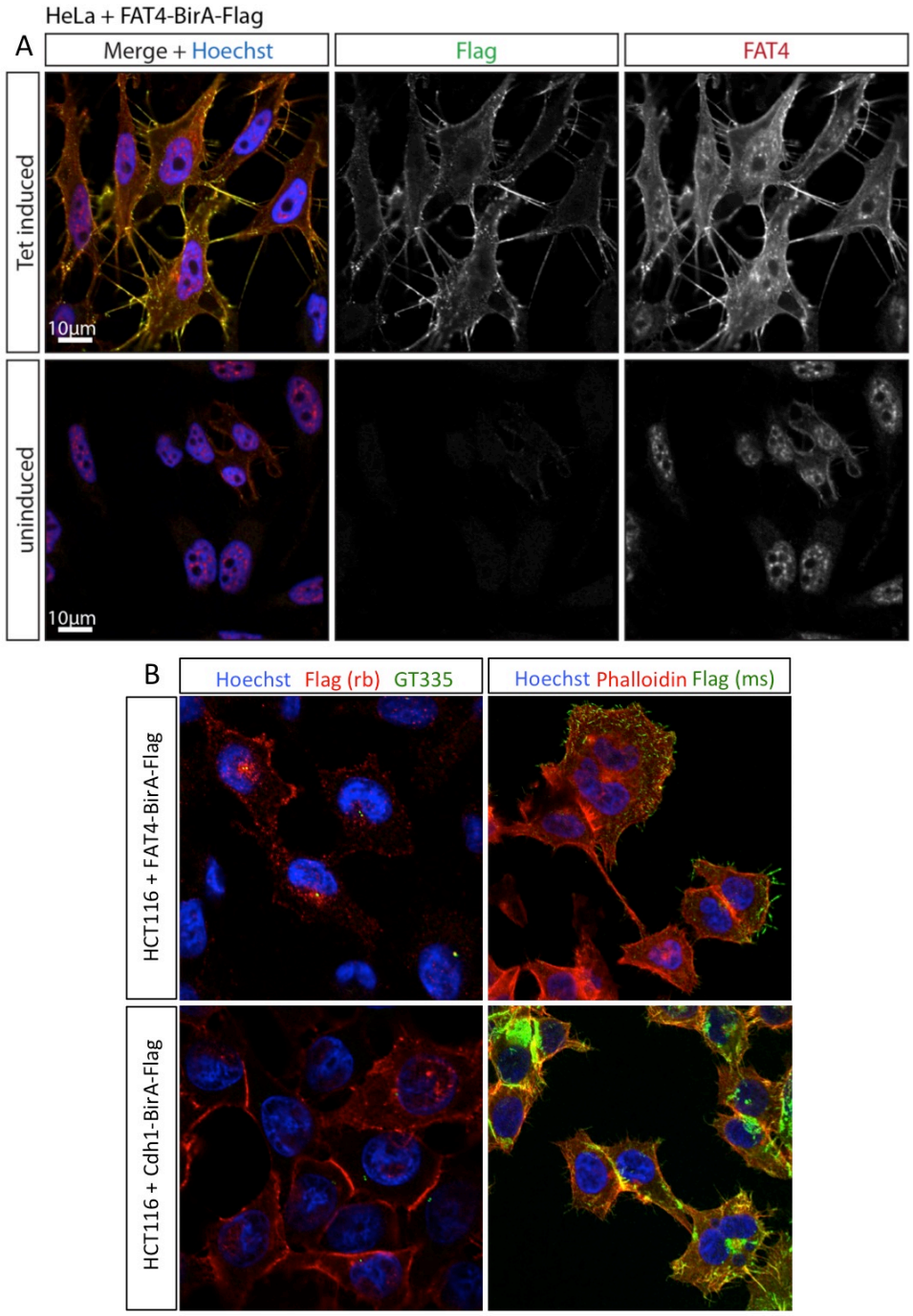

Fig 11.15 Expression test of HeLa and HCT116 stable cell lines for BioID
(A) Stable HeLa cell lines cultured with or without Tet. FAT4-BF expression is only detectable after Tet induction. FAT4 staining co-localizes with Flag staining at cell membranes and filopodia. (B) Stable HCT116 cell lines (Tet induced). FAT4-BF is not expressed in all cells and detectable along cell protrusions. Cdh1-BF localizes to cell-cell contacts and cell protrusions.

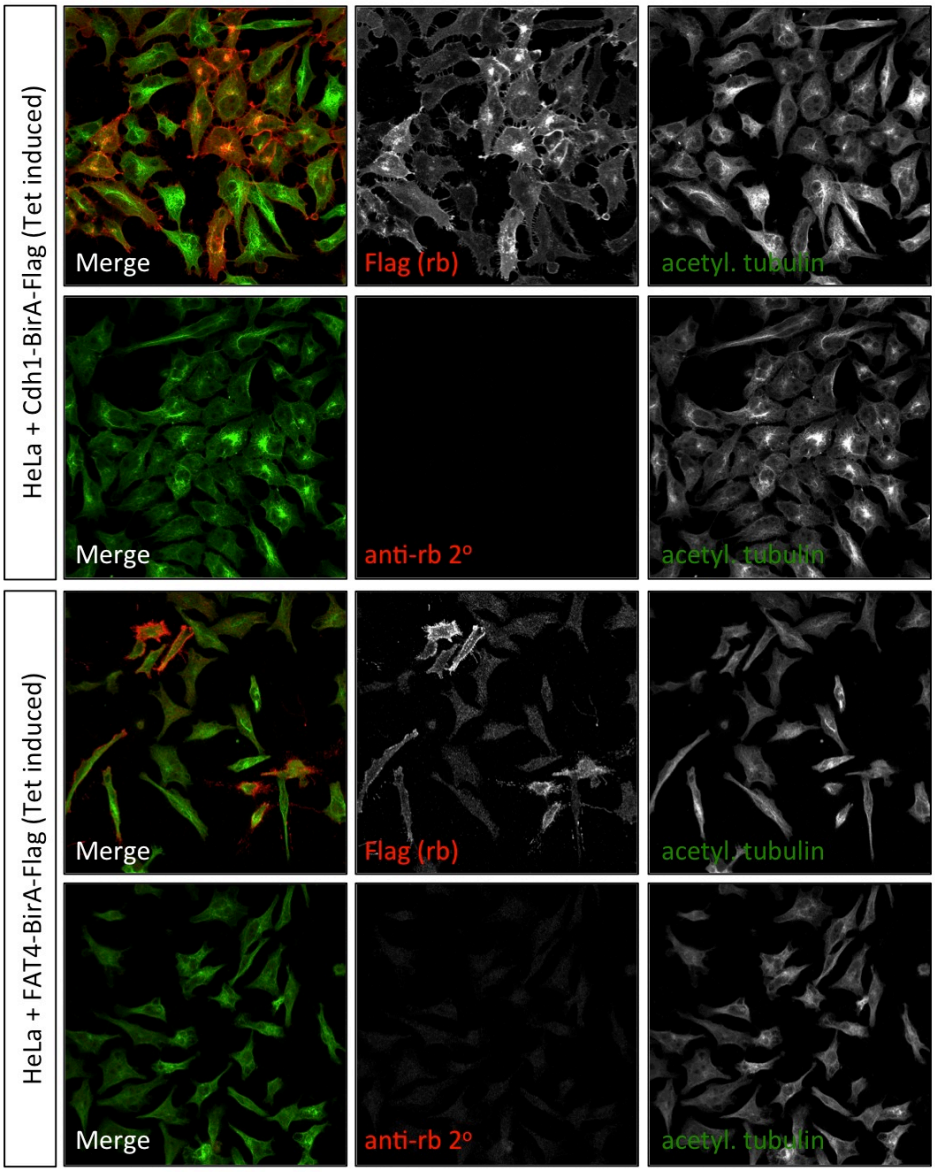

Fig 11.16 Expression test of HeLa stable cell lines for BioID
Stable HeLa cell lines are induced by Tetracycline over night. Flag staining indicates expression of BirA*-Flag tagged FAT4 and Cdh1 constructs. Anti-rb secondary antibody is used as control of staining specificity (no primary antibody used).

Table 11.3 FAT4 and Cdh1 BioID in HeLa cells
All FAT4 hits are shown. Cdh1 hits with an average of > 30 peptides are listed. Full list is shown in Appendix Table 13.4

Bait	Prey	Full Name	Spectra	Average	SAINT	Top 2 Controls	Freq. in Controls
FAT4	FAT4	FAT atypical cadherin 4	517|617	567	**1**	0|0	0/53
FAT4	HSPA5	Heat shock protein family A (Hsp70) member 5	56|81	68.5	**1**	23|22	51/53
FAT4	LIX1L	Limb and CNS expressed 1 like	7|10	8.5	**1**	0|0	0/53
FAT4	JPH1	Junctophilin 1	6|8	7	**0.97**	2|2	4/53
FAT4	LTBP1	Latent transforming growth factor beta binding protein 1	7|5	6	**1**	0|0	0/53
FAT4	FAT1	FAT atypical cadherin 1	3|5	4	**0.99**	0|0	0/53
FAT4	PPFIA1	PTPRF interacting protein alpha 1	2|4	3	**0.93**	0|0	0/53
Cdh1	CTNNA1	Catenin alpha 1	209|199	204	**1**	5|4	8/53
Cdh1	CTNNB1	Catenin beta 1	96|107	101.5	**1**	0|0	0/53
Cdh1	SCRIB	Scribbled planar cell polarity protein	92|89	90.5	**0.99**	42|42	34/53
Cdh1	ARHGAP21	Rho gtpase activating protein 21	66|69	67.5	**1**	10|9	25/53
Cdh1	TRIP11	Thyroid hormone receptor interactor 11	68|62	65	**1**	12|12	18/53
Cdh1	PLEKHA5	Pleckstrin homology domain containing A5	60|65	62.5	**1**	10|8	12/53
Cdh1	GOLGA3	Golgin A3	43|50	46.5	**1**	15|14	26/53
Cdh1	NHS	NHS actin remodeling regulator	44|39	41.5	**1**	8|7	20/53
Cdh1	JUP	Junction plakoglobin	40|39	39.5	**1**	15|15	34/53
Cdh1	VPS13B	Vacuolar protein sorting 13 homolog B (yeast)	34|45	39.5	**1**	0|0	0/53
Cdh1	GOLGA2	Golgin A2	38|40	39	**0.98**	20|19	34/53
Cdh1	KIDINS220	Kinase D-interacting substrate 220kda	27|38	32.5	**1**	9|8	22/53

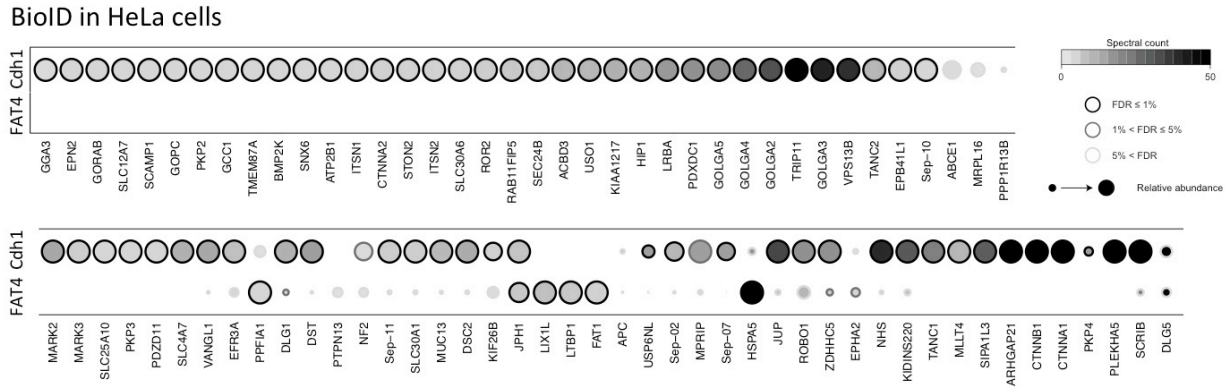

Fig 11.17 Visualization of HeLa BioID
Visual comparison of Cdh1 and FAT4 HeLa BioIDs. Few significant hits are found in FAT4 BioID, including LIX1L and FAT1.

Table 11.4 FAT4 and Cdh1 BioID in HCT116 cells
All FAT4 hits are shown. Cdh1 hits with an average of > 20 peptides are listed. Full list is shown in Appendix Table 13.3

		Top2 controls		FAT4-BirAFlag in HCT116		Cdh1-BirAFlag in HCT116	
Name	**Full Gene Name**			**Average**	**SAINT**	**Average**	**SAINT**
CDH1	*E-cadherin*					**197.25**	**n.a.**
FAT4	*FAT atypical cadherin 4*			**494.5**	**n.a.**		
LIX1L	***limb and CNS expressed 1 like***			**15.75**	**1.00**		
JUP	*junction plakoglobin*	13	12	**10.75**		**376.5**	**1.00**
EPB41L2	*erythrocyte membrane protein band 4.1-like 2*	49	42	**10.5**		**172.5**	**1.00**
SEPT9	*septin 9*	21	19	**9**		**72**	**1.00**
CTNNA1	*catenin alpha 1*	4	2	**7.25**		**1639**	**1.00**
EPHA2	*EPH receptor A2*	21	17	**7.25**		**84.75**	**1.00**
WWOX	*WW domain containing oxidoreductase*	14	14	**7**		**40.75**	**0.76**
ECH1	***enoyl-CoA hydratase 1, peroxisomal***			**7**	**1.00**	**1.25**	
VANGL1	*VANGL planar cell polarity protein 1*	3	1	**6.5**		**85.5**	**1.00**
MIF	***macrophage migration inhibitory factor (glycosylation-inhibiting factor)***			**6.5**	**1.00**		
EPB41	*erythrocyte membrane protein band 4.1*	46	39	**3**		**122.75**	**1.00**
SLC3A2	*solute carrier family 3 (amino acid transporter heavy chain), member 2*	5	3	**3**		**14.25**	**0.78**
MLLT4	*myeloid/lymphoid or mixed-lineage leukemia; translocated to, 4*	16	12	**2.75**		**194.25**	**1.00**
DSG2	*desmoglein 2*	4	3	**2.5**		**207.75**	**1.00**
NUMB	*numb homolog (Drosophila)*	6	5	**1.75**		**34.5**	**1.00**
CYFIP1	*cytoplasmic FMR1 interacting protein 1*	5	5	**1.5**		**23**	**0.95**
ERBB2IP	*erbb2 interacting protein*	4	3	**0.75**		**239.25**	**1.00**
CTNND1	*catenin delta 1*	12	11	**0.25**		**675.5**	**1.00**
CTNNB1	*catenin beta 1*	7	7			**926.5**	**1.00**
CTNNA2	*catenin alpha 2*					**220.5**	**1.00**
ANK3	*ankyrin 3, node of Ranvier (ankyrin G)*					**146.25**	**1.00**
VPS13B	*vacuolar protein sorting 13 homolog B (yeast)*					**121**	**1.00**
MARK2	*MAP/microtubule affinity-regulating kinase 2*	1				**66.75**	**1.00**
MYO1B	*myosin IB*	16	16			**66.75**	**1.00**
PKP4	*plakophilin 4*					**51.25**	**1.00**
DLG1	*discs, large homolog 1 (Drosophila)*	9	3			**46.25**	**1.00**
SEPT11	*septin 11*	13	12			**44**	**1.00**
DLG5	*discs, large homolog 5 (Drosophila)*	5	3			**39.25**	**1.00**
CDH3	*cadherin 3, type 1, P-cadherin (placental)*					**37**	**1.00**
FAM129B	*family with sequence similarity 129 member B*	3	2			**28.5**	**1.00**
SEPT6	*septin 6*	8				**26.75**	**0.92**
USP6NL	*USP6 N-terminal like*					**25.5**	**1.00**
PPFIBP1	*PTPRF interacting protein, binding protein 1 (liprin beta 1)*	8	4			**25**	**1.00**
EFR3A	*EFR3 homolog A*	4	4			**24.5**	**1.00**
UTRN	*utrophin*	1				**24.25**	**1.00**

11.1.8 FAT4 localization

Little is known about the localization of FAT4 within cells and tissues, and if FAT4 is regulated through subcellular localization or membrane availability. So far, antibody limitations have precluded detailed analysis of FAT4 localization at the membrane or elsewhere, except for one specific FAT4 antibody generated by the Tanoue lab, which labeled apical junctions in cortical neuron precursors (Ishiuchi et al., 2009). However, while previous work in our lab had found strong

centrosomal signal in MDCK cells (Saburi et al., 2008), the FAT4 antibody specificity was never fully confirmed. I therefore used the newly established FAT4 cell lines and knockdown tools to re-address the specificity of available FAT4 antibodies for use in immunofluorescence.

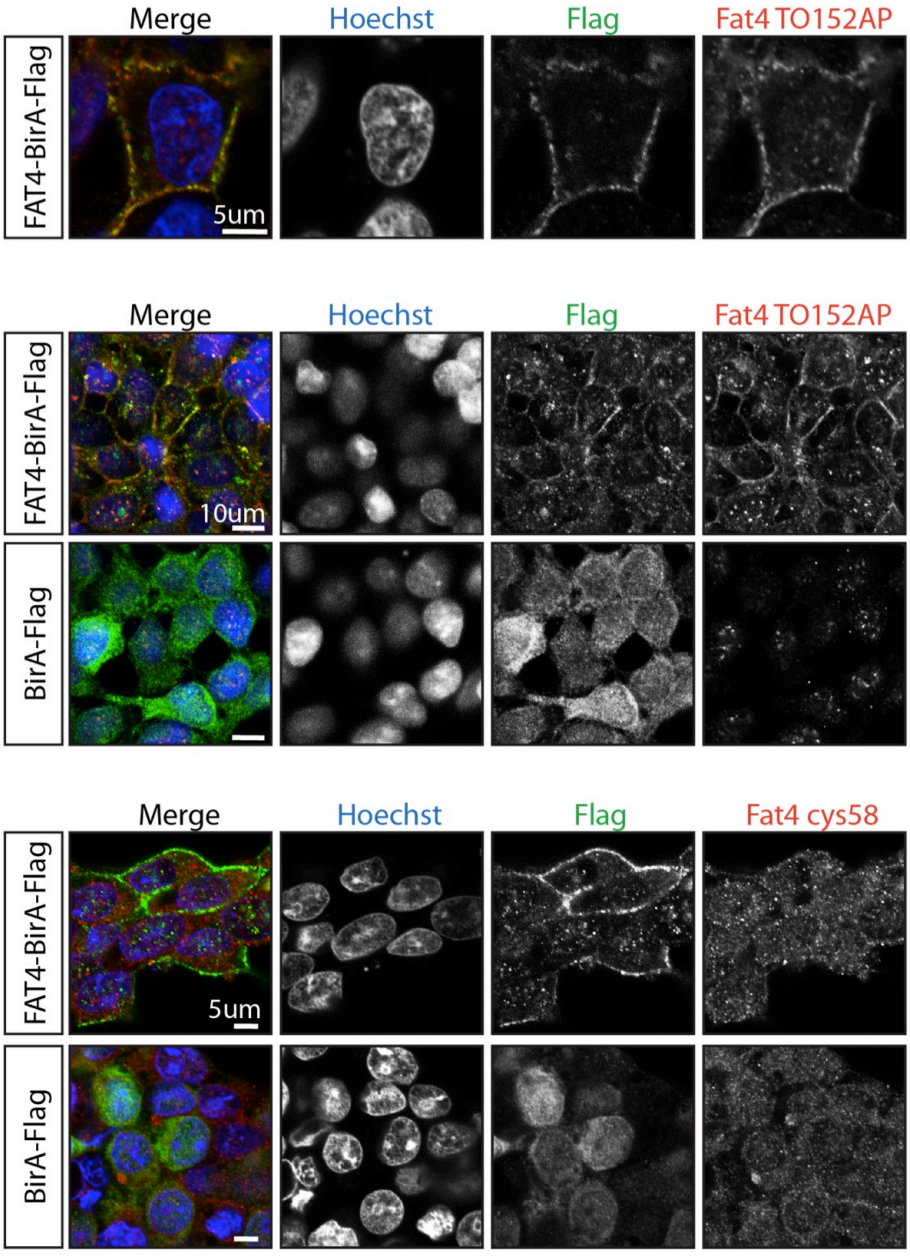

Fig 11.18 FAT4 antibody tests in HEK293 stable cell lines
HEK293 stable cells are Tet induced and stained with antibodies as indicated. FAT4 TO152AP shows strong colocalization with Flag staining in FAT4-BirA*-Flag expressing but not BirA*-Flag expressing cells. FAT4 cys58 antibody appears to be unspecific.

Of several antibodies made in our lab, TO152AP, an affinity-purified polyclonal antibody that had been raised against the entire intracellular domain of FAT4, was most specific. It detected overexpressed FAT4-BF in HEK293 T-REx and HeLa T-REx cells, as well as constitutively expressed FAT4-YFP in MCF7 cells. In contrast, our homemade peptide antibody FAT4cys58 did not recognize overexpressed FAT4-BF (Fig. 11.18). Unfortunately, while potent in detecting FAT4 protein on Western blots, TO152AP did not seem to reliably recognize endogenous FAT4 in immunofluorescence stainings. A difference in signal intensity was seen between mouse embryonic fibroblasts (MEFs) derived from wildtype mice and MEFs from *Fat4* knockout mice. However, signal intensity and quality was low and did not allow detection of detailed structures (Fig. 11.19).

In HeLa T-REx cells that hadn't been induced for FAT4-BF expression, TO152AP only showed a nuclear signal (Fig. 11.15). In RPE-1 cells, TO152AP similarly labeled nuclei without detecting protein at the plasma membrane. Interestingly, when co-stained with a centrosomal marker, it became clear that TO152AP also labeled centrosomes in RPE-1 cells. However, neither centrosomal nor nuclear signals decreased upon FAT4 knockdown, suggesting that these signals are likely unspecific. Similar results were obtained with a commercial FAT4 antibody (Novus), which is raised against an extracellular FAT4 peptide spanning EGF repeats and LaminiG-like domains. The Novus antibody detected overexpressed FAT4, such as FAT4-YFP in MCF7 cells (Fig. 11.19). In RPE-1 cells it labeled centrosomes and short filaments of unknown origin, but both signals were not affected by FAT4 knockdown, suggesting they are unspecific (Fig. 11.20). In summary, the FAT4 antibodies TO152AP and Novus can reliably detect overexpressed but not endogenous FAT4 in immunofluorescence stainings. In HeLa, MCF7 and HCT116 cells, overexpressed FAT4 was mainly localized at the plasma membrane, along actin-rich protrusions and filopodia and in the cytosol in a punctate pattern, possibly reflecting vesicles. A FAT4 signal was further occasionally found at the centrosome and the midbody (Fig. 11.21). FAT4-YFP and CDH1/E-cad partially colocalized at cell-cell contacts of MCF7 cells, suggesting that a physical or functional interaction of the two is possible (Fig. 11.21B).

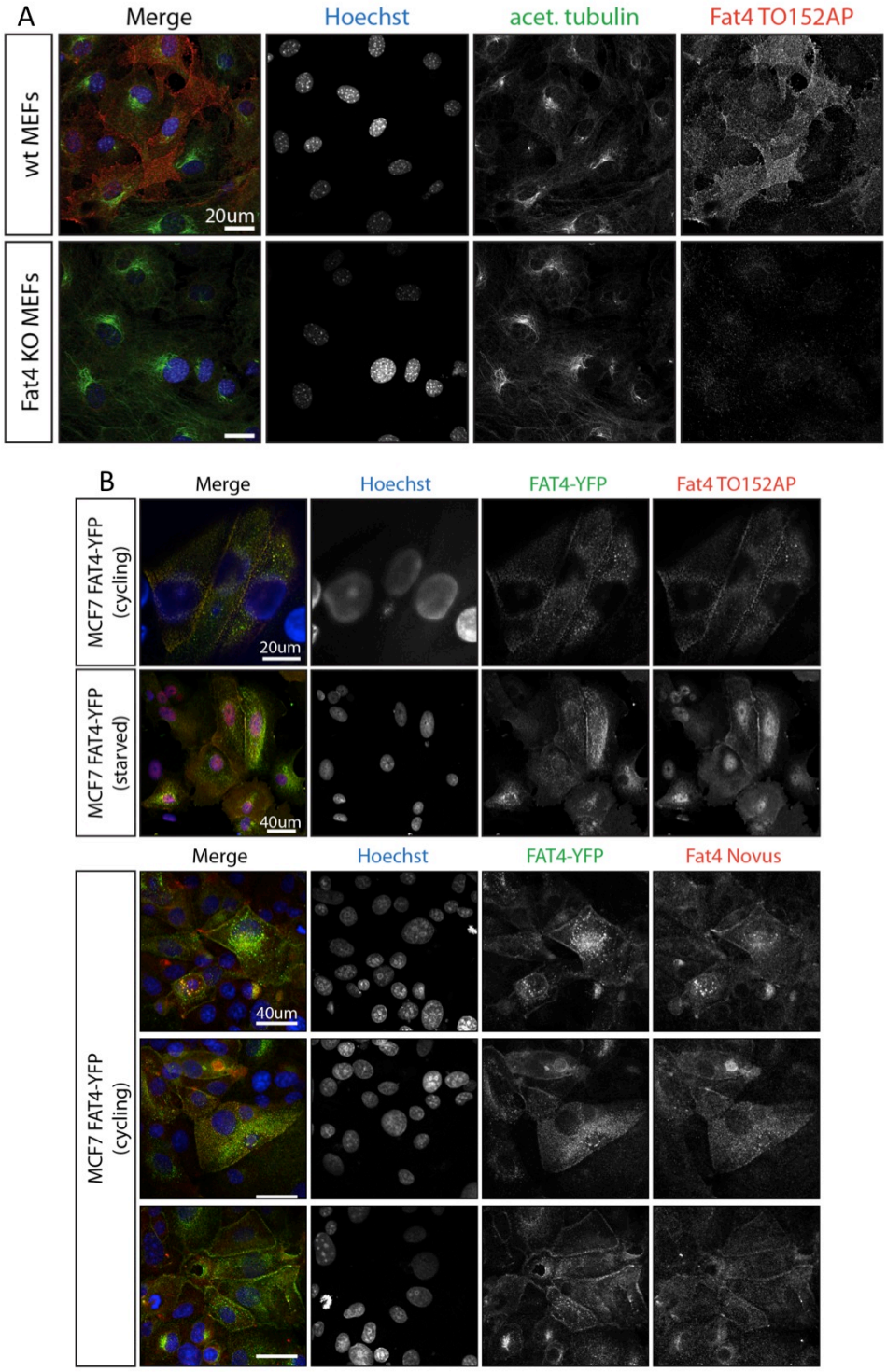

Fig 11.19 FAT4 staining in mouse embryonic fibroblasts and MCF7 cells
(A) Mouse embryonic fibroblasts from wildtype or Fat4-/- embryos. TO152AP antibody detects endogenous Fat4 but with low sensitivity. (B) TO152AP and Novus antibodies recognize overexpressed FAT4-YFP in MCF7 cells. FAT4-YFP localizes to cell-cell contacts and cytoplasmic spots, possibly representing vesicles.

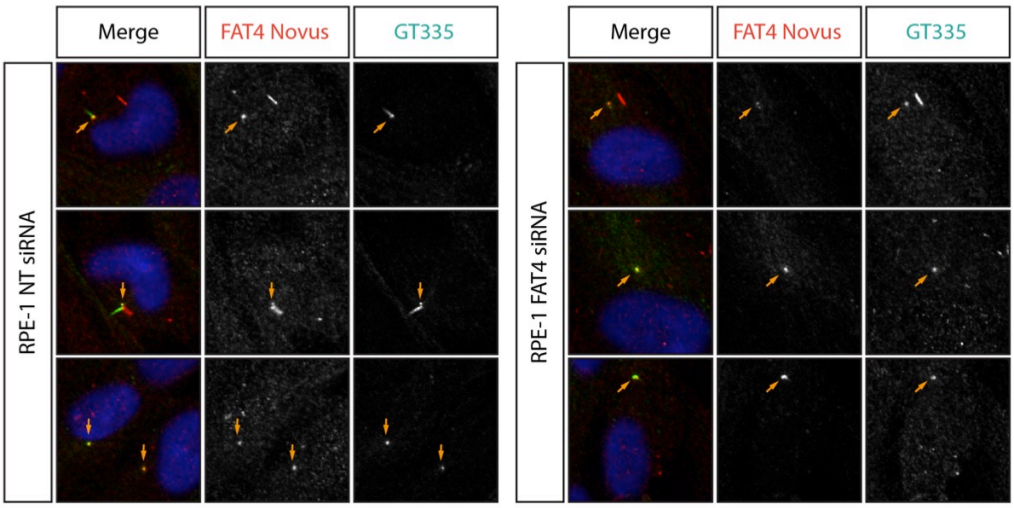

Fig 11.20 FAT4 antibody staining in RPE-1 cells
RPE-1 cells transfected with siRNAs for 72h. Centrosomes and cilia are marked by GT335. FAT4 Novus antibody labels centrosomes (orange arrows) and filamentous structures of unknown nature, but signal intensity is not affected by FAT4 knockdown (FAT4 siRNA pool (#1+3+4)), indicating the signal is unspecific.

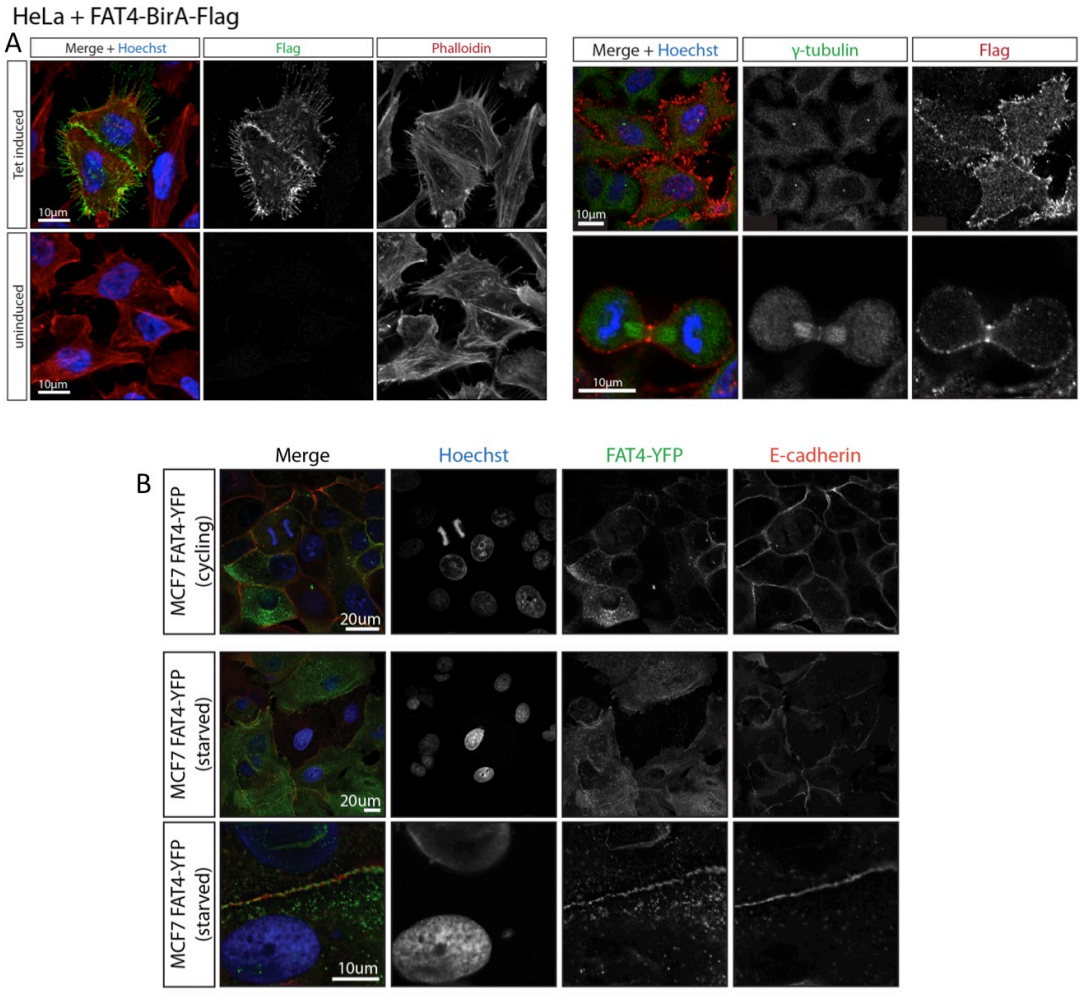

Fig 11.21 FAT4 localization in HeLa and MCF7 cells
(A) HeLa cells uninduced or induced for FAT4-BirA*-Flag expression. FAT4-BirA*-Flag localizes to cell protrusions, partially colocalizing with Phalloidin. Occasionally FAT4-BirA*-Flag localizes to the midbody. (B) FAT4-YFP partially colocalizes with E-cadherin at cell-cell junctions.

11.2 Investigation of a functional link between FAT4 and primary cilia

11.2.1 Loss of Fat4 causes renal cysts in mice

Fat4 mutant mice exhibit kidney cysts at birth, with regions of morphologically abnormal or missing cilia (Saburi et al., 2008). A growing body of evidence suggests that cystic kidney disease and primary cilia defects are linked, as many proteins involved in cystic pathologies localize to and function at the cilium or basal body (Yoder et al., 2002; Yoder, 2007). Additionally, multiple connections between cilia and PCP have been identified (Ross et al., 2005; Antic et al., 2010; Hashimoto et al., 2010; Song et al., 2010; Tissir et al., 2010; Wallingford and Mitchell, 2011; Boutin et al., 2014). Defects in primary cilia often affect several organs and can cause diverse ciliopathies. Also, *Fat4* knockout mice show phenotypes in different organs that resemble ciliopathic defects, such as skeletal malformations, brain abnormalities caused by impaired neuronal migration, as well as cochlea and kidney defects (Saburi et al., 2008; Mao et al., 2011a; Cappello et al., 2013; Badouel et al., 2015). I therefore wondered if Fat4 plays a direct role in cilium biology.

11.2.2 FAT4 knockdown affects primary cilia in RPE-1 cells

As a first step, I addressed if FAT4 plays a role in cilium formation or maintenance. RPE-1 cells are the most commonly used cell culture tool to study primary cilia and are a robust and easy to manipulate experimental system. Cells were typically serum-starved for a duration of 48h – 72h, as starvation can induce primary cilium formation in a significant population of cells (Tucker et al., 1979; Vorobjev and Chentsov Yu, 1982).

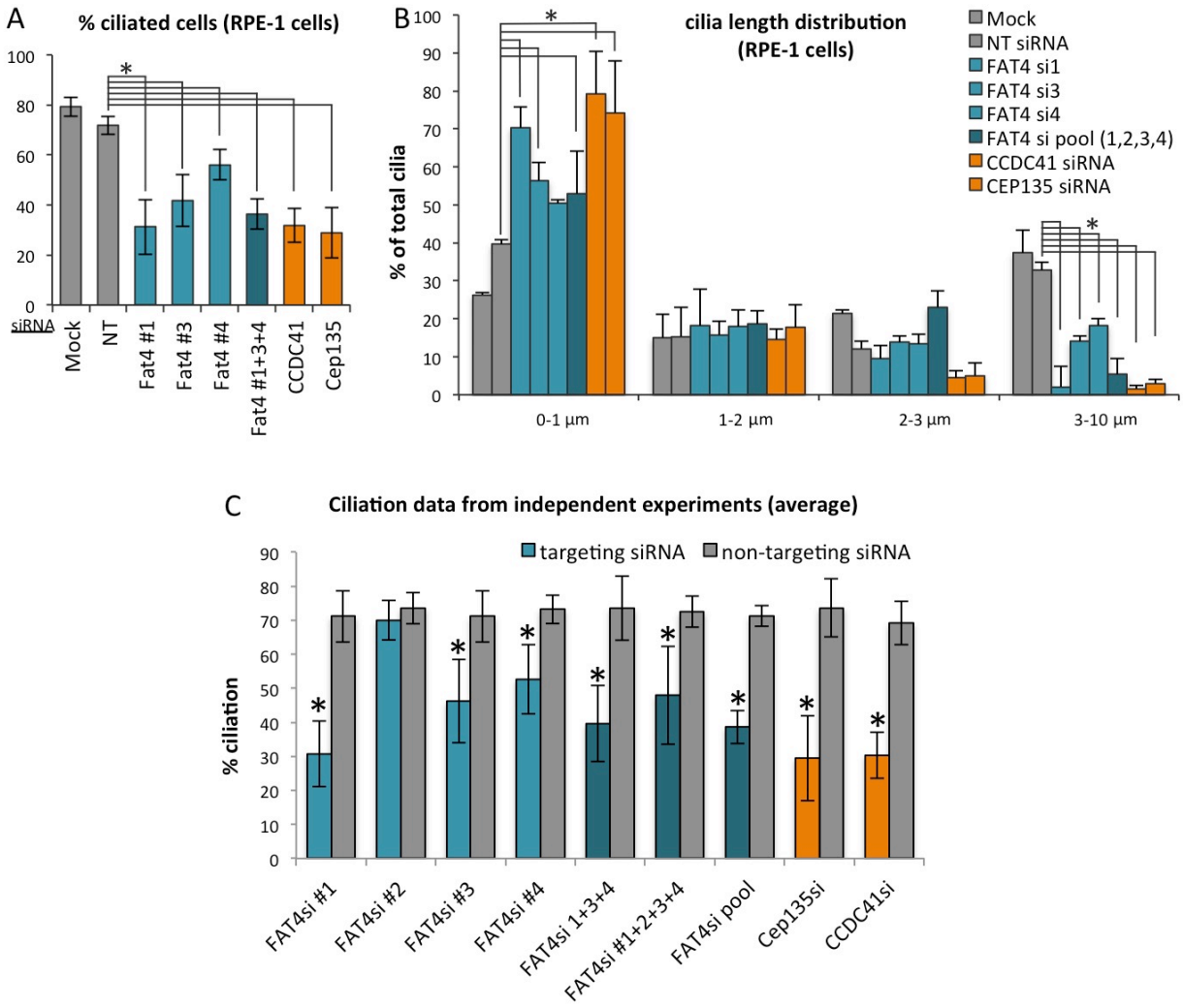

Fig 11.22 Ciliation and cilia length are reduced in FAT4 knockdown cells
FAT4 knockdown by siRNAs in RPE-1 cells. CCDC41 and Cep135 are known regulators of ciliogenesis and their knockdown serves as positive controls. Mock is transfection reagent only. NT is non-targeting siRNA. (A, B) 3 independent FAT4 siRNAs (#1, #3, #4) and their pool cause reduction in the number of ciliated cells and reduced cilia lengt within a cell population (G-slides; n=3 experiments with 2 technical replicates each; ttest to NT with * = $p < 0.05$). (C) Percentage of ciliation averaged over several experiments. Each targeting siRNA is compared to non-targeting siRNA values from the same experiments. Numbers of biological replicates (+ technical repeats) are as following: FAT4si #1: n=5 (+3); FAT4si #2: n=3 (+2); FAT4si #3: n=5 (+3); FAT4si #4: n=4 (+2); FAT4si #1+3+4: n=13 (+4); FAT4si #1+2+3+4: n=2 (+2); FAT4si pool: n=2 (+2). All error bars represent standard deviations. Student's t-test: * = $p<0.05$.

In collaboration with Dr. Laurence Pelletier's lab, I quantitatively tested the effect of FAT4 knockdown by four individual siRNAs and their pool on ciliation of starved RPE-1 cells (see also Fig. 11.7). For RPE-1 culture, transfection and stainings, I used special coverslips with small wells that are separated by hydrophobic coating (G-slides), which allow synchronous processing of separately transfected cells. Cells on G-slides were stained with the DNA dye Hoechst and antibodies against the basal body marker gamma-tubulin and the ciliary axoneme marker Arl13b. Automatic imaging and image processing was used to detect primary cilia and measure axoneme lengths (method described in (Gupta et al., 2015)). Strikingly, 3 of the 4 siRNAs targeting FAT4, as well as their pool, reduced the number of ciliated cells within the population significantly. The magnitude of the effect was comparable to knockdown of the positive controls CEP135, a centrosomal protein essential for ciliogenesis in RPE-1 cells (Gupta et al., 2015) and CCDC41, a centriolar appendages protein required for docking of the ciliary vesicle to the mother centriole (Joo et al., 2013). In addition to a lower percentage of ciliated cells, most remaining cilia were also significantly shorter (Fig. 11.22).

These results were not just due to loss of the assessed cilia marker, since different combinations of cilia stainings (such as Arl13b and GT335) and centrosome stainings (gamma-tubulin, GT335, centrin, pericentrin) showed the cilia loss (Fig. 11.26; 11.27; 11.29). Together, these data suggested a role for FAT4 in cilia formation or maintenance.

11.2.3 The role of FAT1 in primary cilia

As Fat4 and Fat1 interact and function together (Badouel et al., 2015), and loss of *Fat1* enhances the kidney cysts of *Fat4* mutant mice (Saburi et al., 2012), I also tested if FAT1 similarly played a role in cilium formation or maintenance. Three individual siRNAs strongly reduced FAT1 protein as assessed by Western blot, however did not consistently affect cilia numbers in RPE-1 cells, despite a mild trend towards a reduction in ciliation (Fig. 11.23). Two out of three FAT1 siRNAs, as well as the siRNA pool, caused a reduction in cilia length, similarly to FAT4 knockdown cells. Together, this suggested a minor role for FAT1 in cilium

morphology. Interestingly, FAT1 staining of starved RPE-1 cells showed a signal at the cell cortex, as well as along ciliary axonemes. However, while FAT1 knockdown strongly reduced the cortical signal, it did not result in a clear reduction of ciliary staining (Fig. 11.23D). Therefore, the specificity of the ciliary staining remained questionable. On the other hand, persisting protein at primary cilia of FAT1 knockdown cells could also mask requirements for FAT1 in this organelle.

Surprisingly, I noticed that FAT1 levels were increased in cells treated with the FAT4 siRNA pool (#1+3+4) (Fig. 11.24). To test if FAT1 is compensating for FAT4 depletion, I assessed cilia in cells with single or double knockdowns of both proteins. FAT1, FAT4 double knockdown resulted in the same strength of a ciliation defect as the FAT4 knockdown alone (Fig. 11.23). This suggested that, even if the observed increase in FAT1 protein level represented a compensatory mechanism in response to loss of FAT4, it had no significant effect on ciliation.

11.2.4 Localization of FAT4

How could FAT4 regulate primary cilia? Other transmembrane proteins, such as TMEM67 (MKS3/Meckelin) or Polycystins, are well-established regulators of cilia function and localize to the ciliary membrane (Pazour et al., 2002; Yoder et al., 2002; Dawe et al., 2007). Unfortunately, antibody difficulties precluded the investigation of FAT4 protein localization in RPE-1 cells. I occasionally detected weak signals of overexpressed FAT4-YFP or FAT4-BF along primary cilia in HEK293 T-REx cells, but could not consistently repeat these findings. HEK293 cells are also extremely sensitive to starvation and therefore not a good model system to study cilia. The HeLa and MCF7 cell lines stably expressing FAT4 fusion proteins don't ciliate, as commonly observed for transformed cells.

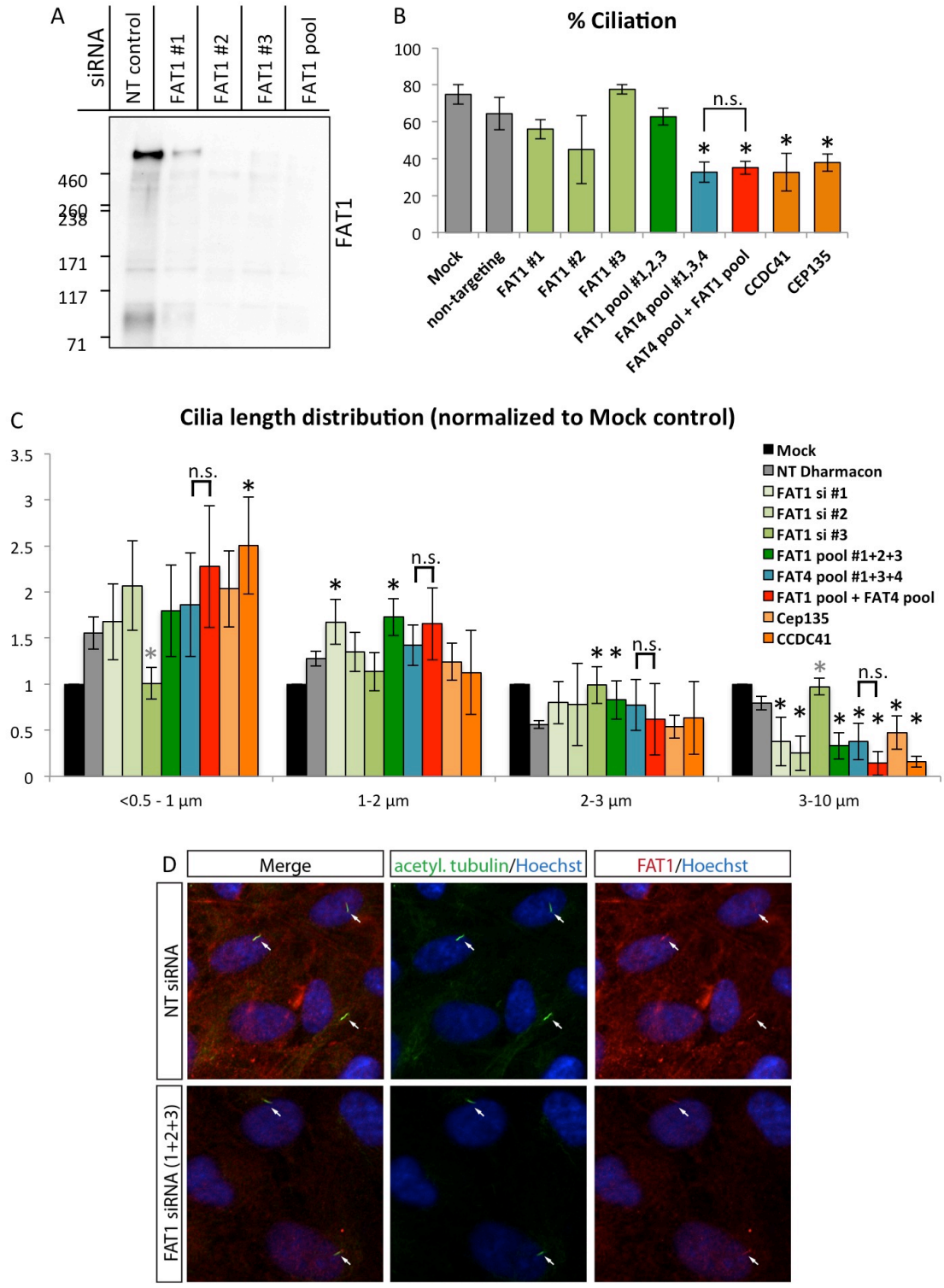

Fig 11.23 FAT1 knockdown does not affect ciliation of RPE-1 cells
(A) Western blot of RPE-1 cells treated with FAT1 siRNAs for 72h. (B) FAT1 knockdown does not cause reduction in the number of ciliated cells within a population of RPE-1 cells. FAT1 and FAT4 double knockdown is indistinguishable from FAT4 knockdown. (C) Two out of three FAT1 siRNAs and the siRNA pool cause significant shortening of cilia. No significant enhancement in cilia shortening is found from FAT1, FAT4 double knockdown. (D) RPE-1 cells starved for 48h and treated with siRNAs for 72h. FAT1 staining is detected at the cell cortex and along cilia, but cilia signal persists after FAT1 knockdown. All error bars represent standard deviations.

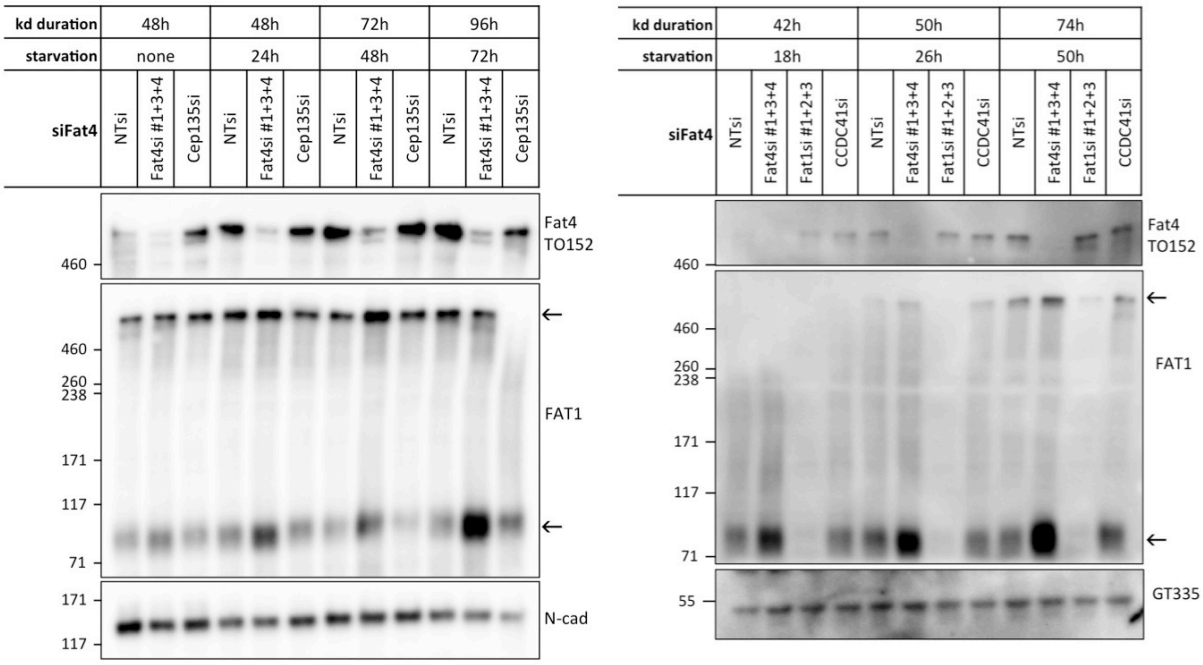

Fig 11.24 FAT1 levels are enhanced in FAT4 knockdown cells
RPE-1 cells are treated with siRNAs and starve as indicated. Noticeable increase in FAT1 levels (full-length (500kDa) and processed (85kDa)) is detected at all time points.

To circumvent antibody limitations, I chose to use CRISPR/Cas9 to tag the endogenous *FAT4* gene in RPE-1 cells with a GFP-coding cassette. However, although these cells express the FAT4-GFP fusion protein as assessed by Western blot (Fig. 11.7D), I was unable to detect a specific GFP signal in live and fixed cells. I tested different fixation methods and GFP antibodies, but autofluorescence of the cells (both live and fixed) and non-specific background staining of the GFP antibodies did not allow for a very sensitive detection. It is therefore possible that endogenous FAT4-GFP protein levels are too low for detection by this approach. Attempts to generate FAT4-YFP or FAT4-BF overexpressing RPE-1 cells were unsuccessful. It therefore remains unknown where FAT4 localizes in RPE-1 cells.

11.2.5 FAT4 BioID using ciliated HEK293 cells

The original FAT4 BioID had identified Septins (SEPT3, SEPT5, SEPT7, SEPT8 and SEPT10) as proximity interactors. Septins have multiple functions in cells, which range from roles in the cytoskeleton, cell motility, cytokinesis to vesicle trafficking and cilium formation (Cesario and Bartles, 1994; Schmidt and Nichols, 2004; Ihara et al., 2005; Kissel et al., 2005; Steels et al., 2007; Xie et al., 2007; Estey et al., 2010; Kwitny et al., 2010). However, the BioID was performed in cycling cells, where only a small population of cells was expected to be ciliated. In order to test if a cilium signature within proximity interactors would emerge under ciliated conditions, I had included ciliated samples in the Velos FAT4 BioID. I employed a starvation protocol that had been used successfully to elicit centrosomal interactome changes upon ciliation (Gupta et al., 2015). For this "ciliated" BioID, cells were induced, biotin treated and harvested under serum starvation.

The ciliated BioID was surprisingly similar to BioID from cycling cells with no clear enrichment of cilia-associated proximity interactors (Table 11.2; 11.5). An enrichment of Septins as expected from the QEHF BioID was not confirmed and only SEPT8 was found in ciliated runs. Interestingly, several components of the actin regulating WAVE regulatory complex (WRC) were enriched in the ciliated FAT4 BioID, but not in controls or ciliated Cdh1 runs. These included Abl-interactor 1 (ABI1), NCK-associated protein 1 (NCKAP1) and Cytoplasmic FMR1 Interacting Protein 1 and 2 (CYFIP1, CYFIP2). This might indicate an involvement of FAT4 with the actin cytoskeleton. Also, DLG1, LLG1 and to a lesser extent SCRIB were preferentially found in the ciliated FAT4 BioID and although they are shared interactors with Cdh1, a similar enrichment was not seen in the ciliated Cdh1 BioID. Therefore, starvation treatment changes the FAT4 proximity interaction network. However, as ciliated conditions did not promote spatial association of FAT4 with ciliary proteins, a functional link to primary cilia remained elusive.

Table 11.5 Comparison of cycling and starved Velos BioID runs
Hits increasing (green) or decreasing (red) in starvation shown. fc=fold change.

Gene Name	Full name	Top 4 controls								FAT4 BioID cycling (Velos)								FAT4 BioID starved (Velos)								Comparison cycling vs. starved	
										pool A		pool B		Total		SAINT		pool A		pool B		Total		SAINT			
										#1	#2	#1	#2					#1	#2	#1	#2					fc	p-value
FAT4	*FAT atypical cadherin 4*									1173	1380	1108	1415	5076				1120	949	1385	1006	4460				0.9	2.6E-01
SSRP1	*structure specific recognition protein 1*	5	3							32	24	20	28	104	1.00											0.0	5.6E-05
SUPT16H	*SPT16 homolog, facilitates chromatin remodeling subunit*	6	5							22	31	17	27	97	0.98											0.0	2.1E-04
DLG1	*discs large homolog 1*									17	23	15	29	84	1.00			49	40	71	56	216	1.00			2.6	3.9E-03
CYFIP2	*cytoplasmic FMR1 interacting protein 2*	4	4							23	21	18	16	78	0.99			54	43	52	47	196	1.00			2.5	5.6E-05
PTPN13	*protein tyrosine phosphatase, non-receptor type 13*	3								20	20	19	15	74	1.00			6	7	13	11	37	0.93			0.5	3.9E-03
ADD3	*adducin 3*	7	7	6	5					14	18	13	28	73				39	30	51	44	164	1.00			2.2	6.6E-03
ANK3	*ankyrin 3, node of Ranvier (ankyrin G)*									13	9	17	17	56	1.00			53	35	53	46	187	1.00			3.3	4.2E-04
CYFIP1	*cytoplasmic FMR1 interacting protein 1*	12								22		16	16	54				51	35	48	38	172	0.98			3.2	2.9E-03
PHACTR4	*phosphatase and actin regulator 4*	2								9	9	7	9	34	0.99			22	18	26	21	87	1.00			2.6	2.6E-04
NCKAP1	*NCK associated protein 1*	2								7	8	8	9	32	0.99			54	39	48	37	178	1.00			5.6	9.6E-05
LEMD3	*LEM domain containing 3*	4	4							4	10	4	6	24				12	12	17	11	52	0.92			2.2	1.2E-02
CKAP4	*cytoskeleton-associated protein 4*	4	4	3						6	3	6	8	23				12	11	10	15	48	0.95			2.1	5.8E-03
VAPB	*VAMP (vesicle-associated membrane protein)-associated protein B and C*	6	6	4	3					6	9	4	3	22				14	17	28	16	75	0.92			3.4	8.1E-03
PTPN1	*protein tyrosine phosphatase, non-receptor type 1*	4								6	8	3	3	20				11	14	15	12	52	0.96			2.6	1.9E-03
SSR4	*signal sequence receptor, delta*									5	6	4	4	19	1.00			13	11	9	9	42	1.00			2.2	1.7E-03
TACC1	*transforming acidic coiled-coil containing protein 1*	4	2							2	5	3	8	18				14	10	17	11	52	0.96			2.9	6.2E-03
ESYT2	*extended synaptotagmin like protein 2*									4	4	6	3	17	1.00			14	13	11	14	52	1.00			3.1	9.0E-05
CDIPT	*CDP-diacylglycerol--inositol 3-phosphatidyltransferase*									3		8	6	17				11	10	13	14	48	1.00			2.8	7.7E-03
OCLN	*occludin*									3	2	5	6	16	0.98					3		3				0.2	3.3E-02
STIM1	*stromal interaction molecule 1*									4		5	6	15				13	7	8	7	35	1.00			2.3	4.2E-02
ECH1	*enoyl-CoA hydratase 1, peroxisomal*	2								3	6	3		12				13	7	13	10	43	0.99			3.6	6.3E-03
OSBPL8	*oxysterol binding protein like 8*									3		3	3	9				10	10	13	9	42	1.00			4.7	3.6E-04
ABI1	*abl interactor 1*										3	3	3	9				10	8	7	8	33	1.00			3.7	8.6E-04
SRPR	*SRP receptor alpha subunit*	2								4		4		8				6	6	6	4	22	0.91			2.8	3.2E-02
KANK2	*KN motif and ankyrin repeat domains 2*										4	4		8				5	4	6	6	21	1.00			2.6	4.1E-02
LLGL1	*lethal giant larvae homolog 1 (Drosophila)*											3	4	7				9	10	14	9	42	1.00			6.0	1.4E-03
HSD17B12	*hydroxysteroid (17-beta) dehydrogenase 12*	3									4			4				7	4	10	11	32	0.87			8.0	9.6E-03
CTNND1	*catenin delta 1*	3										3		3				6	6	17	7	36	0.89			12.0	2.5E-02
SNTB2	*syntrophin beta 2*	3										3		3				7	8	10	7	32	0.92			10.7	4.1E-04
SEPT8	*septin 8*																	18	14	17	10	59	1.00			>	1.8E-04
HSPA12A	*heat shock protein family A (Hsp70) member 12A*																	4	9	8	7	28	1.00			>	6.4E-04
LSR	*lipolysis stimulated lipoprotein receptor*																	7	5	9	4	25	1.00			>	1.3E-03
ROR2	*receptor tyrosine kinase-like orphan receptor 2*																	6	3	7	4	20	1.00			>	1.5E-03
PALM	*paralemmin*																	5	3	7	4	19	1.00			>	1.4E-03
CXADR	*coxsackie virus and adenovirus receptor*																	6	3	5	3	17	0.99			>	1.3E-03

11.2.6 FAT4 knockdown affects cilia maintenance

A net reduction of primary cilia can be caused by defects in cilium formation or in cilium maintenance. To distinguish between these two scenarios, I performed a set of preliminary starvation time courses and quantified ciliation at each time point. In a three-day starvation time course experiment, RPE-1 cells transfected with non-targeting siRNA showed an increase in ciliation with increasing starvation times. Interestingly, cells treated with FAT4 siRNAs showed a similar percentage of ciliation as control cells after one day of starvation, but subsequently lost cilia on day 2 and day 3 of starvation. The control knockdown with Cep135 siRNAs resulted in a steadily low ciliation phenotype throughout the time course, in agreement with its function in early cilium formation (Fig. 11.25A; experimental time lines are shown in the figure). This experiment suggested that cilia are first established but cannot be maintained in FAT4 knockdown cells. Western blot analysis confirmed efficient FAT4 protein depletion at each time point (Fig. 11.24).

In this experiment. however, also the duration of knockdown increased with prolonged starvation, which might modulate the phenotype. To address if the gradual loss of cilia was caused by prolonged knockdown rather than starvation, I cultured siRNA-transfected RPE-1 cells for three days before starting the starvation time course. The results were less dramatic than from the first experimental setup (possibly because siRNA concentrations within the cells were diluted from prolonged culturing), but showed the same trend: after one day of starvation FAT4 knockdown cells had cilia numbers indistinguishable from control cells, but while control cells increased their cilia numbers with prolonged starvation, FAT4 knockdown cells gradually lost cilia. Knockdown of CCDC41, which is essential for cilium formation, showed low cilia numbers throughout the experiment and even established some new cilia late in starvation (Fig. 11.25B). Together, these observations suggested a role for FAT4 in cilium maintenance.

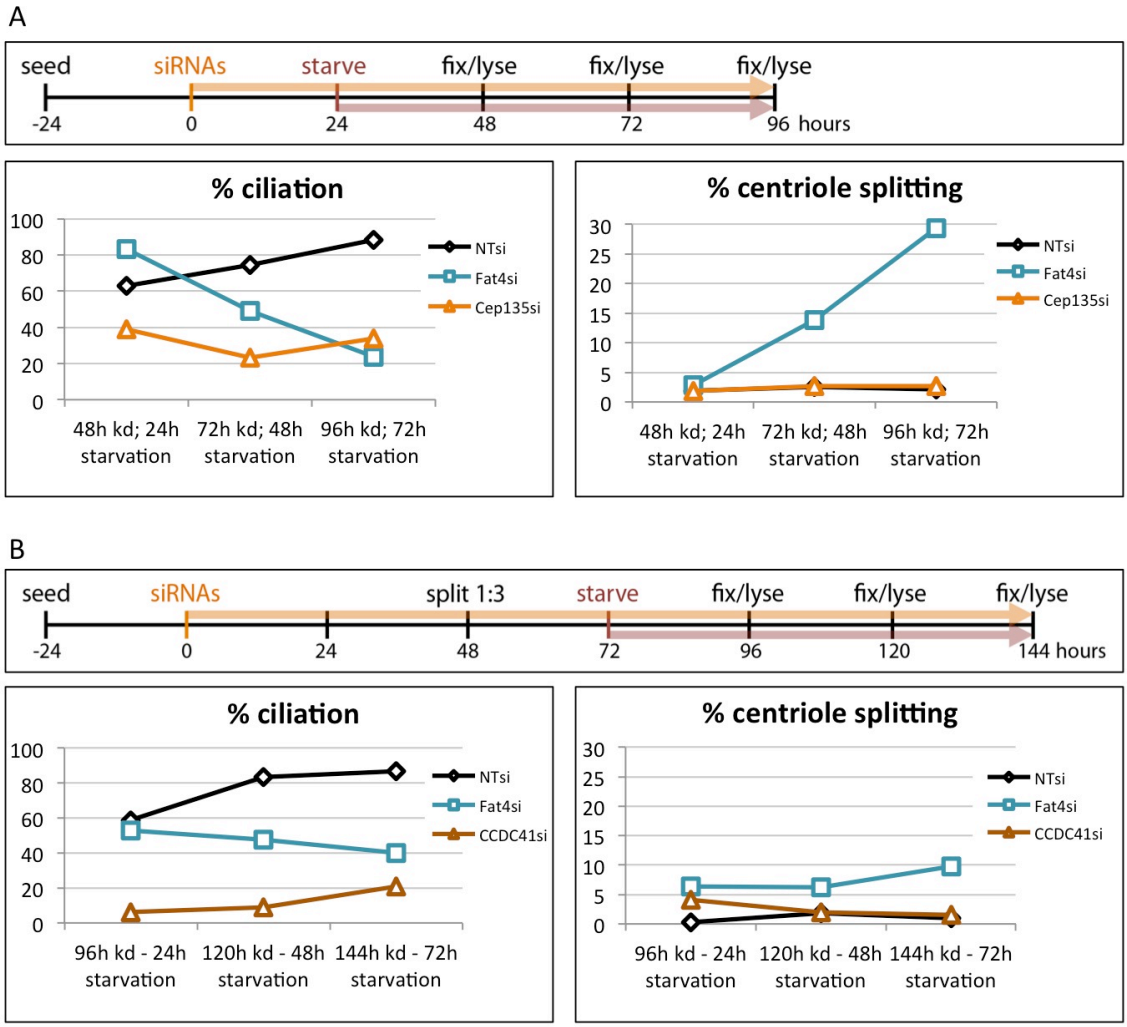

Fig 11.25 FAT4 knockdown cells lose cilia over time
Two independent experiments (see time line for experimental setup) assess ciliation of RPE-1 cells over time. In both cases, cells were starved for 1, 2 and 3 days but in the context of different knockdown (kd) durations. Cilia number within the population and number of cells with split centrioles were counted at each starvation time point (>300 cells counted for each data point). Both experiments show a similar percentage of ciliation after 24h of starvation for non-targeting (NT) siRNA and FAT4 siRNA (siRNA pool #1+3+4) treated cells. In NT siRNA treated cells ciliation increases with prolonged starvation, while FAT4 siRNA treated cells show reduction of ciliation with prolonged starvation, suggesting a problem in cilia maintenance. Knockdown of the controls CCDC41 and Cep135 show low ciliation at all times, consistent with their roles in ciliogenesis. Centriole splitting is only observed in FAT4 siRNA treated cells and increases with prolonged starvation.

In agreement with this, I found that requirements for early cilium assembly were not disrupted in FAT4 knockdown cells. FAT4 knockdown cells showed normal Cep164 staining, a marker for mother centriole appendages required for docking of the ciliary vesicle (Fig. 11.27A). I also tested if the centriolar cap, which needs to be removed specifically from the mother (but not the daughter) centriole to allow ciliogenesis, was removed successfully in FAT4 knockdown cells. Indeed, most cells showed staining for the centriolar cap protein CP110 on only one centriole, whether or not a cilium was present (Fig. 11.26A). Additionally, preliminary results indicated that the transition zone protein NPHP1 was localized properly at the base of remaining cilia in FAT4 knockdown cells and it also seemed to be recruited to most unciliated mother centrioles (Fig. 11.26B). Therefore, these requirements for early ciliogenesis were not affected by knockdown of FAT4.

Cilia maintenance is not well understood and it is often not properly distinguished between ciliogenesis and cilia maintenance defects, as both result in a net reduction of cilia. Intraflagellar transport (IFT) proteins can be important for cilia maintenance, but no obvious defect of the IFT member IFT88 was observed in FAT4 knockdown cells (Fig. 11.27B). Staining of other IFT proteins and more extensive marker analysis might shed light on the molecular changes in FAT4 knockdown cells. Different post-translational modifications (PTMs) stabilize microtubules in cilia and are implicated in cilia maintenance. Therefore, levels of glutamylated, acetylated and glycylated tubulin should be assessed in starvation time courses to address if tubulin stability is altered in FAT4 knockdown cells.

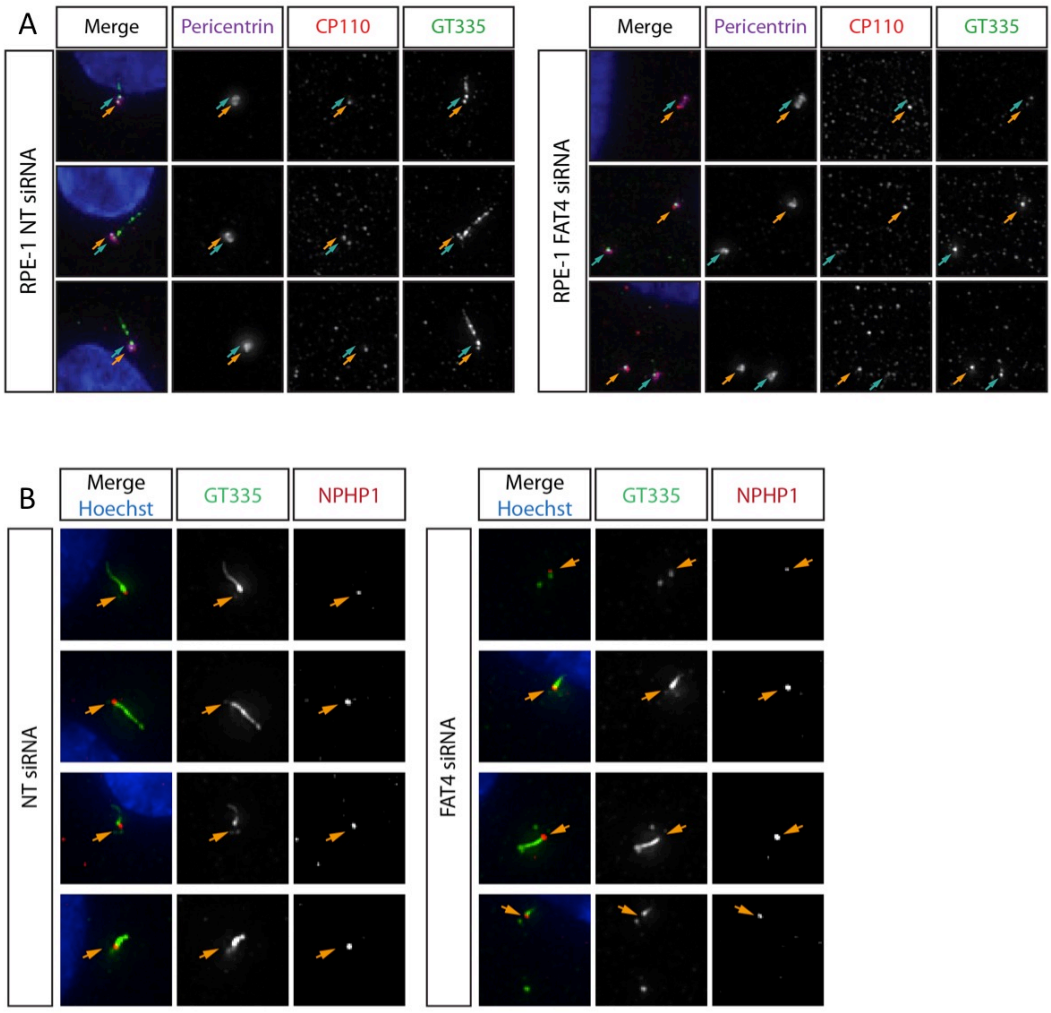

Fig 11.26 CP110 and NPHP1 are unaffected in FAT4 knockdown cells
(A, B) RPE-1 cells are stained with antibodies as indicated after 72h starvation. Percicentrin marks centrosomal region, GT335 labels centrioles and ciliary axonemes. FAT4 siRNA = siRNA pool (#1+3+4). (A) CP110 removal from the mother centriole is a requirement for ciliogenesis. FAT4 knockdown cells have lost CP110 from one of the two centrioles (blue arrow; presumably mother centriole) even in the absence of a primary cilium. (B) NPHP1 is a transition zone protein. It is recruited apparently normally to the mother centriole and labels the transition zone in FAT4 knockdown cells.

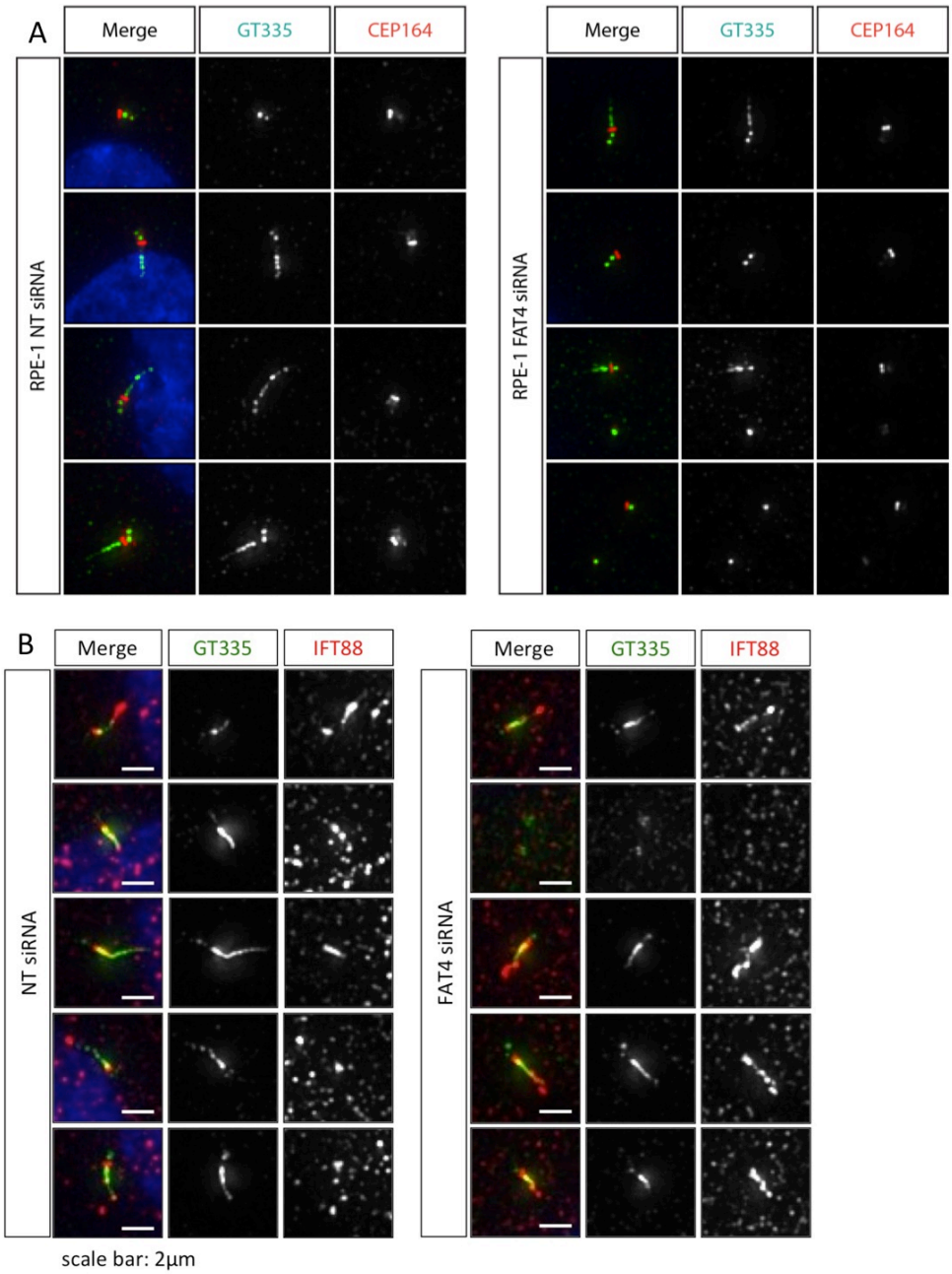

Fig 11.27 CEP164 and IFT88 localization is unaffected in FAT4 knockdown cells

(A, B) RPE-1 cells are stained with antibodies as indicated after 72h starvation. GT335 labels centrioles and ciliary axonemes. FAT4 siRNA = siRNA pool (#1+3+4). (A) CEP164 is a component of centriolar distal appendages and transition fibers in ciliated cells. Cep164 localization to the mother centriole and the base of the cilium is unaffected in FAT4 knockdown cells. (B) IFT88 is a member of the intraflagellar transport machinery and localizes normally along remaining ciliary axonemes in FAT4 knockdown cells. Weak signal is detected in the absence of cilia.

11.2.7 *Fat4* knockout does not affect cilia in the developing mouse cortex

As primary cilia of radial glia cells are important for proper cortex development, I tested if *Fat4* mutant mice had visible abnormalities of cortical cilia. In brain sections of *Fat4* knockout mice and their littermate controls, I labeled cilia with acetylated tubulin or Arl13b and gamma-tubulin and examined radial glia cells in the ventricular walls. However, I did not see defects in ciliation of *Fat4* mutant cells at embryonic day 16 (E16) or postnatal day 0/birth (P0). The same was true for *Fat4/Fat1* double knockout mice that exhibit severe exencephaly at E14 (Badouel et al., 2015). Finally, whole-mount preparations of ventricular walls from a *Fat4* mutant pup at P0 showed mature primary cilia and developing multiciliated cells in the ependyma, indistinguishable from littermate controls (Fig. 11.28).

In summary, no major cilia defects were found in the developing cortex of *Fat4* knockout mice. Therefore, the observed neuronal migration defects in these mice are unlikely due to loss of cilia.

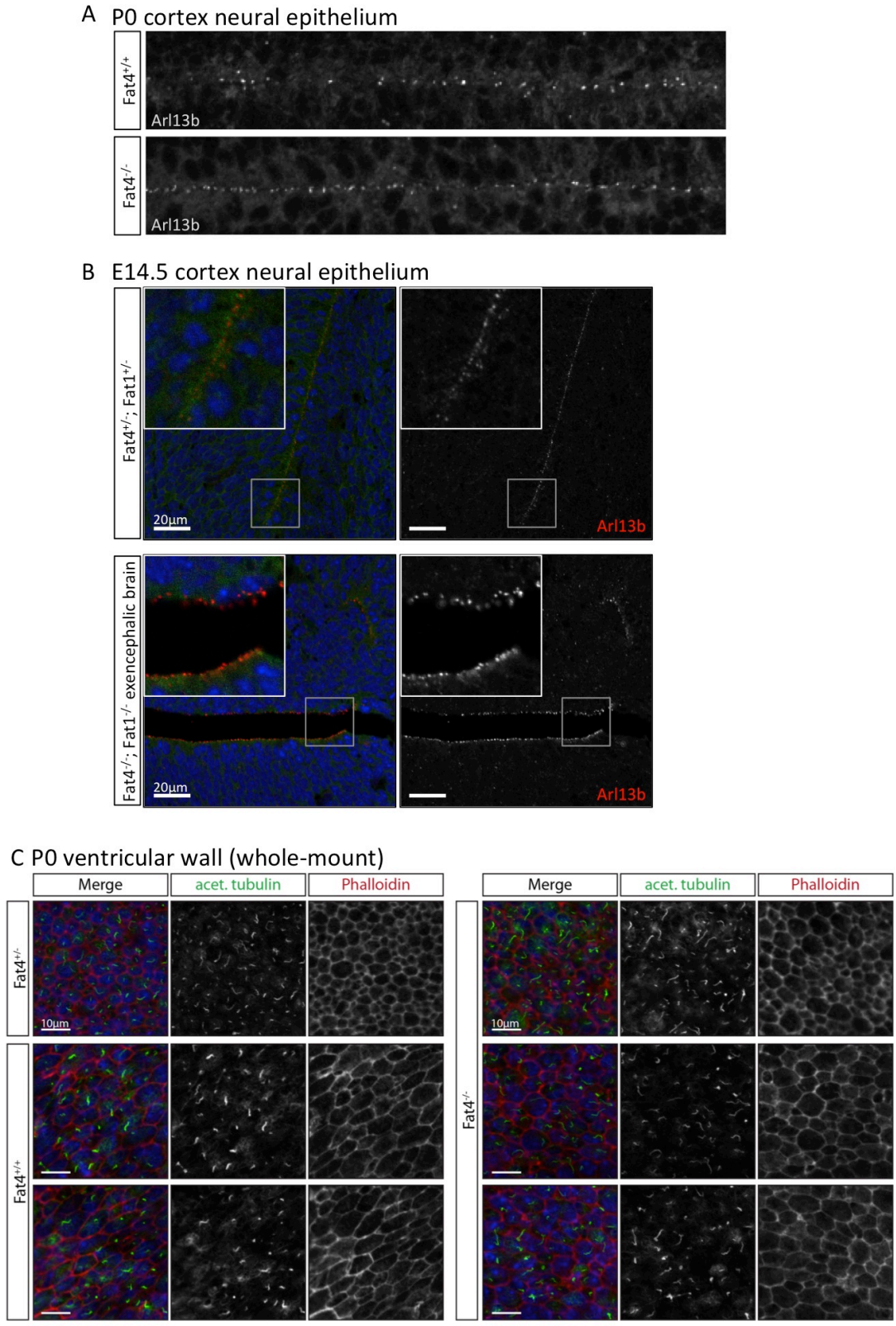

Fig 11.28 Fat4 knockout mice have no obvious defect in cilia of the cortex neural epithelium.

Cilia of the cortical neural epithelium are present at birth of Fat4 knockout mice, shown in sections (A) and whole-mount (C). Fat4, Fat1 double knockout mice exhibit exencephaly but no obvious loss of primary cilia (B).

11.2.8 FAT4 knockdown affects centrosome cohesion and positioning

Immunofluorescence stainings of cilia and basal bodies also revealed a striking centriole cohesion defect upon FAT4 depletion by the siRNA pool (#1+3+4): in starved cells, the centriolar pair, which is usually found in close proximity, was splitting and the two centrioles moved apart from each other. This could be readily observed by staining for gamma-tubulin and pericentrin (Fig. 11.29; 11.30). As the resolution of these stainings is limited and cannot unambiguously distinguish between centriole splitting and duplicated centrosomes, I also used an antibody against glutamylated tubulin (GT335), which gave a sharp centriolar signal and indicated that mother and daughter centriole were indeed separated. Finally, I also confirmed the centriolar splitting in RPE-1 cells stably expressing centrin-GFP that had been transfected with FAT4 siRNAs (Fig. 11.31; 11.26). The observed centriole splitting is a striking phenotype not observed in control knockdowns of Cep135 and CCDC41 or in FAT1 knockdowns. Centriole splitting occurred mainly after longer starvation, such as 48 to 72 hours, as also observed in starvation time courses (Fig. 11.25) (centriole splitting as defined by percentage of cells with intercentriolar distance > 2µm: non-targeting siRNA = 1.9% (± 0.6%); FAT4 siRNA pool (#1+3+4) = 32.8% (± 11.0%); 4 independent experiments; 300-500 analyzed cells each).

Proteins involved in inter-centriolar linkage are the so-called linker proteins, C-Nap1, Rootletin, Cep68, Centlein and LRRC45 (Fry et al., 1998; Bahe et al., 2005; Yang et al., 2006; Graser et al., 2007b; He et al., 2013; Fang et al., 2014). C-Nap1 localizes to the distal ends of centrioles where it serves as a scaffold to connect the other linker proteins to the centrioles (Fry et al., 1998). The strongest centriole cohesion defects are found upon loss of C-Nap1 and Rootletin. C-Nap1 binds Rootletin, which forms fibrous structures thought to connect the two centrioles (Bahe et al., 2005). Linker proteins are regulated in the cell cycle and dissociate from centrioles at the onset of mitosis to allow centrosome separation and formation of spindle poles. Knockdown of linker proteins results in precocious centriolar splitting (Fry et al., 1998; Bahe et al., 2005; Yang et al., 2006; Graser et al., 2007b; He et al., 2013; Fang et al., 2014).

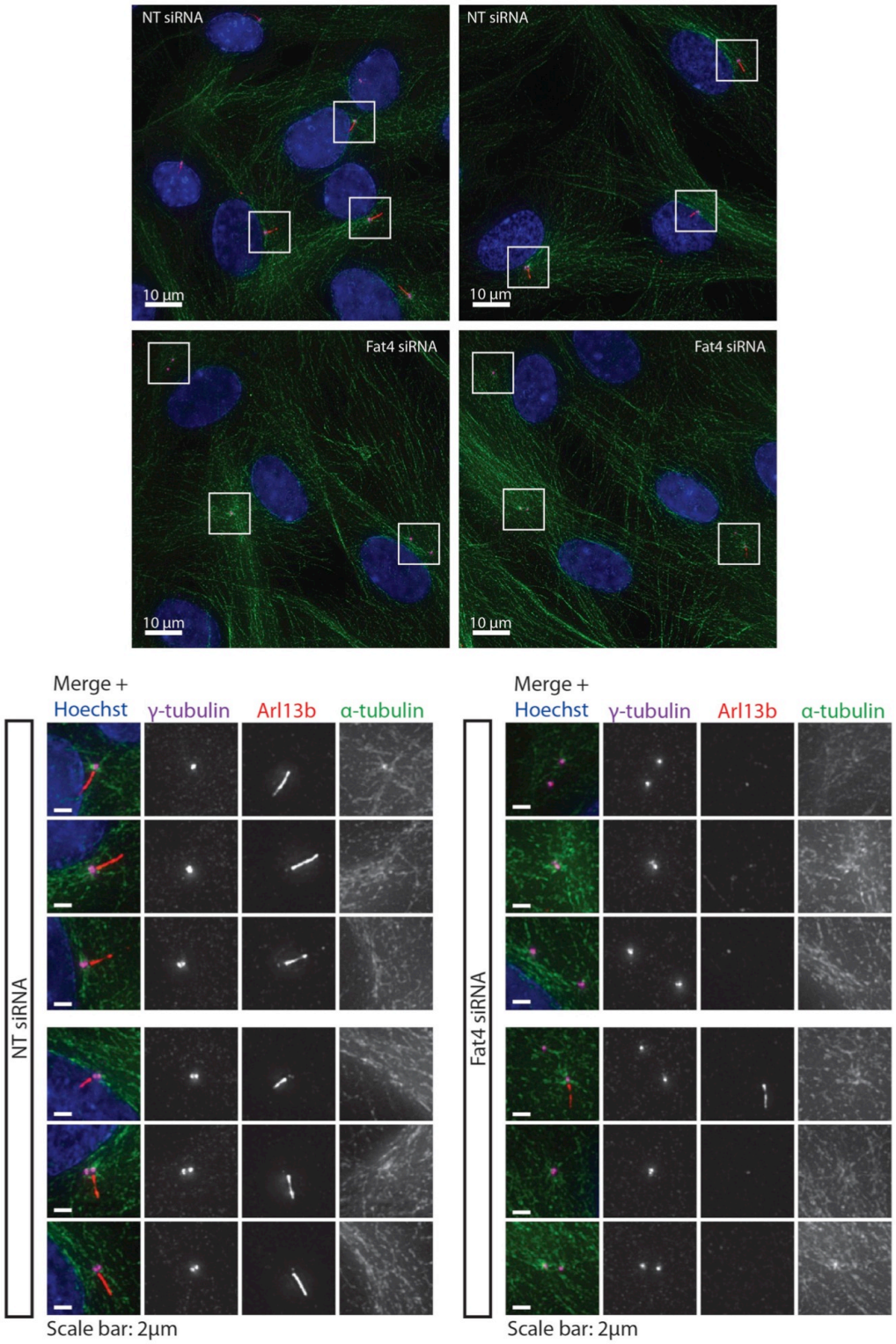

Fig 11.29 FAT4 knockdown causes centriole splitting
RPE-1 cells are stained with antibodies as indicated after 72h starvation. FAT4 siRNA = siRNA pool (#1+3+4). Loss of primary cilia (marked by ARL13B) and splitting of the centrosome (marked by γ-tubulin) is evident in FAT4 knockdown cells.

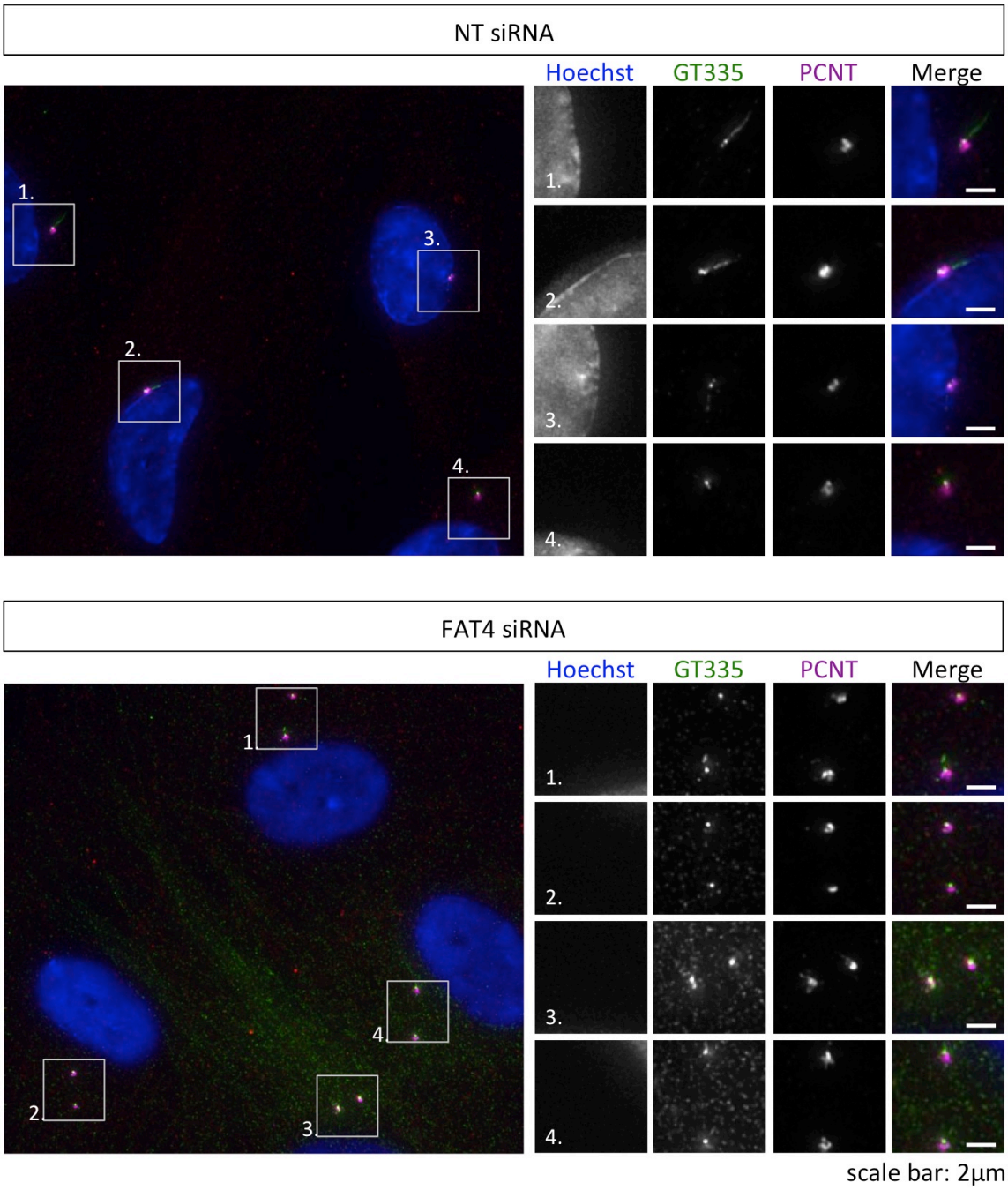

Fig 11.30 GT335 staining shows centriole splitting
RPE-1 cells are stained with antibodies as indicated after 72h starvation. FAT4 siRNA = siRNA pool (#1+3+4). GT335 labels centrioles and ciliary axonemes, PCNT = Pericentrin labels pericentriolar material.

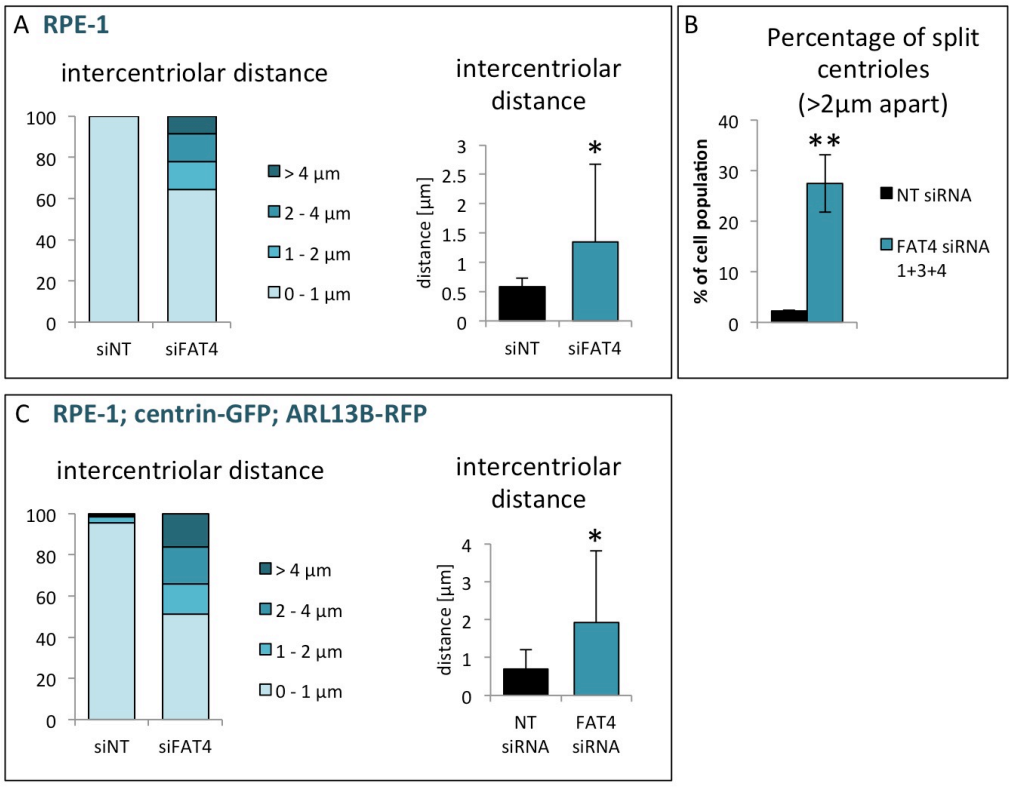

Fig 11.31 Quantification of centriole splitting
RPE-1 cells treated with non-targeting (NT) siRNA or FAT4 siRNAs (pool #1+3+4) and starved for 72h. Intercentriolar distances of RPE-1 cells (A) or RPE-1 cells stably expressing Centrin-GFP and ARL13B-RFP (C) is shown binned into size categories or averaged over all values. Per condition, more than 50 cells (A) or more than 150 cells (C) were measured. Student's t-test: * = $p < 0.05$. (B) Percentage of cells with split centrioles (distance > 2µm apart) within a cell population was averaged over 4 independent experiments. 300 – 500 cells were counted per experiment and sample. Student's t-test ** = $p < 0.0005$. All error bars represent standard deviation.

To test if FAT4 knockdown cells have impaired intercentriolar linkers, I stained cells for Rootletin. Rootletin was still localized at FAT4 knockdown centrioles, but Rootletin fibers often did not seem to connect split centrioles anymore, due to their increased distance (Fig. 11.32). Occasionally, centrioles without Rootletin signal were seen. A very preliminary C-Nap1 staining indicated that also C-Nap1 localization was unaffected in FAT4 knockdown cells.

A recent study found that microtubules control centriole/centrosome cohesion semi-redundantly with linker proteins and that mild microtubule depolymerizing treatment of wildtype cells caused around 30% of centrioles to split (>2µm), without obvious impairment of linker protein localization (Panic et

al., 2015). Stainings of disconnected Rootletin fibers emanating from both centrioles are reminiscent of FAT4 knockdown cells (Panic et al., 2015). Therefore, it would be interesting to test if FAT4 knockdown cells have impaired microtubule stability or dynamics.

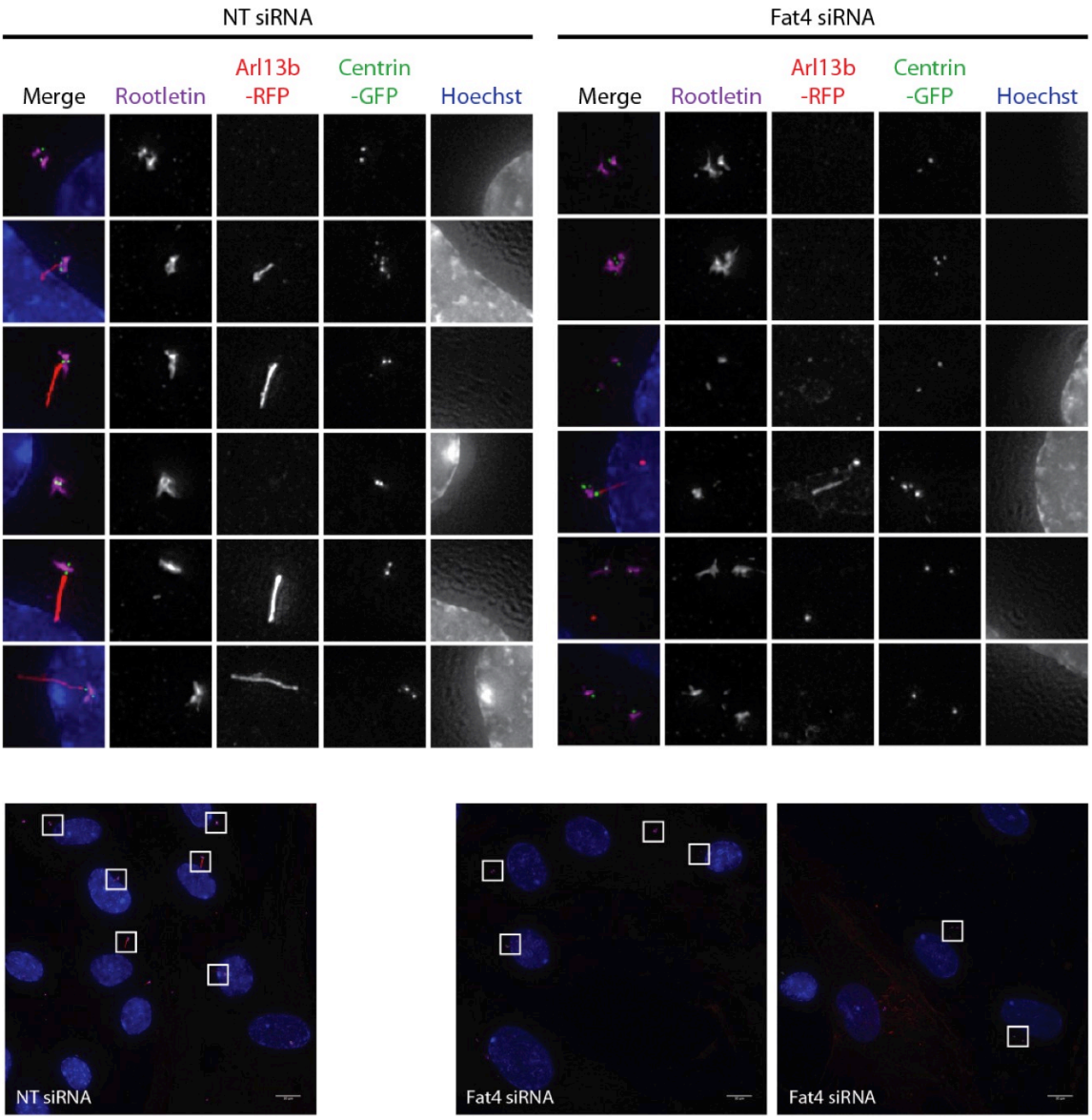

Fig 11.32 Rootletin fibers are present in FAT4 knockdown cells
RPE-1 cells stably expressing centrin-GFP and ARL13B-RFP are stained with antibodies as indicated after 72h starvation. FAT4 siRNA = siRNA pool (#1+3+4). Rootletin fibers still emanate from most split centrioles but are no longer connected.

11.2.9 FAT4 knockdown causes a centrosome positioning defect

Another phenotype of starved FAT4 knockdown cells was a significant increase in centrosome-nucleus distance. In wildtype cells, the centrosome is usually found in close proximity to the nucleus. Dr. Mikhail Bashkurov from the LTRI high-content screening facility developed a script for automated detection of centrosomes and nuclei to measure their shortest distance. Statistically significant centrosome-nucleus distances were found with three FAT4 siRNAs, but not with FAT1, CEP135 or CCDC41 siRNAs (Fig. 11.33).

This phenomenon is not well understood, and while several molecules involved in nucleus-centrosome association have been identified, the molecular mechanism of this process is largely unknown. Modifications of the actin cytoskeleton, microtubular network or nuclear envelope can lead to centrosome positioning defects (Burakov and Nadezhdina, 2013). Interestingly, mice mutant for the dynein regulators *Lis1* or *Ndel1* show an increase in centrosome-nucleus distance, which is tightly correlated to their neuronal migration defect (Youn et al., 2009). This is reminiscent of the neuronal migration defect in *Fat4* knockout mice (Zakaria et al., 2014; Badouel et al., 2015), and centrosome positioning should be addressed in this context.

Strikingly, there did not seem to be a clear correlation between centriole splitting and increased nucleus-centrosome distance, and it remained unclear if they were linked. Microtubules are involved in both centriole cohesion and nucleus-centrosome connection, however there is so far no evidence for a role of FAT4 in microtubule regulation. *Drosophila* Fat appears to regulate microtubule network polarity, however mainly of non-centrosomal microtubules (Harumoto et al., 2010), and it is unknown whether this is conserved in mammalian cells. Finally, alpha-tubulin and gamma-tubulin stainings appeared normal in FAT4 knockdown cells (Fig. 11.29).

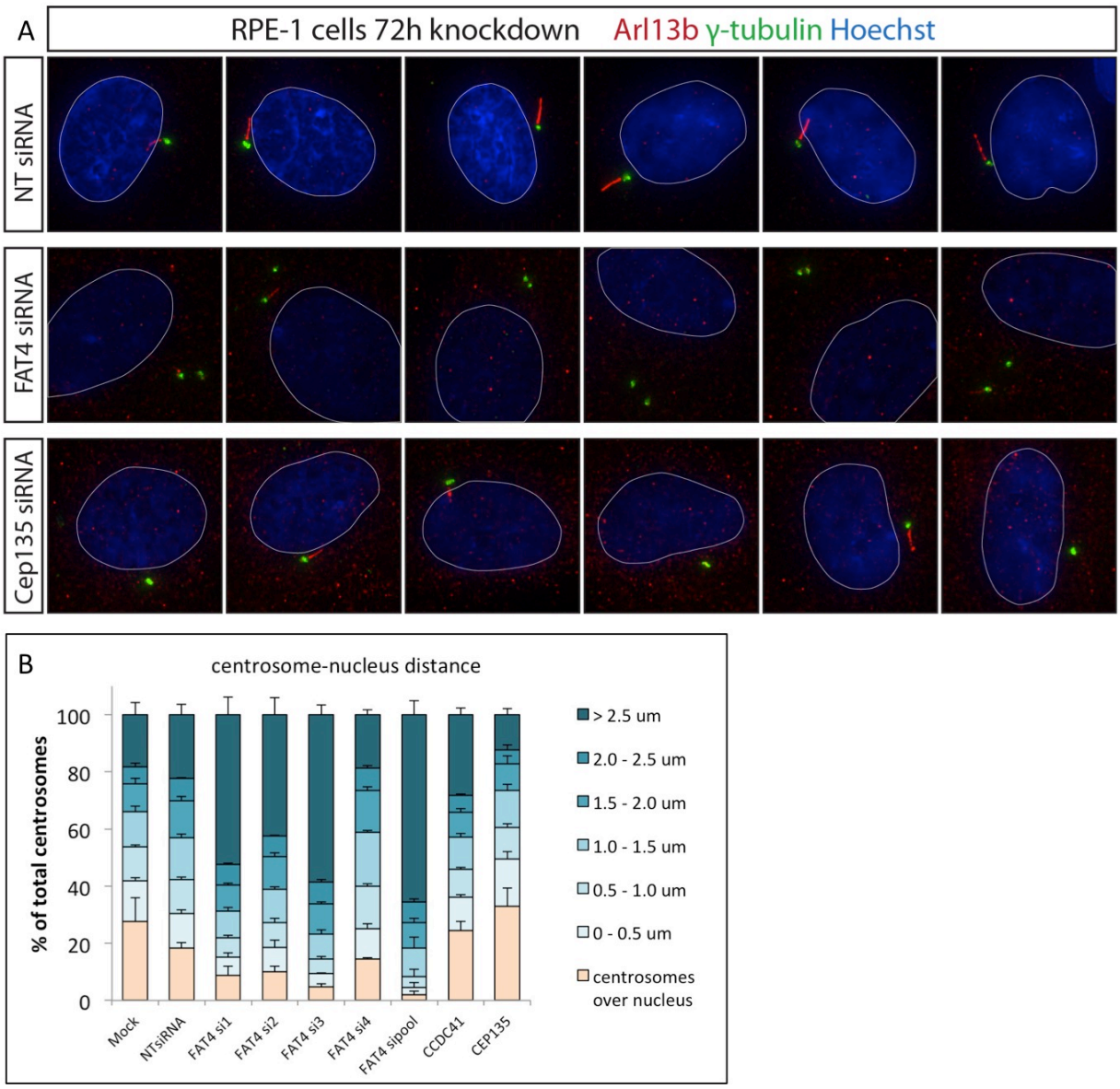

Fig 11.33 FAT4 knockdown causes centrosome positioning defects
(A) RPE-1 cells are stained with antibodies as indicated after 72h starvation. FAT4 siRNA = siRNA pool (#1+3+4). FAT4 knockdown causes increased distances between the (split) centrosome and the nucleus. (B) RPE-1 cells are transfected with siRNAs as indicated on G-slides and starved for 48h. Automated measurement of centrosome-nucleus distance (based on γ-tubulin and Hoechst staining) was performed from two independent experiments with technical duplicates each. Error bars represent standard deviations.

11.2.10 FAT4 knockdown affects Golgi apparatus size

Localizations of centrosome and Golgi apparatus (GA) are tightly linked in mammalian cells. During interphase, microtubules nucleated and anchored at the centrosome provide tracks for the transportation of Golgi membranes to the center of the cell, resulting in the typically observed pericentriolar GA position near the nucleus. To test if the altered centrosome position and cohesion in FAT4 knockdown cells affected GA positioning, I stained FAT4 knockdown RPE-1 cells with the GA markers Gm130 and Giantin. While GAs were still organized in a pericentriolar fashion, the FAT4 siRNA pool strikingly resulted in a strong increase of the area occupied by the GA, as determined by manual and automated GA area analysis (Fig. 11.34; 11.35; 11.36; 11.37). The phenotype seemed more prominent under starved conditions but was also seen in cycling cells (Fig. 11.35; 11.37). Additionally, Western blots showed increased levels of Gm130, the GA marker Golgin97 and the endoplasmic reticulum and GA marker Calnexin, both in cycling and starved cells (Fig. 11.37). This suggested that the GA was in fact increased in size. No similar phenotype was found upon knockdown of FAT1, Cep135, CCDC41 or using non-targeting siRNAs. Additionally, GAs in FAT1, FAT4 double knockdown cells were indistinguishable from those in FAT4 knockdown cells (Fig. 11.34; Fig 11.36).

The GA and the centrosome are functionally interconnected in many aspects and transport from the GA to the basal body is crucial for proper cilium establishment and function. Whether and how the observed centrosome, cilium and GA phenotypes are linked remains an open question.

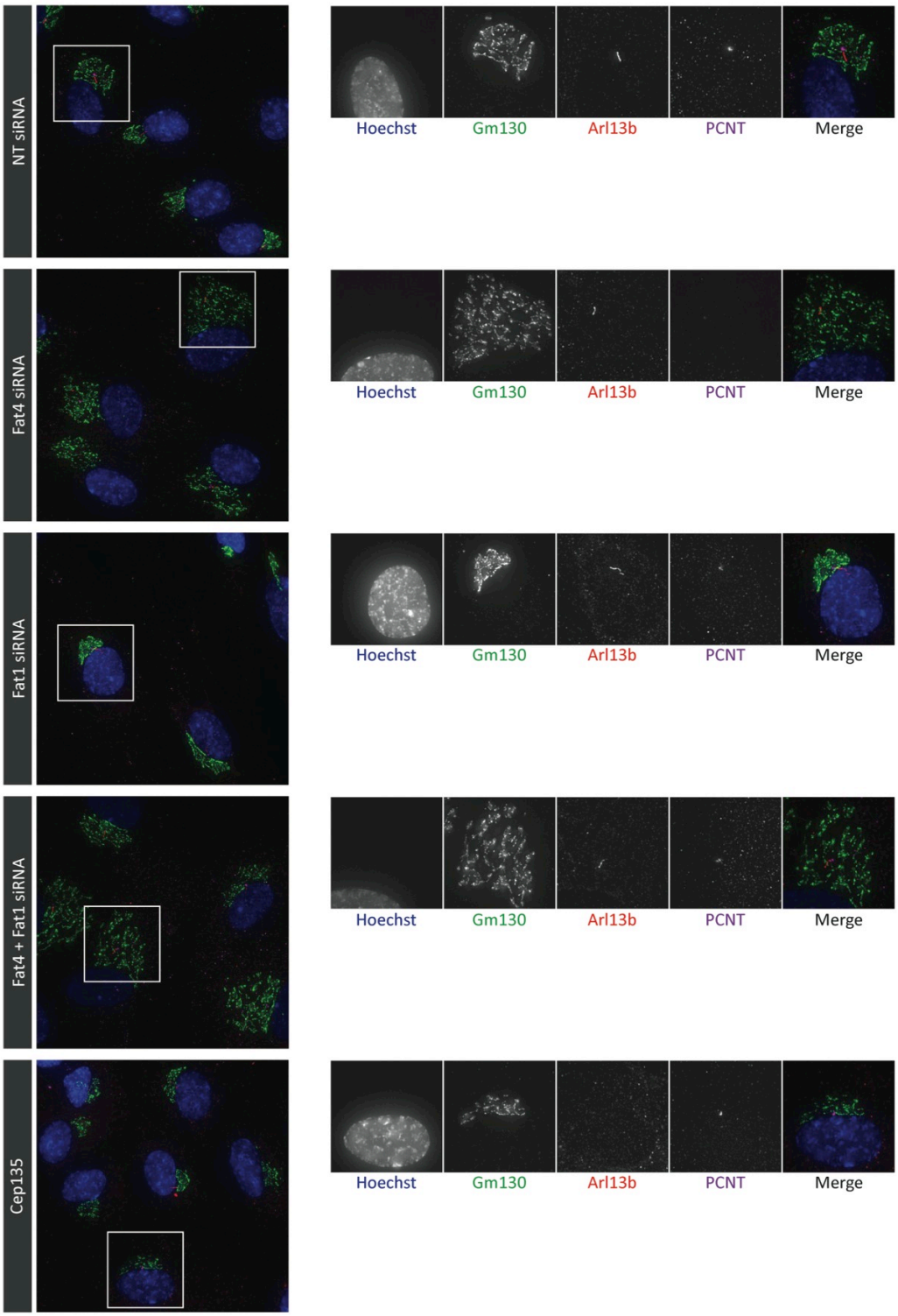

Fig 11.34 FAT4 but not FAT1 knockdown causes GA enlargement
RPE-1 cells are stained with antibodies as indicated after 72h starvation. FAT4 siRNA = siRNA pool (#1+3+4); FAT1 siRNA = siRNAs #1+2. Golgi apparatus (GA) is enlarged in FAT4 and FAT4, FAT1 double knockdown cells.

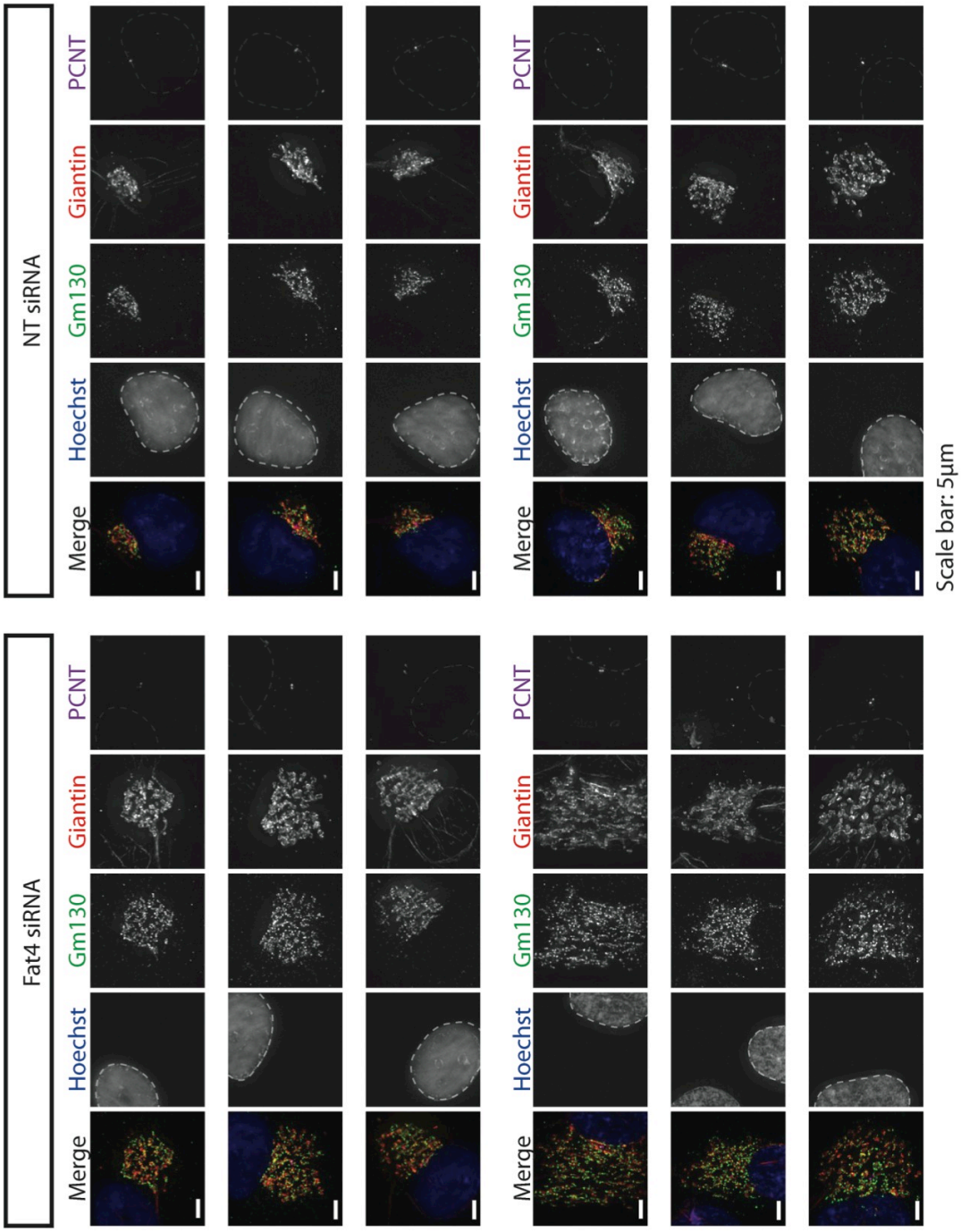

Fig 11.35 GA enlargement in FAT4 knockdown cells occurs in cycling cells
Cycling RPE-1 cells are stained with antibodies as indicated. FAT4 siRNA = siRNA pool (#1+3+4). Both GA makers Gm130 and Giantin show increased GA areas in FAT4 knockdown cells. Dotted line highlights nuclei and nucleus position in PCNT channel.

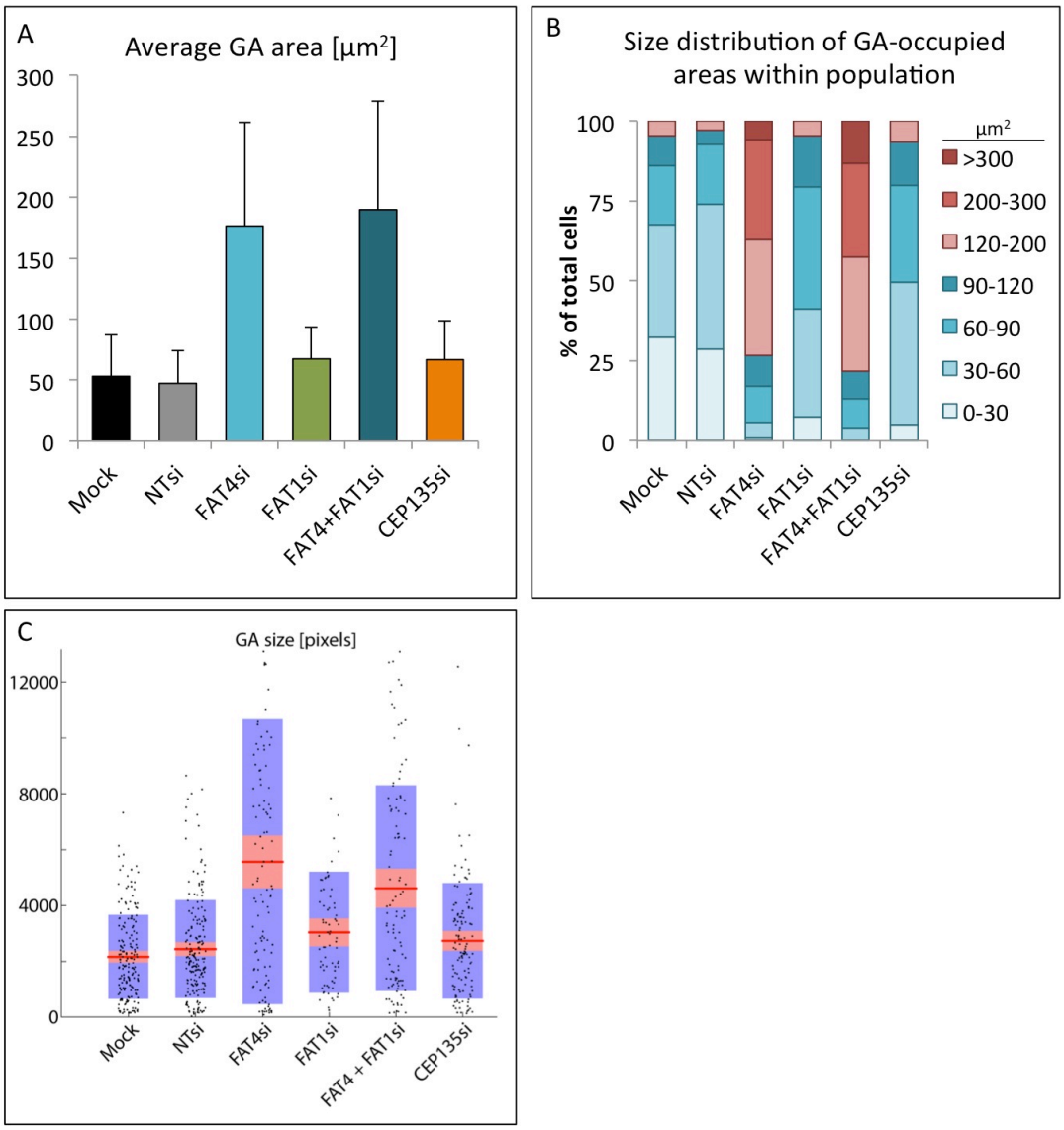

Fig 11.36 Quantification of Golgi apparatus area
Golgi apparatus (GA) measurements based on staining shown in Fig. 11.34 (A, B) Manual GA measurements are shown averaged (A) or as size distributions (B). > 100 cells measured per condition. (C) Automated GA measurement shown in a scatter column graph. 95% confidence interval (1.96 SEM) is in pink and 1 SD (standard deviation) is in blue.

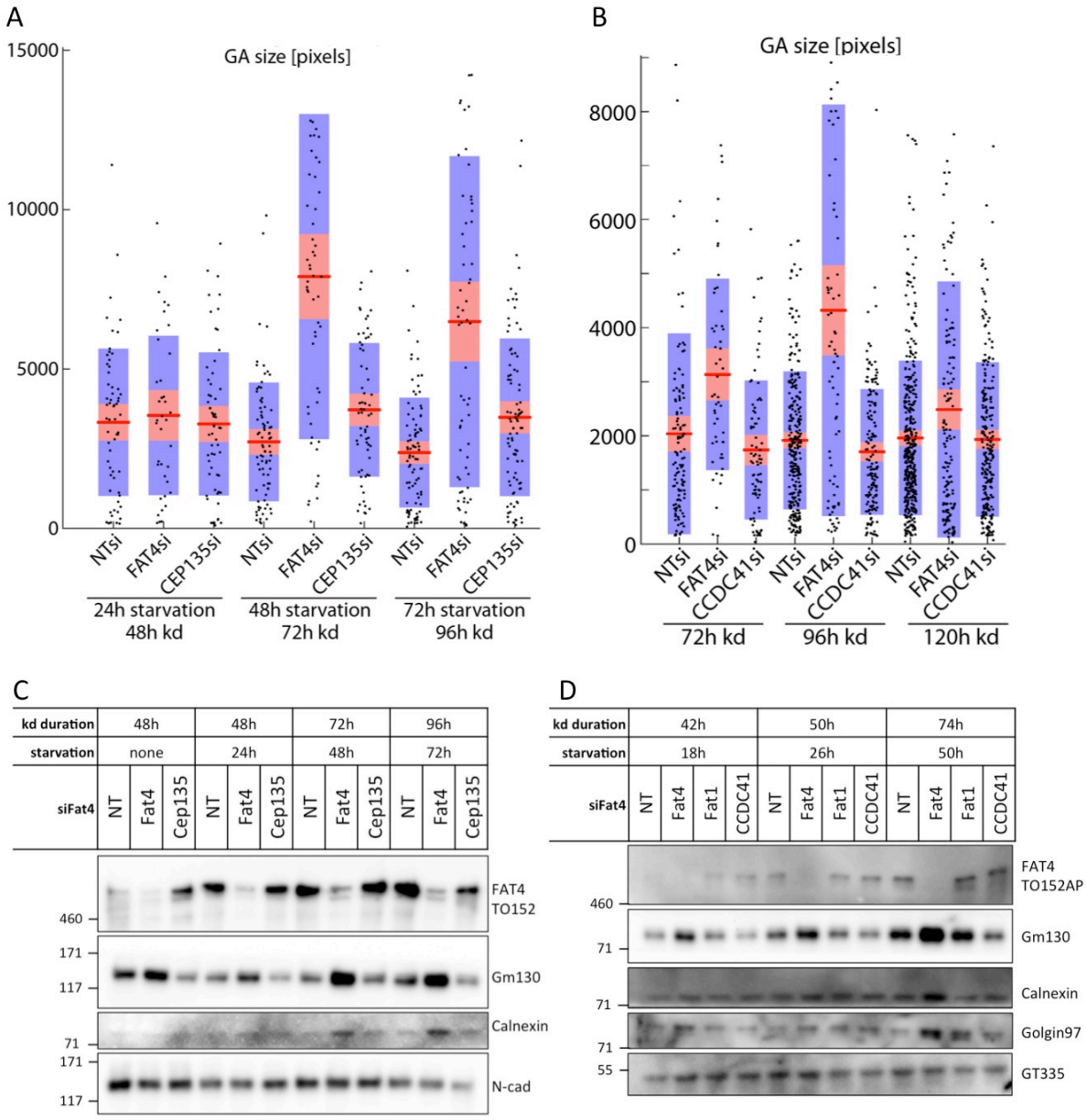

Fig 11.37 Golgi enlargement in cycling and starved cells

(A, B) Golgi apparatus (GA) measurements from RPE-1 cells after different starvation and knockdown times. Automated GA measurement shown in a scatter column graph. 95% confidence interval (1.96 SEM) is in pink and 1 SD (standard deviation) is in blue. FAT4si = FAT4 siRNA pool (#1+3+4); NTsi = non-targeting siRNA. (A) starvation time course. (B) cycling cells with prolonged siRNA treatment. (C, D) Western blot analysis of RPE-1 cels with non-targeting (NT) siRNA, FAT4 siRNA (pool #1+3+4) or FAT1 siRNA (pool #1+2+3). Cep135 siRNA pool and CCDC41 siRNA pool serve as controls. Levels of GA markers Gm130, Calnexin and Golgin97 are increased in FAT4 knockdown samples.

11.2.11 FAT4 knockdown affects RPE-1 cell migration

As centrosome positioning correlates with and is suggested to be important for cell migration directionality in many cells (Gotlieb et al., 1981; Kupfer et al., 1982), I also performed cell culture wound healing assays. I wounded confluent monolayers of RPE-1 cells that had either been transfected with the FAT4 siRNA pool (#1+3+4), FAT1 siRNA pool (#1+2+3) or non-targeting siRNA. Wounds were scratched using 10ul pipette tips and wound closure was monitored by time-lapse imaging over 6-12h. While the wound closure speed of FAT1 knockdown cells was indistinguishable from control knockdown cells, FAT4 knockdown caused a significant reduction in wound closure speed (Fig. 11.38). To address if this was due to a slower migration speed or a problem in oriented migration, I fixed and stained closing wounds 3-4h after scratching and analyzed Golgi apparatus (GA) positioning in relation to the migration front within the first 2 rows of cells. In most mammalian cells, GA and centrosome are positioned towards the leading edge, in the direction of migration. While there was a trend of decreased GA orientation in FAT4 knockdown cells, this was not statistically significant (Fig. 11.38). In summary, FAT4 knockdown impaired either migration speed or directionality in RPE-1 cells.

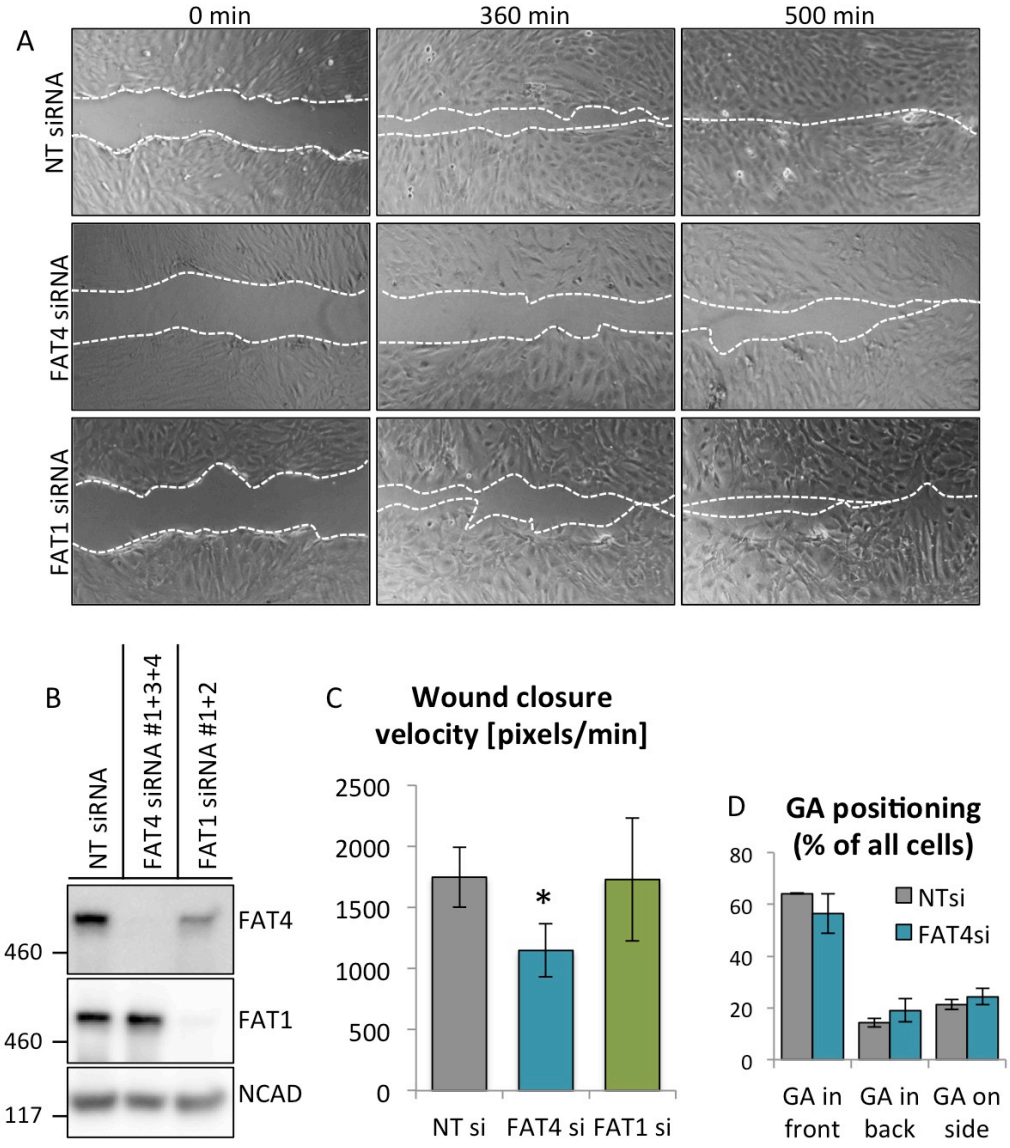

Fig 11.38 Wound healing assays

RPE-1 cells transfected with siRNAs as indicated. FAT4 siRNA pool (#1+3+4) and FAT1 siRNA pool (#1+2+3) were used. Efficient knockdown is shown by Western blot (B). (A) Representative wounds show delay of wound closure in FAT4 knockdown cells. (C) Wound closure velocity assessed by live imaging. Values are from four independent experiments with each four different wounds per condition (averages are over 16 wounds per condition); * = $p < 0.0001$. (D) GA position in relation to wound and nucleus. First three rows of cells at wound border were counted. Bar graph shows average over two independent experiments. All error bars represent standard deviations.

11.2.12 Rescue attempt of FAT4 knockdown phenotypes

In order to prove the specificity of the used FAT4 siRNAs, I attempted to set up a rescue experiment. Since the *FAT4* gene is extremely large, I decided against mutating individual siRNA recognition sites. Instead, I designed siRNAs targeting the FAT4 3'UTR and tried to generate RPE-1 cells stably expressing the FAT4-YFP or FAT4-BF constructs, which both lack the *FAT4* 3'UTR and are therefore siRNA resistant. However, despite testing different transfection strategies, numerous trials of generating stable RPE-1 cells failed. Most likely, this was due to the immense size and therefore low integration efficiency of the *FAT4* construct (23kb). When using the highly efficient Flp-In system to generate HEK293 and HCT116 cells stably expressing FAT4, I had already noticed that the integration efficiency of *FAT4-BF* was around 10-times lower than that of *Cdh1-BF* or *GFP-BF*. Another possibility is that FAT4 overexpression is deleterious to RPE-1 cells or integration of the large gene poses a competitive disadvantage during the rather slow selection process with Zeocin. We, and also our collaborators working with full-length FAT4, encountered similar problems in several cell lines.

I noticed however, that the two FAT4 siRNAs targeting the 3'UTR did not show the same cilia, centrosome and GA phenotypes as the previously established siRNAs. However, both siRNAs strongly reduced FAT4 protein (Fig. 11.39). I therefore tested three additional siRNAs targeting a region of exon 17 that codes for the FAT4 intracellular domain. Curiously, one of them (siRNA #intra2) strongly upregulated FAT4 protein. Only one of the two remaining siRNAs caused a mild ciliation defect, shorter cilia and split centrioles, while the other showed none of these phenotypes. Both siRNAs efficiently reduced FAT4 full-length protein levels on Western blots. This suggested that a reduction of FAT4 was not necessarily linked to cilia or centrosome defects and made clear that additional tests were needed to address if the previously observed phenotypes were caused by a loss of FAT4 or by an off-target effect.

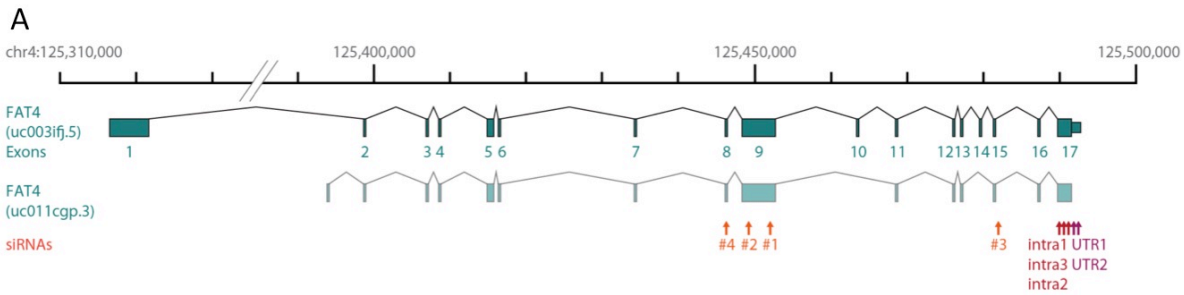

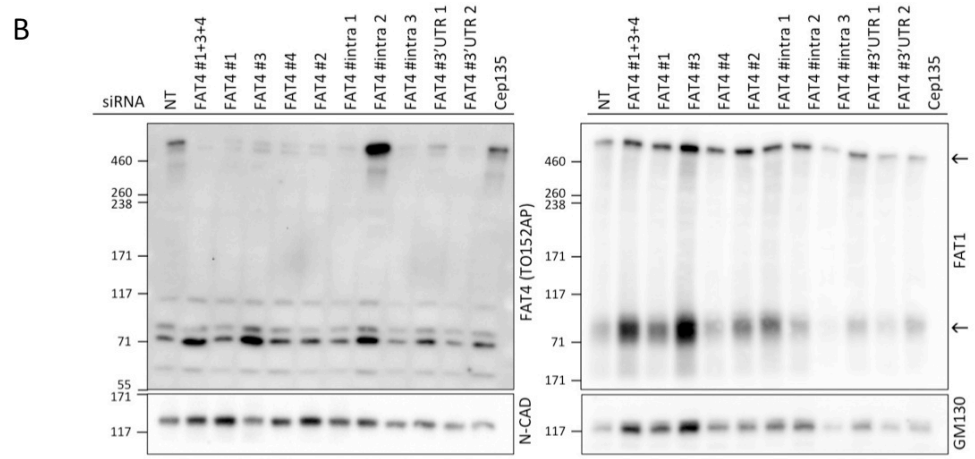

C

FAT4 siRNAs:	Pool: #1+3+4	Fat4 #1	Fat4 #3	Fat4 #4	Fat4 #2	Fat4 #intra1	Fat4 #intra2	Fat4 #intra3	Fat4 #3'UTR1	Fat4 #3'UTR2
targeting exon	8,9, 15	9	15	8	9	17	17	17	17	17
knockdown of full-length protein	x	x	x	x	x	x	in-crease	x	x	x
reduced ciliation G-slides (48h starvation, 72h kd)	+++	+++	++	+	/	+	nA	/	/	/
reduced ciliation manual (72h starvation, 96h kd)	+++	+++	+	+++	+	/	/	nA	/	nA
short cilia	x	x	x	x	nA	x	nA	/	/	/
Golgi size increase	+++	++	+++	++	+	+	de-crease	nA	/	nA
increased centrosome-nucleus distance	+++	+++	++	+	++	/	nA	/	/	/
centriole splitting	++	++	/	+++	/	++	/	nA	/	nA

Fig 11.39 Comparison of individual FAT4 siRNAs

(A) Schematic of FAT4 transcripts and siRNA targeting regions. Gencode transcripts as annotated in UCSC genome browser (genome GRCh38/hg38). Exons are in blue. Targeting exons of independent siRNAs are depicted. Exon numbering according to the longest transcript (uc003ifj.5). (B) Western blot analysis of individual FAT4 siRNAs. Full-length FAT4 protein (540kDa) is reduced in all siRNAs except siRNA #intra2. Arrows indicate FAT1 full-length and processed protein. (C) Summary of observed phenotypes for each FAT4 siRNA (+;++;+++ indicate different phenotype strengths; / = no phenotype; nA = not addressed).

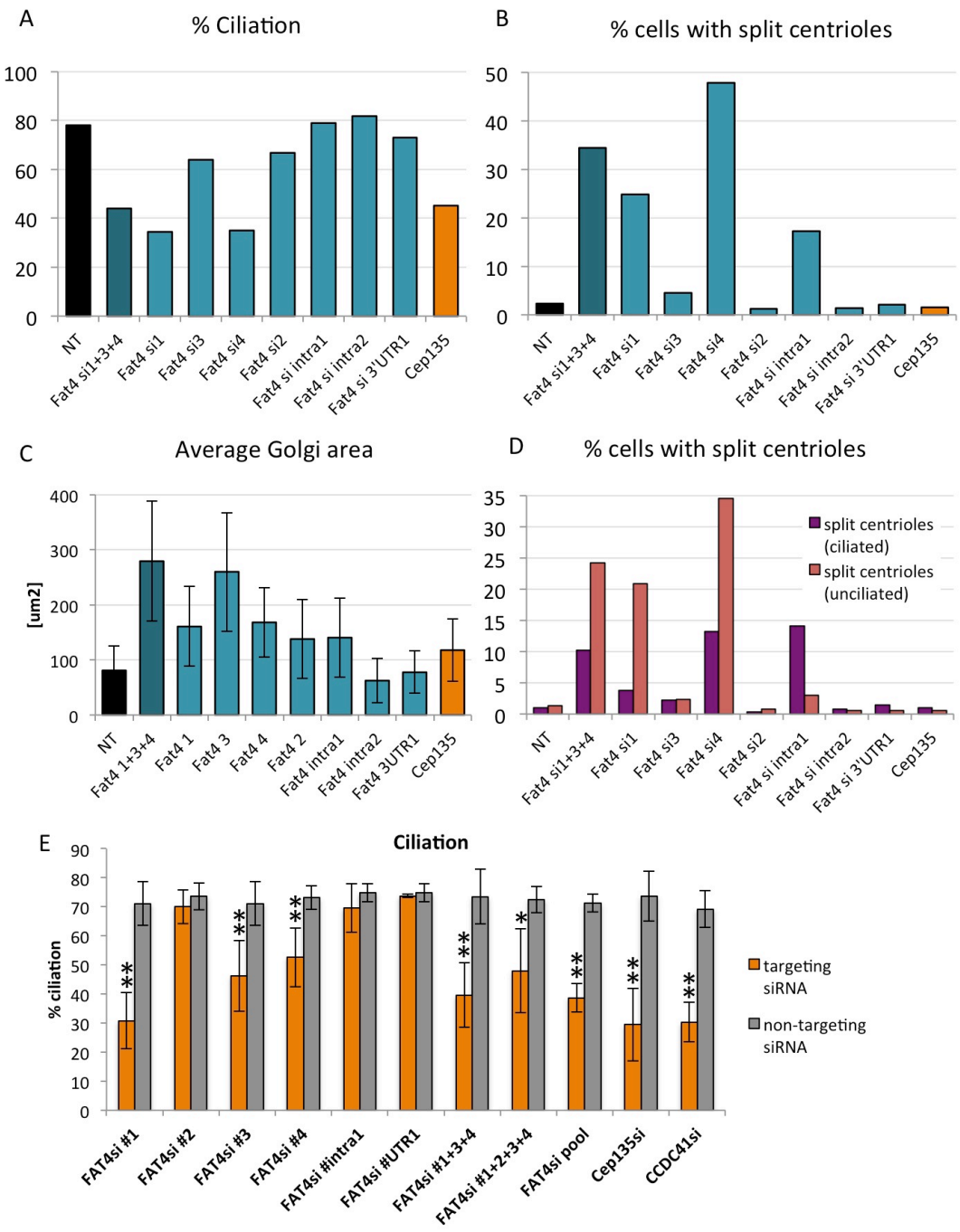

Fig 11.40 Analysis of phenotypes caused by individual FAT4 siRNAs
RPE-1 cells were transfected with siRNAs as indicated and starved for 72h. (A, B, D) Ciliation and centriole splitting was assessed based on ARL13B, γ-tubulin and Pericentrin stainings. > 500 cells were counted for each condition. (C) Manual GA area was based on GM130 staining. > 100 cells were measured per condition. (D) Percentage of ciliation averaged over several experiments. Each targeting siRNA is compared to non-targeting siRNA values from the same experiments. Numbers of biological replicates (+ technical repeats) are as following: non-targeting siRNA: FAT4si #1 n=5(+3); FAT4si #2 n=3(+2); FAT4si #3 n=5(+3); FAT4si #4 n=4(+2); FAT4si #intra1 n=2(+1); FAT4si #UTR1 n=2(+1); FAT4si #1+3+4 n=13(+4); FAT4si #1+2+3+4 n=2(+2); FAT4si pool (= #1+3+4+intra1+intra3+UTR1+UTR2) n=2(+2); Cep135 n=11(+5); CCDC41 n=6(+5). Error bars represent standard deviations. Student's t-test: * = $p < 0.05$; ** = $p < 0.001$

11.2.13 Multiple outcomes using independent FAT4 siRNAs

These findings prompted me to analyze all siRNAs individually and I found strong differences between them (see Fig. 11.39; 11.40). None of the observed phenotypes was found with all siRNAs. The GA phenotype was seen most prominently with one siRNA (siRNA #3) and only to a lesser degree with four others. The cilia and centrosome phenotypes were found (in varying strengths) with multiple siRNAs and with siRNA pools. Strikingly, siRNAs did not necessarily cause both centrosome and cilia defects, further suggesting that they are independent phenotypes. For example, siRNA #3 caused ciliation defects and increased centrosome-nucleus distance, but no centriole splitting. In contrast, siRNA #4 caused ciliation defects and strong centriole splitting, but did not increase nucleus-centrosome distance. siRNA #intra1 caused only mild cilia defects but clear centriole splitting. Finally, a clear increase of FAT1 protein as described earlier, was found only with siRNA #3 and the siRNA pool (#1+3+4), suggesting FAT1 increase is not a general compensational reaction to the depletion of FAT4 (Fig. 11.39B). Although it seemed unlikely that multiple independent siRNAs share the same off-target effect, these results highlighted that FAT4 function could not be addressed confidently by RNAi.

11.2.14 Generation of *FAT4* mutant cell lines by CRISPR/Cas9

In order to address if the observed siRNA phenotypes were due to loss of FAT4 and could be replicated in *FAT4* mutant cells, I generated *FAT4* knockout RPE-1 cell lines using CRISPR/Cas9. To direct the Cas9 endonuclease to the *FAT4* gene and to generate InDels (small insertions or deletions), I chose 4 different guide RNAs (gRNAs) targeting exon 1 and exon 9, as well as a combination of two gRNAs targeting exon 1 (see Fig. 11.41A). I cloned the gRNAs into a vector containing Cas9 as well as a GFP cassette, which allowed sorting of individual successfully transfected cells by flow cytometry, to generate clonal cell lines. I screened around 100 colonies by sequencing and tested promising candidate lines by Western blot. 23 clones lost the full-length FAT4 protein or reduced levels below the detection limit. Interestingly, on Western blot none of the lower bands, including the lower doublet, that were detected by the FAT4 antibodies

(TO152AP and Novus) were changed, again suggesting that only the full-length FAT4 band is specific (Fig. 11.41).

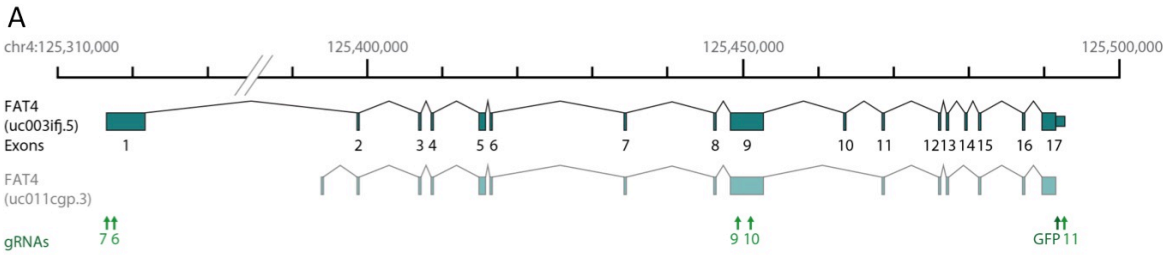

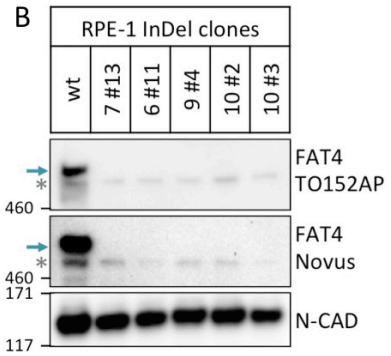

C

gRNA	targeting exon	# clones sequenced	# clones selected for WB	# clones lose FAT4 protein
6	1	22	13	4
7	1	25	13	8
6+7	1	28	13	7
9	9	9	5	2
10	9	10	7	4
total		94	51	22 (=23%)

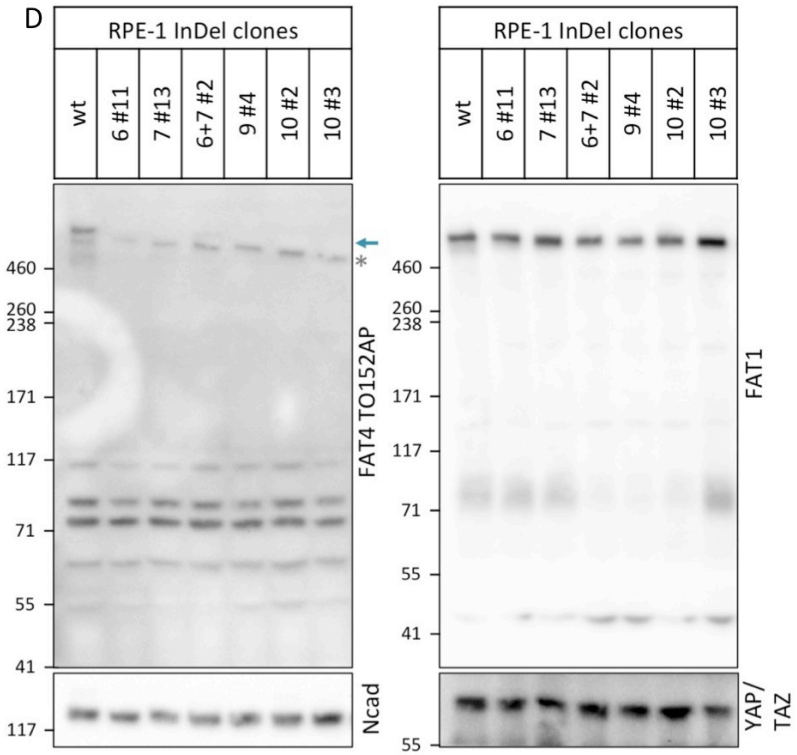

Fig 11.41 *FAT4* mutant RPE-1 cell lines by CRISPR/Cas9-mediated InDels
(A) Schematic of FAT4 transcripts and gRNA targeting regions. Gencode transcripts as annotated in UCSC genome browser (genome GRCh38/hg38). Exons are in blue. Exon numbering according to the longest transcript (uc003ifj.5). (B, D) Western blot confirmation of *FAT4* mutant cell lines. Full-length FAT4 (arrow in (D)) is undetectable in different mutant clones. wt = wildtype RPE-1 cells. Asterisk mark the likely non-specific lower doublet band. (C) Summary of CRISPR/Cas9 efficiency to generate *FAT4* mutant cells.

I selected several independent clones originating from different gRNAs that had lost FAT4 protein and tested their capacity to ciliate. However, starvation of these CRISPR InDel mutants did not show the phenotypes found by RNAi (Fig. 11.42). Two cell lines with clean mutations expected to cause premature translation stops in either exon 1 or exon 9 were further analyzed quantitatively. No difference in ciliation or centriole cohesion was found (Fig. 11.42D). This suggests that full-length FAT4 is either dispensable for cilium formation and maintenance or that non-acute loss of FAT4 can be functionally compensated in RPE-1 cells.

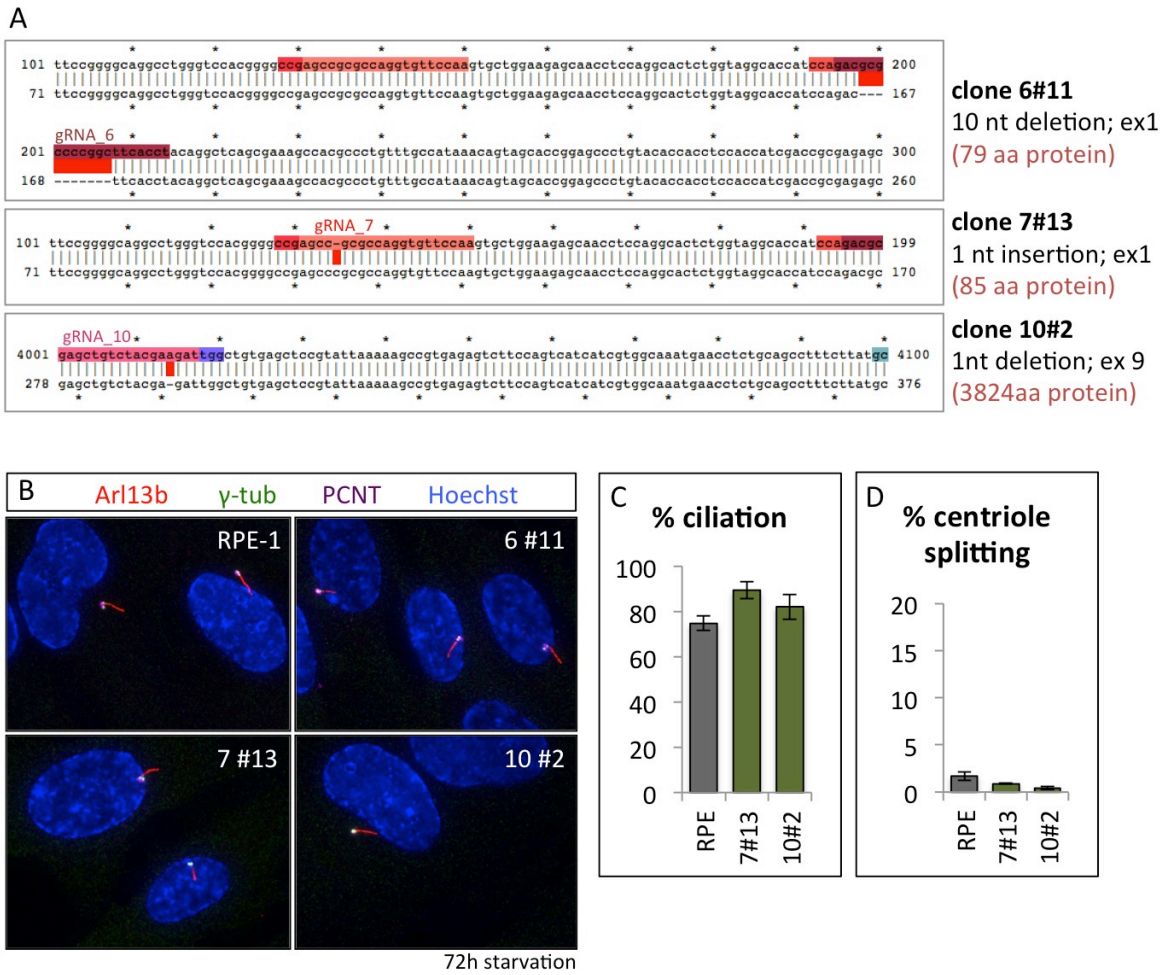

Fig 11.42 *FAT4* CRISPR InDel lines don't show cilia or centrosome defects
Three independent RPE-1 CRISPR InDel lines that result in frame-shift mutations in the *FAT4* gene (A) show mature cilia after 72h of starvation (B). (C) Ciliation and centriole cohesion are unaffected in FAT4 InDel cell lines. Data from two independent experiments, > 300 cells counted each. Error bars represent standard deviation.

11.2.15 Generation of a full *FAT4* knockout cell line

One shorter FAT4 isoform lacking exon 1, exon 10, exon 14 and the 3'UTR is annotated in Gencode (Harrow et al., 2012). And although I only detected a 540kDa FAT4 band in RPE-1 cells, there could be undetected shorter isoforms expressed. To rule out the possibility that remaining FAT4 isoforms might rescue FAT4 function in InDel lines, I used CRISPR/Cas9 to delete nearly the entire FAT4 coding region. I co-transfected RPE-1 cells with Cas9 and two gRNAs simultaneously, one targeting exon 1 close to the translation start site, and the second targeting the exon 17 3'UTR (see Fig. 11.41; 11.43). I FACS sorted individual cells and grew them clonally. The efficiency for generating this large deletion of over 15kb was much lower than for introducing InDels. I screened over 60 clonal lines by PCR-genotyping and Western blot analysis. While 6 clones genotyped positive for the deletion on at least one allele, only 2 clones lost FAT4 protein as judged by Western blot analysis (Fig. 11.43D). I was able to confirm one of the two lines by Sanger sequencing, NC55, which showed a clean deletion of 14'874bp. If the remaining coding region still produced a peptide, it would measure 49aa of FAT4 extracellular domain and unlikely be functional (Fig. 11.43C).

However, similar to the InDel results, the cells of NC55 were able to ciliate apparently normally in a 72h starvation window. Further, no obvious changes in centrosome positioning, centriole coherence or GA size were detected (Fig. 11.44).

I then asked if the absence of a phenotype was due to compensational events within the cells, which had been cultured from the single-cell stage for several weeks prior to the experiment. In the case of compensation one would expect the cells to be resistant against FAT4 siRNAs, unless the phenotypes observed from siRNAs were indeed off-target effects. Yet, additional treatment of NC55 with the FAT4 siRNA pool (#1+3+4) caused strong cilia, centrosome and GA defects, as had been previously found in wildtype RPE-1 cells (Fig. 11.44). This indicates that these phenotypes are caused by an inherent property of certain siRNAs, either in concert with or in parallel to a reduction of FAT4.

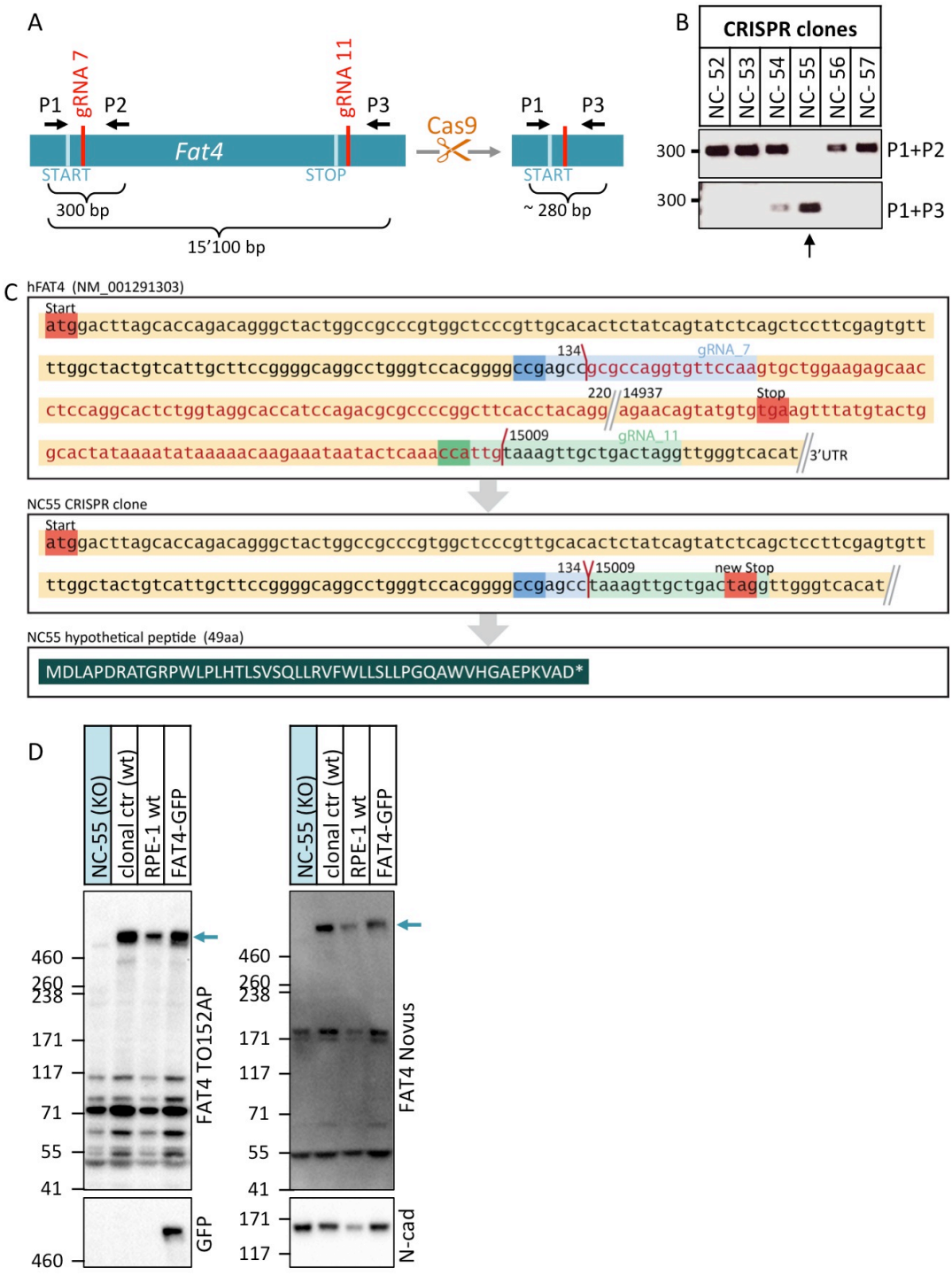

Fig 11.43 *FAT4* knockout RPE-1 cell line by CRISPR/Cas9-mediated gene excision

(A) Schematic of CRISPR/Cas9 *FAT4* gene excision strategy. Primers P1, P2 and P3 were used for genotyping to screen colonies for excision events. (B) Clone NC-55 tests positive for *FAT4* gene excision by genotyping. (C) Sequence information of NC-55 from Sanger sequencing. The remaining *FAT4* gene sequence in N-C55 hypothetically translates to a 49aa peptide. (D) Western blot analysis of NC-55 with two FAT4 antibodies indicates that only the full-length FAT4 band is specific.

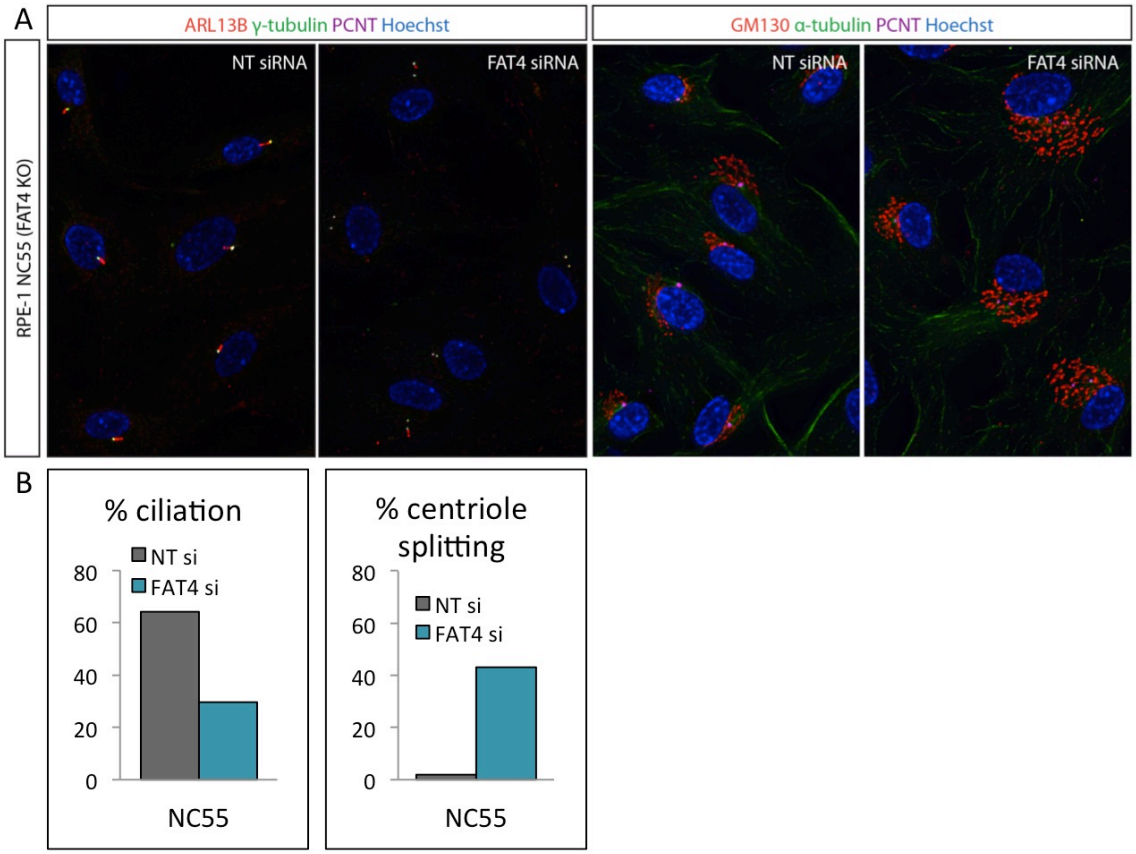

Fig 11.44 *FAT4* excision cell line NC-55 still reacts to FAT4 siRNAs
NC-55 cells are transfected with non-targeting (NT) siRNA or FAT4 siRNA pool (#1+3+4) and starved for 72h. Ciliation is strongly reduced, centriole splitting is strongly increased and GA area is visibly enlarged only in FAT4 knockdown cells, indicating these effects are unrelated to FAT4.

12 Discussion Chapter B

12.1 Lessons from FAT4 BioID and cell culture tools

Fat4 plays important roles during development of various organs and has putative implications in cancer formation or progression. Yet, our understanding of its involvement in these processes is strongly limited through a lack of known biochemical interactors that could link Fat4 mechanistically to other signaling pathways. We therefore asked if we could identify novel interactors of Fat4. Mass spectrometry has become the method of choice to identify candidate molecular interactions in an unbiased manner. As conventional affinity-purification coupled to mass spectrometry techniques have limited success with transmembrane proteins, we used BioID to identify proximity interactions of human FAT4.

12.1.1 FAT4 and the Scribble, Dlg and Lgl module

BioID of full-length FAT4 was performed in HEK293 cells and other cell lines by a former student, Nicole Liscio, and me in collaboration with Dr. Brain Raught's and Dr. Anne-Claude Gingras' groups. A first high-sensitive mass spectrometry approach (referred to as QEHF) revealed an extensive list of high-fidelity FAT4 proximity interactors. Two of the four known FAT4 interactors that have been validated by co-IP in cells and tissue, LIX1L and MPDZ, were recovered in this list, which emphasized the validity of our approach. Interestingly, both LIX1L and MPDZ were retrieved with low peptide numbers, suggesting that other hits with low abundance might be real and meaningful and should be considered for future biochemical and functional validation. A lower-sensitivity follow-up BioID experiment (referred to as Velos) retrieved fewer proximity interactors, but showed a robust 38% overlap of high-confidence interactors with the previous QEHF runs. While I have investigated a few of them, they should also be considered priority candidate interactors for future follow-up screening.

Several proteins associated with adherens junctions and the basolateral membrane of epithelial cells are shared hits of both FAT4 BioIDs. One prominent

group consists of SCRIB, DLG1 and LLGL1. These proteins were first studied in *Drosophila*, where their homologs Scribble (Scrib), Discs large (Dlg) and Lethal giant larvae (Lgl), respectively, localize to septate junctions and cooperate to regulate apical-basal polarity (Woods et al., 1996; Woods et al., 1997; Bilder et al., 2000; Bilder and Perrimon, 2000). More recent studies also suggest that they are involved in the Hippo pathway, however the underlying mechanisms are largely unknown (Grzeschik et al., 2010; Chen et al., 2012; Verghese et al., 2012). While *scrib*, *dlg* and *lgl* appear to act in a common genetic pathway, this is less clear in mammalian systems (Bilder et al., 2000; Wodarz, 2000). Mammalian Scrib, for example, seems to play a more important role in PCP rather than apico-basal polarity (Montcouquiol et al., 2003). In mammalian epithelia, Scrib localizes to adherens junctions and the basolateral membrane (Dow et al., 2003; Navarro et al., 2005). *Scrib* mutant mice exhibit typical PCP phenotypes, including impaired neural tube closure and defects in outer hair cell misalignment in the organ of Corti. They also show a strong genetic interaction with *Vangl2* (Montcouquiol et al., 2003). These phenotypes, albeit stronger, are reminiscent of *Fat4* mutant mice (Saburi et al., 2008). In the heart, *Scrib* is required for proper localization of Vangl2, suggesting that Scrib acts as a scaffold for Vangl2 and potentially other PCP components (Phillips et al., 2007). *Dlg1* knockout mice also show phenotypes reminiscent of defective PCP signaling, such as heart morphogenesis defects, skeletal defects, as well as shortened cochleae but no hair cell abnormalities (Iizuka-Kogo et al., 2015). Again, several of these phenotypes are similarly observed in *Fat4* mutant mice (Saburi et al., 2008; Saburi et al., 2012). Therefore, *Fat4*, *Scrib* and *Dlg1* share several phenotypic similarities in mice. It is plausible that the corresponding proteins also interact functionally during organ development.

I was unable to co-immunoprecipitate endogenous SCRIB and DLG1 with full-length FAT4 (Fig. 11.5), however these are challenging experiments due to the low expression and transmembrane nature of FAT4 and due to the fact that all of these proteins are very large. The BioID technique is not based on physical interactions and therefore can identify prey that interacts transiently or is merely positioned in close proximity to the bait. Therefore it might be impossible

to recapitulate certain BioID "interactions" by affinity-based approaches. However, considering the overlap of phenotypes and the high BioID peptide numbers and SAINT scores, biological interactions between Fat4 and Scrib or Dlg1 seem possible and should be considered in the future.

12.1.2 Potential conservation of FAT4 interaction with EPB41L1

Another basolateral protein, EPB41L1, was identified in both FAT4 BioIDs. Interestingly, EPB41L1 is a FERM-domain containing protein and a homolog of *Drosophila* Coracle (Cora), which has been identified as an interactor of Fat in a mass spectrometry screen in *Drosophila* S2 cells (Kwon et al., 2013). Although this interaction has not been validated further, it is intriguing that it might be conserved between *Drosophila* and humans. In *Drosophila*, Cora forms a functional complex with the related FERM-domain protein Yurt to establish apical-basal polarity through negative regulation of the apical Crb complex (Laprise et al., 2009). The Yurt homolog EPB41L5 is found in the more sensitive QEHF FAT4 BioID runs, indicating that FAT4 might interact with both EPB41L1 and EPB41L5. Strikingly, overexpression of EPB41L5 causes apical constriction in MDCK cells (Nakajima and Tanoue, 2010), which is the opposite of the apical dilation phenotype observed in *Fat4* mutant neural progenitor cells (Badouel et al., 2015). However, attempts to validate an interaction between truncated Fat4 (Fat4ΔECD) and EPB41L5 in HEK293 cells were unsuccessful (Dr. Caroline Badouel*, unpublished data*).

Other interactors that should be considered for follow-up studies are MARK1-3, the mammalian homologs of *Drosophila* Par-1, which is involved in apico-basal polarity and regulates Hippo signaling in flies (Benton and St Johnston, 2003; Huang et al., 2013). Further, JUP/Plakoglobin is a beta-catenin family protein known to interact with classical cadherins to relay cadherin signaling and association with the cytoskeleton (Butz et al., 1992). A putative beta-catenin binding site has been identified in the FAT4 ICD and should be tested for its ability to interact with JUP or CTNNB1/beta-catenin, which was also detected in the QEHF BioID, but with lower peptide numbers.

12.1.3 An interaction between FAT4 and CTNND1/p120 catenin

Another catenin, CTNND1/p120 catenin was amongst the most abundant high-confidence proximity interactors of the QEHF FAT4 BioID. Interestingly, it was only enriched in the Velos BioID from starved cells, suggesting that a possible interaction is stabilized under these conditions. I was able to validate the interaction between endogenous FAT4 and p120 in independent co-immunoprecipitation experiments (Fig. 11.5). FAT4 and p120 further appear to exist in a super-molecular complex (Fig. 11.5I). However, due to the uncertainty about the specificity of the Fat4 antibody, the BN-PAGE experiment should be repeated with FAT4 depleted cells, to confirm the FAT4 signal.

To address if Fat4 could regulate p120, we assessed if loss of *Fat4* in murine intestines affected p120 protein. However, no obvious changes in p120 levels or localization were found, and loss of *Fat4* did not cause pathological abnormalities (Fig. 11.6). Similarly, cultured cells did not show differences in p120 localization or levels after FAT4 knockdown (Fig. 11.8). We therefore concluded that p120 is not dependent on Fat4 for membrane localization in this tissue and loss of Fat4 does not cause similar defects as loss of p120.

p120 is a known interactor and regulator of various classical cadherins, which contain a juxtamembrane p120 binding motif (Daniel and Reynolds, 1995; Yap et al., 1998; Thoreson et al., 2000) (reviewed in (Reynolds, 2007)). While a similar p120 binding motif is missing in Fat4, the observed interaction between the endogenous proteins suggests that Fat4 and p120 are associated in Eph4 cells, either through direct or indirect interaction (Fig. 11.5). p120 competes with other p120-catenin subfamily members, PKP4/p0071 and ARVCF and CTNND2, for binding to classical cadherins (Mariner et al., 2000). Interestingly, PKP4 is also found in the QEHF FAT4 BioID (Table 11.1), and it is tempting to hypothesize that a similar relationship exists between p120-catenin family members and FAT4, as seen with classical cadherins. When bound to a classical cadherin, p120-catenins promote cadherin clustering (Yap et al., 1998; Thoreson et al., 2000) and membrane stability by reducing its endocytosis (Ireton et al., 2002; Davis et al., 2003; Xiao et al., 2003). If a similar relationship exists between

Fat4 and p120, we would expect to rather see a difference of Fat4 levels in *p120* mutant tissue than *vice versa*. Unfortunately, this analysis was precluded by the lack of a Fat4 antibody with specificity in immunofluorescence (see also Fig. 11.6).

As a first approach, however, this could be addressed in one of the cell culture systems expressing tagged FAT4 (such as HEK293 cells expressing FAT4-YFP or FAT4-BF) by RNAi-mediated p120 knockdown. If p120 stabilizes FAT4, reduction of p120 should also reduce membrane levels of FAT4. Original studies investigating the relationship between CDH1 and p120 have further used cadherin-deficient L-cells or A431D cells to show that p120 is cytoplasmic in the absence of cadherins but recruited to the plasma membrane upon CDH1 expression (Thoreson et al., 2000). Similar experiments are conceivable to investigate if FAT4 can recruit p120.

Interestingly, targeted loss of *p120* has been reported to cause convergent-extension defects of the cochlea, but no polarity defects in inner ear hair cells (Chacon-Heszele et al., 2012). *p120* and *Vangl2* show mild genetic interactions, and *Vangl2* ablation results in decreased p120 levels (Chacon-Heszele et al., 2012), therefore it is possible that *p120* functions downstream of *Vangl2* during cochlea convergent extension. *Fat4* mutant mice have similar cochlea extension defects and genetically interact with *Vangl2*, hence a physical and functional interaction between these three proteins is conceivable. Indeed, VANGL2 is a high-confidence proximity interactor in both QEHF and Velos FAT4 BioIDs (Fig. 11.14). An interesting finding is that the convergent extension and hair cell orientation defects in PCP mutants appear to be genetically separable (Chacon-Heszele et al., 2012); therefore p120 could be involved in the convergent extension process branch downstream of Vangl2 and/or downstream or upstream of Fat4. While this is purely speculative, genetic interaction studies between *p120* and *Fat4* might answer some of these questions.

Additonally, similarities between *p120* and *Fat4* mutant kidneys exist. While not all phenotypes overlap, targeted ablation of *p120* during kidney development

results in hypoplastic kidneys with prenatal cysts in proximal tubules (Marciano et al., 2011), which is highly reminiscent of *Fat4* mutants (Saburi et al., 2008; Mao et al., 2011a). Both mouse models further show abnormal cilia in cystic epithelia (Saburi et al., 2008; Marciano et al., 2011). *Fat4* and *p120* mutant kidneys also exhibit reduced numbers of glomeruli (Marciano et al., 2011; Bagherie-Lachidan et al., 2015). In summary, several parallels exist between *p120* and *Fat4* mutant tissue, and it is tempting to speculate that p120 and Fat4 are molecularly connected.

12.1.4 Putative interactions between FAT4 and VANGL proteins

Both VANGL homologs, VANGL2 and VANGL1, are FAT4 BioID hits (QEHF and Velos; see Table 11.1 and 11.2; Fig. 11.14). A high unspecific background signal of the available VANGL2 antibody precluded its testing in FAT4 pulldowns. Therefore, it remains an open question whether these proximity interactors reflect physical interactions between FAT4 and VANGL proteins. Although loss of *Fat4* and core PCP genes all result in hair cell polarity defects, the severity of these defects varies, and the relationship between the two PCP "modules" (as defined in *Drosophila*) is poorly understood (Wang et al., 2005; Wang et al., 2006b; Saburi et al., 2008; Saburi et al., 2012). However, no obvious genetic interaction between *Fat4* and *Vangl2* was found in hair cell orientation in the organ of Corti (Saburi et al., 2012). This is in contrast to strong genetic interactions observed between *Scrib* and *Vangl2* or *Dvl2* and *Vangl2*, which result in severe patterning defects in the same tissue (Montcouquiol et al., 2003; Wang et al., 2005). Additionally, Frizzled 6 (Fz6) asymmetric localization in misoriented *Fat4* mutant hair cells was found to be unaffected (Saburi et al., 2012). Therefore, these data hint towards independent functions of Fat4 and Vangl2 (or other core PCP proteins) in hair cell polarity. Yet, to strengthen this hypothesis, Vangl2 localization should be addressed in the organ of Corti of *Fat4* mutant mice (see also (Montcouquiol et al., 2006; Jones et al., 2008)).

Interestingly, *Ift88* knockout mice similarly exhibit hair cell rotation defects (amongst other PCP-like phenotypes), despite correct Vangl2 localization (Jones et al., 2008). While in *Ift88* mutants hair cells are likely affected due to loss of the

kinocilium, the sensory cilium in the vertex of the stereocilia (which is a defect not seen in *Vangl2* or *Fat4* mutants (Montcouquiol et al., 2003; Saburi et al., 2008)), this demonstrates another case of an inner ear polarity defect apparently independent of core PCP (Jones et al., 2008). Whether loss of *Ift88* or other kinocilium-associated proteins affects PCP signaling downstream of Vangl2 or as part of a parallel polarity-regulating pathway remains to be investigated. Similarly, the relationship between Ift88 and Fat4 is unexplored in the organ of Corti and elsewhere. It would be very interesting, also with regard to a potential link of Fat4 and cilia, to investigate whether *Ift88* and *Fat4* genetically interact in the inner ear or other tissues.

In view of a possible physical interaction between Fat4 and Vangl2 as indicated by BioID, it should lastly be noted that *Fat4* and *Vangl2* do genetically interact in cochlea elongation and kidney development (Saburi et al., 2008; Saburi et al., 2012). Therefore, cooperative functions of Fat4 and Vangl2 might be executed through direct or indirect interaction in these processes. Considering the controversy in *Drosophila* whether the Fat/Ds and core PCP modules are communicating, it will be interesting to address this topic further in mammals.

12.1.5 FAT4 interactions with the Hippo pathway

Only few FAT4 BioID hits were associated with Hippo signaling, such as NF2 and SCRIB. I could not validate interactions between NF2 or SCRIB with FAT4, and FAT4 knockdown in RPE-1 cells did not cause consistent changes of LATS and YAP that would indicate a simple role for FAT4 as an upstream Hippo pathway activator like in *Drosophila*. Whether FAT4 regulates the Hippo pathway in mammals is a longstanding question, and conflicting data have been published, which will require further investigation to reconcile. Since the *Fat4* knockout mouse does not show obvious overproliferation phenotypes or altered YAP activity (Saburi et al., 2008; Mao et al., 2011a; Saburi et al., 2012; Badouel et al., 2015; Bagherie-Lachidan et al., 2015), evidence argues against a major role for Fat4 in mammalian Hippo signaling.

12.1.6 FAT4 shares most BioID interactors with Cdh1

A striking observation was that FAT4 proximity interactors are reminiscent of the interactome of Cdh1/E-cadherin. Indeed, when compared to a recently published dataset of CDH1 BioID interactors, many of the FAT4 interactions were shared. We therefore directly compared both baits in the Velos BioIDs, and found similar results, with 66% of all FAT4 proximity interactors also present in Cdh1 runs.

The strong overlap between the FAT4 and CDH1 proteomes could imply that FAT4 and CDH1 functionally interact and share a common network of proteins to function in similar processes. Alternatively, the overlap might occur because most of the shared interactors are not specific to either FAT4 or Cdh1, but represent common interactors of general transmembrane proteins.

Several of the shared preys are known interactors and functional partners of Cdh1, which would argue against the second hypothesis and suggest that the enriched proximity interactors are more specific than "frequent flyers". To further address this issue, we compared our data with published BioID data of other transmembrane proteins. These interactomes had recently become available as part of a proteomics screen for centrosomal and ciliary proteins, and were performed under very similar conditions as the FAT4 BioID (Gupta et al., 2015).

Strikingly, 38 of the 50 shared interactors between Cdh1 and FAT4 are also high-confidence interactors of at least one of seven presumably unrelated transmembrane proteins (TMEM17, TMEM67, TMEM237, TMEM216, TCTN1, TCTN2, TCTN3) (Fig. 12.1). While this does not exclude that some of these interactions are specific shared interactors of several baits, greater caution should be used when following up on these hits. I noticed an especially high overlap of FAT4 with the transmembrane protein TMEM17, and that many adherens junction proteins were shared between both baits (Fig. 12.2). Little is known about TMEM17 apart from a function in the ciliary transition zone, and only assumptions can be made about its relationship to FAT4 or CDH1. This also

emphasizes that these analyses are difficult to judge, as without a better understanding of the molecular functions and interconnections between different baits, specific hits might be easily filtered out. On the other hand, a stringent comparison as described here is potent to uncover exclusive interactors that are highly specific to the bait of interest. Only 14 FAT4 interactors (Velos BioID) remain after common interactions with Cdh1 and other transmembrane proteins are filtered out (Fig. 12.1). These include LIX1L, as well as the components of the heterodimeric FACT (facilitates chromatin transcription) complex (SSRP1 and SUPT16H), which is involved in chromatin remodeling and was associated with tumor progression (Orphanides et al., 1998; Garcia et al., 2013). p120 on the other hand is shared between all three lists. When all FAT4 proximity interactors are combined (QEHF+Velos), 116 interactors are exclusively found with FAT4 but not Cdh1 or unrelated membrane proteins (Fig. 12.2), although it is unclear if there was higher overlap if the Cdh1 and transmembrane bait BioIDs had been performed on a high-sensitivity QEHF as well. The FAT4 interactomes should be viewed as a resource and filtered depending on the exact question that is being asked. As with all proteomics data, FAT4 BioID hits should be confirmed in a different system prior to more in-depth follow-up work.

Co-immunoprecipitation experiments, such as described in Fig. 11.5, can serve as a first validation step of BioID hits. However, due to the nature of BioID, affinity-purification experiments are often not an ideal approach to confirm data. Problems arise for proteins with lower solubility, such as FAT4, which is a large transmembrane protein, as are many of its proximity interactors. Co-IPs with these proteins are challenging and not an optimal screening approach to filter out specific interactors. Another issue is that BioID can capture transient interactors that might not bind stably to a bait of interest and can therefore not be recovered in affinity purification techniques. Possible validation experiments include PLA (proximity ligation assay (Fredriksson et al., 2002)), to address if the bait protein closely colocalizes with a proximity interactor (<40nm distance).

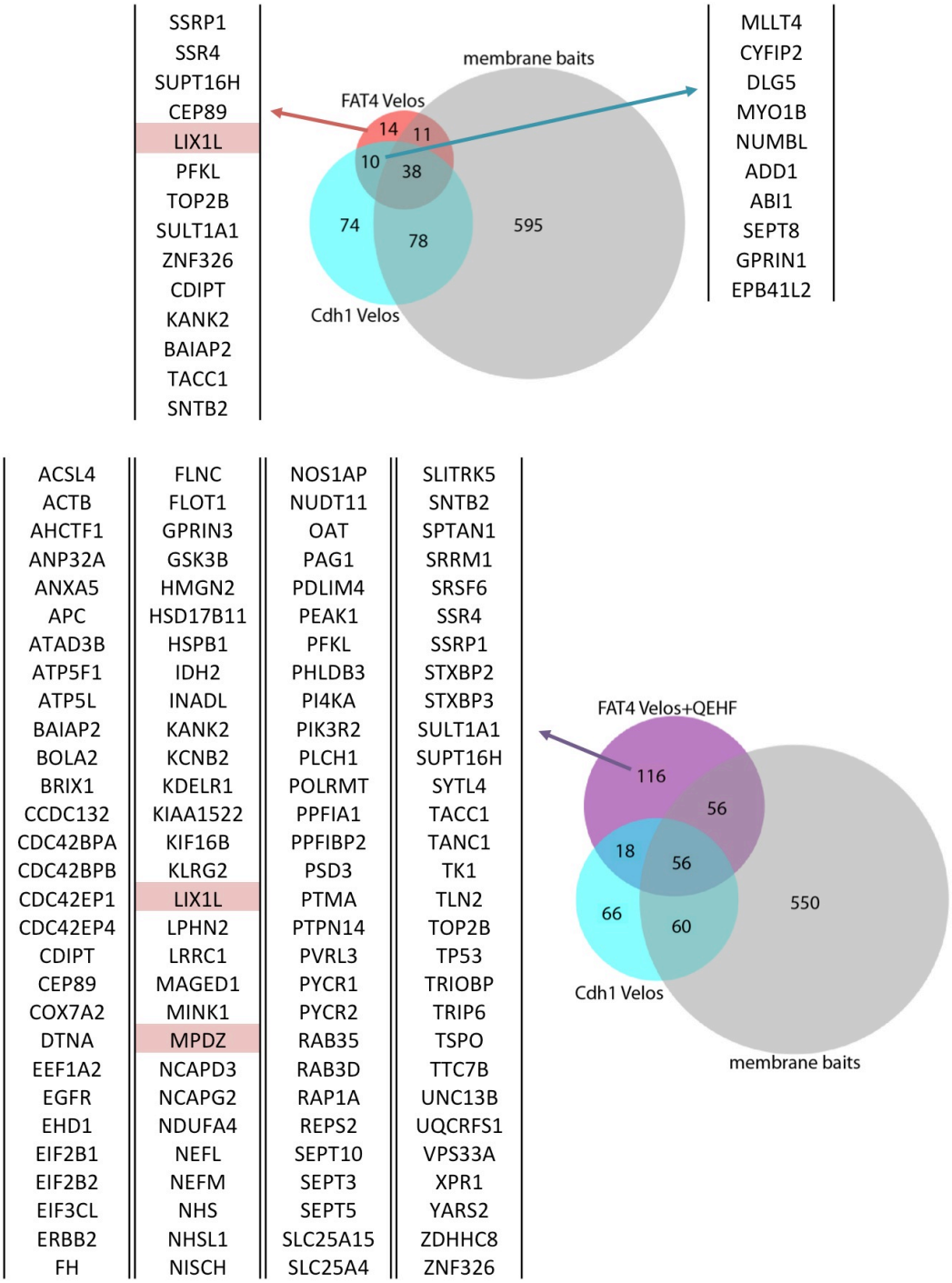

Fig 12.1 Comparison of FAT4 and Cdh1 BioIDs with BioID data from other membrane baits

Gene lists show unique FAT4 Velos hits (top left), hits shared between FAT4 and Cdh1 (Velos) but distinct from unrelated membrane baits (top right) and unique FAT4 hits from QEHF and Velos BioIDs combined (bottom). Known FAT4 interactors LIX1L and MPDZ are highlighted.

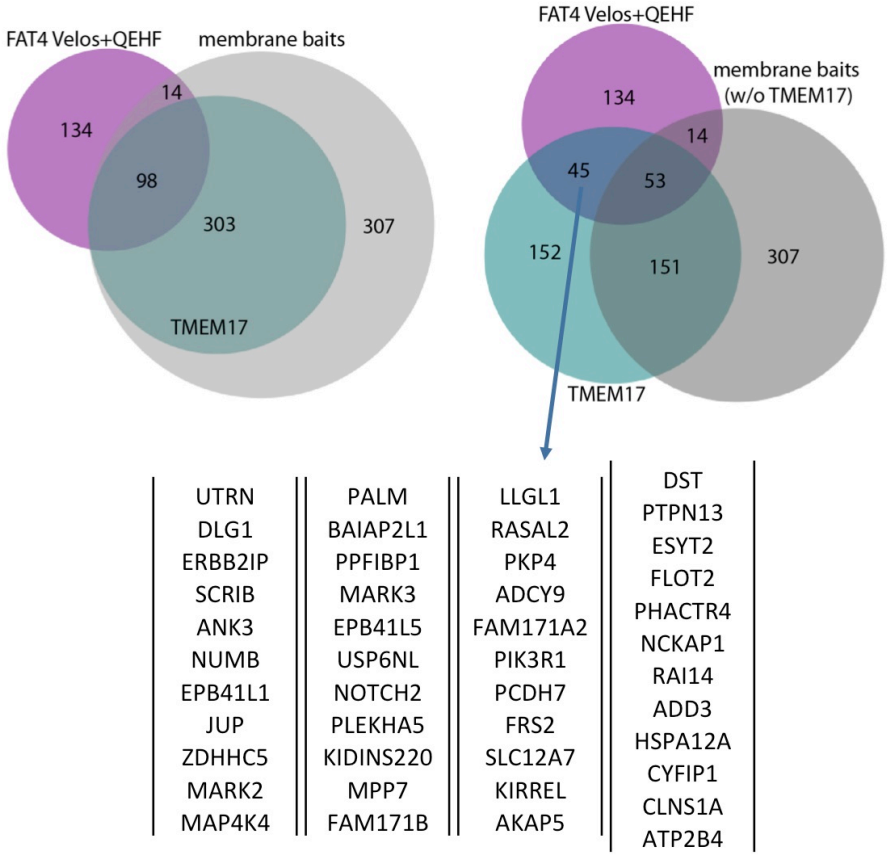

Fig 12.2 Comparison of FAT4 BioID hits with TMEM17 and other membrane baits
When comparing FAT4 BioID hits (Velos and QEHF combined) with TMEM17 (one of the 7 presumably unrelated membrane baits) separately from other membrane baits, it becomes clear that TMEM17 accounts for 40% of overlap between FAT4 and membrane baits (right Venn diagram). Shared proximity interactors between FAT4 and TMEM17 are listed. Hits uniquely found in FAT4 BioIDs should be prioritized for follow-up studies. However, as the function of TMEM17 and its relationship to FAT4 are unknown, some of the shared proximity interactors might still be specific to both baits.

12.1.7 Advantages and caveats of BioID

BioID is a powerful technology to identify weak and transient interactors, as well as to study less soluble baits that are challenging to use in conventional affinity-purification approaches. The modified (promiscuous) BirA* activates free biotin and converts it into biotinoyl-5'-AMP, which is highly reactive and modifies the closest available primary amine of a protein (Lane et al., 1964). Biotinoyl-5'-AMP is short-lived, which limits the biotinylation radius of the BirA*-tagged bait.

BioID studies of nuclear pore complex proteins found that the biotinylation radius extends approximately 10nm from the bait (Kim et al., 2014a). BirA*-tagging of the N- and C-terminus of ZO-1 revealed distinct subsets of interactors, supporting a biotinylation range of less than 20nm (Van Itallie et al., 2013). Therefore, BioID usually uncovers the limited neighborhood of a bait, including some indirect interactors.

A caveat of BioID is that the biotinylation time frame is rather long (biotin treatment occurs over night before the cells are harvested), as is the half-life of biotin modifications. Therefore, the BirA*-tagged bait might biotinylate proteins that it comes into contact with as it traffics through different subcellular compartments or as it is targeted for degradation. Such proximity interactors are less likely to be involved in bait protein signaling or to provide information about bait protein function. In the future, combinations of traditional BioID and newly developed techniques with shorter biotinylation windows (such as APEX labeling (Martell et al., 2012; Rhee et al., 2013)) might help narrowing down specific interactors.

12.1.8 FAT4 and actin regulation

Interestingly, localization of exogenous FAT4 was frequently found at filopodia and membrane protrusions (in HeLa and HCT116 cells, Fig. 11.15; 11.21). These are sites of active actin cytoskeleton dynamics and FAT4 localization to these structures might be associated with the finding that several proteins involved in actin remodeling are enriched in the FAT4 BioIDs, especially under starvation. Whether FAT4 might control actin dynamics similarly to or in concert with FAT1 remains to be addressed in the future. No obvious changes in the F-actin network (Phalloidin stainings) have been found in FAT4 knockdown cells, however defects might be subtle and require more sensitive detection methods.

12.2 A link between FAT4 and cilia

In chapter B I also investigated a potential role for FAT4 in cilia biology. *Fat4* mutant mice exhibit cystic kidney defects before birth, which are accompanied by occasional cilia abnormalities in the cystic tissue. Although not fully

elucidated, cystic kidney defects are highly correlated with primary cilia defects and are a common feature of syndromic ciliopathies (for an overview see (Tobin and Beales, 2009)). *Fat4* mutant mice also exhibit other phenotypes that resemble those associated with defective cilia, such as neural migration defects, skeletal abnormalities and cochlea hair cell misorientation (Jones et al., 2008; Saburi et al., 2008; Badouel et al., 2015). Investigation of primary cilia in prenatal kidney tubules is technically challenging, and a requirement for tissue sections limits a complete assessment of cilia in these three-dimensional structures. I therefore decided to study the relationship of FAT4 and cilia in a cell culture model system, which allows addressing detailed mechanistic questions and performing artificial manipulations.

12.2.1 Cilia and centrosome defects are potentially off-target effects

Using siRNA-mediated knockdown in RPE-1 cells, I indeed found that FAT4 knockdown correlated with shortening and loss of primary cilia (Fig. 11.22). Time course experiments indicated that FAT4 knockdown did not impair initial ciliogenesis but rather cilium stability or maintenance of mature cilia (see Fig. 11.25). Accordingly, early requirements for cilium formation were not found affected, such as centriolar cap removal (CP110; Fig. 11.26), distal appendages (Cep164; Fig. 11.27) and recruitment of transition zone and IFT proteins (NPHP1; IFT88; Fig. 11.26; 11.27).

Since *Fat4* and *Fat1* genetically interact during kidney tubule elongation and loss of one allele of *Fat1* in *Fat4* mutant mice significantly enhances renal cysts (Saburi et al., 2012), I also investigated if knockdown of FAT1 causes cilia defects. Overall ciliation in FAT1 knockdown cells was variable and on average not significantly reduced, although a similar shortening of cilia was observed (Fig. 11.23). A mild involvement in cilia elongation or maintenance is therefore possible. However, double knockdown of FAT4 and FAT1 did not enhance the FAT4 phenotypes (Fig. 11.23; Fig. 11.34).

In contrast to reduction of FAT1, FAT4 knockdown also resulted in strong, unexpected centrosomal phenotypes. When arrested in G0, centrosome

positioning in relation to the nucleus was abnormal, with a significant increase of centrosome-nucleus distance (Fig. 11.33). Additionally, the distance between both centrioles frequently exceeded the normally observed range of 0-2µm (Fig. 11.29-31), which is considered centrosome splitting (Meraldi and Nigg, 2001). While similar centriole splitting can be caused by defects in the intercentriolar linker, localization of the linker protein Rootletin appeared unaffected in FAT4 knockdown cells (Fig. 11.32). The molecular cause of the observed centrosomal phenotypes is presently unknown.

Consistent with other mutants resulting in increased centrosome-nucleus distance, FAT4 knockdown cells showed reduced capacity to close a wound of their monolayer through migration (Fig. 11.38). I also observed a concomitant increase in Golgi apparatus (GA) size, which might add to the migration defect. As GA and centrosomal orientation correlate with directed cell migration (Gotlieb et al., 1981; Kupfer et al., 1982; Wakida et al., 2010), I performed experiments to test if GA orientation during wound healing was perturbed in FAT4 knockdown cells. However, preliminary results did not show significant defects.

I subsequently discovered that out of four additional siRNAs targeting a different exon of *FAT4*, only one mildly showed some of the discussed phenotypes. Careful individual analysis of each siRNA indicated that there was no apparent correlation between cilia, centrosome or GA changes and strong reduction of (full-length) FAT4 protein (Fig. 11.39).

The large size and low genome integration efficiency of FAT4 prevented me from establishing the required tools for siRNA rescue experiments. Instead, I used CRISPR/Cas9 to engineer RPE-1 cell lines with premature translation stops in exon 1 and exon 9 of *FAT4*, as well as one cell line (NC55) where 99% of the entire *FAT4* coding region was excised (Fig. 11.43). However, the mutant cell lines investigated did not exhibit centrosome positioning or cohesion defects, no apparent GA enlargement and no loss of primary cilia (Fig. 11.42-44). In addition, siRNA treatment of NC55, which should not produce any mRNA

containing the siRNA targeting sequences, caused strong cilia and centrosome phenotypes (Fig. 11.44). Therefore, the absence of observed phenotypes in the mutant cell lines cannot be explained by compensatory mechanisms.

Unfortunately, my data don't allow drawing definite conclusions about a role for FAT4 in primary cilia. The absence of obvious structural defects in FAT4 knockout cells argues that FAT4 is not required for primary cilium formation or maintenance, at least under standard culture conditions. If these cells exhibit more subtle defects, such as problems in cilia composition, signaling or stability, remains to be investigated. Yet, the fact that additional treatment with FAT4 siRNAs of *FAT4* knockout (NC55) cells causes severe cilia defects, suggests that these are due to an off-target effect instead or in addition to loss of FAT4.

However, while I cannot exclude this scenario, it appears unlikely that three out of eight independent siRNAs would cause the same phenotypes by regulating other genes off-target. It is also striking that the observed defects occur in organelles that are functionally linked to each other and are interdependent (centrosome, cilium, GA). In an effort to identify potential off-target genes, I found no putative off-target common to the phenotype-causing siRNAs that could easily explain the observed phenotypes (see also below). Additionally, I tested different siRNA pools (consisting of 3, 4 or 8 different FAT4 siRNAs), which showed strong and robust cilia phenotypes (Fig. 11.22). Pooled siRNAs are commonly used for higher confidence, as each individual siRNA within the pool has a lower concentration, which should reduce individual off-target effects (Hannus et al., 2014).

An alternative explanation is that the siRNA phenotypes are caused by a combination of specific and off-target effects. If reduction of FAT4 levels sensitized the cells and their cilia or centrosomes for other, potentially more general stressors, FAT4 depletion alone might not show strong phenotypes. However, in combination with an off-target effect, the sensitized cells would show a stronger phenotype, similar as observed in genetic interactions. While this is merely speculative, this "two-hit" hypothesis could explain the observed

discrepancy between siRNAs and CRISPR mutants and even the differences between individual siRNAs.

The only way to truly test if loss of FAT4 is required for the siRNA-mediated phenotypes is a rescue experiment. One possibility is to overexpress a siRNA-resistant form of *FAT4* in these cells and assess if this can rescue or suppress any of the phenotypes. Unfortunately, I was unable to establish RPE-1 cells ectopically expressing FAT4, most likely due to the enormous size of *FAT4*, which also precludes the use of lentiviruses for higher genome integration efficiency. Another possibility is to introduce silent mutations in one or several siRNA targeting regions of FAT4 (for example using the CRISPR/Cas9 system), to render it siRNA resistant, which should be considered for future investigations.

12.2.2 Analysis of potential FAT4 siRNA off-targets

To address if any of the siRNAs have a high chance to target the same off-target gene, I blasted (NCBI; Blast-n) the targeting sequence of each siRNA and compared the results. No overlap between blast hits with 63% sequence coverage or higher (which equals a match of 13nt or more) was found between any two siRNA sequences (Table 12.1).

siRNAs have also been shown to be able to regulate gene expression in a manner similar to microRNAs (miRNAs) (Lai, 2002), which can cause severe off-target effects. In this case, only a part of the siRNA recognizes a complementary nucleotide sequence, which can affect gene expression (Jackson et al., 2003; Tschuch et al., 2008). Binding and regulation through miRNAs frequently occurs in the 3'UTR of target transcripts (Lai, 2002).

This mode of action of siRNAs is difficult to predict reliably, however, different computational tools have been developed to identify long lists of putative miRNA off-target sequences for siRNAs. I employed the GESS algorithm (Sigoillot et al., 2012; Yilmazel et al., 2014), which screens a library of either human protein coding transcripts or just 3'UTRs for matches with a 7 nt seed region within each siRNA. The program also allows comparing siRNAs that share a phenotype

("active siRNAs") with those that don't show the phenotype ("inactive siRNAs"). Enrichment of off-targets of active sequences is statistically evaluated in comparison with inactive sequences. The tool is intended for large siRNA data sets, such as in genome-wide RNAi screens, but can be employed for smaller lists as well. When the active (i.e. cilium-defect causing) FAT4 siRNAs #1, #3 and #4 are compared to inactive siRNAs (#2, #intra1, #intra3, #UTR1, #UTR2) in GESS (addressing 7-mer homology of guide strands to the full human protein coding transcript library), 23 putative miRNA off-target genes are identified in all active siRNAs that occur in less than 2 inactive siRNAs. None of these genes has reported cilia defects, except DNAAF2, which encodes dynein arms in motile cilia and DNAAF2 loss leads specifically to defects in motile cilia (Table 12.2).

In summary, it remains elusive how the different siRNAs affect similar processes and whether this is related to FAT4 knockdown or a common set of off-target genes. Neither nucleotide blasting nor GESS analysis can fully address potential off-targets and are merely a mean to narrow down candidate genes for further experimental investigation.

Entire siRNA screens have recovered lists of false-positive candidate genes due to shared miRNA off-targets of the active siRNA sequences (Sigoillot et al., 2012). But it should be noted that such screening methods specifically search for a desired phenotype and therefore are more prone to enrich their "hit" lists with siRNAs that cause off-target effects with the same or a similar phenotype. As an example, in a siRNA screen for new TGF-beta pathway components, 391 siRNAs initially scored out of 18,869 tested siRNAs, however most of the 391 siRNAs were later confirmed to cause off-target reduction of TGF-beta receptor 2 expression, both experimentally and as predicted by GESS (Schultz et al., 2011; Sigoillot et al., 2012). Therefore, in this case less than 2% of all tested siRNA sequences caused a phenotype due to shared off-targets.

In contrast, a coincidental overlap of off-target effects of 3 out of 8 independently designed FAT4 siRNAs would indicate a higher off-target frequency. If indeed the observed siRNA phenotypes are off-target effects, as experiments with FAT4

knockout cells suggest, extreme caution employing RNAi strategies should be exercised. Considering that many screening methods and molecular characterizations within the last 15 years relied on siRNAs and that only in recent years siRNA rescue techniques have become common practice to validate their specificity, we should keep the possibility of off-target effects in mind when interpreting these data.

Table 12.1 Blast-n results of siRNA target sequences
Genes containing regions with homology to siRNA targeting sequences are shown (criterium: less than six mismatches in 19bp)

siRNA	Symbol	Full name	Mismatches
siRNA 1	SPOCK2	sparc/osteonectin, cwcv and kazal-like domains proteoglycan (testican) 2	5/19
	LOC105372711	ncRNA	5/19
siRNA 2	SNX30	sorting nexin family member 30	1/19
	CD209	CD209 molecule	4/19
	CLEC4M	C-type lectin domain family 4 member M	4/19
	LINC00339	long intergenic non-protein coding RNA 339	5/19
	ZNF75A	zinc finger protein 75a	5/19
	FMO5	flavin containing monooxygenase 5	5/19
	VSIG10L	V-set and immunoglobulin domain containing 10 like	5/19
siRNA 3	DARS2	aspartyl-tRNA synthetase 2, mitochondrial	5/19
	CTH	cystathionine gamma-lyase	5/19
siRNA 4	FMN1	formin 1	5/19
	LINC01452	prostate cancer associated transcript 5 (non-protein coding)	5/19
siRNA intra1	LOC105371483	ncRNA	2/19
	PRKDC	protein kinase, DNA-activated, catalytic polypeptide	5/19
	LINC00701	long intergenic non-protein coding RNA 701	5/19
siRNA intra2	RC3H1	ring finger and CCCH-type domains 1	1/19
	BEND7	BEN domain containing 7	5/19
	NEK8	NIMA related kinase 8	5/19
	MPHOSPH8	M-phase phosphoprotein 8	5/19
	GFM1	G elongation factor, mitochondrial 1	5/19
	DDR2	discoidin domain receptor tyrosine kinase 2	5/19
siRNA intra3	PTCHD1	patched domain containing 1	4/19
	RNF22	tripartite motif containing 3	4/19
	FBXW8	F-box and WD repeat domain containing 8	4/19
	SPOCK3	sparc/osteonectin, cwcv and kazal-like domains proteoglycan (testican) 3	4/19
	RPRD1A	regulation of nuclear pre-mRNA domain containing 1A	5/19
	EVI2B	ecotropic viral integration site 2B	5/19
	FAM13B	family with sequence similarity 13 member B	5/19
	ASPSCR1	alveolar soft part sarcoma chromosome region, candidate 1	5/19
	IGSF10	immunoglobulin superfamily member 10	5/19
	VPRBP	Vpr (HIV-1) binding protein	5/19
siRNA 3'UTR 1	SWAP70	SWAP switching B-cell complex 70kDa subunit	2/19
	LOC105374499	ncRNA	2/19
	STX3	syntaxin 3	4/19
	SART3	squamous cell carcinoma antigen recognized by T-cells 3	5/19
siRNA 3'UTR 2	none	none	-

Table 12.2 GESS off-target analysis

siRNAs causing the same phenotype (active) were compared to siRNAs without an effect (inactive) for overlap of putative off-targets. GESS results are listed for putative off-targets shared between all active and less than 2 inactive siRNAs.

Potential off-targets enriched for siRNAs #1, #3, #4 (affecting ciliation)	
AHNAK2	AHNAK nucleoprotein 2
ANLN	anillin actin binding protein
BMPR1A	bone morphogenetic protein receptor type 1A
CENPN	centromere protein N
CPPED1	calcineurin-like phosphoesterase domain containing 1
CTNS	cystinosin, lysosomal cystine transporter
DNAAF2	dynein (axonemal) assembly factor 2
FMNL2	formin like 2
GOLGA7B	golgin A7 family member B
GPR133	adhesion G protein-coupled receptor D1
IQCA1	IQ motif containing with AAA domain 1
KIF18A	kinesin family member 18A
KLHDC4	kelch domain containing 4
NUTM2A	NUT family member 2A
NUTM2B	NUT family member 2B
PCDH10	protocadherin 10
PDE4DIP	phosphodiesterase 4D interacting protein
PHF15	jade family PHD finger 2
PTGFR	prostaglandin F receptor
RGS6	regulator of G-protein signaling 6
RGS8	regulator of G-protein signaling 8
SETDB2	SET domain bifurcated 2
SLC4A5	solute carrier family 4 member 5

Potential off-targets enriched for siRNAs #1, #4, #intra1 (centriole splitting)	
AGRN	agrin
AHNAK2	AHNAK nucleoprotein 2
ATAD1	ATPase family, AAA domain containing 1
CHD5	chromodomain helicase DNA binding protein 5
DNAAF2	dynein (axonemal) assembly factor 2
DNAJC10	DnaJ heat shock protein family (Hsp40) member C10
ERCC3	excision repair cross-complementation group 3
GCLC	glutamate-cysteine ligase catalytic subunit
HECA	hdc homolog, cell cycle regulator
KCNU1	potassium calcium-activated channel subfamily U member 1
KLHDC4	kelch domain containing 4
LMBR1	limb development membrane protein 1
MAP3K13	mitogen-activated protein kinase kinase kinase 13
NOL8	nucleolar protein 8
PALD1	phosphatase domain containing, paladin 1
PCDH10	protocadherin 10
PDE2A	phosphodiesterase 2A
SLC10A7	solute carrier family 10 member 7
SLC4A5	solute carrier family 4 member 5
TBC1D19	TBC1 domain family member 19
TMEM132C	transmembrane protein 132C
TP73	tumor protein p73
UMODL1	uromodulin like 1
WDR87	WD repeat domain 87
ZNF423	zinc finger protein 423

Potential off-targets enriched for siRNAs #1, #2, #3, #4, #intra1 (affecting Golgi size)	
ABCB1	ATP binding cassette subfamily B member 1
DOCK5	dedicator of cytokinesis 5
DOCK7	dedicator of cytokinesis 7
FAT2	FAT atypical cadherin 2
FOXN3	forkhead box N3

12.2.3 New insight into FAT4 through new cell culture tools

It will be useful to address some of the open questions and future experiments suggested here with the newly established cell lines generated in this study. Endogenous *FAT4* has been mutated, deleted and tagged with GFP in RPE-1 cells using the CRISPR/Cas9 technology, therefore these cell lines represent molecularly "cleaner" tools than the previous overexpression and knockdown approaches. As a first step, I used these cells to confirm the specificity of FAT4 antibodies for use on Western blots. Interestingly, it appears that only a high-molecular band (likely representing full-length FAT4) corresponds to FAT4 protein and that FAT4 in RPE-1 cells does not appear to undergo a similar cleavage event as observed for *Drosophila* Fat (which mainly exists in a processed form of 450kDa + 110kDa) (Fig. 11.7). It will be interesting to use the FAT4-GFP cells to test interactions between FAT4 and BioID hits in endogenous co-immunoprecipitation (using GFP-trap beads), proximity ligation assays and blue native PAGE experiments. Especially the interaction between FAT4 and p120 should be addressed in more detail. I wasn't able to detect the endogenous FAT4-GFP in preliminary immunofluorescence stainings, but signal amplifaction techniques, such as tyramide signal amplification (van Gijlswijk et al., 1997) or Streptavidin-signal amplification might help to detect low FAT4-GFP expression. To understand FAT4 function, it will be important to analyze its localization, which so far has not been possible due to a lack of specific antibodies for use in immunofluorescence. Lastly, FAT4 knockout cells, such as the NC55 cell line, will provide a FAT4 negative control for future biochemical or molecular studies.

12.2.4 Molecular causes of *Fat4* mutant kidney cysts

Fat4 mutant mice exhibit kidney cysts associated with both OCD and cilia defects (Saburi et al., 2008). Why does loss of *Fat4* cause kidney cyst formation? The morphogenetic mechanisms underlying kidney tubule development and how they are affected by mutations in the multitude of genes that have been associated with renal cysts, is still poorly understood. Hh, Wnt/PCP, Hippo and mTOR signaling pathways have been implicated in cystic kidney disease (Brook-Carter et al., 1994; Simons et al., 2005; Hu et al., 2006; Shillingford et al., 2006;

Hossain et al., 2007; Makita et al., 2008; Patel et al., 2008; Bonnet et al., 2009; Happe et al., 2009; Karner et al., 2009; Shillingford et al., 2010; Zullo et al., 2010). Additionally, a striking correlation between cilia defects and kidney cysts exists, but how exactly cilia might function in cyst development is not known (Watnick and Germino, 2003; Yoder, 2007; Winyard and Jenkins, 2011; Lee and Somlo, 2014). One model suggests that cilia sense renal fluid flow and elicit a cellular response, such as by regulating intracellular calcium levels (Praetorius and Spring, 2001; Nauli et al., 2003; Li et al., 2009). Also abnormal oriented cell division (OCD) correlates with cyst formation in several models and has been suggested as the direct cause for tubule dilation (Fischer et al., 2006; Jonassen et al., 2008; Patel et al., 2008; Luyten et al., 2010). However, affecting OCD does not automatically cause kidney cysts (Nishio et al., 2010) and it remains controversial if OCD defects are primary or secondary to cyst development (Luyten et al., 2010; Nishio et al., 2010). Unfortunately, the cell culture models in my study did not answer if Fat4 plays a role in cilia structure or function. It therefore remains unsolved what the mechanistic causes for *Fat4* mutant kidney cyst development are.

12.3 Outlook

Throughout this project, I have generated multiple tools to address FAT4 molecular function and to understand FAT4 biology. I have established multiple cell lines expressing full-length FAT4, validated FAT4 antibodies and identified potential FAT4 interactors in BioID experiments from HEK293, HeLa and HCT116 cells. I have established efficient siRNA-mediated knockdown protocols, although we need to better understand why several siRNAs result in different phenotypes. As cilia and centrosome defects observed with siRNAs appear to be results of off-target effects, these findings highlight that RNAi technology should be used with caution and complemented with rescue experiments. Finally, I have generated multiple independent FAT4 mutant cell lines that either have early frame-shift mutations within the *FAT4* gene or a deletion of the entire gene that will facilitate future studies concerning molecular functions of FAT4.

Very few tools to molecularly explore FAT4 had been developed in the past, and the large size of FAT4 had limited the use of biochemical and cell culture techniques to study its function. The herein described newly established cell lines, interactomes and initial data will hopefully be a useful resource and help to understand FAT4 biology in the future.

13 Appendix

Table 13.1 Full list FAT4 BioID (QEHF) HEK293 cells

Gene ID	Gene Name	Full name	Top 2 controls		FAT4 BioID (QEHF dataset) pool A tech#1	pool A tech #2	pool B tech #1	pool B tech #2	Total	SAINT
79633	**FAT4**	*FAT atypical cadherin 4*			1153	1152	1160	1151	**4616**	**NA**
948469	**birA**	*E.Coli biotin ligase*	1919	1748	744	777	755	797	**3073**	**NA**
7402	**UTRN**	*Utrophin*	36	36	156	152	168	163	**639**	**1.00**
1739	**DLG1**	*Discs large homolog 1, scribble cell polarity complex component*	31	28	138	138	137	135	**548**	**1.00**
55914	**ERBB2IP**	*Erbb2 interacting protein*	32	30	152	116	138	140	**546**	**1.00**
23513	**SCRIB**	*Scribbled planar cell polarity protein*	24	21	125	136	138	135	**534**	**1.00**
1829	**DSG2**	*Desmoglein 2*	20	15	122	118	128	138	**506**	**1.00**
989	**SEPT7**	*Septin 7*	28	25	98	106	101	108	**413**	**1.00**
114787	**GPRIN1**	*G protein regulated inducer of neurite outgrowth 1*	5	4	90	97	96	89	**372**	**1.00**
288	**ANK3**	*Ankyrin 3, node of Ranvier (ankyrin G)*	21	21	90	87	95	88	**360**	**1.00**
60	**ACTB**	*Actin, beta*			51	56	63	55	**225**	**1.00**
1500	**CTNND1**	*Catenin delta 1*	10	9	58	55	55	55	**223**	**1.00**
25909	**AHCTF1**	*AT-hook containing transcription factor 1*	18	14	56	53	60	52	**221**	**1.00**
8650	**NUMB**	*Numb homolog (Drosophila)*	9	8	50	54	59	55	**218**	**1.00**
2036	**EPB41L1**	*Erythrocyte membrane protein band 4.1-like 1*	5	4	45	39	49	52	**185**	**1.00**
3728	**JUP**	*Junction plakoglobin*	10	9	45	45	49	44	**183**	**1.00**
81839	**VANGL1**	*VANGL planar cell polarity protein 1*	2	2	43	46	45	41	**175**	**1.00**
4741	**NEFM**	*Neurofilament, medium polypeptide*			34	38	49	52	**173**	**1.00**
56704	**JPH1**	*Junctophilin 1*	3		38	41	40	35	**154**	**1.00**
4430	**MYO1B**	*Myosin IB*	7	6	39	39	40	36	**154**	**1.00**
3151	**HMGN2**	*High mobility group nucleosomal binding domain 2*			43	37	38	34	**152**	**1.00**
1917	**EEF1A2**	*Eukaryotic translation elongation factor 1 alpha 2*	8	7	35	37	37	35	**144**	**1.00**
25921	**ZDHHC5**	*Zinc finger DHHC-type containing 5*			33	33	36	35	**137**	**1.00**
2011	**MARK2**	*Microtubule affinity regulating kinase 2*	3		33	31	33	30	**127**	**1.00**
6709	**SPTAN1**	*Spectrin alpha, non-erythrocytic 1*	6	5	28	25	32	32	**117**	**1.00**
57216	**VANGL2**	*VANGL planar cell polarity protein 2*			28	28	26	24	**106**	**1.00**
9448	**MAP4K4**	*Mitogen-activated protein kinase kinase kinase kinase 4*			30	27	26	22	**105**	**1.00**
5064	**PALM**	*Paralemmin*	8	5	29	23	25	26	**103**	**1.00**
10458	**BAIAP2**	*BAI1 associated protein 2*	6	4	27	25	25	20	**97**	**1.00**
55971	**BAIAP2L1**	*BAI1 associated protein 2 like 1*	4	4	21	22	26	27	**96**	**1.00**
8496	**PPFIBP1**	*PPFIA binding protein 1*	2		22	25	24	24	**95**	**1.00**
4140	**MARK3**	*Microtubule affinity regulating kinase 3*	5		24	24	21	22	**91**	**0.98**
11180	**WDR6**	*WD repeat domain 6*	5	2	21	26	21	21	**89**	**1.00**
291	**SLC25A4**	*Solute carrier family 25 member 4*	6	4	15	25	24	24	**88**	**0.96**
57669	**EPB41L5**	*Erythrocyte membrane protein band 4.1 like 5*	4	3	22	25	21	19	**87**	**1.00**
8773	**SNAP23**	*Synaptosome associated protein 23kda*	7	7	21	22	22	22	**87**	**0.97**
23176	**SEPT8**	*Septin 8*	4	3	22	20	20	19	**81**	**1.00**

Gene ID	Gene Name	Full name	Top 2 controls		FAT4 BioID (QEHF dataset) pool A tech#1	pool A tech #2	pool B tech #1	pool B tech #2	Total	SAINT
2318	**FLNC**	*Filamin C*			20	20	17	21	**78**	**1.00**
9231	**DLG5**	*Discs large homolog 5*			17	18	18	23	**76**	**1.00**
79834	**PEAK1**	*Pseudopodium enriched atypical kinase 1*	6	5	18	17	23	17	**75**	**0.95**
9712	**USP6NL**	*USP6 N-terminal like*			19	20	20	15	**74**	**1.00**
4747	**NEFL**	*Neurofilament, light polypeptide*			18	17	18	18	**71**	**1.00**
6520	**SLC3A2**	*Solute carrier family 3 member 2*			18	17	17	16	**68**	**1.00**
3315	**HSPB1**	*Heat shock protein family B (small) member 1*			16	17	16	15	**64**	**1.00**
4853	**NOTCH2**	*Notch 2*	3		15	19	16	14	**64**	**0.99**
54477	**PLEKHA5**	*Pleckstrin homology domain containing A5*	4	4	15	13	17	18	**63**	**0.97**
128077	**LIX1L**	*Limb and CNS expressed 1 like*			13	15	18	16	**62**	**1.00**
57498	**KIDINS220**	*Kinase D-interacting substrate 220kda*			16	15	15	15	**61**	**1.00**
51599	**LSR**	*Lipolysis stimulated lipoprotein receptor*	2		16	18	14	13	**61**	**1.00**
26003	**GORASP2**	*Golgi reassembly stacking protein 2*	4	3	16	15	15	13	**59**	**0.99**
1837	**DTNA**	*Dystrobrevin alpha*	4	3	15	14	16	12	**57**	**0.98**
26050	**SLITRK5**	*SLIT and NTRK like family member 5*			19	13	13	11	**56**	**1.00**
6645	**SNTB2**	*Syntrophin beta 2*	5	3	13	16	14	13	**56**	**0.94**
4771	**NF2**	*Neurofibromin 2 (merlin)*	2		12	15	14	11	**52**	**1.00**
143098	**MPP7**	*Membrane protein, palmitoylated 7*	2		9	13	14	15	**51**	**0.99**
57648	**KIAA1522**	*Kiaa1522*			13	12	12	13	**50**	**1.00**
3418	**IDH2**	*Isocitrate dehydrogenase 2 (NADP+), mitochondrial*			11	9	16	13	**49**	**1.00**
54862	**CC2D1A**	*Coiled-coil and C2 domain containing 1A*	4	3	13	10	12	14	**49**	**0.85**
1824	**DSC2**	*Desmocollin 2*			9	10	13	12	**44**	**1.00**
165215	**FAM171B**	*Family with sequence similarity 171 member B*			12	13	11	8	**44**	**1.00**
1525	**CXADR**	*Coxsackie virus and adenovirus receptor*			9	8	14	12	**43**	**1.00**
728689	**EIF3CL**	*Eukaryotic translation initiation factor 3 subunit C-like*			11	12	11	9	**43**	**1.00**
55240	**STEAP3**	*STEAP3 metalloreductase*			13	10	10	10	**43**	**1.00**
26092	**TOR1AIP1**	*Torsin 1A interacting protein 1*	2		11	9	13	10	**43**	**0.99**
7205	**TRIP6**	*Thyroid hormone receptor interactor 6*	3		13	11	7	12	**43**	**0.89**
5819	**PVRL2**	*Nectin cell adhesion molecule 2*			9	10	11	12	**42**	**1.00**
151011	**SEPT10**	*Septin 10*			8	12	10	11	**41**	**1.00**
9524	**TECR**	*Trans-2,3-enoyl-coa reductase*	2		9	9	11	11	**40**	**0.98**
55299	**BRIX1**	*BRX1, biogenesis of ribosomes*	2	2	8	10	13	9	**40**	**0.96**
493	**ATP2B4**	*Atpase plasma membrane Ca2+ transporting 4*			9	9	10	11	**39**	**1.00**
11188	**NISCH**	*Nischarin*			11	9	12	7	**39**	**1.00**
5784	**PTPN14**	*Protein tyrosine phosphatase, non-receptor type 14*			12	10	6	11	**39**	**1.00**
10890	**RAB10**	*RAB10, member RAS oncogene family*			9	11	9	10	**39**	**1.00**
6811	**STX5**	*Syntaxin 5*	3		11	9	9	10	**39**	**0.89**
50488	**MINK1**	*Misshapen-like kinase 1*			11	8	8	11	**38**	**1.00**
25945	**PVRL3**	*Nectin cell adhesion molecule 3*			8	8	12	10	**38**	**1.00**
7157	**TP53**	*Tumor protein p53*	3		10	9	8	11	**38**	**0.87**
100505818	**LOC100505818**	*Entry replaced with MLLT4*			8	5	12	12	**37**	**1.00**

Gene ID	Gene Name	Full name	Top 2 controls	FAT4 BioID (QEHF dataset) pool A tech#1	pool A tech #2	pool B tech #1	pool B tech #2	Total	SAINT
8572	**PDLIM4**	*PDZ and LIM domain 4*		10	7	9	11	**37**	**1.00**
1956	**EGFR**	*Epidermal growth factor receptor*		8	6	12	10	**36**	**1.00**
55227	**LRRC1**	*Leucine rich repeat containing 1*		9	9	9	9	**36**	**1.00**
6558	**SLC12A2**	*Solute carrier family 12 member 2*		9	9	10	7	**35**	**1.00**
1499	**CTNNB1**	*Catenin beta 1*	2	8	9	9	9	**35**	**0.96**
3996	**LLGL1**	*Lethal giant larvae homolog 1, scribble cell polarity complex component*	2 2	9	6	9	11	**35**	**0.85**
8727	**CTNNAL1**	*Catenin alpha like 1*		7	9	6	11	**33**	**1.00**
10938	**EHD1**	*EH domain containing 1*		9	8	7	9	**33**	**1.00**
100506658	**OCLN**	*Occludin*	2	9	8	7	9	**33**	**0.95**
8500	**PPFIA1**	*PTPRF interacting protein alpha 1*		9	10	5	8	**32**	**1.00**
9462	**RASAL2**	*RAS protein activator like 2*		6	8	11	7	**32**	**1.00**
324	**APC**	*Adenomatous polyposis coli*		8	5	8	10	**31**	**1.00**
5296	**PIK3R2**	*Phosphoinositide-3-kinase regulatory subunit 2*		8	9	7	7	**31**	**1.00**
8502	**PKP4**	*Plakophilin 4*		6	6	12	7	**31**	**1.00**
83461	**CDCA3**	*Cell division cycle associated 3*		6	8	8	8	**30**	**1.00**
5413	**SEPT5**	*Septin 5*		9	9	6	6	**30**	**1.00**
5831	**PYCR1**	*Pyrroline-5-carboxylate reductase 1*		10	7	6	6	**29**	**1.00**
11021	**RAB35**	*RAB35, member RAS oncogene family*		8	6	9	6	**29**	**1.00**
115	**ADCY9**	*Adenylate cyclase 9*		9	4	7	8	**28**	**1.00**
219	**ALDH1B1**	*Aldehyde dehydrogenase 1 family member B1*		6	8	8	5	**27**	**1.00**
23580	**CDC42EP4**	*CDC42 effector protein 4*		7	6	6	7	**26**	**1.00**
284069	**FAM171A2**	*Family with sequence similarity 171 member A2*		7	6	7	6	**26**	**1.00**
5757	**PTMA**	*Prothymosin, alpha*		6	8	5	7	**26**	**1.00**
10497	**UNC13B**	*Unc-13 homolog B (C. Elegans)*		6	7	6	6	**25**	**1.00**
10945	**KDELR1**	*KDEL endoplasmic reticulum protein retention receptor 1*	2	7	6	6	6	**25**	**0.84**
285513	**GPRIN3**	*GPRIN family member 3*		5	5	7	7	**24**	**1.00**
2932	**GSK3B**	*Glycogen synthase kinase 3 beta*		8	6	3	7	**24**	**1.00**
54407	**SLC38A2**	*Solute carrier family 38 member 2*		5	6	6	7	**24**	**1.00**
55627	**SMPD4**	*Sphingomyelin phosphodiesterase 4*		8	6	3	7	**24**	**1.00**
23266	**LPHN2**	*Adhesion G protein-coupled receptor L2*		6	4	7	6	**23**	**1.00**
55824	**PAG1**	*Phosphoprotein membrane anchor with glycosphingolipid microdomains 1*		6	5	5	7	**23**	**1.00**
23362	**PSD3**	*Pleckstrin and Sec7 domain containing 3*		5	6	5	7	**23**	**1.00**
8140	**SLC7A5**	*Solute carrier family 7 member 5*		5	6	6	6	**23**	**1.00**
57224	**NHSL1**	*NHS like 1*		6	5	6	5	**22**	**1.00**
23007	**PLCH1**	*Phospholipase C eta 1*		5	6	6	5	**22**	**1.00**
5906	**RAP1A**	*RAP1A, member of RAS oncogene family*		4	5	8	5	**22**	**1.00**
10550	**ARL6IP5**	*ADP ribosylation factor like gtpase 6 interacting protein 5*		5	6	5	5	**21**	**1.00**
29801	**ZDHHC8**	*Zinc finger DHHC-type containing 8*		3	4	8	6	**21**	**1.00**
9722	**NOS1AP**	*Nitric oxide synthase 1 adaptor protein*		6	6	3	5	**20**	**1.00**
5295	**PIK3R1**	*Phosphoinositide-3-kinase regulatory subunit 1*		5	5	7	3	**20**	**1.00**
54901	**CDKAL1**	*CDK5 regulatory subunit associated protein 1*		4	6	3	6	**19**	**1.00**

Gene ID	Gene Name	Full name	Top 2 controls	FAT4 BioID (QEHF dataset) pool A tech#1	pool A tech #2	pool B tech #1	pool B tech #2	Total	SAINT
		like 1							
23197	**FAF2**	*Fas associated factor family member 2*		4	4	6	5	**19**	**1.00**
4942	**OAT**	*Ornithine aminotransferase*		5	6	5	3	**19**	**1.00**
9545	**RAB3D**	*RAB3D, member RAS oncogene family*		4	5	5	5	**19**	**1.00**
55964	**SEPT3**	*Septin 3*		3	6	4	6	**19**	**1.00**
8777	**MPDZ**	*Multiple PDZ domain crumbs cell polarity complex component*		7	6	2	4	**19**	**0.98**
308	**ANXA5**	*Annexin A5*		3	4	6	5	**18**	**1.00**
4162	**MCAM**	*Melanoma cell adhesion molecule*		3	4	6	5	**18**	**1.00**
54892	**NCAPG2**	*Non-SMC condensin II complex subunit G2*		5	3	5	5	**18**	**1.00**
5099	**PCDH7**	*Protocadherin 7*		4	6	3	5	**18**	**1.00**
6535	**SLC6A8**	*Solute carrier family 6 member 8*		4	6	5	3	**18**	**1.00**
85461	**TANC1**	*Tetratricopeptide repeat, ankyrin repeat and coiled-coil containing 1*		3	5	6	4	**18**	**1.00**
83660	**TLN2**	*Talin 2*		3	5	5	4	**17**	**1.00**
9372	**ZFYVE9**	*Zinc finger FYVE-type containing 9*		4	4	4	5	**17**	**1.00**
6814	**STXBP3**	*Syntaxin binding protein 3*		6	3	5	3	**17**	**0.99**
11078	**TRIOBP**	*TRIO and F-actin binding protein*		4	7	3	3	**17**	**0.99**
8495	**PPFIBP2**	*PPFIA binding protein 2*		6	4	5	2	**17**	**0.98**
83858	**ATAD3B**	*Atpase family, AAA domain containing 3B*		4	4	5	3	**16**	**1.00**
10632	**ATP5L**	*ATP synthase, H+ transporting, mitochondrial Fo complex subunit G*		4	4	4	4	**16**	**1.00**
55092	**TMEM51**	*Transmembrane protein 51*		3	4	4	5	**16**	**1.00**
8476	**CDC42BPA**	*CDC42 binding protein kinase alpha*		2	4	5	5	**16**	**0.98**
201595	**STT3B**	*STT3B, catalytic subunit of the oligosaccharyltransferase complex*		4	5	2	5	**16**	**0.98**
11135	**CDC42EP1**	*CDC42 effector protein 1*		4	3	4	4	**15**	**1.00**
10818	**FRS2**	*Fibroblast growth factor receptor substrate 2*		4	3	4	4	**15**	**1.00**
9500	**MAGED1**	*MAGE family member D1*		4	5	3	3	**15**	**0.99**
23310	**NCAPD3**	*Non-SMC condensin II complex subunit D3*		3	5	4	3	**15**	**0.99**
29920	**PYCR2**	*Pyrroline-5-carboxylate reductase family member 2*		3	3	5	4	**15**	**0.99**
7083	**TK1**	*Thymidine kinase 1, soluble*		3	5	4	3	**15**	**0.99**
515	**ATP5F1**	*ATP synthase, H+ transporting, mitochondrial Fo complex subunit B1*		4	2	4	5	**15**	**0.98**
65108	**MARCKSL1**	*MARCKS-like 1*		2	5	4	4	**15**	**0.98**
552900	**BOLA2**	*Bola family member 2*		4	4	3	3	**14**	**0.99**
4267	**CD99**	*CD99 molecule*		3	3	3	5	**14**	**0.99**
6431	**SRSF6**	*Serine/arginine-rich splicing factor 6*		3	3	3	5	**14**	**0.99**
65082	**VPS33A**	*VPS33A, CORVET/HOPS core subunit*		3	4	4	3	**14**	**0.99**
9213	**XPR1**	*Xenotropic and polytropic retrovirus receptor 1*		3	3	4	4	**14**	**0.99**
8125	**ANP32A**	*Acidic nuclear phosphoprotein 32 family member A*		4	3	3	3	**13**	**0.99**
9578	**CDC42BPB**	*CDC42 binding protein kinase beta*		3	3	3	4	**13**	**0.99**
10207	**INADL**	*PATJ, crumbs cell polarity complex component*		4	3	3	3	**13**	**0.99**
4810	**NHS**	*NHS actin remodeling regulator*		3	4	3	3	**13**	**0.99**
1967	**EIF2B1**	*Eukaryotic translation initiation factor 2B subunit alpha*		3	3	5	2	**13**	**0.98**

Gene ID	Gene Name	Full name	Top 2 controls	FAT4 BioID (QEHF dataset)					
				pool A		pool B			
				tech#1	tech #2	tech #1	tech #2	Total	SAINT
10723	**SLC12A7**	*Solute carrier family 12 member 7*		2	3	4	4	**13**	**0.98**
10250	**SRRM1**	*Serine and arginine repetitive matrix 1*		4	4	3	2	**13**	**0.98**
10478	**SLC25A17**	*Solute carrier family 25 member 17*		2	2	4	5	**13**	**0.97**
51067	**YARS2**	*Tyrosyl-trna synthetase 2*		4	2	2	5	**13**	**0.97**
55243	**KIRREL**	*Kin of IRRE like (Drosophila)*		3	3	3	3	**12**	**0.99**
5442	**POLRMT**	*Polymerase (RNA) mitochondrial*		3	3	3	3	**12**	**0.99**
9495	**AKAP5**	*A-kinase anchoring protein 5*		2	3	4	3	**12**	**0.98**
55610	**CCDC132**	*VPS50, EARP/GARPII complex subunit*		3	2	4	3	**12**	**0.98**
1947	**EFNB1**	*Ephrin-B1*		2	3	4	3	**12**	**0.98**
9312	**KCNB2**	*Potassium voltage-gated channel subfamily B member 2*		2	3	4	3	**12**	**0.98**
55614	**KIF16B**	*Kinesin family member 16B*		3	2	3	4	**12**	**0.98**
5297	**PI4KA**	*Phosphatidylinositol 4-kinase alpha*		2	4	3	3	**12**	**0.98**
9185	**REPS2**	*RALBP1 associated Eps domain containing 2*		4	3	2	3	**12**	**0.98**
145567	**TTC7B**	*Tetratricopeptide repeat domain 7B*		3	4	2	3	**12**	**0.98**
2182	**ACSL4**	*Acyl-coa synthetase long-chain family member 4*		2	5	2	3	**12**	**0.97**
84902	**CEP89**	*Centrosomal protein 89kda*		4	4	2	2	**12**	**0.97**
653583	**PHLDB3**	*Pleckstrin homology like domain family B member 3*		2	3	2	5	**12**	**0.97**
10211	**FLOT1**	*Flotillin 1*		3	3	3	2	**11**	**0.98**
4697	**NDUFA4**	*NDUFA4, mitochondrial complex associated*		3	3	3	2	**11**	**0.98**
23478	**SEC11A**	*SEC11 homolog A, signal peptidase complex subunit*		2	2	4	3	**11**	**0.97**
55676	**SLC30A6**	*Solute carrier family 30 member 6*		2	3	4	2	**11**	**0.97**
81539	**SLC38A1**	*Solute carrier family 38 member 1*		2	2	4	3	**11**	**0.97**
57181	**SLC39A10**	*Solute carrier family 39 member 10*		2	4	3	2	**11**	**0.97**
6813	**STXBP2**	*Syntaxin binding protein 2*		2	2	3	4	**11**	**0.97**
94121	**SYTL4**	*Synaptotagmin like 4*		2	2	4	3	**11**	**0.97**
2271	**FH**	*Fumarate hydratase*		2	2	5	2	**11**	**0.95**
400793	**C1orf226**	*Chromosome 1 open reading frame 226*		2	3	2	3	**10**	**0.96**
79143	**MBOAT7**	*Membrane bound O-acyltransferase domain containing 7*		3	3	2	2	**10**	**0.96**
94005	**PIGS**	*Phosphatidylinositol glycan anchor biosynthesis class S*		3	2	3	2	**10**	**0.96**
6548	**SLC9A1**	*Solute carrier family 9 member A1*		3	2	2	3	**10**	**0.96**
84928	**TMEM209**	*Transmembrane protein 209*		2	2	3	3	**10**	**0.96**
7386	**UQCRFS1**	*Ubiquinol-cytochrome c reductase, Rieske iron-sulfur polypeptide 1*		2	2	3	3	**10**	**0.96**
1186	**CLCN7**	*Chloride voltage-gated channel 7*		2	2	2	4	**10**	**0.95**
2064	**ERBB2**	*Erb-b2 receptor tyrosine kinase 2*		2	3	2	2	**9**	**0.95**
373156	**GSTK1**	*Glutathione S-transferase kappa 1*		2	2	3	2	**9**	**0.95**
346689	**KLRG2**	*Killer cell lectin like receptor G2*		2	3	2	2	**9**	**0.95**
10206	**TRIM13**	*Tripartite motif containing 13*		3	2	2	2	**9**	**0.95**
706	**TSPO**	*Translocator protein*		2	3	2	2	**9**	**0.95**
29914	**UBIAD1**	*Ubia prenyltransferase domain containing 1*		3	2	2	2	**9**	**0.95**
10897	**YIF1A**	*Yip1 interacting factor homolog A, membrane trafficking protein*		2	2	2	3	**9**	**0.95**
1347	**COX7A2**	*Cytochrome c oxidase subunit 7A2*		2	2	2	2	**8**	**0.94**

Gene ID	Gene Name	Full name	Top 2 controls	FAT4 BioID (QEHF dataset)					
				pool A		pool B			
				tech#1	tech #2	tech #1	tech #2	Total	SAINT
8892	**EIF2B2**	*Eukaryotic translation initiation factor 2B subunit beta*		2	2	2	2	**8**	**0.94**
51170	**HSD17B11**	*Hydroxysteroid (17-beta) dehydrogenase 11*		2	2	2	2	**8**	**0.94**
55190	**NUDT11**	*Nudix hydrolase 11*		2	2	2	2	**8**	**0.94**
10166	**SLC25A15**	*Solute carrier family 25 member 15*		2	2	2	2	**8**	**0.94**

Table 13.2 FAT4 and Cdh1 BioID (Velos) HEK293 cells

Full list of hits. MB = membrane baits; indicates the number of BioID runs that showed significant enrichment of a prey. 7 unrelated transmembrane baits were used for this comparison, each analyzed under cycling and starved conditions (= 14 MB total)

								FAT4 BioID Cycling						FAT4 BioID Starved						ECAD BioID Cycling						ECAD BioID Starved					
Gene ID	Gene Name	Full name	MB	Top 4 controls				A#1	A#2	B#1	B#2	Total	SAINT	A#1	A#2	B#1	B#2	Total	SAINT	A#1	A#2	B#1	B#2	Total	SAINT	A#1	A#2	B#1	B#2	Total	SAINT
948469	birA	*E.Coli biotin ligase*		6178	3390	3260	3094	595	656	626	624	**2501**	**NA**	574	614	612	604	**2404**	**NA**	941	956	885	904	**3686**	**NA**	777	776	714	733	**3000**	**NA**
999	CDH1	*Cadherin 1*																		65	63	68	68	**264**	**NA**	64	60	63	66	**253**	**NA**
79633	FAT4	*FAT atypical cadherin 4*						1173	1380	1108	1415	**5076**	**NA**	1120	949	1385	1006	**4460**	**NA**												
4301	MLLT4	*Myeloid/lymphoid or mixed-lineage leukemia; translocated to, 4*		42	34	33	32	166	202	155	213	**736**	**1.00**	228	203	299	209	**939**	**1.00**	391	373	394	380	**1538**	**1.00**	426	414	406	425	**1671**	**1.00**
667	DST	*Dystonin*	**1**	6	5	3	3	83	101	75	127	**386**	**1.00**	59	52	96	75	**282**	**1.00**	15	14	14	16	**59**	**0.97**	6	10	5	5	**26**	
8471	IRS4	*Insulin receptor substrate 4*	**3**	27	25	20	19	81	122	80	88	**371**	**1.00**	54	36	69	55	**214**		142	136	139	147	**564**	**1.00**	39	37	39	33	**148**	
55914	ERBB2IP	*Erbb2 interacting protein*	**1**	11	4	4	4	80	95	75	97	**347**	**1.00**	90	83	118	92	**383**	**1.00**	141	127	131	137	**536**	**1.00**	174	169	176	168	**687**	**1.00**
23344	ESYT1	*Extended synaptotagmin protein 1*	**8**	10	8	8	6	46	46	42	51	**185**	**1.00**	64	56	75	61	**256**	**1.00**	41	42	44	43	**170**	**1.00**	40	33	35	33	**141**	**1.00**
23513	SCRIB	*Scribbled planar cell polarity protein*	**2**					40	52	39	45	**176**	**1.00**	75	56	112	74	**317**	**1.00**	79	78	89	95	**341**	**1.00**	85	71	85	74	**315**	**1.00**
7402	UTRN	*Utrophin*	**1**	15	11	9	8	36	37	37	37	**147**	**1.00**	50	44	93	69	**256**	**1.00**	25	13	17	10	**65**		24	14	15	14	**67**	
1969	EPHA2	*EPH receptor A2*	**3**	4	4	3	2	35	37	22	41	**135**	**1.00**	48	29	62	31	**170**	**1.00**	53	56	53	44	**206**	**1.00**	60	60	53	58	**231**	**1.00**
1829	DSG2	*Desmoglein 2*	**3**	4				30	34	24	38	**126**	**1.00**	45	48	73	45	**211**	**1.00**	93	99	90	80	**362**	**1.00**	70	70	75	75	**290**	**1.00**
3728	JUP	*Junction plakoglobin*	**2**	5	4			27	35	23	37	**122**	**1.00**	32	21	30	32	**115**	**1.00**	177	160	177	177	**691**	**1.00**	163	144	172	164	**643**	**1.00**
6749	SSRP1	*Structure specific recognition protein 1*		5	3			32	24	20	28	**104**	**1.00**																		
11198	SUPT16H	*SPT16 homolog, facilitates chromatin remodeling subunit*		6	5			22	31	17	27	**97**	**0.99**																		
1739	DLG1	*Discs large homolog 1, scribble cell polarity complex component*	**2**					17	23	15	29	**84**	**1.00**	49	40	71	56	**216**	**1.00**	56	71	64	51	**242**	**1.00**	63	72	59	68	**262**	**1.00**
81839	VANGL1	*VANGL planar cell polarity protein 1*	**5**					19	22	18	24	**83**	**1.00**	16	20	34	16	**86**	**1.00**	55	55	62	61	**233**	**1.00**	44	37	47	43	**171**	**1.00**
26999	CYFIP2	*Cytoplasmic FMR1 interacting protein 2*		4	4			23	21	18	16	**78**	**1.00**	54	43	52	47	**196**	**1.00**		22	22	23	**67**		22	18	19	16	**75**	**0.99**
5783	PTPN13	*Protein tyrosine phosphatase, non-receptor type 13*	**1**	3				20	20	19	15	**74**	**1.00**	6	7	13	11	**37**	**0.95**	10	9	10	9	**38**	**0.98**						
8650	NUMB	*Numb homolog (Drosophila)*	**2**					12	29	9	21	**71**	**1.00**	13	11	35	11	**70**	**1.00**	51	43	59	50	**203**	**1.00**	39	41	37	34	**151**	**1.00**
7155	TOP2B	*Topoisomerase (DNA) II beta*		5	4	4		23	20	9	18	**70**	**0.85**																		
288	ANK3	*Ankyrin 3, node of Ranvier (ankyrin G)*	**1**					13	9	17	17	**56**	**1.00**	53	35	53	46	**187**	**1.00**	113	106	110	111	**440**	**1.00**	133	115	132	135	**515**	**1.00**
10652	YKT6	*YKT6 v-SNARE homolog (S. Cerevisiae)*	**8**	5	4			19	10	11	11	**51**	**0.89**	12	9	16	14	**51**	**0.90**	35	33	39	36	**143**	**1.00**	43	42	41	39	**165**	**1.00**
9253	NUMBL	*Numb homolog (Drosophila)-like*		3				6	20	3	22	**51**	**0.88**	12	6	14		**32**		41	35	38	41	**155**	**1.00**	25	22	22	22	**91**	**1.00**
2011	MARK2	*Microtubule affinity regulating kinase 2*	**2**					12	13	8	11	**44**	**1.00**	6	7	9	5	**27**	**1.00**	72	68	57	71	**268**	**1.00**	44	49	43	45	**181**	**1.00**
65979	PHACTR4	*Phosphatase and actin regulator 4*	**2**	2				9	9	7	9	**34**	**0.99**	22	18	26	21	**87**	**1.00**	17	14	13	24	**68**	**1.00**	27	36	35	24	**122**	**1.00**
4430	MYO1B	*Myosin IB*		2				3	9	12	10	**34**	**0.93**	8	11	12	18	**49**	**1.00**	17	8	16	15	**56**	**1.00**	6	5	5	9	**25**	**0.96**
10787	NCKAP1	*NCK associated protein 1*	**1**	2				7	8	8	9	**32**	**0.99**	54	39	48	37	**178**	**1.00**	9	6	11	11	**37**	**0.99**	13	13	13	9	**48**	**1.00**
6817	SULT1A1	*Sulfotransferase family 1A member 1*		4	3			7	9	8	7	**31**	**0.79**																		
64746	ACBD3	*Acyl-coa binding domain containing 3*	**4**	4	2			10	6	7	7	**30**	**0.81**	4		6	4	**14**		51	51	51	55	**208**	**1.00**	48	54	37	44	**183**	**1.00**
55971	BAIAP2L1	*BAI1 associated protein 2 like 1*	**2**					5	10	6	8	**29**	**1.00**	16	9	16	6	**47**	**1.00**		2		2	**4**							
4140	MARK3	*Microtubule affinity regulating kinase 3*	**2**					7	7	5	9	**28**	**1.00**	6	4	8	3	**21**	**1.00**	44	37	41	43	**165**	**1.00**	30	35	32	34	**131**	**1.00**
57216	VANGL2	*VANGL planar cell polarity protein 2*	**3**					3	6	9	9	**27**	**1.00**	8	12	21	12	**53**	**1.00**	31	27	24	27	**109**	**1.00**	15	8	18	10	**51**	**1.00**
5211	PFKL	*Phosphofructokinase, liver type*		3				9	3	8	6	**26**	**0.86**	3	9	5	9	**26**	**0.85**												
9231	DLG5	*Discs large homolog 5*						3	7	5	6	**21**	**1.00**	2	3	10	2	**17**	**0.98**	2	2	2	5	**11**	**0.97**						
284695	ZNF326	*Zinc finger protein 326*		4				5	7	4	5	**21**	**0.76**																		
84902	CEP89	*Centrosomal protein 89kda*						9	4	5	2	**20**	**0.99**	3	6	5	8	**22**	**1.00**	6	4			**10**							
6748	SSR4	*Signal sequence receptor, delta*						5	6	4	4	**19**	**1.00**	13	11	9	9	**42**	**1.00**										2	**2**	

Gene ID	Gene Name	Full name	MB	Top 4 controls				FAT4 BioID Cycling						FAT4 BioID Starved						ECAD BioID Cycling						ECAD BioID Starved					
								A#1	A#2	B#1	B#2	Total	SAINT	A#1	A#2	B#1	B#2	Total	SAINT	A#1	A#2	B#1	B#2	Total	SAINT	A#1	A#2	B#1	B#2	Total	SAINT
128077	**LIX1L**	*Limb and CNS expressed 1 like*						6	7	2	4	**19**	**0.99**	7	6	6	7	**26**	**1.00**												
57488	**ESYT2**	*Extended synaptotagmin protein 2*	***2***					4	4	6	3	**17**	**1.00**	14	13	11	14	**52**	**1.00**	4	6	7	5	**22**	**1.00**	4	5	2		**11**	
2319	**FLOT2**	*Flotillin 2*	***2***					4	5	4	3	**16**	**1.00**	11	6	10	4	**31**	**1.00**	31	31	32	30	**124**	**1.00**	22	21	18	24	**85**	**1.00**
100506658	**OCLN**	*Occludin*	***3***					3	2	5	6	**16**	**0.99**			3		**3**		18	17	12	15	**62**	**1.00**	13	17	19	16	**65**	**1.00**
9631	**NUP155**	*Nucleoporin 155kda*	***3***					2	6	5	2	**15**	**0.98**			2	2	**4**		10	4	4	7	**25**	**1.00**	4	3	4	6	**17**	**1.00**
65992	**DDRGK1**	*DDRGK domain containing 1*	***4***					2	2	2	2	**8**	**0.95**			4		**4**		5			3	**8**		4			4	**8**	
2037	**EPB41L2**	*Erythrocyte membrane protein band 4.1-like 2*		39	39	34	32	86	114	63	99	**362**		109	90	161	105	**465**	**0.76**	157	169	174	178	**678**	**1.00**	153	158	149	155	**615**	**1.00**
26064	**RAI14**	*Retinoic acid induced 14*	***1***	16	12	10	9	31	48	21	53	**153**		73	42	91	46	**252**	**1.00**	35	35	34	29	**133**	**0.77**	30	28	23	23	**104**	
23191	**CYFIP1**	*Cytoplasmic FMR1 interacting protein 1*	***1***	12				22		16	16	**54**		51	35	48	38	**172**	**0.99**	21	22		25	**68**		20		19		**39**	
120	**ADD3**	*Adducin 3*	***2***	7	7	6	5	14	18	13	28	**73**		39	30	51	44	**164**	**1.00**	48	46	45	44	**183**	**1.00**	30	31	29	25	**115**	**1.00**
118	**ADD1**	*Adducin 1*		11	8	6	6	21	25	10	31	**87**		34	26	39	27	**126**	**1.00**	57	58	58	58	**231**	**1.00**	35	36	30	36	**137**	**1.00**
92140	**MTDH**	*Metadherin*	***4***	10	5	4	3	4	5	5	4	**18**		15	19	33	18	**85**	**0.78**	8	8	5		**21**		19	13	11	14	**57**	
114787	**GPRIN1**	*G protein regulated inducer of neurite outgrowth 1*		7				4	7	5	9	**25**		17	12	41	11	**81**	**0.94**	20	23	19	31	**93**	**0.98**	35	38	31	34	**138**	**1.00**
9217	**VAPB**	*VAMP (vesicle-associated membrane protein)-associated protein B and C*	***4***	6	6	4	3	6	9	4	3	**22**		14	17	28	16	**75**	**0.94**	28	32	29	30	**119**	**1.00**	47	45	49	40	**181**	**1.00**
1207	**CLNS1A**	*Chloride nucleotide-sensitive channel 1A*	***2***	5	4	4	3	13	16	10	12	**51**		14	14	21	13	**62**	**0.97**	31	23	30	24	**108**	**1.00**	20	22	16	17	**75**	**1.00**
23176	**SEPT8**	*Septin 8*												18	14	17	10	**59**	**1.00**	22	21	26	28	**97**	**1.00**	21	21	12	16	**70**	**1.00**
2036	**EPB41L1**	*Erythrocyte membrane protein band 4.1-like 1*	***2***								13	**13**		15		24	16	**55**	**0.75**	16		24	23	**63**	**0.75**	25	22	23	24	**94**	**1.00**
5770	**PTPN1**	*Protein tyrosine phosphatase, non-receptor type 1*	***8***	4				6	8	3	3	**20**		11	14	15	12	**52**	**0.98**	18	21	13	20	**72**	**0.99**	23	27	27	26	**103**	**1.00**
6867	**TACC1**	*Transforming acidic coiled-coil containing protein 1*		4	2			2	5	3	8	**18**		14	10	17	11	**52**	**0.98**		3	3	2	**8**		7	5	7		**19**	
23592	**LEMD3**	*LEM domain containing 3*	***7***	4	4			4	10	4	6	**24**		12	12	17	11	**52**	**0.95**	77	66	78	66	**287**	**1.00**	72	49	56	56	**233**	**1.00**
10423	**CDIPT**	*CDP-diacylglycerol--inositol 3-phosphatidyltransferase*						3		8	6	**17**		11	10	13	14	**48**	**1.00**							7	6		7	**20**	
10970	**CKAP4**	*Cytoskeleton-associated protein 4*	***13***	4	4	3		6	3	6	8	**23**		12	11	10	15	**48**	**0.97**	6	9	8	2	**25**		17	24	16	20	**77**	**1.00**
1891	**ECH1**	*Enoyl-coa hydratase 1, peroxisomal*	***1***	2				3	6	3		**12**		13	7	13	10	**43**	**1.00**												
3996	**LLGL1**	*Lethal giant larvae homolog 1, scribble cell polarity complex component*	***1***							3	4	**7**		9	10	14	9	**42**	**1.00**	11	10	9	12	**42**	**1.00**	8	8	8	8	**32**	**1.00**
114882	**OSBPL8**	*Oxysterol binding protein like 8*	***6***					3		3	3	**9**		10	10	13	9	**42**	**1.00**	5		2		**7**		10	13	11	11	**45**	**1.00**
1500	**CTNND1**	*Catenin delta 1*	***4***	3						3		**3**		6	6	17	7	**36**	**0.93**	264	248	250	241	**1003**	**1.00**	326	339	326	345	**1336**	**1.00**
6786	**STIM1**	*Stromal interaction molecule 1*	***6***					4		5	6	**15**		13	7	8	7	**35**	**1.00**	3			3	**6**			5	5		**10**	
10006	**ABI1**	*Abl interactor 1*							3	3	3	**9**		10	8	7	8	**33**	**1.00**	6	6	4	7	**23**	**1.00**	6	7	14	10	**37**	**1.00**
6645	**SNTB2**	*Syntrophin beta 2*		3						3		**3**		7	8	10	7	**32**	**0.95**	4		4	4	**12**		3	3			**6**	
51144	**HSD17B12**	*Hydroxysteroid (17-beta) dehydrogenase 12*	***2***	3					4			**4**		7	4	10	11	**32**	**0.91**		4			**4**		5	6	5	4	**20**	**0.83**
259217	**HSPA12A**	*Heat shock protein family A (Hsp70) member 12A*	***2***											4	9	8	7	**28**	**1.00**												
51599	**LSR**	*Lipolysis stimulated lipoprotein receptor*	***4***											7	5	9	4	**25**	**1.00**				5	**5**		4	9		4	**17**	
6734	**SRPR**	*SRP receptor alpha subunit*	***11***	2				4		4		**8**		6	6	6	4	**22**	**0.94**	7	11	5	8	**31**	**0.98**	11	11	16	5	**43**	**0.98**
25959	**KANK2**	*KN motif and ankyrin repeat domains 2*							4	4		**8**		5	4	6	6	**21**	**1.00**												
4920	**ROR2**	*Receptor tyrosine kinase-like orphan receptor 2*	***3***											6	3	7	4	**20**	**1.00**	13	13	16	12	**54**	**1.00**	12	10	9	10	**41**	**1.00**
10458	**BAIAP2**	*BAI1 associated protein 2*									8	**8**		3	5	7	5	**20**	**1.00**				2	**2**							
5064	**PALM**	*Paralemmin*	***2***											5	3	7	4	**19**	**1.00**			6	6	**12**			5	4	5	**14**	
1525	**CXADR**	*Coxsackie virus and adenovirus receptor*	***4***											6	3	5	3	**17**	**1.00**												
1495	**CTNNA1**	*Catenin alpha 1*												2				**2**		749	720	723	721	**2913**	**1.00**	1034	1030	1141	1125	**4330**	**1.00**
1499	**CTNNB1**	*Catenin beta 1*																		407	385	369	355	**1516**	**1.00**	356	351	333	341	**1381**	**1.00**
2035	**EPB41**	*Erythrocyte membrane protein band 4.1*		49	41	34	32	60	84	39	79	**262**		102	59	149	80	**390**		163	158	157	162	**640**	**1.00**	152	151	141	147	**591**	**1.00**
58513	**EPS15L1**	*Epidermal growth factor receptor pathway substrate 15-like 1*		47	39	36	32	30	33	34	29	**126**		50	37	37	34	**158**		100	99	103	106	**408**	**1.00**	58	64	76	75	**273**	

Gene ID	Gene Name	Full name	MB	Top 4 controls				FAT4 BioID Cycling						FAT4 BioID Starved						ECAD BioID Cycling						ECAD BioID Starved					
								A#1	A#2	B#1	B#2	Total	SAINT	A#1	A#2	B#1	B#2	Total	SAINT	A#1	A#2	B#1	B#2	Total	SAINT	A#1	A#2	B#1	B#2	Total	SAINT
1496	**CTNNA2**	*Catenin alpha 2*																		89	86	95	89	**359**	**1.00**	119	117	133	133	**502**	**1.00**
144100	**PLEKHA7**	*Pleckstrin homology domain containing A7*																		85	80	70	78	**313**	**1.00**	78	70	70	82	**300**	**1.00**
54477	**PLEKHA5**	*Pleckstrin homology domain containing A5*	***2***						3			**3**								72	74	80	79	**305**	**1.00**	70	91	76	73	**310**	**1.00**
987	**LRBA**	*LPS responsive beige-like anchor protein*	***3***	20	19	17	16	3		3	3	**9**					2	**2**		66	66	74	77	**283**	**1.00**	59	54	40	48	**201**	
58533	**SNX6**	*Sorting nexin 6*																		62	63	68	71	**264**	**1.00**	53	57	56	51	**217**	**1.00**
9685	**CLINT1**	*Clathrin interactor 1*	***2***	23	22	21	11			3	2	**5**			6	5	5	**16**		66	65	65	68	**264**	**1.00**	47	58	54	62	**221**	
4735	**SEPT2**	*Septin 2*		21	19	17	15	23	26	18	32	**99**		42	33	46	34	**155**		63	57	60	64	**244**	**1.00**	46	54	52	53	**205**	**0.83**
54464	**XRN1**	*5'-3' exoribonuclease 1*		22	15	13	12	10	15	7	10	**42**		11	9	11	7	**38**		51	52	58	49	**210**	**1.00**	40	34	29	33	**136**	
9765	**ZFYVE16**	*Zinc finger FYVE-type containing 16*		8	7	5	4	7	8	12	14	**41**		8	4	9	10	**31**		47	46	56	54	**203**	**1.00**	27	26	32	31	**116**	**1.00**
6453	**ITSN1**	*Intersectin 1*		6	5	3	2		5	2	5	**12**		6	9	12	6	**33**		49	42	53	59	**203**	**1.00**	33	28	30	23	**114**	**1.00**
8301	**PICALM**	*Phosphatidylinositol binding clathrin assembly protein*																		56	52	49	43	**200**	**1.00**	37	43	37	49	**166**	**1.00**
989	**SEPT7**	*Septin 7*		22	14	8	8	20	25	16	24	**85**		31	26	40	20	**117**		45	47	53	52	**197**	**0.95**	37	33	27	30	**127**	
56829	**ZC3HAV1**	*Zinc finger CCCH-type containing, antiviral 1*	***2***	19	18	13	10	17	16	14	19	**66**		14	10	8	9	**41**		42	47	51	50	**190**	**1.00**	16	17	15	11	**59**	
7159	**TP53BP2**	*Tumor protein p53 binding protein 2*		7	2	2		2	4	2	2	**10**		4			3	**7**		41	47	47	48	**183**	**1.00**	37	35	31	32	**135**	**1.00**
23042	**PDXDC1**	*Pyridoxal-dependent decarboxylase domain containing 1*	***4***							3	3	**6**								41	40	48	50	**179**	**1.00**	21	20	24	14	**79**	**1.00**
6642	**SNX1**	*Sorting nexin 1*		15	15	13	9	5	7		8	**20**			6	5	4	**15**		44	43	43	43	**173**	**1.00**	28	25	29	26	**108**	
80223	**RAB11FIP1**	*RAB11 family interacting protein 1 (class I)*								4		**4**					5	**5**		41	44	50	34	**169**	**1.00**	31	26	30	27	**114**	**1.00**
317762	**CCDC85C**	*Coiled-coil domain containing 85C*																		33	40	51	45	**169**	**1.00**	31	31	29	28	**119**	**1.00**
55752	**SEPT11**	*Septin 11*		15	14	14	9	17	22	17	22	**78**		29	21	37	18	**105**		36	37	42	45	**160**	**0.98**	36	33	37	39	**145**	**0.79**
157680	**VPS13B**	*Vacuolar protein sorting 13 homolog B (yeast)*																		38	36	44	41	**159**	**1.00**	57	46	51	36	**190**	**1.00**
3267	**AGFG1**	*Arfgap with FG repeats 1*		4										5	3		6	**14**		32	40	39	42	**153**	**1.00**	31	27	29	39	**126**	**1.00**
7082	**TJP1**	*Tight junction protein 1*		14	11	4	4	2	3		3	**8**		8	8	7	7	**30**		36	36	43	37	**152**	**0.99**	37	39	37	30	**143**	**0.97**
163	**AP2B1**	*Adaptor related protein complex 2 beta 1 subunit*		7	7	6	6													29	27	39	51	**146**	**1.00**	37	28	24	27	**116**	**1.00**
8867	**SYNJ1**	*Synaptojanin 1*		4	3										4			**4**		36	34	38	30	**138**	**1.00**	31	25	28	31	**115**	**1.00**
54862	**CC2D1A**	*Coiled-coil and C2 domain containing 1A*																		33	32	40	32	**137**	**1.00**	28	33	32	32	**125**	**1.00**
160	**AP2A1**	*Adaptor related protein complex 2 alpha 1 subunit*		2																28	38	35	35	**136**	**1.00**	25	29	29	30	**113**	**1.00**
57584	**ARHGAP21**	*Rho gtpase activating protein 21*		3																30	29	30	30	**119**	**1.00**	32	31	29	28	**120**	**1.00**
161	**AP2A2**	*Adaptor related protein complex 2 alpha 2 subunit*																		27	29	26	37	**119**	**1.00**	24	27	32	28	**111**	**1.00**
64744	**SMAP2**	*Small arfgap2*	***2***																	30	28	31	27	**116**	**1.00**	16	15	18	17	**66**	**1.00**
55676	**SLC30A6**	*Solute carrier family 30 member 6*	***5***																	24	26	30	35	**115**	**1.00**	31	29	32	24	**116**	**1.00**
51429	**SNX9**	*Sorting nexin 9*		5	5	3	2							4	3	4	4	**15**		29	31	28	26	**114**	**1.00**	26	19	31	18	**94**	**1.00**
9218	**VAPA**	*VAMP associated protein A*	***4***	10	9	7	7	6	9	6		**21**		20	17	26	26	**89**		31	24	30	29	**114**	**0.99**	44	39	45	40	**168**	**1.00**
2060	**EPS15**	*Epidermal growth factor receptor pathway substrate 15*	***2***	11	9	7	4													20	24	40	28	**112**	**0.86**	15	6	6	12	**39**	
23368	**PPP1R13B**	*Protein phosphatase 1 regulatory subunit 13B*																		28	25	30	26	**109**	**1.00**	31	27	23	24	**105**	**1.00**
11311	**VPS45**	*Vacuolar protein sorting 45 homolog (S. Cerevisiae)*	***2***																	29	29	27	20	**105**	**1.00**	27	41	34	32	**134**	**1.00**
26056	**RAB11FIP5**	*RAB11 family interacting protein 5 (class I)*	***1***																	25	23	26	29	**103**	**1.00**	21	22	23	20	**86**	**1.00**
64924	**SLC30A5**	*Solute carrier family 30 member 5*	***5***																	24	25	24	25	**98**	**1.00**	22	23	20	20	**85**	**1.00**
22905	**EPN2**	*Epsin 2*	***1***																	30	23	21	24	**98**	**1.00**	19	22	15	21	**77**	**1.00**
10298	**PAK4**	*P21 protein (Cdc42/Rac)-activated kinase 4*	***2***	4				4	4	3		**11**				4		**4**		22	19	29	28	**98**	**1.00**	11	11	11	10	**43**	**0.96**
56288	**PARD3**	*Par-3 family cell polarity regulator*	***1***																	20	26	27	25	**98**	**1.00**		8	13	11	**32**	
100505818	**LOC100505818**	*Entry replaced with MLLT4*		7	6	6	5	6	16		9	**31**		15		21	3	**39**		24	22	26	24	**96**	**1.00**	31	28	24	21	**104**	**1.00**
5500	**PPP1CB**	*Protein phosphatase 1 catalytic subunit beta*		16	4									9				**9**		24	27	23	20	**94**	**0.86**	17	21		22	**60**	
121441	**NEDD1**	*Neural precursor cell expressed, developmentally down-regulated 1*																		23	22	27	21	**93**	**1.00**	12	10	13	9	**44**	**1.00**

Gene ID	Gene Name	Full name	MB	Top 4 controls	FAT4 BioID Cycling						FAT4 BioID Starved						ECAD BioID Cycling						ECAD BioID Starved					
					A#1	A#2	B#1	B#2	Total	SAINT	A#1	A#2	B#1	B#2	Total	SAINT	A#1	A#2	B#1	B#2	Total	SAINT	A#1	A#2	B#1	B#2	Total	SAINT
9522	**SCAMP1**	*Secretory carrier membrane protein 1*	***4***														25	22	23	22	**92**	**1.00**	26	21	23	18	**88**	**1.00**
10427	**SEC24B**	*SEC24 homolog B, COPII coat complex component*	***4***		4		2		**6**		3			5	**8**		25	20	22	23	**90**	**1.00**	22	24	25	23	**94**	**1.00**
55681	**SCYL2**	*SCY1 like pseudokinase 2*	***1***														19	21	20	27	**87**	**1.00**	21	20	20	16	**77**	**1.00**
23355	**VPS8**	*VPS8, CORVET complex subunit*															18	22	23	22	**85**	**1.00**	32	23	24	27	**106**	**1.00**
4952	**OCRL**	*Oculocerebrorenal syndrome of Lowe*	***1***														17	20	20	27	**84**	**1.00**	13	15	11	11	**50**	**1.00**
11336	**EXOC3**	*Exocyst complex component 3*	***2***														22	20	15	26	**83**	**1.00**	24	25	35	23	**107**	**1.00**
200894	**ARL13B**	*ADP ribosylation factor like gtpase 13B*	***1***										2	4	**6**		21	16	21	23	**81**	**1.00**	18	13	17	14	**62**	**1.00**
23094	**SIPA1L3**	*Signal-induced proliferation-associated 1 like 3*									10				**10**		21	16	20	21	**78**	**1.00**	29	27	31	25	**112**	**1.00**
9146	**HGS**	*Hepatocyte growth factor-regulated tyrosine kinase substrate*	***2***			5			**5**		2		5		**7**		19	19	18	21	**77**	**1.00**	7	18	12	14	**51**	**1.00**
22841	**RAB11FIP2**	*RAB11 family interacting protein 2 (class I)*															17	20	18	19	**74**	**1.00**	20	16	19	19	**74**	**1.00**
55789	**DEPDC1B**	*DEP domain containing 1B*	***5***	6 5 3	5	4		7	**16**		4	2			**6**		21	16	20	17	**74**	**0.99**	7	8	9	8	**32**	
1173	**AP2M1**	*Adaptor related protein complex 2 mu 1 subunit*		3 3													19	16	15	21	**71**	**1.00**	11	14	16	10	**51**	**0.99**
22874	**PLEKHA6**	*Pleckstrin homology domain containing A6*															20	16	17	17	**70**	**1.00**	22	18	23	23	**86**	**1.00**
51248	**PDZD11**	*PDZ domain containing 11*	***2***														16	19	16	17	**68**	**1.00**	19	19	24	18	**80**	**1.00**
9372	**ZFYVE9**	*Zinc finger FYVE-type containing 9*															13	14	19	22	**68**	**1.00**			3	2	**5**	
140775	**SMCR8**	*Smith-Magenis syndrome chromosome region, candidate 8*	***1***														19	14	18	15	**66**	**1.00**	22	21	22	22	**87**	**1.00**
6643	**SNX2**	*Sorting nexin 2*	***1***														16	16	17	16	**65**	**1.00**	17	12	11	10	**50**	**1.00**
9950	**GOLGA5**	*Golgin A5*	***4***														12	17	17	17	**63**	**1.00**	29	26	24	16	**95**	**1.00**
23673	**STX12**	*Syntaxin 12*	***3***														17	15	15	16	**63**	**1.00**	15	18	19	15	**67**	**1.00**
8027	**STAM**	*Signal transducing adaptor molecule*	***4***	3													15	17	19	12	**63**	**1.00**	11	12	12	14	**49**	**0.99**
56243	**KIAA1217**	*Kiaa1217*		2													21	15	12	13	**61**	**1.00**	42	46	37	42	**167**	**1.00**
10409	**BASP1**	*Brain abundant membrane attached signal protein 1*											2	4	**6**		16	13	17	14	**60**	**1.00**	17	22	12	23	**74**	**1.00**
4026	**LPP**	*LIM domain containing preferred translocation partner in lipoma*		6 3													13	14	14	18	**59**	**0.94**	35	32	37	30	**134**	**1.00**
6811	**STX5**	*Syntaxin 5*	***5***														15	16	13	14	**58**	**1.00**	20	17	17	19	**73**	**1.00**
55117	**SLC6A15**	*Solute carrier family 6 member 15*	***4***														16	14	15	13	**58**	**1.00**	3		5	3	**11**	
55255	**WDR41**	*WD repeat domain 41*	***5***									2			**2**		14	18	9	16	**57**	**1.00**	15	12	12	10	**49**	**1.00**
9341	**VAMP3**	*Vesicle associated membrane protein 3*	***5***	3	2	5	2	3	**12**		4	2			**6**		16	17	13	10	**56**	**0.99**	11	13	16	15	**55**	**0.99**
55717	**WDR11**	*WD repeat domain 11*	***4***	4 4 4 3									3		**3**		12	14	16	14	**56**	**0.97**	11	10	11	5	**37**	
6636	**SNRPF**	*Small nuclear ribonucleoprotein polypeptide F*		6 5 5 3													14	15	13	14	**56**	**0.77**	12	13	10	11	**46**	
6558	**SLC12A2**	*Solute carrier family 12 member 2*	***6***														12	14	13	16	**55**	**1.00**	5		4	7	**16**	
26003	**GORASP2**	*Golgi reassembly stacking protein 2*	***4***	6													13	14	13	15	**55**	**0.95**	8	15	14	12	**49**	**0.92**
55240	**STEAP3**	*STEAP3 metalloreductase*	***4***														16	12	12	14	**54**	**1.00**	7	5	10	9	**31**	**1.00**
10979	**FERMT2**	*Fermitin family member 2*	***2***				5		**5**								13	15	13	12	**53**	**1.00**	12	12	11	8	**43**	**1.00**
151963	**MB21D2**	*Mab-21 domain containing 2*	***3***	3													11	10	15	17	**53**	**0.99**	6	7	16	9	**38**	**0.95**
85377	**MICALL1**	*MICAL like 1*															13	13	15	11	**52**	**1.00**	5			4	**9**	
9497	**SLC4A7**	*Solute carrier family 4 member 7*	***4***			5	3	2	**10**			3	4	3	**10**		18	9	12	12	**51**	**1.00**						
7414	**VCL**	*Vinculin*		4													13	12	13	13	**51**	**0.98**	16	17	25	19	**77**	**1.00**
8773	**SNAP23**	*Synaptosome associated protein 23kda*	***4***			6		5	**11**		4	5	8		**17**		13	11	15	11	**50**	**1.00**	7	10	18	12	**47**	**1.00**
10484	**SEC23A**	*Sec23 homolog A, COPII coat complex component*	***2***				4		**4**				4		**4**		11	13	15	11	**50**	**1.00**	14	17	17	13	**61**	**1.00**
157769	**FAM91A1**	*Family with sequence similarity 91 member A1*	***4***	3 3 2 2													12	12	13	12	**49**	**1.00**	11	7	9	7	**34**	
115548	**FCHO2**	*FCH domain only 2*										2			**2**		12	10	12	13	**47**	**1.00**	8	9	16	7	**40**	**1.00**
8417	**STX7**	*Syntaxin 7*	***4***														14	8	14	11	**47**	**1.00**	13	10	11	14	**48**	**1.00**
23256	**SCFD1**	*Sec1 family domain containing 1*	***4***														10	12	14	10	**46**	**1.00**	11	16	20	21	**68**	**1.00**
50618	**ITSN2**	*Intersectin 2*		2													11	14	12	8	**45**	**1.00**	7	4			**11**	

Gene ID	Gene Name	Full name	MB	Top 4 controls				FAT4 BioID Cycling						FAT4 BioID Starved						ECAD BioID Cycling						ECAD BioID Starved					
								A#1	A#2	B#1	B#2	Total	SAINT	A#1	A#2	B#1	B#2	Total	SAINT	A#1	A#2	B#1	B#2	Total	SAINT	A#1	A#2	B#1	B#2	Total	SAINT
10483	**SEC23B**	*Sec23 homolog B, COPII coat complex component*	***3***	3																12	10	12	10	**44**	**0.99**	11	9	10	10	**40**	**0.98**
8727	**CTNNAL1**	*Catenin alpha like 1*																		13	9	9	12	**43**	**1.00**		3			**3**	
6844	**VAMP2**	*Vesicle associated membrane protein 2*	***4***																	11	11	9	11	**42**	**1.00**	9	9	12	12	**42**	**1.00**
79830	**ZMYM1**	*Zinc finger MYM-type containing 1*																		11	9	10	9	**39**	**1.00**						
26276	**VPS33B**	*VPS33B, late endosome and lysosome associated*																		11	8	8	11	**38**	**1.00**		4		7	**11**	
64145	**ZFYVE20**	*Rabenosyn, RAB effector*																		9	9	6	12	**36**	**1.00**	10	11	14	15	**50**	**1.00**
526	**ATP6V1B2**	*Atpase H+ transporting V1 subunit B2*																		9	7	10	10	**36**	**1.00**	8	8	7	8	**31**	**1.00**
3092	**HIP1**	*Huntingtin interacting protein 1*	***1***																	6	6	15	9	**36**	**1.00**						
9107	**MTMR6**	*Myotubularin related protein 6*	***1***																	9	11	6	9	**35**	**1.00**	7	10	6	8	**31**	**1.00**
738	**C11orf2**	*VPS51, GARP complex subunit*																		11	7	10	7	**35**	**1.00**		5	5		**10**	
23301	**EHBP1**	*EH domain binding protein 1*	***2***	3																8	7	12	8	**35**	**0.96**	3	2		3	**8**	
11180	**WDR6**	*WD repeat domain 6*	***3***					2	2		2	**6**		3		10	7	**20**		7	9	6	9	**31**	**1.00**		3	4	4	**11**	
5286	**PIK3C2A**	*Phosphatidylinositol-4-phosphate 3-kinase catalytic subunit type 2 alpha*																	8	7	11	5	**31**	**1.00**		2	3	5		**10**	
144402	**CPNE8**	*Copine 8*	**2**																	9	8	8	6	**31**	**1.00**	2	2		3	**7**	
152503	**SH3D19**	*SH3 domain containing 19*																		5	9	9	8	**31**	**1.00**						
66036	**MTMR9**	*Myotubularin related protein 9*																		9	9	8	4	**30**	**1.00**	6	8	7	4	**25**	**1.00**
10254	**STAM2**	*Signal transducing adaptor molecule 2*	**3**																	8	7	6	9	**30**	**1.00**	5	5	5	2	**17**	**0.99**
56704	**JPH1**	*Junctophilin 1*	**6**							6	6	**12**				5		**5**		6	5	10	7	**28**	**1.00**			2		**2**	
26092	**TOR1AIP1**	*Torsin 1A interacting protein 1*	**11**					6	4		4	**14**			4	5	6	**15**		6	4	9	8	**27**	**1.00**	21	20	15	15	**71**	**1.00**
9223	**MAGI1**	*Membrane associated guanylate kinase, WW and PDZ domain containing 1*																		7	6	6	8	**27**	**1.00**	3		6		**9**	
25921	**ZDHHC5**	*Zinc finger DHHC-type containing 5*	**2**											8		10	3	**21**		8	5	5	6	**24**	**1.00**	6	6	7	5	**24**	**1.00**
57120	**GOPC**	*Golgi-associated PDZ and coiled-coil motif containing*	**4**					3	3	4		**10**								8	3	8	5	**24**	**1.00**	3	3		6	**12**	
10160	**FARP1**	*FERM, ARH/rhogef and pleckstrin domain protein 1*														4	3	**7**		10	6	3	4	**23**	**1.00**	4	3	7	4	**18**	**1.00**
400793	**C1orf226**	*Chromosome 1 open reading frame 226*																		3	7	5	8	**23**	**1.00**	5	4	3		**12**	
5295	**PIK3R1**	*Phosphoinositide-3-kinase regulatory subunit 1*	**1**																	7	6	6	4	**23**	**1.00**						
11196	**SEC23IP**	*SEC23 interacting protein*	**3**																	3	6	7	6	**22**	**1.00**	6	3	3	4	**16**	**1.00**
1824	**DSC2**	*Desmocollin 2*	**2**											4		3	3	**10**		9	4	5	4	**22**	**1.00**	4	5		6	**15**	
57579	**FAM135A**	*Family with sequence similarity 135 member A*																		3	6	5	8	**22**	**1.00**						
57670	**KIAA1549**	*Kiaa1549*	**1**																	8	5	5	3	**21**	**1.00**				3	**3**	
23041	**MON2**	*MON2 homolog, regulator of endosome-to-Golgi trafficking*																		6	7	5	3	**21**	**1.00**	3				**3**	
81539	**SLC38A1**	*Solute carrier family 38 member 1*	**4**																	5	5	4	4	**18**	**1.00**		4		2	**6**	
4771	**NF2**	*Neurofibromin 2 (merlin)*														2	2	**4**		5	3	4	5	**17**	**1.00**	5	4	2	3	**14**	**0.99**
7112	**TMPO**	*Thymopoietin*	**6**	103	89	85	78	85	88	58	88	**319**		97	57	102	74	**330**		188	186	179	177	**730**		235	251	242	239	**967**	**1.00**
3930	**LBR**	*Lamin B receptor*	**8**	32	31	27	27	39	47	27	42	**155**		57	30	69	42	**198**		65	78	68	70	**281**		92	101	82	94	**369**	**1.00**
10424	**EMD**	*Emerin*	**9**	11	10	10	9	11	29	7	24	**71**		22	11	31	10	**74**		25	25	26	20	**96**		24	35	29	32	**120**	**0.76**
58477	**ARVCF**	*Armadillo repeat gene deleted in velocardiofacial syndrome*		3																5	4	3		**12**		32	31	24	28	**115**	**1.00**
287	**PGRMC2**	*Progesterone receptor membrane component 2*	**10**	6	5	4	4	7	13	4	6	**30**		9	8	10	8	**35**		11	14	12	10	**47**		22	27	25	30	**104**	**1.00**
119	**PKP4**	*Plakophilin 4*	**2**											7				**7**		14		12	10	**36**		21	30	21	22	**94**	**1.00**
8502	**SORBS1**	*Sorbin and SH3 domain containing 1*																		9		6	2	**17**		18	18	17	21	**74**	**1.00**
83461	**PVRL2**	*Nectin cell adhesion molecule 2*	**4**																		3	2	5	**10**		18	10	18	18	**64**	**1.00**
23065	**ANK2**	*Ankyrin 2, neuronal*												13		8		**21**				16		**16**		15	15	13	15	**58**	**1.00**
9712	**SEC22B**	*SEC22 homolog B, vesicle trafficking protein (gene/pseudogene)*	**8**	5	3										3		2	**5**		6		9	6	**21**		12	12	15	11	**50**	**0.94**

Gene ID	Gene Name	Full name	MB	Top 4 controls	FAT4 BioID Cycling						FAT4 BioID Starved						ECAD BioID Cycling						ECAD BioID Starved					
					A#1	A#2	B#1	B#2	Total	SAINT	A#1	A#2	B#1	B#2	Total	SAINT	A#1	A#2	B#1	B#2	Total	SAINT	A#1	A#2	B#1	B#2	Total	SAINT
10580	**CCDC47**	*Coiled-coil domain containing 47*	**12**																4	6	**10**		14	13	10	10	**47**	**1.00**
55684	**CDCA3**	*Cell division cycle associated 3*	**4**									3		3	**6**					2	**2**		11	11	12	10	**44**	**1.00**
26060	**SRPRB**	*SRP receptor beta subunit*	**4**					4	**4**				8	3	**11**		7	2	6		**15**		11	10	6	7	**34**	**1.00**
10529	**KIAA0090**	*ER membrane protein complex subunit 1*									3				**3**		3				**3**		12	5	10	6	**33**	**1.00**
421	**TTC35**	*ER membrane protein complex subunit 2*																					7	10	5	6	**28**	**1.00**
5819	**USP6NL**	*USP6 N-terminal like*	**1**											2	**2**		3	3		4	**10**		7	5	7	7	**26**	**1.00**
57003	**C9orf72**	*Chromosome 9 open reading frame 72*																	6	4	**10**		9	7	7	3	**26**	**1.00**
203228	**TPD52L2**	*Tumor protein D52-like 2*		3													2	6	3	6	**17**		4	5	4	11	**24**	**0.83**
92344	**C9orf86**	*RAB, member RAS oncogene family-like 6*															4	3		9	**16**		7	5	5	6	**23**	**1.00**
819	**NEBL**	*Nebulette*															5	5	4		**14**		5	7	4	7	**23**	**1.00**
8615	**GORAB**	*Golgin, RAB6-interacting*	**2**															2	3	4	**9**		7	4	7	5	**23**	**1.00**
9694	**CAMLG**	*Calcium modulating ligand*	**9**															4			**4**		4	6	6	7	**23**	**1.00**
55165	**USO1**	*USO1 vesicle transport factor*	**2**														3				**3**		6	3	5	9	**23**	**1.00**
3927	**CEP55**	*Centrosomal protein 55kda*																					7	6	5	3	**21**	**1.00**
23163	**ADD2**	*Adducin 2*									4		4	2	**10**			4	5	7	**16**		4	5	6	5	**20**	**1.00**
9554	**CHMP5**	*Charged multivesicular body protein 5*		3													5	5	5	2	**17**		5	5	5	5	**20**	**0.84**
51510	**APPL1**	*Adaptor protein, phosphotyrosine interacting with PH domain and leucine zipper 1*	**1**														5	5	5		**15**		6	3	4	4	**17**	**1.00**
7165	**LASP1**	*LIM and SH3 protein 1*																					3	4	4	6	**17**	**1.00**
2010	**GGA3**	*Golgi-associated, gamma adaptin ear containing, ARF binding protein 3*	**1**																3	4	**7**		2	2	7	3	**14**	**0.98**

Table 13.3 All hits of FAT4 and Cdh1 BioID in HCT116 cells

					Cdh1-BirA*-Flag in HCT116						FAT4-BirA*-Flag in HCT116							
					pool A		pool B				pool A		pool B					
Gene ID	Gene Name		Top2 controls		#1	#2	#1	#2	Total	SAINT	#1	#2	#1	#2	Total	SAINT	log2 fc vs Cdh1	p-value
999	**CDH1**	Cadherin 1			204	189	197	199	**7890**	**n.a.**								
79633	**FAT4**	FAT atypical cadherin 4									514	552	439	473	**1978**	**n.a.**		
128077	**LIX1L**	**Limb and CNS expressed 1 like**									**14**	**19**	**18**	**12**	**63**	**1.00**	***6.00***	***7.6E-05***
3728	**JUP**	Junction plakoglobin	13	12	381	385	355	385	**1506**	**1.00**	15	14	8	6	**43**		*-5.10*	*5.2E-09*
2037	**EPB41L2**	Erythrocyte membrane protein band 4.1-like 2	49	42	186	187	148	169	**690**	**1.00**	17	14	7	4	**42**		*-4.01*	*2.8E-06*
10801	**SEPT9**	Septin 9	21	19	67	68	74	79	**288**	**1.00**	11	10	9	6	**36**		*-2.97*	*7.6E-07*
1495	**CTNNA1**	Catenin alpha 1	4	2	1727	1652	1570	1607	**6556**	**1.00**	14	10	3	2	**29**		*-7.77*	*5.4E-09*
1969	**EPHA2**	EPH receptor A2	21	17	82	84	82	91	**339**	**1.00**	4	8	9	8	**29**		*-3.50*	*6.0E-08*
51741	**WWOX**	WW domain containing oxidoreductase	14	14	44	43	42	34	**163**	**0.76**	11	7	6	4	**28**		*-2.50*	*1.7E-05*
1891	**ECH1**	**Enoyl-coa hydratase 1, peroxisomal**			**1**		**2**	**2**	**5**		**8**	**12**	**5**	**3**	**28**	**1.00**	***2.27***	***2.9E-02***
81839	**VANGL1**	VANGL planar cell polarity protein 1	3	1	90	84	76	92	**342**	**1.00**	7	9	6	4	**26**		*-3.67*	*7.4E-07*
4282	**MIF**	**Macrophage migration inhibitory factor**									**6**	**6**	**6**	**8**	**26**	**1.00**	***4.75***	***1.3E-05***
2035	**EPB41**	Erythrocyte membrane protein band 4.1	46	39	125	115	128	123	**491**	**1.00**	3	6	1	2	**12**		*-5.24*	*1.6E-08*
6520	**SLC3A2**	Solute carrier family 3 member 2	5	3	17	16	10	14	**57**	**0.78**	3	4	4	1	**12**		*-2.16*	*5.8E-04*
4301	**MLLT4**	Myeloid/lymphoid or mixed-lineage leukemia; translocated to, 4	16	12	210	198	175	194	**777**	**1.00**	3	2	3	3	**11**		*-6.02*	*2.0E-07*
1829	**DSG2**	Desmoglein 2	4	3	228	211	186	206	**831**	**1.00**	3	7			**10**		*-6.24*	*4.1E-07*
8650	**NUMB**	Numb homolog (Drosophila)	6	5	35	40	34	29	**138**	**1.00**	2	5			**7**		*-4.12*	*1.4E-05*
23191	**CYFIP1**	Cytoplasmic FMR1 interacting protein 1	5	5	23	15	30	24	**92**	**0.95**			3	3	**6**		*-3.73*	*5.3E-04*
55914	**ERBB2IP**	Erbb2 interacting protein	4	3	264	254	203	236	**957**	**1.00**		3			**3**		*-7.90*	*2.0E-06*
1500	**CTNND1**	Catenin delta 1	12	11	677	678	670	677	**2702**	**1.00**	1				**1**		*-10.40*	*3.0E-14*
1499	**CTNNB1**	Catenin beta 1	7	7	962	914	880	950	**3706**	**1.00**							*-11.86*	*4.3E-09*
1496	**CTNNA2**	Catenin alpha 2			240	219	212	211	**882**	**1.00**							*-9.79*	*5.4E-08*
288	**ANK3**	Ankyrin 3, node of Ranvier (ankyrin G)			141	147	133	164	**585**	**1.00**							*-9.19*	*5.4E-07*
157680	**VPS13B**	Vacuolar protein sorting 13 homolog B (yeast)			116	108	129	131	**484**	**1.00**							*-8.92*	*5.5E-07*
2011	**MARK2**	Microtubule affinity regulating kinase 2	1		72	73	60	62	**267**	**1.00**							*-8.07*	*1.0E-06*
4430	**MYO1B**	Myosin IB	16	16	80	75	54	58	**267**	**1.00**							*-8.07*	*4.3E-05*
8502	**PKP4**	Plakophilin 4			52	54	50	49	**205**	**1.00**							*-7.69*	*6.9E-09*
1739	**DLG1**	Discs large homolog 1, scribble cell polarity complex component	9	3	50	48	44	43	**185**	**1.00**							*-7.54*	*1.4E-07*
55752	**SEPT11**	Septin 11	13	12	41	39	43	53	**176**	**1.00**							*-7.47*	*7.8E-06*
9231	**DLG5**	Discs large homolog 5	5	3	46	49	26	36	**157**	**1.00**							*-7.30*	*2.9E-04*
1001	**CDH3**	Cadherin 3			41	30	38	39	**148**	**1.00**							*-7.22*	*4.9E-06*
64855	**FAM129B**	Family with sequence similarity 129 member B	3	2	30	22	33	29	**114**	**1.00**							*-6.85*	*1.8E-05*
23157	**SEPT6**	Septin 6	8		24	22	26	35	**107**	**0.92**							*-6.75*	*8.6E-05*
9712	**USP6NL**	USP6 N-terminal like			27	23	26	26	**102**	**1.00**							*-6.69*	*1.0E-07*
8496	**PPFIBP1**	PPFIA binding protein 1	8	4	21	24	28	27	**100**	**1.00**							*-6.66*	*4.1E-06*

					Cdh1-BirA*-Flag in HCT116						FAT4-BirA*-Flag in HCT116							
					pool A		pool B				pool A		pool B					
Gene ID	**Gene Name**		Top2 controls		#1	#2	#1	#2	Total	SAINT	#1	#2	#1	#2	Total	SAINT	*log2 fc vs Cdh1*	*p-value*
23167	**EFR3A**	EFR3 homolog A	4	4	27	22	24	25	**98**	**1.00**							*-6.63*	*3.9E-07*
7402	**UTRN**	Utrophin	1		31	18	26	22	**97**	**1.00**							*-6.61*	*1.3E-04*
55240	**STEAP3**	STEAP3 metalloreductase			22	14	24	19	**79**	**1.00**							*-6.32*	*1.0E-04*
1207	**CLNS1A**	Chloride nucleotide-sensitive channel 1A	1		19	13	15	19	**66**	**1.00**							*-6.07*	*3.4E-05*
56288	**PARD3**	Par-3 family cell polarity regulator			19	17	9	13	**58**	**1.00**							*-5.88*	*6.1E-04*
64924	**SLC30A5**	Solute carrier family 30 member 5	1		17	17	12	11	**57**	**1.00**							*-5.86*	*1.1E-04*
8773	**SNAP23**	Synaptosome associated protein 23kda	3	2	16	16	13	12	**57**	**1.00**							*-5.86*	*8.9E-06*
1956	**EGFR**	Epidermal growth factor receptor			14	12	11	15	**52**	**1.00**							*-5.73*	*7.5E-06*
4140	**MARK3**	Microtubule affinity regulating kinase 3			12	16	12	12	**52**	**1.00**							*-5.73*	*1.3E-05*
6645	**SNTB2**	Syntrophin beta 2	1		14	14	12	12	**52**	**1.00**							*-5.73*	*5.0E-07*
10787	**NCKAP1**	NCK associated protein 1	3	2	10	10	16	14	**50**	**0.97**							*-5.67*	*1.6E-04*
9743	**ARHGAP32**	Rho gtpase activating protein 32			13	10	11	10	**44**	**1.00**							*-5.49*	*4.5E-06*
57584	**ARHGAP21**	Rho gtpase activating protein 21	2		12	9	11	10	**42**	**0.98**							*-5.43*	*3.4E-06*
51599	**LSR**	Lipolysis stimulated lipoprotein receptor	1	1	13	12	6	8	**39**	**1.00**							*-5.32*	*1.1E-03*
56924	**PAK6**	P21 protein (Cdc42/Rac)-activated kinase 6			7	8	11	8	**34**	**1.00**							*-5.13*	*6.4E-05*
55676	**SLC30A6**	Solute carrier family 30 member 6			10	8	9	7	**34**	**1.00**							*-5.13*	*1.2E-05*
8985	**PLOD3**	Procollagen-lysine, 2-oxoglutarate 5-dioxygenase 3			13	12	4	4	**33**	**1.00**							*-5.09*	*1.5E-02*
81539	**SLC38A1**	Solute carrier family 38 member 1			10	8	5	8	**31**	**1.00**							*-5.00*	*2.9E-04*
8573	**CASK**	Calcium/calmodulin-dependent serine protein kinase (MAGUK family)			8	8	4	7	**27**	**1.00**							*-4.81*	*3.8E-04*
113828	**FAM83F**	Family with sequence similarity 83 member F			8	5	8	6	**27**	**1.00**							*-4.81*	*1.1E-04*
9497	**SLC4A7**	Solute carrier family 4 member 7	2		7	6	6	7	**26**	**0.84**							*-4.75*	*5.0E-07*
642273	**FAM110C**	Family with sequence similarity 110 member C			6	6	7	6	**25**	**1.00**							*-4.70*	*2.7E-07*
23256	**SCFD1**	Sec1 family domain containing 1	1		5	5	3	7	**20**	**1.00**							*-4.39*	*8.7E-04*
81848	**SPRY4**	Sprouty RTK signaling antagonist 4	1	1	4	4	4	6	**18**	**1.00**							*-4.25*	*1.1E-04*
25921	**ZDHHC5**	Zinc finger DHHC-type containing 5			6	3	4	5	**18**	**1.00**							*-4.25*	*4.3E-04*
3783	**KCNN4**	Potassium calcium-activated channel subfamily N member 4	1		7	3	2	2	**14**	**0.96**							*-3.91*	*2.6E-02*
26064	**RAI14**	Retinoic acid induced 14	1		2	2	2	2	**8**	**0.93**							*-3.17*	-

Table 13.4 All hits of FAT4 and Cdh1 BioID in HeLa cells

Bait	Prey	Full Name	Spectra	Average	SAINT	Top 2 Controls	Freq. in Controls
FAT4	FAT4	FAT atypical cadherin 4	517|617	567	**1**	0|0	0/53
FAT4	HSPA5	Heat shock protein family A (Hsp70) member 5	56|81	68.5	**1**	23|22	51/53
FAT4	LIX1L	Limb and CNS expressed 1 like	7|10	8.5	**1**	0|0	0/53
FAT4	JPH1	Junctophilin 1	6|8	7	**0.97**	2|2	4/53
FAT4	LTBP1	Latent transforming growth factor beta binding protein 1	7|5	6	**1**	0|0	0/53
FAT4	FAT1	FAT atypical cadherin 1	3|5	4	**0.99**	0|0	0/53
FAT4	PPFIA1	PTPRF interacting protein alpha 1	2|4	3	**0.93**	0|0	0/53
Cdh1	CTNNA1	Catenin alpha 1	209|199	204	**1**	5|4	8/53
Cdh1	CTNNB1	Catenin beta 1	96|107	101.5	**1**	0|0	0/53
Cdh1	SCRIB	Scribbled planar cell polarity protein	92|89	90.5	**0.99**	42|42	34/53
Cdh1	ARHGAP21	Rho gtpase activating protein 21	66|69	67.5	**1**	10|9	25/53
Cdh1	TRIP11	Thyroid hormone receptor interactor 11	68|62	65	**1**	12|12	18/53
Cdh1	PLEKHA5	Pleckstrin homology domain containing A5	60|65	62.5	**1**	10|8	12/53
Cdh1	GOLGA3	Golgin A3	43|50	46.5	**1**	15|14	26/53
Cdh1	NHS	NHS actin remodeling regulator	44|39	41.5	**1**	8|7	20/53
Cdh1	JUP	Junction plakoglobin	40|39	39.5	**1**	15|15	34/53
Cdh1	VPS13B	Vacuolar protein sorting 13 homolog B (yeast)	34|45	39.5	**1**	0|0	0/53
Cdh1	GOLGA2	Golgin A2	38|40	39	**0.98**	20|19	34/53
Cdh1	KIDINS220	Kinase D-interacting substrate 220kda	27|38	32.5	**1**	9|8	22/53
Cdh1	SIPA1L3	Signal-induced proliferation-associated 1 like 3	31|27	29	**1**	0|0	0/53
Cdh1	GOLGA4	Golgin A4	22|34	28	**1**	5|2	3/53
Cdh1	TANC1	Tetratricopeptide repeat, ankyrin repeat and coiled-coil containing 1	25|21	23	**1**	2|0	1/53
Cdh1	ROBO1	Roundabout guidance receptor 1	24|18	21	**0.92**	10|10	28/53
Cdh1	GOLGA5	Golgin A5	17|23	20	**1**	5|3	4/53
Cdh1	CCDC88C	Coiled-coil domain containing 88C	13|25	19	**1**	0|0	0/53
Cdh1	ZDHHC5	Zinc finger DHHC-type containing 5	21|17	19	**1**	3|2	3/53
Cdh1	PDXDC1	Pyridoxal-dependent decarboxylase domain containing 1	18|19	18.5	**1**	2|0	1/53
Cdh1	LRBA	LPS responsive beige-like anchor protein	18|16	17	**1**	2|0	1/53
Cdh1	SEPT7	Septin 7	15|17	16	**1**	5|5	14/53
Cdh1	DST	Dystonin	18|13	15.5	**1**	0|0	0/53
Cdh1	PKP4	Plakophilin 4	19|12	15.5	**1**	4|3	3/53
Cdh1	USP6NL	USP6 N-terminal like	15|16	15.5	**1**	0|0	0/53
Cdh1	MARK2	Microtubule affinity regulating kinase 2	12|16	14	**1**	3|2	2/53
Cdh1	VANGL1	VANGL planar cell polarity protein 1	13|13	13	**1**	0|0	0/53
Cdh1	DLG1	Discs large homolog 1, scribble cell polarity complex component	12|12	12	**1**	0|0	0/53
Cdh1	DSC2	Desmocollin 2	9|15	12	**1**	2|0	1/53
Cdh1	SLC4A7	Solute carrier family 4 member 7	10|14	12	**1**	2|2	3/53
Cdh1	HIP1	Huntingtin interacting protein 1	12|11	11.5	**1**	0|0	0/53
Cdh1	KIAA1217	Kiaa1217	10|12	11	**1**	0|0	0/53
Cdh1	SEPT2	Septin 2	11|11	11	**0.99**	3|2	9/53
Cdh1	USO1	USO1 vesicle transport factor	12|10	11	**1**	6|4	14/53
Cdh1	ACBD3	Acyl-coa binding domain containing 3	12|8	10	**1**	0|0	0/53
Cdh1	MLLT4	Myeloid/lymphoid or mixed-lineage leukemia; translocated to, 4	10|10	10	**1**	0|0	0/53
Cdh1	MUC13	Mucin 13, cell surface associated	9|11	10	**0.96**	0|0	0/53
Cdh1	TANC2	Tetratricopeptide repeat, ankyrin repeat and coiled-coil containing 2	10|10	10	**1**	4|4	13/53
Cdh1	EFR3A	EFR3 homolog A	6|11	8.5	**0.91**	3|3	6/53
Cdh1	JPH1	Junctophilin 1	9|7	8	**0.99**	2|2	4/53
Cdh1	SEC24B	SEC24 homolog B, COPII coat complex component	7|6	6.5	**0.93**	3|2	4/53
Cdh1	RAB11FIP5	RAB11 family interacting protein 5 (class I)	4|8	6	**1**	0|0	0/53
Cdh1	MARK3	Microtubule affinity regulating kinase 3	5|6	5.5	**1**	0|0	0/53
Cdh1	ROR2	Receptor tyrosine kinase-like orphan receptor 2	6|5	5.5	**1**	2|0	1/53
Cdh1	SEPT11	Septin 11	4|7	5.5	**0.98**	0|0	0/53
Cdh1	SLC30A1	Solute carrier family 30 member 1	4|7	5.5	**1**	0|0	0/53

Bait	Prey	Full Name	Spectra	Average	SAINT	Top 2 Controls	Freq. in Controls
Cdh1	CCDC88A	Coiled-coil domain containing 88A	3|7	5	**0.99**	0|0	0/53
Cdh1	EPB41L1	Erythrocyte membrane protein band 4.1-like 1	6|4	5	**0.94**	2|2	2/53
Cdh1	ITSN2	Intersectin 2	3|6	4.5	**0.99**	0|0	0/53
Cdh1	SLC30A6	Solute carrier family 30 member 6	5|4	4.5	**1**	0|0	0/53
Cdh1	CDH1	Cadherin 1	4|4	4	**1**	0|0	0/53
Cdh1	CTNNA2	Catenin alpha 2	3|5	4	**0.99**	0|0	0/53
Cdh1	ITSN1	Intersectin 1	2|6	4	**0.94**	0|0	0/53
Cdh1	KIF26B	Kinesin family member 26B	3|5	4	**0.99**	0|0	0/53
Cdh1	STON2	Stonin 2	4|4	4	**1**	0|0	0/53
Cdh1	ATP2B1	Atpase plasma membrane Ca2+ transporting 1	2|5	3.5	**0.92**	0|0	0/53
Cdh1	BMP2K	BMP2 inducible kinase	5|2	3.5	**0.92**	0|0	0/53
Cdh1	GCC1	GRIP and coiled-coil domain containing 1	3|4	3.5	**0.98**	0|0	0/53
Cdh1	GOPC	Golgi-associated PDZ and coiled-coil motif containing	5|2	3.5	**0.92**	0|0	0/53
Cdh1	PKP2	Plakophilin 2	3|4	3.5	**0.98**	0|0	0/53
Cdh1	PKP3	Plakophilin 3	4|3	3.5	**0.98**	0|0	0/53
Cdh1	SEPT10	Septin 10	3|4	3.5	**0.98**	0|0	0/53
Cdh1	SLC25A10	Solute carrier family 25 member 10	3|4	3.5	**0.95**	2|0	1/53
Cdh1	SNX6	Sorting nexin 6	4|3	3.5	**0.98**	0|0	0/53
Cdh1	TMEM87A	Transmembrane protein 87A	3|4	3.5	**0.98**	0|0	0/53
Cdh1	EPN2	Epsin 2	2|4	3	**0.92**	0|0	0/53
Cdh1	GORAB	Golgin, RAB6-interacting	2|4	3	**0.92**	0|0	0/53
Cdh1	PDZD11	PDZ domain containing 11	3|3	3	**0.97**	0|0	0/53
Cdh1	SCAMP1	Secretory carrier membrane protein 1	3|3	3	**0.97**	0|0	0/53
Cdh1	SLC12A7	Solute carrier family 12 member 7	4|2	3	**0.92**	0|0	0/53
Cdh1	GGA3	Golgi-associated, gamma adaptin ear containing, ARF binding protein 3	3|2	2.5	**0.91**	0|0	0/53
Cdh1	RASSF8	Ras association domain family member 8	2|3	2.5	**0.91**	0|0	0/53

14 Bibliography

A - B

→ Adler, P. N., Charlton, J. and Liu, J. (1998) 'Mutations in the cadherin superfamily member gene dachsous cause a tissue polarity phenotype by altering frizzled signaling', *Development* 125(5): 959-68.

→ Afzelius, B. A. (1976) 'A human syndrome caused by immotile cilia', *Science* 193(4250): 317-9.

→ Ambegaonkar, A. A., Pan, G., Mani, M., Feng, Y. and Irvine, K. D. (2012) 'Propagation of Dachsous-Fat planar cell polarity', *Current biology : CB* 22(14): 1302-8.

→ Amonlirdviman, K., Khare, N. A., Tree, D. R., Chen, W. S., Axelrod, J. D. and Tomlin, C. J. (2005) 'Mathematical modeling of planar cell polarity to understand domineering nonautonomy', *Science* 307(5708): 423-6.

→ Andersen, S. S. (1999) 'Molecular characteristics of the centrosome', *International review of cytology* 187: 51-109.

→ Anderson, R. G. (1972) 'The three-dimensional structure of the basal body from the rhesus monkey oviduct', *The Journal of cell biology* 54(2): 246-65.

→ Angus, L., Moleirinho, S., Herron, L., Sinha, A., Zhang, X., Niestrata, M., Dholakia, K., Prystowsky, M. B., Harvey, K. F., Reynolds, P. A. et al. (2012) 'Willin/FRMD6 expression activates the Hippo signaling pathway kinases in mammals and antagonizes oncogenic YAP', *Oncogene* 31(2): 238-50.

→ Antic, D., Stubbs, J. L., Suyama, K., Kintner, C., Scott, M. P. and Axelrod, J. D. (2010) 'Planar cell polarity enables posterior localization of nodal cilia and left-right axis determination during mouse and Xenopus embryogenesis', *PloS one* 5(2): e8999.

→ Axelrod, J. D. (2001) 'Unipolar membrane association of Dishevelled mediates Frizzled planar cell polarity signaling', *Genes & development* 15(10): 1182-7.

→ Bachmann, A., Schneider, M., Theilenberg, E., Grawe, F. and Knust, E. (2001) 'Drosophila Stardust is a partner of Crumbs in the control of epithelial cell polarity', *Nature* 414(6864): 638-43.

→ Badouel, C., Gardano, L., Amin, N., Garg, A., Rosenfeld, R., Le Bihan, T. and McNeill, H. (2009) 'The FERM-domain protein Expanded regulates Hippo pathway activity via direct interactions with the transcriptional activator Yorkie', *Developmental cell* 16(3): 411-20.

→ Badouel, C., Zander, M. A., Liscio, N., Bagherie-Lachidan, M., Sopko, R., Coyaud, E., Raught, B., Miller, F. D. and McNeill, H. (2015) 'Fat1 interacts with Fat4 to regulate neural tube closure, neural progenitor proliferation and apical constriction during mouse brain development', *Development* 142(16): 2781-91.

→ Baena-Lopez, L. A., Baonza, A. and Garcia-Bellido, A. (2005) 'The orientation of cell divisions determines the shape of Drosophila organs', *Current biology : CB* 15(18): 1640-4.

→ Bagherie-Lachidan, M., Reginensi, A., Pan, Q., Zaveri, H. P., Scott, D. A., Blencowe, B. J., Helmbacher, F. and McNeill, H. (2015) 'Stromal Fat4 acts non-autonomously with Dchs1/2 to restrict the nephron progenitor pool', *Development* 142(15): 2564-73.

→ Bahe, S., Stierhof, Y. D., Wilkinson, C. J., Leiss, F. and Nigg, E. A. (2005) 'Rootletin forms centriole-associated filaments and functions in centrosome cohesion', *The Journal of cell biology* 171(1): 27-33.

→ Baker, N. E. (2001) 'Cell proliferation, survival, and death in the Drosophila eye', *Seminars in cell & developmental biology* 12(6): 499-507.

→ Barlow, J. L., Drynan, L. F., Hewett, D. R., Holmes, L. R., Lorenzo-Abalde, S., Lane, A. L., Jolin, H. E., Pannell, R., Middleton, A. J., Wong, S. H. et al. (2010) 'A p53-dependent mechanism underlies macrocytic anemia in a mouse model of human 5q- syndrome', *Nature medicine* 16(1): 59-66.

→ Barral, Y., Mermall, V., Mooseker, M. S. and Snyder, M. (2000) 'Compartmentalization of the cell cortex by septins is required for maintenance of cell polarity in yeast', *Molecular cell* 5(5): 841-51.

→ Bastock, R., Strutt, H. and Strutt, D. (2003) 'Strabismus is asymmetrically localised and binds to Prickle and Dishevelled during Drosophila planar polarity patterning', *Development* 130(13): 3007-14.

→ Belozerov, V. E., Lin, Z. Y., Gingras, A. C., McDermott, J. C. and Michael Siu, K. W. (2012) 'High-resolution protein interaction map of the Drosophila melanogaster p38 mitogen-activated protein kinases reveals limited functional redundancy', *Molecular and cellular biology* 32(18): 3695-706.

→ Bennett, F. C. and Harvey, K. F. (2006) 'Fat cadherin modulates organ size in Drosophila via the Salvador/Warts/Hippo signaling pathway', *Current biology : CB* 16(21): 2101-10.

→ Benton, R. and St Johnston, D. (2003) 'Drosophila PAR-1 and 14-3-3 inhibit Bazooka/PAR-3 to establish complementary cortical domains in polarized cells', *Cell* 115(6): 691-704.

→ Bichsel, S. J., Tamaskovic, R., Stegert, M. R. and Hemmings, B. A. (2004) 'Mechanism of activation of NDR (nuclear Dbf2-related) protein kinase by the hMOB1 protein', *The Journal of biological chemistry* 279(34): 35228-35.

→ Bilder, D., Li, M. and Perrimon, N. (2000) 'Cooperative regulation of cell polarity and growth by Drosophila tumor suppressors', *Science* 289(5476): 113-6.

→ Bilder, D. and Perrimon, N. (2000) 'Localization of apical epithelial determinants by the basolateral PDZ protein Scribble', *Nature* 403(6770): 676-80.

→ Blaumueller, C. M. and Mlodzik, M. (2000) 'The Drosophila tumor suppressor expanded regulates growth, apoptosis, and patterning during development', *Mechanisms of development* 92(2): 251-62.

→ Boggiano, J. C. and Fehon, R. G. (2012) 'Growth control by committee: intercellular junctions, cell polarity, and the cytoskeleton regulate Hippo signaling', *Developmental cell* 22(4): 695-702.

→ Boggon, T. J., Murray, J., Chappuis-Flament, S., Wong, E., Gumbiner, B. M. and Shapiro, L. (2002) 'C-cadherin ectodomain structure and implications for cell adhesion mechanisms', *Science* 296(5571): 1308-13.

→ Boisvieux-Ulrich, E., Laine, M. C. and Sandoz, D. (1989) 'In vitro effects of taxol on ciliogenesis in quail oviduct', *Journal of cell science* 92 (Pt 1): 9-20.

→ Bonnet, C. S., Aldred, M., von Ruhland, C., Harris, R., Sandford, R. and Cheadle, J. P. (2009) 'Defects in cell polarity underlie TSC and ADPKD-associated cystogenesis', *Human molecular genetics* 18(12): 2166-76.

→ Bornens, M. (2002) 'Centrosome composition and microtubule anchoring mechanisms', *Current opinion in cell biology* 14(1): 25-34.

→ Bosch, J. A., Sumabat, T. M., Hafezi, Y., Pellock, B. J., Gandhi, K. D. and Hariharan, I. K. (2014) 'The Drosophila F-box protein Fbxl7 binds to the protocadherin fat and regulates Dachs localization and Hippo signaling', *eLife* 3: e03383.

→ Bossuyt, W., Chen, C. L., Chen, Q., Sudol, M., McNeill, H., Pan, D., Kopp, A. and Halder, G. (2014) 'An evolutionary shift in the regulation of the Hippo pathway between mice and flies', *Oncogene* 33(10): 1218-28.

→ Bosveld, F., Bonnet, I., Guirao, B., Tlili, S., Wang, Z., Petitalot, A., Marchand, R., Bardet, P. L., Marcq, P., Graner, F. et al. (2012) 'Mechanical control of morphogenesis by Fat/Dachsous/Four-jointed planar cell polarity pathway', *Science* 336(6082): 724-7.

→ Boutin, C., Labedan, P., Dimidschstein, J., Richard, F., Cremer, H., Andre, P., Yang, Y., Montcouquiol, M., Goffinet, A. M. and Tissir, F. (2014) 'A dual role for planar cell polarity genes in ciliated cells', *Proceedings of the National Academy of Sciences of the United States of America* 111(30): E3129-38.

→ Brazelton, W. J., Amundsen, C. D., Silflow, C. D. and Lefebvre, P. A. (2001) 'The bld1 mutation identifies the Chlamydomonas osm-6 homolog as a gene required for flagellar assembly', *Current biology : CB* 11(20): 1591-4.

→ Breslow, D. K., Koslover, E. F., Seydel, F., Spakowitz, A. J. and Nachury, M. V. (2013) 'An in vitro assay for entry into cilia reveals unique properties of the soluble diffusion barrier', *The Journal of cell biology* 203(1): 129-47.

→ Bretscher, A., Gary, R. and Berryman, M. (1995) 'Soluble ezrin purified from placenta exists as stable monomers and elongated dimers with masked C-terminal ezrin-radixin-moesin association domains', *Biochemistry* 34(51): 16830-7.

→ Brinkman, E. K., Chen, T., Amendola, M. and van Steensel, B. (2014) 'Easy quantitative assessment of genome editing by sequence trace decomposition', *Nucleic acids research* 42(22): e168.

→ Brittle, A., Thomas, C. and Strutt, D. (2012) 'Planar polarity specification through asymmetric subcellular localization of Fat and Dachsous', *Current biology : CB* 22(10): 907-14.

→ Brittle, A. L., Repiso, A., Casal, J., Lawrence, P. A. and Strutt, D. (2010) 'Four-jointed modulates growth and planar polarity by reducing the affinity of dachsous for fat', *Current biology : CB* 20(9): 803-10.
→ Brook-Carter, P. T., Peral, B., Ward, C. J., Thompson, P., Hughes, J., Maheshwar, M. M., Nellist, M., Gamble, V., Harris, P. C. and Sampson, J. R. (1994) 'Deletion of the TSC2 and PKD1 genes associated with severe infantile polycystic kidney disease--a contiguous gene syndrome', *Nature genetics* 8(4): 328-32.
→ Bryant, P. J., Huettner, B., Held, L. I., Jr., Ryerse, J. and Szidonya, J. (1988) 'Mutations at the fat locus interfere with cell proliferation control and epithelial morphogenesis in Drosophila', *Developmental biology* 129(2): 541-54.
→ Burakov, A. V. and Nadezhdina, E. S. (2013) 'Association of nucleus and centrosome: magnet or velcro?', *Cell biology international* 37(2): 95-104.
→ Butz, S., Stappert, J., Weissig, H. and Kemler, R. (1992) 'Plakoglobin and beta-catenin: distinct but closely related', *Science* 257(5073): 1142-4.

C - D

→ Cai, J., Feng, D., Hu, L., Chen, H., Yang, G., Cai, Q., Gao, C. and Wei, D. (2015) 'FAT4 functions as a tumour suppressor in gastric cancer by modulating Wnt/beta-catenin signalling', *British journal of cancer* 113(12): 1720-9.
→ Camargo, F. D., Gokhale, S., Johnnidis, J. B., Fu, D., Bell, G. W., Jaenisch, R. and Brummelkamp, T. R. (2007) 'YAP1 increases organ size and expands undifferentiated progenitor cells', *Current biology : CB* 17(23): 2054-60.
→ Cappello, S., Gray, M. J., Badouel, C., Lange, S., Einsiedler, M., Srour, M., Chitayat, D., Hamdan, F. F., Jenkins, Z. A., Morgan, T. et al. (2013) 'Mutations in genes encoding the cadherin receptor-ligand pair DCHS1 and FAT4 disrupt cerebral cortical development', *Nature genetics* 45(11): 1300-8.
→ Carreira-Barbosa, F., Concha, M. L., Takeuchi, M., Ueno, N., Wilson, S. W. and Tada, M. (2003) 'Prickle 1 regulates cell movements during gastrulation and neuronal migration in zebrafish', *Development* 130(17): 4037-46.
→ Casal, J., Lawrence, P. A. and Struhl, G. (2006) 'Two separate molecular systems, Dachsous/Fat and Starry night/Frizzled, act independently to confer planar cell polarity', *Development* 133(22): 4561-72.
→ Casal, J., Struhl, G. and Lawrence, P. A. (2002) 'Developmental compartments and planar polarity in Drosophila', *Current biology : CB* 12(14): 1189-98.
→ Castillejo-Lopez, C., Arias, W. M. and Baumgartner, S. (2004) 'The fat-like gene of Drosophila is the true orthologue of vertebrate fat cadherins and is involved in the formation of tubular organs', *The Journal of biological chemistry* 279(23): 24034-43.
→ Cesario, M. M. and Bartles, J. R. (1994) 'Compartmentalization, processing and redistribution of the plasma membrane protein CE9 on rodent spermatozoa. Relationship of the annulus to domain boundaries in the plasma membrane of the tail', *Journal of cell science* 107 (Pt 2): 561-70.
→ Chacon-Heszele, M. F., Ren, D., Reynolds, A. B., Chi, F. and Chen, P. (2012) 'Regulation of cochlear convergent extension by the vertebrate planar cell polarity pathway is dependent on p120-catenin', *Development* 139(5): 968-78.
→ Chae, J., Kim, M. J., Goo, J. H., Collier, S., Gubb, D., Charlton, J., Adler, P. N. and Park, W. J. (1999) 'The Drosophila tissue polarity gene starry night encodes a member of the protocadherin family', *Development* 126(23): 5421-9.
→ Chan, E. H., Nousiainen, M., Chalamalasetty, R. B., Schafer, A., Nigg, E. A. and Sillje, H. H. (2005) 'The Ste20-like kinase Mst2 activates the human large tumor suppressor kinase Lats1', *Oncogene* 24(12): 2076-86.
→ Chen, C. L., Gajewski, K. M., Hamaratoglu, F., Bossuyt, W., Sansores-Garcia, L., Tao, C. and Halder, G. (2010) 'The apical-basal cell polarity determinant Crumbs regulates Hippo signaling in Drosophila', *Proceedings of the National Academy of Sciences of the United States of America* 107(36): 15810-5.
→ Chen, C. L., Schroeder, M. C., Kango-Singh, M., Tao, C. and Halder, G. (2012) 'Tumor suppression by cell competition through regulation of the Hippo pathway', *Proceedings of the National Academy of Sciences of the United States of America* 109(2): 484-9.

→ Chen, E. Y., Tan, C. M., Kou, Y., Duan, Q., Wang, Z., Meirelles, G. V., Clark, N. R. and Ma'ayan, A. (2013) 'Enrichr: interactive and collaborative HTML5 gene list enrichment analysis tool', *BMC bioinformatics* 14: 128.

→ Chen, W. S., Antic, D., Matis, M., Logan, C. Y., Povelones, M., Anderson, G. A., Nusse, R. and Axelrod, J. D. (2008) 'Asymmetric homotypic interactions of the atypical cadherin flamingo mediate intercellular polarity signaling', *Cell* 133(6): 1093-105.

→ Chih, B., Liu, P., Chinn, Y., Chalouni, C., Komuves, L. G., Hass, P. E., Sandoval, W. and Peterson, A. S. (2012) 'A ciliopathy complex at the transition zone protects the cilia as a privileged membrane domain', *Nature cell biology* 14(1): 61-72.

→ Cho, E., Feng, Y., Rauskolb, C., Maitra, S., Fehon, R. and Irvine, K. D. (2006) 'Delineation of a Fat tumor suppressor pathway', *Nature genetics* 38(10): 1142-50.

→ Cho, E. and Irvine, K. D. (2004) 'Action of fat, four-jointed, dachsous and dachs in distal-to-proximal wing signaling', *Development* 131(18): 4489-500.

→ Choi, H., Larsen, B., Lin, Z. Y., Breitkreutz, A., Mellacheruvu, D., Fermin, D., Qin, Z. S., Tyers, M., Gingras, A. C. and Nesvizhskii, A. I. (2011) 'SAINT: probabilistic scoring of affinity purification-mass spectrometry data', *Nature methods* 8(1): 70-3.

→ Chow, A., Hao, Y. and Yang, X. (2010) 'Molecular characterization of human homologs of yeast MOB1', *International journal of cancer. Journal international du cancer* 126(9): 2079-89.

→ Chretien, D., Buendia, B., Fuller, S. D. and Karsenti, E. (1997) 'Reconstruction of the centrosome cycle from cryoelectron micrographs', *Journal of structural biology* 120(2): 117-33.

→ Ciani, L., Patel, A., Allen, N. D. and ffrench-Constant, C. (2003) 'Mice lacking the giant protocadherin mFAT1 exhibit renal slit junction abnormalities and a partially penetrant cyclopia and anophthalmia phenotype', *Molecular and cellular biology* 23(10): 3575-82.

→ Clark, H. F., Brentrup, D., Schneitz, K., Bieber, A., Goodman, C. and Noll, M. (1995) 'Dachsous encodes a member of the cadherin superfamily that controls imaginal disc morphogenesis in Drosophila', *Genes & development* 9(12): 1530-42.

→ Cohen, E., Binet, S. and Meininger, V. (1988) 'Ciliogenesis and centriole formation in the mouse embryonic nervous system. An ultrastructural analysis', *Biology of the cell / under the auspices of the European Cell Biology Organization* 62(2): 165-9.

→ Comartin, D., Gupta, G. D., Fussner, E., Coyaud, E., Hasegan, M., Archinti, M., Cheung, S. W., Pinchev, D., Lawo, S., Raught, B. et al. (2013) 'CEP120 and SPICE1 cooperate with CPAP in centriole elongation', *Current biology : CB* 23(14): 1360-6.

→ Copeland, N. G., Jenkins, N. A. and Court, D. L. (2001) 'Recombineering: a powerful new tool for mouse functional genomics', *Nature reviews. Genetics* 2(10): 769-79.

→ Corbit, K. C., Aanstad, P., Singla, V., Norman, A. R., Stainier, D. Y. and Reiter, J. F. (2005) 'Vertebrate Smoothened functions at the primary cilium', *Nature* 437(7061): 1018-21.

→ Corbit, K. C., Shyer, A. E., Dowdle, W. E., Gaulden, J., Singla, V., Chen, M. H., Chuang, P. T. and Reiter, J. F. (2008) 'Kif3a constrains beta-catenin-dependent Wnt signalling through dual ciliary and non-ciliary mechanisms', *Nature cell biology* 10(1): 70-6.

→ Cox, B., Hadjantonakis, A. K., Collins, J. E. and Magee, A. I. (2000) 'Cloning and expression throughout mouse development of mfat1, a homologue of the Drosophila tumour suppressor gene fat', *Developmental dynamics : an official publication of the American Association of Anatomists* 217(3): 233-40.

→ Craig, R. and Beavis, R. C. (2004) 'TANDEM: matching proteins with tandem mass spectra', *Bioinformatics* 20(9): 1466-7.

→ Creasy, C. L. and Chernoff, J. (1995a) 'Cloning and characterization of a human protein kinase with homology to Ste20', *The Journal of biological chemistry* 270(37): 21695-700.

→ Creasy, C. L. and Chernoff, J. (1995b) 'Cloning and characterization of a member of the MST subfamily of Ste20-like kinases', *Gene* 167(1-2): 303-6.

→ Crobach, S., Ruano, D., van Eijk, R., Fleuren, G. J., Minderhout, I., Snowdowne, R., Tops, C., van Wezel, T. and Morreau, H. (2015) 'Target-enriched next-generation sequencing reveals differences between primary and secondary ovarian tumors in formalin-fixed, paraffin-embedded tissue', *The Journal of molecular diagnostics : JMD* 17(2): 193-200.

→ Curtin, J. A., Quint, E., Tsipouri, V., Arkell, R. M., Cattanach, B., Copp, A. J., Henderson, D. J., Spurr, N., Stanier, P., Fisher, E. M. et al. (2003) 'Mutation of Celsr1 disrupts planar polarity of inner ear hair cells and causes severe neural tube defects in the mouse', *Current biology : CB* 13(13): 1129-33.

→ Daniel, J. M. and Reynolds, A. B. (1995) 'The tyrosine kinase substrate p120cas binds directly to E-cadherin but not to the adenomatous polyposis coli protein or alpha-catenin', *Molecular and cellular biology* 15(9): 4819-24.
→ Darken, R. S., Scola, A. M., Rakeman, A. S., Das, G., Mlodzik, M. and Wilson, P. A. (2002) 'The planar polarity gene strabismus regulates convergent extension movements in Xenopus', *The EMBO journal* 21(5): 976-85.
→ Das, A., Tanigawa, S., Karner, C. M., Xin, M., Lum, L., Chen, C., Olson, E. N., Perantoni, A. O. and Carroll, T. J. (2013) 'Stromal-epithelial crosstalk regulates kidney progenitor cell differentiation', *Nature cell biology* 15(9): 1035-44.
→ Das, G., Jenny, A., Klein, T. J., Eaton, S. and Mlodzik, M. (2004) 'Diego interacts with Prickle and Strabismus/Van Gogh to localize planar cell polarity complexes', *Development* 131(18): 4467-76.
→ Das, G., Reynolds-Kenneally, J. and Mlodzik, M. (2002) 'The atypical cadherin Flamingo links Frizzled and Notch signaling in planar polarity establishment in the Drosophila eye', *Developmental cell* 2(5): 655-66.
→ Davis, M. A., Ireton, R. C. and Reynolds, A. B. (2003) 'A core function for p120-catenin in cadherin turnover', *The Journal of cell biology* 163(3): 525-34.
→ Dawe, H. R., Adams, M., Wheway, G., Szymanska, K., Logan, C. V., Noegel, A. A., Gull, K. and Johnson, C. A. (2009) 'Nesprin-2 interacts with meckelin and mediates ciliogenesis via remodelling of the actin cytoskeleton', *Journal of cell science* 122(Pt 15): 2716-26.
→ Dawe, H. R., Smith, U. M., Cullinane, A. R., Gerrelli, D., Cox, P., Badano, J. L., Blair-Reid, S., Sriram, N., Katsanis, N., Attie-Bitach, T. et al. (2007) 'The Meckel-Gruber Syndrome proteins MKS1 and meckelin interact and are required for primary cilium formation', *Human molecular genetics* 16(2): 173-86.
→ Day, S. J. and Lawrence, P. A. (2000) 'Measuring dimensions: the regulation of size and shape', *Development* 127(14): 2977-87.
→ Deans, M. R., Antic, D., Suyama, K., Scott, M. P., Axelrod, J. D. and Goodrich, L. V. (2007) 'Asymmetric distribution of prickle-like 2 reveals an early underlying polarization of vestibular sensory epithelia in the inner ear', *The Journal of neuroscience : the official journal of the Society for Neuroscience* 27(12): 3139-47.
→ Deans, M. R., Krol, A., Abraira, V. E., Copley, C. O., Tucker, A. F. and Goodrich, L. V. (2011) 'Control of neuronal morphology by the atypical cadherin Fat3', *Neuron* 71(5): 820-32.
→ Deardorff, M. A., Tan, C., Conrad, L. J. and Klein, P. S. (1998) 'Frizzled-8 is expressed in the Spemann organizer and plays a role in early morphogenesis', *Development* 125(14): 2687-700.
→ Degoutin, J. L., Milton, C. C., Yu, E., Tipping, M., Bosveld, F., Yang, L., Bellaiche, Y., Veraksa, A. and Harvey, K. F. (2013) 'Riquiqui and minibrain are regulators of the hippo pathway downstream of Dachsous', *Nature cell biology* 15(10): 1176-85.
→ Deng, H., Wang, W., Yu, J., Zheng, Y., Qing, Y. and Pan, D. (2015) 'Spectrin regulates Hippo signaling by modulating cortical actomyosin activity', *eLife* 4: e06567.
→ Deng, Y., Matsui, Y., Zhang, Y. and Lai, Z. C. (2013) 'Hippo activation through homodimerization and membrane association for growth inhibition and organ size control', *Developmental biology* 375(2): 152-9.
→ Dishinger, J. F., Kee, H. L., Jenkins, P. M., Fan, S., Hurd, T. W., Hammond, J. W., Truong, Y. N., Margolis, B., Martens, J. R. and Verhey, K. J. (2010) 'Ciliary entry of the kinesin-2 motor KIF17 is regulated by importin-beta2 and RanGTP', *Nature cell biology* 12(7): 703-10.
→ Djiane, A., Riou, J., Umbhauer, M., Boucaut, J. and Shi, D. (2000) 'Role of frizzled 7 in the regulation of convergent extension movements during gastrulation in Xenopus laevis', *Development* 127(14): 3091-100.
→ Domingues, C. and Ryoo, H. D. (2012) 'Drosophila BRUCE inhibits apoptosis through non-lysine ubiquitination of the IAP-antagonist REAPER', *Cell death and differentiation* 19(3): 470-7.
→ Dong, J., Feldmann, G., Huang, J., Wu, S., Zhang, N., Comerford, S. A., Gayyed, M. F., Anders, R. A., Maitra, A. and Pan, D. (2007) 'Elucidation of a universal size-control mechanism in Drosophila and mammals', *Cell* 130(6): 1120-33.
→ Dow, L. E., Brumby, A. M., Muratore, R., Coombe, M. L., Sedelies, K. A., Trapani, J. A., Russell, S. M., Richardson, H. E. and Humbert, P. O. (2003) 'hScrib is a functional homologue of the Drosophila tumour suppressor Scribble', *Oncogene* 22(58): 9225-30.

→ Dowdle, W. E., Robinson, J. F., Kneist, A., Sirerol-Piquer, M. S., Frints, S. G., Corbit, K. C., Zaghloul, N. A., van Lijnschoten, G., Mulders, L., Verver, D. E. et al. (2011) 'Disruption of a ciliary B9 protein complex causes Meckel syndrome', *American journal of human genetics* 89(1): 94-110.

→ Dunne, J., Hanby, A. M., Poulsom, R., Jones, T. A., Sheer, D., Chin, W. G., Da, S. M., Zhao, Q., Beverley, P. C. and Owen, M. J. (1995) 'Molecular cloning and tissue expression of FAT, the human homologue of the Drosophila fat gene that is located on chromosome 4q34-q35 and encodes a putative adhesion molecule', *Genomics* 30(2): 207-23.

E - F

→ Enderle, L. and McNeill, H. (2013) 'Hippo gains weight: added insights and complexity to pathway control', *Science signaling* 6(296): re7.

→ Eng, J. K., Jahan, T. A. and Hoopmann, M. R. (2013) 'Comet: an open-source MS/MS sequence database search tool', *Proteomics* 13(1): 22-4.

→ Estey, M. P., Di Ciano-Oliveira, C., Froese, C. D., Bejide, M. T. and Trimble, W. S. (2010) 'Distinct roles of septins in cytokinesis: SEPT9 mediates midbody abscission', *The Journal of cell biology* 191(4): 741-9.

→ Fan, S., Fogg, V., Wang, Q., Chen, X. W., Liu, C. J. and Margolis, B. (2007) 'A novel Crumbs3 isoform regulates cell division and ciliogenesis via importin beta interactions', *The Journal of cell biology* 178(3): 387-98.

→ Fang, G., Zhang, D., Yin, H., Zheng, L., Bi, X. and Yuan, L. (2014) 'Centlein mediates an interaction between C-Nap1 and Cep68 to maintain centrosome cohesion', *Journal of cell science* 127(Pt 8): 1631-9.

→ Fang, X. and Adler, P. N. (2010) 'Regulation of cell shape, wing hair initiation and the actin cytoskeleton by Trc/Fry and Wts/Mats complexes', *Developmental biology* 341(2): 360-74.

→ Fanto, M., Clayton, L., Meredith, J., Hardiman, K., Charroux, B., Kerridge, S. and McNeill, H. (2003) 'The tumor-suppressor and cell adhesion molecule Fat controls planar polarity via physical interactions with Atrophin, a transcriptional co-repressor', *Development* 130(4): 763-74.

→ Feiguin, F., Hannus, M., Mlodzik, M. and Eaton, S. (2001) 'The ankyrin repeat protein Diego mediates Frizzled-dependent planar polarization', *Developmental cell* 1(1): 93-101.

→ Feng, Y. and Irvine, K. D. (2007) 'Fat and expanded act in parallel to regulate growth through warts', *Proceedings of the National Academy of Sciences of the United States of America* 104(51): 20362-7.

→ Feng, Y. and Irvine, K. D. (2009) 'Processing and phosphorylation of the Fat receptor', *Proceedings of the National Academy of Sciences of the United States of America* 106(29): 11989-94.

→ Fernandez, B. G., Gaspar, P., Bras-Pereira, C., Jezowska, B., Rebelo, S. R. and Janody, F. (2011) 'Actin-Capping Protein and the Hippo pathway regulate F-actin and tissue growth in Drosophila', *Development* 138(11): 2337-46.

→ Ferrante, M. I., Romio, L., Castro, S., Collins, J. E., Goulding, D. A., Stemple, D. L., Woolf, A. S. and Wilson, S. W. (2009) 'Convergent extension movements and ciliary function are mediated by ofd1, a zebrafish orthologue of the human oral-facial-digital type 1 syndrome gene', *Human molecular genetics* 18(2): 289-303.

→ Fisch, C. and Dupuis-Williams, P. (2011) 'Ultrastructure of cilia and flagella - back to the future!', *Biology of the cell / under the auspices of the European Cell Biology Organization* 103(6): 249-70.

→ Fischer, E., Legue, E., Doyen, A., Nato, F., Nicolas, J. F., Torres, V., Yaniv, M. and Pontoglio, M. (2006) 'Defective planar cell polarity in polycystic kidney disease', *Nature genetics* 38(1): 21-3.

→ Fletcher, G. C., Elbediwy, A., Khanal, I., Ribeiro, P. S., Tapon, N. and Thompson, B. J. (2015) 'The Spectrin cytoskeleton regulates the Hippo signalling pathway', *The EMBO journal* 34(7): 940-54.

→ Fliegauf, M., Horvath, J., von Schnakenburg, C., Olbrich, H., Muller, D., Thumfart, J., Schermer, B., Pazour, G. J., Neumann, H. P., Zentgraf, H. et al. (2006) 'Nephrocystin specifically localizes to the transition zone of renal and respiratory cilia and photoreceptor connecting cilia', *Journal of the American Society of Nephrology : JASN* 17(9): 2424-33.

→ Follit, J. A., Tuft, R. A., Fogarty, K. E. and Pazour, G. J. (2006) 'The intraflagellar transport protein IFT20 is associated with the Golgi complex and is required for cilia assembly', *Molecular biology of the cell* 17(9): 3781-92.
→ Frame, M. C., Patel, H., Serrels, B., Lietha, D. and Eck, M. J. (2010) 'The FERM domain: organizing the structure and function of FAK', *Nature reviews. Molecular cell biology* 11(11): 802-14.
→ Fredriksson, S., Gullberg, M., Jarvius, J., Olsson, C., Pietras, K., Gustafsdottir, S. M., Ostman, A. and Landegren, U. (2002) 'Protein detection using proximity-dependent DNA ligation assays', *Nature biotechnology* 20(5): 473-7.
→ Fry, A. M., Mayor, T., Meraldi, P., Stierhof, Y. D., Tanaka, K. and Nigg, E. A. (1998) 'C-Nap1, a novel centrosomal coiled-coil protein and candidate substrate of the cell cycle-regulated protein kinase Nek2', *The Journal of cell biology* 141(7): 1563-74.
→ Fuller, S. D., Gowen, B. E., Reinsch, S., Sawyer, A., Buendia, B., Wepf, R. and Karsenti, E. (1995) 'The core of the mammalian centriole contains gamma-tubulin', *Current biology : CB* 5(12): 1384-93.
→ Furukawa, T., Sakamoto, H., Takeuchi, S., Ameri, M., Kuboki, Y., Yamamoto, T., Hatori, T., Yamamoto, M., Sugiyama, M., Ohike, N. et al. (2015) 'Whole exome sequencing reveals recurrent mutations in BRCA2 and FAT genes in acinar cell carcinomas of the pancreas', *Scientific reports* 5: 8829.

G - H

→ Gao, Y. B., Chen, Z. L., Li, J. G., Hu, X. D., Shi, X. J., Sun, Z. M., Zhang, F., Zhao, Z. R., Li, Z. T., Liu, Z. Y. et al. (2014) 'Genetic landscape of esophageal squamous cell carcinoma', *Nature genetics* 46(10): 1097-102.
→ Garcia, H., Miecznikowski, J. C., Safina, A., Commane, M., Ruusulehto, A., Kilpinen, S., Leach, R. W., Attwood, K., Li, Y., Degan, S. et al. (2013) 'Facilitates chromatin transcription complex is an "accelerator" of tumor transformation and potential marker and target of aggressive cancers', *Cell reports* 4(1): 159-73.
→ Garcia-Gonzalo, F. R., Corbit, K. C., Sirerol-Piquer, M. S., Ramaswami, G., Otto, E. A., Noriega, T. R., Seol, A. D., Robinson, J. F., Bennett, C. L., Josifova, D. J. et al. (2011) 'A transition zone complex regulates mammalian ciliogenesis and ciliary membrane composition', *Nature genetics* 43(8): 776-84.
→ Garoia, F., Guerra, D., Pezzoli, M. C., Lopez-Varea, A., Cavicchi, S. and Garcia-Bellido, A. (2000) 'Cell behaviour of Drosophila fat cadherin mutations in wing development', *Mechanisms of development* 94(1-2): 95-109.
→ Gaspar, P., Holder, M. V., Aerne, B. L., Janody, F. and Tapon, N. (2015) 'Zyxin antagonizes the FERM protein expanded to couple F-actin and Yorkie-dependent organ growth', *Current biology : CB* 25(6): 679-89.
→ Gaspar, P. and Tapon, N. (2014) 'Sensing the local environment: actin architecture and Hippo signalling', *Current opinion in cell biology* 31: 74-83.
→ Genevet, A., Wehr, M. C., Brain, R., Thompson, B. J. and Tapon, N. (2010) 'Kibra is a regulator of the Salvador/Warts/Hippo signaling network', *Developmental cell* 18(2): 300-8.
→ Gerdes, J. M., Liu, Y., Zaghloul, N. A., Leitch, C. C., Lawson, S. S., Kato, M., Beachy, P. A., Beales, P. L., DeMartino, G. N., Fisher, S. et al. (2007) 'Disruption of the basal body compromises proteasomal function and perturbs intracellular Wnt response', *Nature genetics* 39(11): 1350-60.
→ Ghossoub, R., Hu, Q., Failler, M., Rouyez, M. C., Spitzbarth, B., Mostowy, S., Wolfrum, U., Saunier, S., Cossart, P., Jamesnelson, W. et al. (2013) 'Septins 2, 7 and 9 and MAP4 colocalize along the axoneme in the primary cilium and control ciliary length', *Journal of cell science* 126(Pt 12): 2583-94.
→ Gilula, N. B. and Satir, P. (1972) 'The ciliary necklace. A ciliary membrane specialization', *The Journal of cell biology* 53(2): 494-509.
→ Gong, Y., Mo, C. and Fraser, S. E. (2004) 'Planar cell polarity signalling controls cell division orientation during zebrafish gastrulation', *Nature* 430(7000): 689-93.
→ Gotlieb, A. I., May, L. M., Subrahmanyan, L. and Kalnins, V. I. (1981) 'Distribution of microtubule organizing centers in migrating sheets of endothelial cells', *The Journal of cell biology* 91(2 Pt 1): 589-94.

→ Goto, T. and Keller, R. (2002) 'The planar cell polarity gene strabismus regulates convergence and extension and neural fold closure in Xenopus', *Developmental biology* 247(1): 165-81.
→ Goulev, Y., Fauny, J. D., Gonzalez-Marti, B., Flagiello, D., Silber, J. and Zider, A. (2008) 'SCALLOPED interacts with YORKIE, the nuclear effector of the hippo tumor-suppressor pathway in Drosophila', *Current biology : CB* 18(6): 435-41.
→ Graser, S., Stierhof, Y. D., Lavoie, S. B., Gassner, O. S., Lamla, S., Le Clech, M. and Nigg, E. A. (2007a) 'Cep164, a novel centriole appendage protein required for primary cilium formation', *The Journal of cell biology* 179(2): 321-30.
→ Graser, S., Stierhof, Y. D. and Nigg, E. A. (2007b) 'Cep68 and Cep215 (Cdk5rap2) are required for centrosome cohesion', *Journal of cell science* 120(Pt 24): 4321-31.
→ Grzeschik, N. A., Parsons, L. M., Allott, M. L., Harvey, K. F. and Richardson, H. E. (2010) 'Lgl, aPKC, and Crumbs regulate the Salvador/Warts/Hippo pathway through two distinct mechanisms', *Current biology : CB* 20(7): 573-81.
→ Gubb, D., Green, C., Huen, D., Coulson, D., Johnson, G., Tree, D., Collier, S. and Roote, J. (1999) 'The balance between isoforms of the prickle LIM domain protein is critical for planar polarity in Drosophila imaginal discs', *Genes & development* 13(17): 2315-27.
→ Guirao, B., Meunier, A., Mortaud, S., Aguilar, A., Corsi, J. M., Strehl, L., Hirota, Y., Desoeuvre, A., Boutin, C., Han, Y. G. et al. (2010) 'Coupling between hydrodynamic forces and planar cell polarity orients mammalian motile cilia', *Nature cell biology* 12(4): 341-50.
→ Guo, Z., Neilson, L. J., Zhong, H., Murray, P. S., Zanivan, S. and Zaidel-Bar, R. (2014) 'E-cadherin interactome complexity and robustness resolved by quantitative proteomics', *Science signaling* 7(354): rs7.
→ Gupta, G. D., Coyaud, E., Goncalves, J., Mojarad, B. A., Liu, Y., Wu, Q., Gheiratmand, L., Comartin, D., Tkach, J. M., Cheung, S. W. et al. (2015) 'A Dynamic Protein Interaction Landscape of the Human Centrosome-Cilium Interface', *Cell* 163(6): 1484-99.
→ Gupta, G. D., Dey, G., Swetha, M. G., Ramalingam, B., Shameer, K., Thottacherry, J. J., Kalappurakkal, J. M., Howes, M. T., Chandran, R., Das, A. et al. (2014) 'Population distribution analyses reveal a hierarchy of molecular players underlying parallel endocytic pathways', *PloS one* 9(6): e100554.
→ Gutzeit, H. O., Eberhardt, W. and Gratwohl, E. (1991) 'Laminin and basement membrane-associated microfilaments in wild-type and mutant Drosophila ovarian follicles', *Journal of cell science* 100 (Pt 4): 781-8.
→ Hale, R. and Strutt, D. (2015) 'Conservation of Planar Polarity Pathway Function Across the Animal Kingdom', *Annual review of genetics* 49: 529-51.
→ Hamaratoglu, F., Gajewski, K., Sansores-Garcia, L., Morrison, C., Tao, C. and Halder, G. (2009) 'The Hippo tumor-suppressor pathway regulates apical-domain size in parallel to tissue growth', *Journal of cell science* 122(Pt 14): 2351-9.
→ Hamaratoglu, F., Willecke, M., Kango-Singh, M., Nolo, R., Hyun, E., Tao, C., Jafar-Nejad, H. and Halder, G. (2006) 'The tumour-suppressor genes NF2/Merlin and Expanded act through Hippo signalling to regulate cell proliferation and apoptosis', *Nature cell biology* 8(1): 27-36.
→ Hamblet, N. S., Lijam, N., Ruiz-Lozano, P., Wang, J., Yang, Y., Luo, Z., Mei, L., Chien, K. R., Sussman, D. J. and Wynshaw-Boris, A. (2002) 'Dishevelled 2 is essential for cardiac outflow tract development, somite segmentation and neural tube closure', *Development* 129(24): 5827-38.
→ Hannus, M., Beitzinger, M., Engelmann, J. C., Weickert, M. T., Spang, R., Hannus, S. and Meister, G. (2014) 'siPools: highly complex but accurately defined siRNA pools eliminate off-target effects', *Nucleic acids research* 42(12): 8049-61.
→ Hao, Y., Chun, A., Cheung, K., Rashidi, B. and Yang, X. (2008) 'Tumor suppressor LATS1 is a negative regulator of oncogene YAP', *The Journal of biological chemistry* 283(9): 5496-509.
→ Happe, H., Leonhard, W. N., van der Wal, A., van de Water, B., Lantinga-van Leeuwen, I. S., Breuning, M. H., de Heer, E. and Peters, D. J. (2009) 'Toxic tubular injury in kidneys from Pkd1-deletion mice accelerates cystogenesis accompanied by dysregulated planar cell polarity and canonical Wnt signaling pathways', *Human molecular genetics* 18(14): 2532-42.
→ Harrow, J., Frankish, A., Gonzalez, J. M., Tapanari, E., Diekhans, M., Kokocinski, F., Aken, B. L., Barrell, D., Zadissa, A., Searle, S. et al. (2012) 'GENCODE: the reference human genome annotation for The ENCODE Project', *Genome research* 22(9): 1760-74.

→ Harumoto, T., Ito, M., Shimada, Y., Kobayashi, T. J., Ueda, H. R., Lu, B. and Uemura, T. (2010) 'Atypical cadherins Dachsous and Fat control dynamics of noncentrosomal microtubules in planar cell polarity', *Developmental cell* 19(3): 389-401.

→ Harvey, K. F. and Hariharan, I. K. (2012) 'The hippo pathway', *Cold Spring Harbor perspectives in biology* 4(8): a011288.

→ Harvey, K. F., Pfleger, C. M. and Hariharan, I. K. (2003) 'The Drosophila Mst ortholog, hippo, restricts growth and cell proliferation and promotes apoptosis', *Cell* 114(4): 457-67.

→ Hashimoto, M., Shinohara, K., Wang, J., Ikeuchi, S., Yoshiba, S., Meno, C., Nonaka, S., Takada, S., Hatta, K., Wynshaw-Boris, A. et al. (2010) 'Planar polarization of node cells determines the rotational axis of node cilia', *Nature cell biology* 12(2): 170-6.

→ He, R., Huang, N., Bao, Y., Zhou, H., Teng, J. and Chen, J. (2013) 'LRRC45 is a centrosome linker component required for centrosome cohesion', *Cell reports* 4(6): 1100-7.

→ Heisenberg, C. P., Tada, M., Rauch, G. J., Saude, L., Concha, M. L., Geisler, R., Stemple, D. L., Smith, J. C. and Wilson, S. W. (2000) 'Silberblick/Wnt11 mediates convergent extension movements during zebrafish gastrulation', *Nature* 405(6782): 76-81.

→ Helps, N. R., Luo, X., Barker, H. M. and Cohen, P. T. (2000) 'NIMA-related kinase 2 (Nek2), a cell-cycle-regulated protein kinase localized to centrosomes, is complexed to protein phosphatase 1', *The Biochemical journal* 349(Pt 2): 509-18.

→ Hildebrandt, F., Benzing, T. and Katsanis, N. (2011) 'Ciliopathies', *The New England journal of medicine* 364(16): 1533-43.

→ Hinchcliffe, E. H., Li, C., Thompson, E. A., Maller, J. L. and Sluder, G. (1999) 'Requirement of Cdk2-cyclin E activity for repeated centrosome reproduction in Xenopus egg extracts', *Science* 283(5403): 851-4.

→ Hossain, Z., Ali, S. M., Ko, H. L., Xu, J., Ng, C. P., Guo, K., Qi, Z., Ponniah, S., Hong, W. and Hunziker, W. (2007) 'Glomerulocystic kidney disease in mice with a targeted inactivation of Wwtr1', *Proceedings of the National Academy of Sciences of the United States of America* 104(5): 1631-6.

→ Hou, R. and Sibinga, N. E. (2009) 'Atrophin proteins interact with the Fat1 cadherin and regulate migration and orientation in vascular smooth muscle cells', *The Journal of biological chemistry* 284(11): 6955-65.

→ Hu, M. C., Mo, R., Bhella, S., Wilson, C. W., Chuang, P. T., Hui, C. C. and Rosenblum, N. D. (2006) 'GLI3-dependent transcriptional repression of Gli1, Gli2 and kidney patterning genes disrupts renal morphogenesis', *Development* 133(3): 569-78.

→ Hu, Q., Milenkovic, L., Jin, H., Scott, M. P., Nachury, M. V., Spiliotis, E. T. and Nelson, W. J. (2010) 'A septin diffusion barrier at the base of the primary cilium maintains ciliary membrane protein distribution', *Science* 329(5990): 436-9.

→ Huang, H. L., Wang, S., Yin, M. X., Dong, L., Wang, C., Wu, W., Lu, Y., Feng, M., Dai, C., Guo, X. et al. (2013) 'Par-1 regulates tissue growth by influencing hippo phosphorylation status and hippo-salvador association', *PLoS biology* 11(8): e1001620.

→ Huang, J., Wu, S., Barrera, J., Matthews, K. and Pan, D. (2005) 'The Hippo signaling pathway coordinately regulates cell proliferation and apoptosis by inactivating Yorkie, the Drosophila Homolog of YAP', *Cell* 122(3): 421-34.

→ Huangfu, D., Liu, A., Rakeman, A. S., Murcia, N. S., Niswander, L. and Anderson, K. V. (2003) 'Hedgehog signalling in the mouse requires intraflagellar transport proteins', *Nature* 426(6962): 83-7.

→ Hulpiau, P. and van Roy, F. (2009) 'Molecular evolution of the cadherin superfamily', *The international journal of biochemistry & cell biology* 41(2): 349-69.

→ Hulpiau, P. and van Roy, F. (2011) 'New insights into the evolution of metazoan cadherins', *Molecular biology and evolution* 28(1): 647-57.

→ Hulsen, T., de Vlieg, J. and Alkema, W. (2008) 'BioVenn - a web application for the comparison and visualization of biological lists using area-proportional Venn diagrams', *BMC genomics* 9: 488.

→ Hurd, T. W., Fan, S. and Margolis, B. L. (2011) 'Localization of retinitis pigmentosa 2 to cilia is regulated by Importin beta2', *Journal of cell science* 124(Pt 5): 718-26.

I - K

→ Ihara, M., Kinoshita, A., Yamada, S., Tanaka, H., Tanigaki, A., Kitano, A., Goto, M., Okubo, K., Nishiyama, H., Ogawa, O. et al. (2005) 'Cortical organization by the septin cytoskeleton is essential for structural and mechanical integrity of mammalian spermatozoa', *Developmental cell* 8(3): 343-52.

→ Iizuka-Kogo, A., Senda, T., Akiyama, T., Shimomura, A., Nomura, R., Hasegawa, Y., Yamamura, K., Kogo, H., Sawai, N. and Matsuzaki, T. (2015) 'Requirement of DLG1 for cardiovascular development and tissue elongation during cochlear, enteric, and skeletal development: possible role in convergent extension', *PloS one* 10(4): e0123965.

→ Ikmi, A., Gaertner, B., Seidel, C., Srivastava, M., Zeitlinger, J. and Gibson, M. C. (2014) 'Molecular evolution of the Yap/Yorkie proto-oncogene and elucidation of its core transcriptional program', *Molecular biology and evolution* 31(6): 1375-90.

→ Ireton, R. C., Davis, M. A., van Hengel, J., Mariner, D. J., Barnes, K., Thoreson, M. A., Anastasiadis, P. Z., Matrisian, L., Bundy, L. M., Sealy, L. et al. (2002) 'A novel role for p120 catenin in E-cadherin function', *The Journal of cell biology* 159(3): 465-76.

→ Ishikawa, H., Tamura, A., Matsui, T., Sasaki, H., Hakoshima, T. and Tsukita, S. (2001) 'Structural conversion between open and closed forms of radixin: low-angle shadowing electron microscopy', *Journal of molecular biology* 310(5): 973-8.

→ Ishikawa, H. O., Takeuchi, H., Haltiwanger, R. S. and Irvine, K. D. (2008) 'Four-jointed is a Golgi kinase that phosphorylates a subset of cadherin domains', *Science* 321(5887): 401-4.

→ Ishiuchi, T., Misaki, K., Yonemura, S., Takeichi, M. and Tanoue, T. (2009) 'Mammalian Fat and Dachsous cadherins regulate apical membrane organization in the embryonic cerebral cortex', *The Journal of cell biology* 185(6): 959-67.

→ Ito, T., Taniguchi, H., Fukagai, K., Okamuro, S. and Kobayashi, A. (2015) 'Inhibitory mechanism of FAT4 gene expression in response to actin dynamics during Src-induced carcinogenesis', *PloS one* 10(2): e0118336.

→ Jackson, A. L., Bartz, S. R., Schelter, J., Kobayashi, S. V., Burchard, J., Mao, M., Li, B., Cavet, G. and Linsley, P. S. (2003) 'Expression profiling reveals off-target gene regulation by RNAi', *Nature biotechnology* 21(6): 635-7.

→ Jaiswal, M., Agrawal, N. and Sinha, P. (2006) 'Fat and Wingless signaling oppositely regulate epithelial cell-cell adhesion and distal wing development in Drosophila', *Development* 133(5): 925-35.

→ Jenny, A., Darken, R. S., Wilson, P. A. and Mlodzik, M. (2003) 'Prickle and Strabismus form a functional complex to generate a correct axis during planar cell polarity signaling', *The EMBO journal* 22(17): 4409-20.

→ Jenny, A., Reynolds-Kenneally, J., Das, G., Burnett, M. and Mlodzik, M. (2005) 'Diego and Prickle regulate Frizzled planar cell polarity signalling by competing for Dishevelled binding', *Nature cell biology* 7(7): 691-7.

→ Jessen, J. R., Topczewski, J., Bingham, S., Sepich, D. S., Marlow, F., Chandrasekhar, A. and Solnica-Krezel, L. (2002) 'Zebrafish trilobite identifies new roles for Strabismus in gastrulation and neuronal movements', *Nature cell biology* 4(8): 610-5.

→ Jia, J., Zhang, L., Zhang, Q., Tong, C., Wang, B., Hou, F., Amanai, K. and Jiang, J. (2005) 'Phosphorylation by double-time/CKIepsilon and CKIalpha targets cubitus interruptus for Slimb/beta-TRCP-mediated proteolytic processing', *Developmental cell* 9(6): 819-30.

→ Jia, J., Zhang, W., Wang, B., Trinko, R. and Jiang, J. (2003) 'The Drosophila Ste20 family kinase dMST functions as a tumor suppressor by restricting cell proliferation and promoting apoptosis', *Genes & development* 17(20): 2514-9.

→ Jonassen, J. A., San Agustin, J., Follit, J. A. and Pazour, G. J. (2008) 'Deletion of IFT20 in the mouse kidney causes misorientation of the mitotic spindle and cystic kidney disease', *The Journal of cell biology* 183(3): 377-84.

→ Jones, C., Roper, V. C., Foucher, I., Qian, D., Banizs, B., Petit, C., Yoder, B. K. and Chen, P. (2008) 'Ciliary proteins link basal body polarization to planar cell polarity regulation', *Nature genetics* 40(1): 69-77.

→ Joo, K., Kim, C. G., Lee, M. S., Moon, H. Y., Lee, S. H., Kim, M. J., Kweon, H. S., Park, W. Y., Kim, C. H., Gleeson, J. G. et al. (2013) 'CCDC41 is required for ciliary vesicle docking to the mother centriole', *Proceedings of the National Academy of Sciences of the United States of America* 110(15): 5987-92.

→ Jung, H. Y., Cho, H., Oh, M. H., Lee, J. H., Lee, H. J., Jang, S. H. and Lee, M. S. (2015) 'Loss of FAT Atypical Cadherin 4 Expression Is Associated with High Pathologic T Stage in Radically Resected Gastric Cancer', *Journal of gastric cancer* 15(1): 39-45.

→ Justice, R. W., Zilian, O., Woods, D. F., Noll, M. and Bryant, P. J. (1995) 'The Drosophila tumor suppressor gene warts encodes a homolog of human myotonic dystrophy kinase and is required for the control of cell shape and proliferation', *Genes & development* 9(5): 534-46.

→ Kanai, F., Marignani, P. A., Sarbassova, D., Yagi, R., Hall, R. A., Donowitz, M., Hisaminato, A., Fujiwara, T., Ito, Y., Cantley, L. C. et al. (2000) 'TAZ: a novel transcriptional co-activator regulated by interactions with 14-3-3 and PDZ domain proteins', *The EMBO journal* 19(24): 6778-91.

→ Kango-Singh, M., Nolo, R., Tao, C., Verstreken, P., Hiesinger, P. R., Bellen, H. J. and Halder, G. (2002) 'Shar-pei mediates cell proliferation arrest during imaginal disc growth in Drosophila', *Development* 129(24): 5719-30.

→ Kaplan, O. I., Molla-Herman, A., Cevik, S., Ghossoub, R., Kida, K., Kimura, Y., Jenkins, P., Martens, J. R., Setou, M., Benmerah, A. et al. (2010) 'The AP-1 clathrin adaptor facilitates cilium formation and functions with RAB-8 in C. elegans ciliary membrane transport', *Journal of cell science* 123(Pt 22): 3966-77.

→ Karner, C. M., Chirumamilla, R., Aoki, S., Igarashi, P., Wallingford, J. B. and Carroll, T. J. (2009) 'Wnt9b signaling regulates planar cell polarity and kidney tubule morphogenesis', *Nature genetics* 41(7): 793-9.

→ Kee, H. L., Dishinger, J. F., Blasius, T. L., Liu, C. J., Margolis, B. and Verhey, K. J. (2012) 'A size-exclusion permeability barrier and nucleoporins characterize a ciliary pore complex that regulates transport into cilia', *Nature cell biology* 14(4): 431-7.

→ Kessner, D., Chambers, M., Burke, R., Agus, D. and Mallick, P. (2008) 'ProteoWizard: open source software for rapid proteomics tools development', *Bioinformatics* 24(21): 2534-6.

→ Kibar, Z., Vogan, K. J., Groulx, N., Justice, M. J., Underhill, D. A. and Gros, P. (2001) 'Ltap, a mammalian homolog of Drosophila Strabismus/Van Gogh, is altered in the mouse neural tube mutant Loop-tail', *Nature genetics* 28(3): 251-5.

→ Kim, D. I., Birendra, K. C., Zhu, W., Motamedchaboki, K., Doye, V. and Roux, K. J. (2014a) 'Probing nuclear pore complex architecture with proximity-dependent biotinylation', *Proceedings of the National Academy of Sciences of the United States of America* 111(24): E2453-61.

→ Kim, H., Xu, H., Yao, Q., Li, W., Huang, Q., Outeda, P., Cebotaru, V., Chiaravalli, M., Boletta, A., Piontek, K. et al. (2014b) 'Ciliary membrane proteins traffic through the Golgi via a Rabep1/GGA1/Arl3-dependent mechanism', *Nature communications* 5: 5482.

→ Kim, S., Lee, K., Choi, J. H., Ringstad, N. and Dynlacht, B. D. (2015) 'Nek2 activation of Kif24 ensures cilium disassembly during the cell cycle', *Nature communications* 6: 8087.

→ Kim, S., Zaghloul, N. A., Bubenshchikova, E., Oh, E. C., Rankin, S., Katsanis, N., Obara, T. and Tsiokas, L. (2011) 'Nde1-mediated inhibition of ciliogenesis affects cell cycle re-entry', *Nature cell biology* 13(4): 351-60.

→ Kim, S. K., Shindo, A., Park, T. J., Oh, E. C., Ghosh, S., Gray, R. S., Lewis, R. A., Johnson, C. A., Attie-Bittach, T., Katsanis, N. et al. (2010) 'Planar cell polarity acts through septins to control collective cell movement and ciliogenesis', *Science* 329(5997): 1337-40.

→ Kinzel, D., Boldt, K., Davis, E. E., Burtscher, I., Trumbach, D., Diplas, B., Attie-Bitach, T., Wurst, W., Katsanis, N., Ueffing, M. et al. (2010) 'Pitchfork regulates primary cilia disassembly and left-right asymmetry', *Developmental cell* 19(1): 66-77.

→ Kiss, A., Troyanovsky, R. B. and Troyanovsky, S. M. (2008) 'p120-catenin is a key component of the cadherin-gamma-secretase supercomplex', *Molecular biology of the cell* 19(10): 4042-50.

→ Kissel, H., Georgescu, M. M., Larisch, S., Manova, K., Hunnicutt, G. R. and Steller, H. (2005) 'The Sept4 septin locus is required for sperm terminal differentiation in mice', *Developmental cell* 8(3): 353-64.

→ Klein, T. J., Jenny, A., Djiane, A. and Mlodzik, M. (2006) 'CKIepsilon/discs overgrown promotes both Wnt-Fz/beta-catenin and Fz/PCP signaling in Drosophila', *Current biology : CB* 16(13): 1337-43.

→ Kleinschmit, A., Koyama, T., Dejima, K., Hayashi, Y., Kamimura, K. and Nakato, H. (2010) 'Drosophila heparan sulfate 6-O endosulfatase regulates Wingless morphogen gradient formation', *Developmental biology* 345(2): 204-14.

→ Klingensmith, J., Nusse, R. and Perrimon, N. (1994) 'The Drosophila segment polarity gene dishevelled encodes a novel protein required for response to the wingless signal', *Genes & development* 8(1): 118-30.
→ Knodler, A., Feng, S., Zhang, J., Zhang, X., Das, A., Peranen, J. and Guo, W. (2010) 'Coordination of Rab8 and Rab11 in primary ciliogenesis', *Proceedings of the National Academy of Sciences of the United States of America* 107(14): 6346-51.
→ Knust, E., Tepass, U. and Wodarz, A. (1993) 'crumbs and stardust, two genes of Drosophila required for the development of epithelial cell polarity', *Development*: 261-8.
→ Kobayashi, T., Tsang, W. Y., Li, J., Lane, W. and Dynlacht, B. D. (2011) 'Centriolar kinesin Kif24 interacts with CP110 to remodel microtubules and regulate ciliogenesis', *Cell* 145(6): 914-25.
→ Kozminski, K. G., Beech, P. L. and Rosenbaum, J. L. (1995) 'The Chlamydomonas kinesin-like protein FLA10 is involved in motility associated with the flagellar membrane', *The Journal of cell biology* 131(6 Pt 1): 1517-27.
→ Kozminski, K. G., Johnson, K. A., Forscher, P. and Rosenbaum, J. L. (1993) 'A motility in the eukaryotic flagellum unrelated to flagellar beating', *Proceedings of the National Academy of Sciences of the United States of America* 90(12): 5519-23.
→ Krasnoperov, V., Lu, Y., Buryanovsky, L., Neubert, T. A., Ichtchenko, K. and Petrenko, A. G. (2002) 'Post-translational proteolytic processing of the calcium-independent receptor of alpha-latrotoxin (CIRL), a natural chimera of the cell adhesion protein and the G protein-coupled receptor. Role of the G protein-coupled receptor proteolysis site (GPS) motif', *The Journal of biological chemistry* 277(48): 46518-26.
→ Kupfer, A., Louvard, D. and Singer, S. J. (1982) 'Polarization of the Golgi apparatus and the microtubule-organizing center in cultured fibroblasts at the edge of an experimental wound', *Proceedings of the National Academy of Sciences of the United States of America* 79(8): 2603-7.
→ Kurbegovic, A., Kim, H., Xu, H., Yu, S., Cruanes, J., Maser, R. L., Boletta, A., Trudel, M. and Qian, F. (2014) 'Novel functional complexity of polycystin-1 by GPS cleavage in vivo: role in polycystic kidney disease', *Molecular and cellular biology* 34(17): 3341-53.
→ Kwitny, S., Klaus, A. V. and Hunnicutt, G. R. (2010) 'The annulus of the mouse sperm tail is required to establish a membrane diffusion barrier that is engaged during the late steps of spermiogenesis', *Biology of reproduction* 82(4): 669-78.
→ Kwon, Y., Vinayagam, A., Sun, X., Dephoure, N., Gygi, S. P., Hong, P. and Perrimon, N. (2013) 'The Hippo signaling pathway interactome', *Science* 342(6159): 737-40.

L - M

→ Lai, E. C. (2002) 'Micro RNAs are complementary to 3' UTR sequence motifs that mediate negative post-transcriptional regulation', *Nature genetics* 30(4): 363-4.
→ Lai, Z. C., Wei, X., Shimizu, T., Ramos, E., Rohrbaugh, M., Nikolaidis, N., Ho, L. L. and Li, Y. (2005) 'Control of cell proliferation and apoptosis by mob as tumor suppressor, mats', *Cell* 120(5): 675-85.
→ Lambert, J. P., Tucholska, M., Go, C., Knight, J. D. and Gingras, A. C. (2015) 'Proximity biotinylation and affinity purification are complementary approaches for the interactome mapping of chromatin-associated protein complexes', *Journal of proteomics* 118: 81-94.
→ Lane, M. D., Rominger, K. L., Young, D. L. and Lynen, F. (1964) 'The Enzymatic Synthesis of Holotranscarboxylase from Apotranscarboxylase and (+)-Biotin. Ii. Investigation of the Reaction Mechanism', *The Journal of biological chemistry* 239: 2865-71.
→ Laprise, P., Lau, K. M., Harris, K. P., Silva-Gagliardi, N. F., Paul, S. M., Beronja, S., Beitel, G. J., McGlade, C. J. and Tepass, U. (2009) 'Yurt, Coracle, Neurexin IV and the Na(+),K(+)-ATPase form a novel group of epithelial polarity proteins', *Nature* 459(7250): 1141-5.
→ Lawrence, P. A., Casal, J. and Struhl, G. (2002) 'Towards a model of the organisation of planar polarity and pattern in the Drosophila abdomen', *Development* 129(11): 2749-60.
→ Lawrence, P. A., Struhl, G. and Casal, J. (2007) 'Planar cell polarity: one or two pathways?', *Nature reviews. Genetics* 8(7): 555-63.
→ Lee, K. H., Johmura, Y., Yu, L. R., Park, J. E., Gao, Y., Bang, J. K., Zhou, M., Veenstra, T. D., Yeon Kim, B. and Lee, K. S. (2012) 'Identification of a novel Wnt5a-CK1varepsilon-Dvl2-Plk1-mediated primary cilia disassembly pathway', *The EMBO journal* 31(14): 3104-17.

→ Lee, S. H. and Somlo, S. (2014) 'Cyst growth, polycystins, and primary cilia in autosomal dominant polycystic kidney disease', *Kidney research and clinical practice* 33(2): 73-8.
→ Lei, Q. Y., Zhang, H., Zhao, B., Zha, Z. Y., Bai, F., Pei, X. H., Zhao, S., Xiong, Y. and Guan, K. L. (2008) 'TAZ promotes cell proliferation and epithelial-mesenchymal transition and is inhibited by the hippo pathway', *Molecular and cellular biology* 28(7): 2426-36.
→ Li, Q., Li, S., Mana-Capelli, S., Roth Flach, R. J., Danai, L. V., Amcheslavsky, A., Nie, Y., Kaneko, S., Yao, X., Chen, X. et al. (2014a) 'The conserved misshapen-warts-Yorkie pathway acts in enteroblasts to regulate intestinal stem cells in Drosophila', *Developmental cell* 31(3): 291-304.
→ Li, W., Cooper, J., Zhou, L., Yang, C., Erdjument-Bromage, H., Zagzag, D., Snuderl, M., Ladanyi, M., Hanemann, C. O., Zhou, P. et al. (2014b) 'Merlin/NF2 loss-driven tumorigenesis linked to CRL4(DCAF1)-mediated inhibition of the hippo pathway kinases Lats1 and 2 in the nucleus', *Cancer cell* 26(1): 48-60.
→ Li, W., You, L., Cooper, J., Schiavon, G., Pepe-Caprio, A., Zhou, L., Ishii, R., Giovannini, M., Hanemann, C. O., Long, S. B. et al. (2010) 'Merlin/NF2 suppresses tumorigenesis by inhibiting the E3 ubiquitin ligase CRL4(DCAF1) in the nucleus', *Cell* 140(4): 477-90.
→ Li, Y., Santoso, N. G., Yu, S., Woodward, O. M., Qian, F. and Guggino, W. B. (2009) 'Polycystin-1 interacts with inositol 1,4,5-trisphosphate receptor to modulate intracellular Ca2+ signaling with implications for polycystic kidney disease', *The Journal of biological chemistry* 284(52): 36431-41.
→ Lim, S. T. (2013) 'Nuclear FAK: a new mode of gene regulation from cellular adhesions', *Molecules and cells* 36(1): 1-6.
→ Lin, D. C., Hao, J. J., Nagata, Y., Xu, L., Shang, L., Meng, X., Sato, Y., Okuno, Y., Varela, A. M., Ding, L. W. et al. (2014) 'Genomic and molecular characterization of esophageal squamous cell carcinoma', *Nature genetics* 46(5): 467-73.
→ Lin, Y. C., Niewiadomski, P., Lin, B., Nakamura, H., Phua, S. C., Jiao, J., Levchenko, A., Inoue, T. and Rohatgi, R. (2013) 'Chemically inducible diffusion trap at cilia reveals molecular sieve-like barrier', *Nature chemical biology* 9(7): 437-43.
→ Ling, C., Zheng, Y., Yin, F., Yu, J., Huang, J., Hong, Y., Wu, S. and Pan, D. (2010) 'The apical transmembrane protein Crumbs functions as a tumor suppressor that regulates Hippo signaling by binding to Expanded', *Proceedings of the National Academy of Sciences of the United States of America* 107(23): 10532-7.
→ Liu, A., Wang, B. and Niswander, L. A. (2005) 'Mouse intraflagellar transport proteins regulate both the activator and repressor functions of Gli transcription factors', *Development* 132(13): 3103-11.
→ Liu, G., Zhang, J., Larsen, B., Stark, C., Breitkreutz, A., Lin, Z. Y., Breitkreutz, B. J., Ding, Y., Colwill, K., Pasculescu, A. et al. (2010) 'ProHits: integrated software for mass spectrometry-based interaction proteomics', *Nature biotechnology* 28(10): 1015-7.
→ Logeat, F., Bessia, C., Brou, C., LeBail, O., Jarriault, S., Seidah, N. G. and Israel, A. (1998) 'The Notch1 receptor is cleaved constitutively by a furin-like convertase', *Proceedings of the National Academy of Sciences of the United States of America* 95(14): 8108-12.
→ Lu, Q., Insinna, C., Ott, C., Stauffer, J., Pintado, P. A., Rahajeng, J., Baxa, U., Walia, V., Cuenca, A., Hwang, Y. S. et al. (2015) 'Early steps in primary cilium assembly require EHD1/EHD3-dependent ciliary vesicle formation', *Nature cell biology* 17(3): 228-40.
→ Luders, J. and Stearns, T. (2007) 'Microtubule-organizing centres: a re-evaluation', *Nature reviews. Molecular cell biology* 8(2): 161-7.
→ Luyten, A., Su, X., Gondela, S., Chen, Y., Rompani, S., Takakura, A. and Zhou, J. (2010) 'Aberrant regulation of planar cell polarity in polycystic kidney disease', *Journal of the American Society of Nephrology : JASN* 21(9): 1521-32.
→ Ma, D., Yang, C. H., McNeill, H., Simon, M. A. and Axelrod, J. D. (2003) 'Fidelity in planar cell polarity signalling', *Nature* 421(6922): 543-7.
→ MacDonald, B. T., Tamai, K. and He, X. (2009) 'Wnt/beta-catenin signaling: components, mechanisms, and diseases', *Developmental cell* 17(1): 9-26.
→ Magg, T., Schreiner, D., Solis, G. P., Bade, E. G. and Hofer, H. W. (2005) 'Processing of the human protocadherin Fat1 and translocation of its cytoplasmic domain to the nucleus', *Experimental cell research* 307(1): 100-8.

→ Mahoney, P. A., Weber, U., Onofrechuk, P., Biessmann, H., Bryant, P. J. and Goodman, C. S. (1991) 'The fat tumor suppressor gene in Drosophila encodes a novel member of the cadherin gene superfamily', *Cell* 67(5): 853-68.
→ Maitra, S., Kulikauskas, R. M., Gavilan, H. and Fehon, R. G. (2006) 'The tumor suppressors Merlin and Expanded function cooperatively to modulate receptor endocytosis and signaling', *Current biology : CB* 16(7): 702-9.
→ Makita, R., Uchijima, Y., Nishiyama, K., Amano, T., Chen, Q., Takeuchi, T., Mitani, A., Nagase, T., Yatomi, Y., Aburatani, H. et al. (2008) 'Multiple renal cysts, urinary concentration defects, and pulmonary emphysematous changes in mice lacking TAZ', *American journal of physiology. Renal physiology* 294(3): F542-53.
→ Mao, Y., Francis-West, P. and Irvine, K. D. (2015) 'Fat4/Dchs1 signaling between stromal and cap mesenchyme cells influences nephrogenesis and ureteric bud branching', *Development* 142(15): 2574-85.
→ Mao, Y., Kucuk, B. and Irvine, K. D. (2009) 'Drosophila lowfat, a novel modulator of Fat signaling', *Development* 136(19): 3223-33.
→ Mao, Y., Mulvaney, J., Zakaria, S., Yu, T., Morgan, K. M., Allen, S., Basson, M. A., Francis-West, P. and Irvine, K. D. (2011a) 'Characterization of a Dchs1 mutant mouse reveals requirements for Dchs1-Fat4 signaling during mammalian development', *Development* 138(5): 947-57.
→ Mao, Y., Rauskolb, C., Cho, E., Hu, W. L., Hayter, H., Minihan, G., Katz, F. N. and Irvine, K. D. (2006) 'Dachs: an unconventional myosin that functions downstream of Fat to regulate growth, affinity and gene expression in Drosophila', *Development* 133(13): 2539-51.
→ Mao, Y., Tournier, A. L., Bates, P. A., Gale, J. E., Tapon, N. and Thompson, B. J. (2011b) 'Planar polarization of the atypical myosin Dachs orients cell divisions in Drosophila', *Genes & development* 25(2): 131-6.
→ Mao, Y., Tournier, A. L., Hoppe, A., Kester, L., Thompson, B. J. and Tapon, N. (2013) 'Differential proliferation rates generate patterns of mechanical tension that orient tissue growth', *The EMBO journal* 32(21): 2790-803.
→ Marciano, D. K., Brakeman, P. R., Lee, C. Z., Spivak, N., Eastburn, D. J., Bryant, D. M., Beaudoin, G. M., 3rd, Hofmann, I., Mostov, K. E. and Reichardt, L. F. (2011) 'p120 catenin is required for normal renal tubulogenesis and glomerulogenesis', *Development* 138(10): 2099-109.
→ Mariner, D. J., Wang, J. and Reynolds, A. B. (2000) 'ARVCF localizes to the nucleus and adherens junction and is mutually exclusive with p120(ctn) in E-cadherin complexes', *Journal of cell science* 113 (Pt 8): 1481-90.
→ Marshall, W. F. and Rosenbaum, J. L. (2001) 'Intraflagellar transport balances continuous turnover of outer doublet microtubules: implications for flagellar length control', *The Journal of cell biology* 155(3): 405-14.
→ Martell, J. D., Deerinck, T. J., Sancak, Y., Poulos, T. L., Mootha, V. K., Sosinsky, G. E., Ellisman, M. H. and Ting, A. Y. (2012) 'Engineered ascorbate peroxidase as a genetically encoded reporter for electron microscopy', *Nature biotechnology* 30(11): 1143-8.
→ Matakatsu, H. and Blair, S. S. (2004) 'Interactions between Fat and Dachsous and the regulation of planar cell polarity in the Drosophila wing', *Development* 131(15): 3785-94.
→ Matakatsu, H. and Blair, S. S. (2006) 'Separating the adhesive and signaling functions of the Fat and Dachsous protocadherins', *Development* 133(12): 2315-24.
→ Matakatsu, H. and Blair, S. S. (2008) 'The DHHC palmitoyltransferase approximated regulates Fat signaling and Dachs localization and activity', *Current biology : CB* 18(18): 1390-5.
→ Matakatsu, H. and Blair, S. S. (2012) 'Separating planar cell polarity and Hippo pathway activities of the protocadherins Fat and Dachsous', *Development* 139(8): 1498-508.
→ Matis, M. and Axelrod, J. D. (2013) 'Regulation of PCP by the Fat signaling pathway', *Genes & development* 27(20): 2207-20.
→ May, S. R., Ashique, A. M., Karlen, M., Wang, B., Shen, Y., Zarbalis, K., Reiter, J., Ericson, J. and Peterson, A. S. (2005) 'Loss of the retrograde motor for IFT disrupts localization of Smo to cilia and prevents the expression of both activator and repressor functions of Gli', *Developmental biology* 287(2): 378-89.
→ Mazelova, J., Ransom, N., Astuto-Gribble, L., Wilson, M. C. and Deretic, D. (2009) 'Syntaxin 3 and SNAP-25 pairing, regulated by omega-3 docosahexaenoic acid, controls the delivery of rhodopsin for the biogenesis of cilia-derived sensory organelles, the rod outer segments', *Journal of cell science* 122(Pt 12): 2003-13.

→ McCartney, B. M. and Fehon, R. G. (1996) 'Distinct cellular and subcellular patterns of expression imply distinct functions for the Drosophila homologues of moesin and the neurofibromatosis 2 tumor suppressor, merlin', *The Journal of cell biology* 133(4): 843-52.
→ McCartney, B. M., Kulikauskas, R. M., LaJeunesse, D. R. and Fehon, R. G. (2000) 'The neurofibromatosis-2 homologue, Merlin, and the tumor suppressor expanded function together in Drosophila to regulate cell proliferation and differentiation', *Development* 127(6): 1315-24.
→ McDermott, K. M., Liu, B. Y., Tlsty, T. D. and Pazour, G. J. (2010) 'Primary cilia regulate branching morphogenesis during mammary gland development', *Current biology : CB* 20(8): 731-7.
→ McGrath, J., Somlo, S., Makova, S., Tian, X. and Brueckner, M. (2003) 'Two populations of node monocilia initiate left-right asymmetry in the mouse', *Cell* 114(1): 61-73.
→ Medina, E., Williams, J., Klipfell, E., Zarnescu, D., Thomas, G. and Le Bivic, A. (2002) 'Crumbs interacts with moesin and beta(Heavy)-spectrin in the apical membrane skeleton of Drosophila', *The Journal of cell biology* 158(5): 941-51.
→ Menco, M. (1980) 'Qualitative and quantitative freeze-fracture studies on olfactory and respiratory epithelial surfaces of frog, ox, rat, and dog. IV. Ciliogenesis and ciliary necklaces (including high-voltage observations)', *Cell and tissue research* 212(1): 1-16.
→ Meng, Z., Moroishi, T., Mottier-Pavie, V., Plouffe, S. W., Hansen, C. G., Hong, A. W., Park, H. W., Mo, J. S., Lu, W., Lu, S. et al. (2015) 'MAP4K family kinases act in parallel to MST1/2 to activate LATS1/2 in the Hippo pathway', *Nature communications* 6: 8357.
→ Meraldi, P., Lukas, J., Fry, A. M., Bartek, J. and Nigg, E. A. (1999) 'Centrosome duplication in mammalian somatic cells requires E2F and Cdk2-cyclin A', *Nature cell biology* 1(2): 88-93.
→ Meraldi, P. and Nigg, E. A. (2001) 'Centrosome cohesion is regulated by a balance of kinase and phosphatase activities', *Journal of cell science* 114(Pt 20): 3749-57.
→ Mitchell, B., Stubbs, J. L., Huisman, F., Taborek, P., Yu, C. and Kintner, C. (2009) 'The PCP pathway instructs the planar orientation of ciliated cells in the Xenopus larval skin', *Current biology : CB* 19(11): 924-9.
→ Mitsui, K., Nakajima, D., Ohara, O. and Nakayama, M. (2002) 'Mammalian fat3: a large protein that contains multiple cadherin and EGF-like motifs', *Biochemical and biophysical research communications* 290(4): 1260-6.
→ Moeller, M. J., Soofi, A., Braun, G. S., Li, X., Watzl, C., Kriz, W. and Holzman, L. B. (2004) 'Protocadherin FAT1 binds Ena/VASP proteins and is necessary for actin dynamics and cell polarization', *The EMBO journal* 23(19): 3769-79.
→ Mohr, O. (1923) Modifications of the sex-ratio through a sex-linked semi-lethal in Drosophila melanogaster (besides notes on an autosomal section deficiency) *Studia Mendelina: Ad Centesimum Diem Natalem Gregorii Mendelii a Grata Patria Celebrandum*: Apud Typos, Brunn, Czechoslovakia.
→ Mohr, O. L. (1929) 'Exaggeration and inhibition phenomena encountered in the analysis of an autosomal dominant', *Zeitschrift fur induktive Abstammungs- und Vererbungslehre* 50: 113-200.
→ Montcouquiol, M., Rachel, R. A., Lanford, P. J., Copeland, N. G., Jenkins, N. A. and Kelley, M. W. (2003) 'Identification of Vangl2 and Scrb1 as planar polarity genes in mammals', *Nature* 423(6936): 173-7.
→ Montcouquiol, M., Sans, N., Huss, D., Kach, J., Dickman, J. D., Forge, A., Rachel, R. A., Copeland, N. G., Jenkins, N. A., Bogani, D. et al. (2006) 'Asymmetric localization of Vangl2 and Fz3 indicate novel mechanisms for planar cell polarity in mammals', *The Journal of neuroscience : the official journal of the Society for Neuroscience* 26(19): 5265-75.
→ Moritz, M., Braunfeld, M. B., Guenebaut, V., Heuser, J. and Agard, D. A. (2000) 'Structure of the gamma-tubulin ring complex: a template for microtubule nucleation', *Nature cell biology* 2(6): 365-70.
→ Murdoch, J. N., Doudney, K., Paternotte, C., Copp, A. J. and Stanier, P. (2001) 'Severe neural tube defects in the loop-tail mouse result from mutation of Lpp1, a novel gene involved in floor plate specification', *Human molecular genetics* 10(22): 2593-601.

N - P

→ Nachury, M. V., Loktev, A. V., Zhang, Q., Westlake, C. J., Peranen, J., Merdes, A., Slusarski, D. C., Scheller, R. H., Bazan, J. F., Sheffield, V. C. et al. (2007) 'A core complex of BBS proteins cooperates with the GTPase Rab8 to promote ciliary membrane biogenesis', *Cell* 129(6): 1201-13.

→ Nagae, S., Tanoue, T. and Takeichi, M. (2007) 'Temporal and spatial expression profiles of the Fat3 protein, a giant cadherin molecule, during mouse development', *Developmental dynamics : an official publication of the American Association of Anatomists* 236(2): 534-43.

→ Nakajima, H. and Tanoue, T. (2010) 'Epithelial cell shape is regulated by Lulu proteins via myosin-II', *Journal of cell science* 123(Pt 4): 555-66.

→ Nakayama, M., Nakajima, D., Yoshimura, R., Endo, Y. and Ohara, O. (2002) 'MEGF1/fat2 proteins containing extraordinarily large extracellular domains are localized to thin parallel fibers of cerebellar granule cells', *Molecular and cellular neurosciences* 20(4): 563-78.

→ Nauli, S. M., Alenghat, F. J., Luo, Y., Williams, E., Vassilev, P., Li, X., Elia, A. E., Lu, W., Brown, E. M., Quinn, S. J. et al. (2003) 'Polycystins 1 and 2 mediate mechanosensation in the primary cilium of kidney cells', *Nature genetics* 33(2): 129-37.

→ Navarro, C., Nola, S., Audebert, S., Santoni, M. J., Arsanto, J. P., Ginestier, C., Marchetto, S., Jacquemier, J., Isnardon, D., Le Bivic, A. et al. (2005) 'Junctional recruitment of mammalian Scribble relies on E-cadherin engagement', *Oncogene* 24(27): 4330-9.

→ Nikolaev, S. I., Rimoldi, D., Iseli, C., Valsesia, A., Robyr, D., Gehrig, C., Harshman, K., Guipponi, M., Bukach, O., Zoete, V. et al. (2012) 'Exome sequencing identifies recurrent somatic MAP2K1 and MAP2K2 mutations in melanoma', *Nature genetics* 44(2): 133-9.

→ Nishio, S., Tian, X., Gallagher, A. R., Yu, Z., Patel, V., Igarashi, P. and Somlo, S. (2010) 'Loss of oriented cell division does not initiate cyst formation', *Journal of the American Society of Nephrology : JASN* 21(2): 295-302.

→ Nolo, R., Morrison, C. M., Tao, C., Zhang, X. and Halder, G. (2006) 'The bantam microRNA is a target of the hippo tumor-suppressor pathway', *Current biology : CB* 16(19): 1895-904.

→ Nonaka, S., Shiratori, H., Saijoh, Y. and Hamada, H. (2002) 'Determination of left-right patterning of the mouse embryo by artificial nodal flow', *Nature* 418(6893): 96-9.

→ Nonaka, S., Tanaka, Y., Okada, Y., Takeda, S., Harada, A., Kanai, Y., Kido, M. and Hirokawa, N. (1998) 'Randomization of left-right asymmetry due to loss of nodal cilia generating leftward flow of extraembryonic fluid in mice lacking KIF3B motor protein', *Cell* 95(6): 829-37.

→ Ocbina, P. J. and Anderson, K. V. (2008) 'Intraflagellar transport, cilia, and mammalian Hedgehog signaling: analysis in mouse embryonic fibroblasts', *Developmental dynamics : an official publication of the American Association of Anatomists* 237(8): 2030-8.

→ Ocbina, P. J., Tuson, M. and Anderson, K. V. (2009) 'Primary cilia are not required for normal canonical Wnt signaling in the mouse embryo', *PloS one* 4(8): e6839.

→ Oh, H. and Irvine, K. D. (2008) 'In vivo regulation of Yorkie phosphorylation and localization', *Development* 135(6): 1081-8.

→ Oh, H. and Irvine, K. D. (2009) 'In vivo analysis of Yorkie phosphorylation sites', *Oncogene* 28(17): 1916-27.

→ Oh, H., Reddy, B. V. and Irvine, K. D. (2009) 'Phosphorylation-independent repression of Yorkie in Fat-Hippo signaling', *Developmental biology* 335(1): 188-97.

→ Oh, H., Slattery, M., Ma, L., Crofts, A., White, K. P., Mann, R. S. and Irvine, K. D. (2013) 'Genome-wide Association of Yorkie with Chromatin and Chromatin-Remodeling Complexes', *Cell reports* 3(2): 309-18.

→ Oishi, I., Kawakami, Y., Raya, A., Callol-Massot, C. and Izpisua Belmonte, J. C. (2006) 'Regulation of primary cilia formation and left-right patterning in zebrafish by a noncanonical Wnt signaling mediator, duboraya', *Nature genetics* 38(11): 1316-22.

→ Oka, T., Mazack, V. and Sudol, M. (2008) 'Mst2 and Lats kinases regulate apoptotic function of Yes kinase-associated protein (YAP)', *The Journal of biological chemistry* 283(41): 27534-46.

→ Orphanides, G., LeRoy, G., Chang, C. H., Luse, D. S. and Reinberg, D. (1998) 'FACT, a factor that facilitates transcript elongation through nucleosomes', *Cell* 92(1): 105-16.

→ Oteiza, P., Koppen, M., Krieg, M., Pulgar, E., Farias, C., Melo, C., Preibisch, S., Muller, D., Tada, M., Hartel, S. et al. (2010) 'Planar cell polarity signalling regulates cell adhesion properties in progenitors of the zebrafish laterality organ', *Development* 137(20): 3459-68.
→ Otto, E. A., Schermer, B., Obara, T., O'Toole, J. F., Hiller, K. S., Mueller, A. M., Ruf, R. G., Hoefele, J., Beekmann, F., Landau, D. et al. (2003) 'Mutations in INVS encoding inversin cause nephronophthisis type 2, linking renal cystic disease to the function of primary cilia and left-right axis determination', *Nature genetics* 34(4): 413-20.
→ Ozawa, M., Ringwald, M. and Kemler, R. (1990) 'Uvomorulin-catenin complex formation is regulated by a specific domain in the cytoplasmic region of the cell adhesion molecule', *Proceedings of the National Academy of Sciences of the United States of America* 87(11): 4246-50.
→ Paintrand, M., Moudjou, M., Delacroix, H. and Bornens, M. (1992) 'Centrosome organization and centriole architecture: their sensitivity to divalent cations', *Journal of structural biology* 108(2): 107-28.
→ Pan, G., Feng, Y., Ambegaonkar, A. A., Sun, G., Huff, M., Rauskolb, C. and Irvine, K. D. (2013) 'Signal transduction by the Fat cytoplasmic domain', *Development* 140(4): 831-42.
→ Pan, J. and Snell, W. J. (2014) 'Organelle size: a cilium length signal regulates IFT cargo loading', *Current biology : CB* 24(2): R75-8.
→ Panic, M., Hata, S., Neuner, A. and Schiebel, E. (2015) 'The centrosomal linker and microtubules provide dual levels of spatial coordination of centrosomes', *PLoS genetics* 11(5): e1005243.
→ Pantalacci, S., Tapon, N. and Leopold, P. (2003) 'The Salvador partner Hippo promotes apoptosis and cell-cycle exit in Drosophila', *Nature cell biology* 5(10): 921-7.
→ Papermaster, D. S., Schneider, B. G. and Besharse, J. C. (1985) 'Vesicular transport of newly synthesized opsin from the Golgi apparatus toward the rod outer segment. Ultrastructural immunocytochemical and autoradiographic evidence in Xenopus retinas', *Investigative ophthalmology & visual science* 26(10): 1386-404.
→ Park, M. and Moon, R. T. (2002) 'The planar cell-polarity gene stbm regulates cell behaviour and cell fate in vertebrate embryos', *Nature cell biology* 4(1): 20-5.
→ Park, T. J., Mitchell, B. J., Abitua, P. B., Kintner, C. and Wallingford, J. B. (2008) 'Dishevelled controls apical docking and planar polarization of basal bodies in ciliated epithelial cells', *Nature genetics* 40(7): 871-9.
→ Parry, M., Rose-Zerilli, M. J., Gibson, J., Ennis, S., Walewska, R., Forster, J., Parker, H., Davis, Z., Gardiner, A., Collins, A. et al. (2013) 'Whole exome sequencing identifies novel recurrently mutated genes in patients with splenic marginal zone lymphoma', *PloS one* 8(12): e83244.
→ Patel, V., Li, L., Cobo-Stark, P., Shao, X., Somlo, S., Lin, F. and Igarashi, P. (2008) 'Acute kidney injury and aberrant planar cell polarity induce cyst formation in mice lacking renal cilia', *Human molecular genetics* 17(11): 1578-90.
→ Pathak, N., Obara, T., Mangos, S., Liu, Y. and Drummond, I. A. (2007) 'The zebrafish fleer gene encodes an essential regulator of cilia tubulin polyglutamylation', *Molecular biology of the cell* 18(11): 4353-64.
→ Pazour, G. J., Dickert, B. L. and Witman, G. B. (1999) 'The DHC1b (DHC2) isoform of cytoplasmic dynein is required for flagellar assembly', *The Journal of cell biology* 144(3): 473-81.
→ Pazour, G. J., San Agustin, J. T., Follit, J. A., Rosenbaum, J. L. and Witman, G. B. (2002) 'Polycystin-2 localizes to kidney cilia and the ciliary level is elevated in orpk mice with polycystic kidney disease', *Current biology : CB* 12(11): R378-80.
→ Pazour, G. J., Wilkerson, C. G. and Witman, G. B. (1998) 'A dynein light chain is essential for the retrograde particle movement of intraflagellar transport (IFT)', *The Journal of cell biology* 141(4): 979-92.
→ Pedrioli, P. G. (2010) 'Trans-proteomic pipeline: a pipeline for proteomic analysis', *Methods in molecular biology* 604: 213-38.
→ Pellikka, M., Tanentzapf, G., Pinto, M., Smith, C., McGlade, C. J., Ready, D. F. and Tepass, U. (2002) 'Crumbs, the Drosophila homologue of human CRB1/RP12, is essential for photoreceptor morphogenesis', *Nature* 416(6877): 143-9.
→ Pellock, B. J., Buff, E., White, K. and Hariharan, I. K. (2007) 'The Drosophila tumor suppressors Expanded and Merlin differentially regulate cell cycle exit, apoptosis, and Wingless signaling', *Developmental biology* 304(1): 102-15.

→ Perkins, L. A., Hedgecock, E. M., Thomson, J. N. and Culotti, J. G. (1986) 'Mutant sensory cilia in the nematode Caenorhabditis elegans', *Developmental biology* 117(2): 456-87.
→ Peters, K. R., Palade, G. E., Schneider, B. G. and Papermaster, D. S. (1983) 'Fine structure of a periciliary ridge complex of frog retinal rod cells revealed by ultrahigh resolution scanning electron microscopy', *The Journal of cell biology* 96(1): 265-76.
→ Phillips, H. M., Rhee, H. J., Murdoch, J. N., Hildreth, V., Peat, J. D., Anderson, R. H., Copp, A. J., Chaudhry, B. and Henderson, D. J. (2007) 'Disruption of planar cell polarity signaling results in congenital heart defects and cardiomyopathy attributable to early cardiomyocyte disorganization', *Circulation research* 101(2): 137-45.
→ Piel, M., Nordberg, J., Euteneuer, U. and Bornens, M. (2001) 'Centrosome-dependent exit of cytokinesis in animal cells', *Science* 291(5508): 1550-3.
→ Poernbacher, I., Baumgartner, R., Marada, S. K., Edwards, K. and Stocker, H. (2012) 'Drosophila Pez acts in Hippo signaling to restrict intestinal stem cell proliferation', *Current biology : CB* 22(5): 389-96.
→ Polesello, C., Huelsmann, S., Brown, N. H. and Tapon, N. (2006) 'The Drosophila RASSF homolog antagonizes the hippo pathway', *Current biology : CB* 16(24): 2459-65.
→ Porter, M. E., Bower, R., Knott, J. A., Byrd, P. and Dentler, W. (1999) 'Cytoplasmic dynein heavy chain 1b is required for flagellar assembly in Chlamydomonas', *Molecular biology of the cell* 10(3): 693-712.
→ Praetorius, H. A. and Spring, K. R. (2001) 'Bending the MDCK cell primary cilium increases intracellular calcium', *The Journal of membrane biology* 184(1): 71-9.
→ Preibisch, S., Saalfeld, S. and Tomancak, P. (2009) 'Globally optimal stitching of tiled 3D microscopic image acquisitions', *Bioinformatics* 25(11): 1463-5.
→ Price, M. A. and Kalderon, D. (2002) 'Proteolysis of the Hedgehog signaling effector Cubitus interruptus requires phosphorylation by Glycogen Synthase Kinase 3 and Casein Kinase 1', *Cell* 108(6): 823-35.
→ Pugacheva, E. N., Jablonski, S. A., Hartman, T. R., Henske, E. P. and Golemis, E. A. (2007) 'HEF1-dependent Aurora A activation induces disassembly of the primary cilium', *Cell* 129(7): 1351-63.

Q - S

→ Qi, C., Zhu, Y. T., Hu, L. and Zhu, Y. J. (2009) 'Identification of Fat4 as a candidate tumor suppressor gene in breast cancers', *International journal of cancer. Journal international du cancer* 124(4): 793-8.
→ Qin, H., Diener, D. R., Geimer, S., Cole, D. G. and Rosenbaum, J. L. (2004) 'Intraflagellar transport (IFT) cargo: IFT transports flagellar precursors to the tip and turnover products to the cell body', *The Journal of cell biology* 164(2): 255-66.
→ Rauch, T. A., Wang, Z., Wu, X., Kernstine, K. H., Riggs, A. D. and Pfeifer, G. P. (2012) 'DNA methylation biomarkers for lung cancer', *Tumour biology : the journal of the International Society for Oncodevelopmental Biology and Medicine* 33(2): 287-96.
→ Rawls, A. S., Guinto, J. B. and Wolff, T. (2002) 'The cadherins fat and dachsous regulate dorsal/ventral signaling in the Drosophila eye', *Current biology : CB* 12(12): 1021-6.
→ Reczek, D. and Bretscher, A. (1998) 'The carboxyl-terminal region of EBP50 binds to a site in the amino-terminal domain of ezrin that is masked in the dormant molecule', *The Journal of biological chemistry* 273(29): 18452-8.
→ Reinacher-Schick, A. and Gumbiner, B. M. (2001) 'Apical membrane localization of the adenomatous polyposis coli tumor suppressor protein and subcellular distribution of the beta-catenin destruction complex in polarized epithelial cells', *The Journal of cell biology* 152(3): 491-502.
→ Ren, F., Zhang, L. and Jiang, J. (2010) 'Hippo signaling regulates Yorkie nuclear localization and activity through 14-3-3 dependent and independent mechanisms', *Developmental biology* 337(2): 303-12.
→ Reynolds, A. B. (2007) 'p120-catenin: Past and present', *Biochimica et biophysica acta* 1773(1): 2-7.
→ Rhee, H. W., Zou, P., Udeshi, N. D., Martell, J. D., Mootha, V. K., Carr, S. A. and Ting, A. Y. (2013) 'Proteomic mapping of mitochondria in living cells via spatially restricted enzymatic tagging', *Science* 339(6125): 1328-31.

→ Ribeiro, P., Holder, M., Frith, D., Snijders, A. P. and Tapon, N. (2014) 'Crumbs promotes expanded recognition and degradation by the SCF(Slimb/beta-TrCP) ubiquitin ligase', *Proceedings of the National Academy of Sciences of the United States of America* 111(19): E1980-9.

→ Ribeiro, P. S., Josue, F., Wepf, A., Wehr, M. C., Rinner, O., Kelly, G., Tapon, N. and Gstaiger, M. (2010) 'Combined functional genomic and proteomic approaches identify a PP2A complex as a negative regulator of Hippo signaling', *Molecular cell* 39(4): 521-34.

→ Robinson, B. S., Huang, J., Hong, Y. and Moberg, K. H. (2010) 'Crumbs regulates Salvador/Warts/Hippo signaling in Drosophila via the FERM-domain protein Expanded', *Current biology : CB* 20(7): 582-90.

→ Rock, R., Schrauth, S. and Gessler, M. (2005) 'Expression of mouse dchs1, fjx1, and fat-j suggests conservation of the planar cell polarity pathway identified in Drosophila', *Developmental dynamics : an official publication of the American Association of Anatomists* 234(3): 747-55.

→ Rodrigues-Campos, M. and Thompson, B. J. (2014) 'The ubiquitin ligase FbxL7 regulates the Dachsous-Fat-Dachs system in Drosophila', *Development* 141(21): 4098-103.

→ Rogulja, D., Rauskolb, C. and Irvine, K. D. (2008) 'Morphogen control of wing growth through the Fat signaling pathway', *Developmental cell* 15(2): 309-21.

→ Roh, M. H., Makarova, O., Liu, C. J., Shin, K., Lee, S., Laurinec, S., Goyal, M., Wiggins, R. and Margolis, B. (2002) 'The Maguk protein, Pals1, functions as an adapter, linking mammalian homologues of Crumbs and Discs Lost', *The Journal of cell biology* 157(1): 161-72.

→ Rohatgi, R., Milenkovic, L. and Scott, M. P. (2007) 'Patched1 regulates hedgehog signaling at the primary cilium', *Science* 317(5836): 372-6.

→ Roper, K. (2012) 'Anisotropy of Crumbs and aPKC drives myosin cable assembly during tube formation', *Developmental cell* 23(5): 939-53.

→ Rosenbaum, J. L. and Child, F. M. (1967) 'Flagellar regeneration in protozoan flagellates', *The Journal of cell biology* 34(1): 345-64.

→ Ross, A. J., May-Simera, H., Eichers, E. R., Kai, M., Hill, J., Jagger, D. J., Leitch, C. C., Chapple, J. P., Munro, P. M., Fisher, S. et al. (2005) 'Disruption of Bardet-Biedl syndrome ciliary proteins perturbs planar cell polarity in vertebrates', *Nature genetics* 37(10): 1135-40.

→ Roux, K. J., Kim, D. I., Raida, M. and Burke, B. (2012) 'A promiscuous biotin ligase fusion protein identifies proximal and interacting proteins in mammalian cells', *The Journal of cell biology* 196(6): 801-10.

→ Saburi, S., Hester, I., Fischer, E., Pontoglio, M., Eremina, V., Gessler, M., Quaggin, S. E., Harrison, R., Mount, R. and McNeill, H. (2008) 'Loss of Fat4 disrupts PCP signaling and oriented cell division and leads to cystic kidney disease', *Nature genetics* 40(8): 1010-5.

→ Saburi, S., Hester, I., Goodrich, L. and McNeill, H. (2012) 'Functional interactions between Fat family cadherins in tissue morphogenesis and planar polarity', *Development* 139(10): 1806-20.

→ Sadeqzadeh, E., de Bock, C. E., Zhang, X. D., Shipman, K. L., Scott, N. M., Song, C., Yeadon, T., Oliveira, C. S., Jin, B., Hersey, P. et al. (2011) 'Dual processing of FAT1 cadherin protein by human melanoma cells generates distinct protein products', *The Journal of biological chemistry* 286(32): 28181-91.

→ Sagner, A., Merkel, M., Aigouy, B., Gaebel, J., Brankatschk, M., Julicher, F. and Eaton, S. (2012) 'Establishment of global patterns of planar polarity during growth of the Drosophila wing epithelium', *Current biology : CB* 22(14): 1296-301.

→ Sambrook, J. and Russell, D. W. (2006) 'Detection of Protein-Protein Interactions Using the GST Fusion Protein Pulldown Technique', *CSH protocols* 2006(1).

→ Sang, L., Miller, J. J., Corbit, K. C., Giles, R. H., Brauer, M. J., Otto, E. A., Baye, L. M., Wen, X., Scales, S. J., Kwong, M. et al. (2011) 'Mapping the NPHP-JBTS-MKS protein network reveals ciliopathy disease genes and pathways', *Cell* 145(4): 513-28.

→ Sansores-Garcia, L., Atkins, M., Moya, I. M., Shahmoradgoli, M., Tao, C., Mills, G. B. and Halder, G. (2013) 'Mask is required for the activity of the Hippo pathway effector Yki/YAP', *Current biology : CB* 23(3): 229-35.

→ Sansores-Garcia, L., Bossuyt, W., Wada, K., Yonemura, S., Tao, C., Sasaki, H. and Halder, G. (2011) 'Modulating F-actin organization induces organ growth by affecting the Hippo pathway', *The EMBO journal* 30(12): 2325-35.

→ Sawada, A., Kiyonari, H., Ukita, K., Nishioka, N., Imuta, Y. and Sasaki, H. (2008) 'Redundant roles of Tead1 and Tead2 in notochord development and the regulation of cell proliferation and survival', *Molecular and cellular biology* 28(10): 3177-89.

→ Schmidt, K. and Nichols, B. J. (2004) 'A barrier to lateral diffusion in the cleavage furrow of dividing mammalian cells', *Current biology : CB* 14(11): 1002-6.

→ Schroeder, M. C. and Halder, G. (2012) 'Regulation of the Hippo pathway by cell architecture and mechanical signals', *Seminars in cell & developmental biology* 23(7): 803-11.

→ Schultz, N., Marenstein, D. R., De Angelis, D. A., Wang, W. Q., Nelander, S., Jacobsen, A., Marks, D. S., Massague, J. and Sander, C. (2011) 'Off-target effects dominate a large-scale RNAi screen for modulators of the TGF-beta pathway and reveal microRNA regulation of TGFBR2', *Silence* 2: 3.

→ Sharan, S. K., Thomason, L. C., Kuznetsov, S. G. and Court, D. L. (2009) 'Recombineering: a homologous recombination-based method of genetic engineering', *Nature protocols* 4(2): 206-23.

→ Sharma, N., Kosan, Z. A., Stallworth, J. E., Berbari, N. F. and Yoder, B. K. (2011) 'Soluble levels of cytosolic tubulin regulate ciliary length control', *Molecular biology of the cell* 22(6): 806-16.

→ Sharma, P. and McNeill, H. (2013) 'Regulation of long-range planar cell polarity by Fat-Dachsous signaling', *Development* 140(18): 3869-81.

→ Shaw, R. J., Paez, J. G., Curto, M., Yaktine, A., Pruitt, W. M., Saotome, I., O'Bryan, J. P., Gupta, V., Ratner, N., Der, C. J. et al. (2001) 'The Nf2 tumor suppressor, merlin, functions in Rac-dependent signaling', *Developmental cell* 1(1): 63-72.

→ Sher, I., Hanemann, C. O., Karplus, P. A. and Bretscher, A. (2012) 'The tumor suppressor merlin controls growth in its open state, and phosphorylation converts it to a less-active more-closed state', *Developmental cell* 22(4): 703-5.

→ Sherman, L., Xu, H. M., Geist, R. T., Saporito-Irwin, S., Howells, N., Ponta, H., Herrlich, P. and Gutmann, D. H. (1997) 'Interdomain binding mediates tumor growth suppression by the NF2 gene product', *Oncogene* 15(20): 2505-9.

→ Shillingford, J. M., Murcia, N. S., Larson, C. H., Low, S. H., Hedgepeth, R., Brown, N., Flask, C. A., Novick, A. C., Goldfarb, D. A., Kramer-Zucker, A. et al. (2006) 'The mTOR pathway is regulated by polycystin-1, and its inhibition reverses renal cystogenesis in polycystic kidney disease', *Proceedings of the National Academy of Sciences of the United States of America* 103(14): 5466-71.

→ Shillingford, J. M., Piontek, K. B., Germino, G. G. and Weimbs, T. (2010) 'Rapamycin ameliorates PKD resulting from conditional inactivation of Pkd1', *Journal of the American Society of Nephrology : JASN* 21(3): 489-97.

→ Shnitsar, I., Bashkurov, M., Masson, G. R., Ogunjimi, A. A., Mosessian, S., Cabeza, E. A., Hirsch, C. L., Trcka, D., Gish, G., Jiao, J. et al. (2015) 'PTEN regulates cilia through Dishevelled', *Nature communications* 6: 8388.

→ Sidor, C. M., Brain, R. and Thompson, B. J. (2013) 'Mask proteins are cofactors of Yorkie/YAP in the Hippo pathway', *Current biology : CB* 23(3): 223-8.

→ Signor, D., Wedaman, K. P., Orozco, J. T., Dwyer, N. D., Bargmann, C. I., Rose, L. S. and Scholey, J. M. (1999) 'Role of a class DHC1b dynein in retrograde transport of IFT motors and IFT raft particles along cilia, but not dendrites, in chemosensory neurons of living Caenorhabditis elegans', *The Journal of cell biology* 147(3): 519-30.

→ Sigoillot, F. D., Lyman, S., Huckins, J. F., Adamson, B., Chung, E., Quattrochi, B. and King, R. W. (2012) 'A bioinformatics method identifies prominent off-targeted transcripts in RNAi screens', *Nature methods* 9(4): 363-6.

→ Sillibourne, J. E., Hurbain, I., Grand-Perret, T., Goud, B., Tran, P. and Bornens, M. (2013) 'Primary ciliogenesis requires the distal appendage component Cep123', *Biology open* 2(6): 535-45.

→ Silva, E., Tsatskis, Y., Gardano, L., Tapon, N. and McNeill, H. (2006) 'The tumor-suppressor gene fat controls tissue growth upstream of expanded in the hippo signaling pathway', *Current biology : CB* 16(21): 2081-9.

→ Simon, M. A. (2004) 'Planar cell polarity in the Drosophila eye is directed by graded Four-jointed and Dachsous expression', *Development* 131(24): 6175-84.

→ Simon, M. A., Xu, A., Ishikawa, H. O. and Irvine, K. D. (2010) 'Modulation of fat:dachsous binding by the cadherin domain kinase four-jointed', *Current biology : CB* 20(9): 811-7.

→ Simons, M., Gloy, J., Ganner, A., Bullerkotte, A., Bashkurov, M., Kronig, C., Schermer, B., Benzing, T., Cabello, O. A., Jenny, A. et al. (2005) 'Inversin, the gene product mutated in nephronophthisis type II, functions as a molecular switch between Wnt signaling pathways', *Nature genetics* 37(5): 537-43.

→ Sing, A., Tsatskis, Y., Fabian, L., Hester, I., Rosenfeld, R., Serricchio, M., Yau, N., Bietenhader, M., Shanbhag, R., Jurisicova, A. et al. (2014) 'The atypical cadherin fat directly regulates mitochondrial function and metabolic state', *Cell* 158(6): 1293-308.

→ Sirajuddin, M., Rice, L. M. and Vale, R. D. (2014) 'Regulation of microtubule motors by tubulin isotypes and post-translational modifications', *Nature cell biology* 16(4): 335-44.

→ Skouloudaki, K., Puetz, M., Simons, M., Courbard, J. R., Boehlke, C., Hartleben, B., Engel, C., Moeller, M. J., Englert, C., Bollig, F. et al. (2009) 'Scribble participates in Hippo signaling and is required for normal zebrafish pronephros development', *Proceedings of the National Academy of Sciences of the United States of America* 106(21): 8579-84.

→ Smalley-Freed, W. G., Efimov, A., Burnett, P. E., Short, S. P., Davis, M. A., Gumucio, D. L., Washington, M. K., Coffey, R. J. and Reynolds, A. B. (2010) 'p120-catenin is essential for maintenance of barrier function and intestinal homeostasis in mice', *The Journal of clinical investigation* 120(6): 1824-35.

→ Smalley-Freed, W. G., Efimov, A., Short, S. P., Jia, P., Zhao, Z., Washington, M. K., Robine, S., Coffey, R. J. and Reynolds, A. B. (2011) 'Adenoma formation following limited ablation of p120-catenin in the mouse intestine', *PloS one* 6(5): e19880.

→ Smith, R. K., Carroll, P. M., Allard, J. D. and Simon, M. A. (2002) 'MASK, a large ankyrin repeat and KH domain-containing protein involved in Drosophila receptor tyrosine kinase signaling', *Development* 129(1): 71-82.

→ Sokol, S. Y. (1996) 'Analysis of Dishevelled signalling pathways during Xenopus development', *Current biology : CB* 6(11): 1456-67.

→ Song, H., Hu, J., Chen, W., Elliott, G., Andre, P., Gao, B. and Yang, Y. (2010) 'Planar cell polarity breaks bilateral symmetry by controlling ciliary positioning', *Nature* 466(7304): 378-82.

→ Sopko, R., Silva, E., Clayton, L., Gardano, L., Barrios-Rodiles, M., Wrana, J., Varelas, X., Arbouzova, N. I., Shaw, S., Saburi, S. et al. (2009) 'Phosphorylation of the tumor suppressor fat is regulated by its ligand Dachsous and the kinase discs overgrown', *Current biology : CB* 19(13): 1112-7.

→ Sorokin, S. (1962) 'Centrioles and the formation of rudimentary cilia by fibroblasts and smooth muscle cells', *The Journal of cell biology* 15: 363-77.

→ Sorokin, S. P. (1968) 'Reconstructions of centriole formation and ciliogenesis in mammalian lungs', *Journal of cell science* 3(2): 207-30.

→ Spalluto, C., Wilson, D. I. and Hearn, T. (2012) 'Nek2 localises to the distal portion of the mother centriole/basal body and is required for timely cilium disassembly at the G2/M transition', *European journal of cell biology* 91(9): 675-86.

→ Squarr, A. J., Brinkmann, K., Chen, B., Steinbacher, T., Ebnet, K., Rosen, M. K. and Bogdan, S. (2016) 'Fat2 acts through the WAVE regulatory complex to drive collective cell migration during tissue rotation', *The Journal of cell biology* 212(5): 591-603.

→ Staley, B. K. and Irvine, K. D. (2012) 'Hippo signaling in Drosophila: recent advances and insights', *Developmental dynamics : an official publication of the American Association of Anatomists* 241(1): 3-15.

→ Stavridi, E. S., Harris, K. G., Huyen, Y., Bothos, J., Verwoerd, P. M., Stayrook, S. E., Pavletich, N. P., Jeffrey, P. D. and Luca, F. C. (2003) 'Crystal structure of a human Mob1 protein: toward understanding Mob-regulated cell cycle pathways', *Structure* 11(9): 1163-70.

→ Steels, J. D., Estey, M. P., Froese, C. D., Reynaud, D., Pace-Asciak, C. and Trimble, W. S. (2007) 'Sept12 is a component of the mammalian sperm tail annulus', *Cell motility and the cytoskeleton* 64(10): 794-807.

→ Stephens, R. E. (1997) 'Synthesis and turnover of embryonic sea urchin ciliary proteins during selective inhibition of tubulin synthesis and assembly', *Molecular biology of the cell* 8(11): 2187-98.

→ Struhl, G., Barbash, D. A. and Lawrence, P. A. (1997) 'Hedgehog acts by distinct gradient and signal relay mechanisms to organise cell type and cell polarity in the Drosophila abdomen', *Development* 124(11): 2155-65.

→ Struhl, G., Casal, J. and Lawrence, P. A. (2012) 'Dissecting the molecular bridges that mediate the function of Frizzled in planar cell polarity', *Development* 139(19): 3665-74.

→ Strutt, D. (2009) 'Gradients and the specification of planar polarity in the insect cuticle', *Cold Spring Harbor perspectives in biology* 1(5): a000489.
→ Strutt, D., Johnson, R., Cooper, K. and Bray, S. (2002) 'Asymmetric localization of frizzled and the determination of notch-dependent cell fate in the Drosophila eye', *Current biology : CB* 12(10): 813-24.
→ Strutt, D. and Strutt, H. (2007) 'Differential activities of the core planar polarity proteins during Drosophila wing patterning', *Developmental biology* 302(1): 181-94.
→ Strutt, D. I. (2001) 'Asymmetric localization of frizzled and the establishment of cell polarity in the Drosophila wing', *Molecular cell* 7(2): 367-75.
→ Strutt, H., Mundy, J., Hofstra, K. and Strutt, D. (2004) 'Cleavage and secretion is not required for Four-jointed function in Drosophila patterning', *Development* 131(4): 881-90.
→ Strutt, H., Price, M. A. and Strutt, D. (2006) 'Planar polarity is positively regulated by casein kinase Iepsilon in Drosophila', *Current biology : CB* 16(13): 1329-36.
→ Strutt, H. and Strutt, D. (2002) 'Nonautonomous planar polarity patterning in Drosophila: dishevelled-independent functions of frizzled', *Developmental cell* 3(6): 851-63.
→ Strutt, H. and Strutt, D. (2008) 'Differential stability of flamingo protein complexes underlies the establishment of planar polarity', *Current biology : CB* 18(20): 1555-64.
→ Strutt, H. and Strutt, D. (2009) 'Asymmetric localisation of planar polarity proteins: Mechanisms and consequences', *Seminars in cell & developmental biology* 20(8): 957-63.
→ Sugiyama, Y., Shelley, E. J., Badouel, C., McNeill, H. and McAvoy, J. W. (2015) 'Atypical Cadherin Fat1 Is Required for Lens Epithelial Cell Polarity and Proliferation but Not for Fiber Differentiation', *Investigative ophthalmology & visual science* 56(6): 4099-107.
→ Sun, S., Reddy, B. V. and Irvine, K. D. (2015) 'Localization of Hippo signalling complexes and Warts activation in vivo', *Nature communications* 6: 8402.

T - V

→ Tada, M. and Smith, J. C. (2000) 'Xwnt11 is a target of Xenopus Brachyury: regulation of gastrulation movements via Dishevelled, but not through the canonical Wnt pathway', *Development* 127(10): 2227-38.
→ Takeuchi, M., Nakabayashi, J., Sakaguchi, T., Yamamoto, T. S., Takahashi, H., Takeda, H. and Ueno, N. (2003) 'The prickle-related gene in vertebrates is essential for gastrulation cell movements', *Current biology : CB* 13(8): 674-9.
→ Takizawa, P. A., DeRisi, J. L., Wilhelm, J. E. and Vale, R. D. (2000) 'Plasma membrane compartmentalization in yeast by messenger RNA transport and a septin diffusion barrier', *Science* 290(5490): 341-4.
→ Tanos, B. E., Yang, H. J., Soni, R., Wang, W. J., Macaluso, F. P., Asara, J. M. and Tsou, M. F. (2013) 'Centriole distal appendages promote membrane docking, leading to cilia initiation', *Genes & development* 27(2): 163-8.
→ Tanoue, T. and Takeichi, M. (2004) 'Mammalian Fat1 cadherin regulates actin dynamics and cell-cell contact', *The Journal of cell biology* 165(4): 517-28.
→ Tanoue, T. and Takeichi, M. (2005) 'New insights into Fat cadherins', *Journal of cell science* 118(Pt 11): 2347-53.
→ Tao, W., Zhang, S., Turenchalk, G. S., Stewart, R. A., St John, M. A., Chen, W. and Xu, T. (1999) 'Human homologue of the Drosophila melanogaster lats tumour suppressor modulates CDC2 activity', *Nature genetics* 21(2): 177-81.
→ Tapon, N., Harvey, K. F., Bell, D. W., Wahrer, D. C., Schiripo, T. A., Haber, D. and Hariharan, I. K. (2002) 'salvador Promotes both cell cycle exit and apoptosis in Drosophila and is mutated in human cancer cell lines', *Cell* 110(4): 467-78.
→ Taylor, J., Abramova, N., Charlton, J. and Adler, P. N. (1998) 'Van Gogh: a new Drosophila tissue polarity gene', *Genetics* 150(1): 199-210.
→ Tepass, U., Theres, C. and Knust, E. (1990) 'crumbs encodes an EGF-like protein expressed on apical membranes of Drosophila epithelial cells and required for organization of epithelia', *Cell* 61(5): 787-99.
→ Theisen, H., Purcell, J., Bennett, M., Kansagara, D., Syed, A. and Marsh, J. L. (1994) 'dishevelled is required during wingless signaling to establish both cell polarity and cell identity', *Development* 120(2): 347-60.

→ Thompson, B. J. and Cohen, S. M. (2006) 'The Hippo pathway regulates the bantam microRNA to control cell proliferation and apoptosis in Drosophila', *Cell* 126(4): 767-74.
→ Thoreson, M. A., Anastasiadis, P. Z., Daniel, J. M., Ireton, R. C., Wheelock, M. J., Johnson, K. R., Hummingbird, D. K. and Reynolds, A. B. (2000) 'Selective uncoupling of p120(ctn) from E-cadherin disrupts strong adhesion', *The Journal of cell biology* 148(1): 189-202.
→ Tissir, F., Qu, Y., Montcouquiol, M., Zhou, L., Komatsu, K., Shi, D., Fujimori, T., Labeau, J., Tyteca, D., Courtoy, P. et al. (2010) 'Lack of cadherins Celsr2 and Celsr3 impairs ependymal ciliogenesis, leading to fatal hydrocephalus', *Nature neuroscience* 13(6): 700-7.
→ Tobin, J. L. and Beales, P. L. (2009) 'The nonmotile ciliopathies', *Genetics in medicine : official journal of the American College of Medical Genetics* 11(6): 386-402.
→ Tree, D. R., Shulman, J. M., Rousset, R., Scott, M. P., Gubb, D. and Axelrod, J. D. (2002) 'Prickle mediates feedback amplification to generate asymmetric planar cell polarity signaling', *Cell* 109(3): 371-81.
→ Tschuch, C., Schulz, A., Pscherer, A., Werft, W., Benner, A., Hotz-Wagenblatt, A., Barrionuevo, L. S., Lichter, P. and Mertens, D. (2008) 'Off-target effects of siRNA specific for GFP', *BMC molecular biology* 9: 60.
→ Tsou, M. F. and Stearns, T. (2006) 'Mechanism limiting centrosome duplication to once per cell cycle', *Nature* 442(7105): 947-51.
→ Tucker, R. W., Pardee, A. B. and Fujiwara, K. (1979) 'Centriole ciliation is related to quiescence and DNA synthesis in 3T3 cells', *Cell* 17(3): 527-35.
→ Udan, R. S., Kango-Singh, M., Nolo, R., Tao, C. and Halder, G. (2003) 'Hippo promotes proliferation arrest and apoptosis in the Salvador/Warts pathway', *Nature cell biology* 5(10): 914-20.
→ Usui, T., Shima, Y., Shimada, Y., Hirano, S., Burgess, R. W., Schwarz, T. L., Takeichi, M. and Uemura, T. (1999) 'Flamingo, a seven-pass transmembrane cadherin, regulates planar cell polarity under the control of Frizzled', *Cell* 98(5): 585-95.
→ van Gijlswijk, R. P., Zijlmans, H. J., Wiegant, J., Bobrow, M. N., Erickson, T. J., Adler, K. E., Tanke, H. J. and Raap, A. K. (1997) 'Fluorochrome-labeled tyramides: use in immunocytochemistry and fluorescence in situ hybridization', *The journal of histochemistry and cytochemistry : official journal of the Histochemistry Society* 45(3): 375-82.
→ Van Hateren, N. J., Das, R. M., Hautbergue, G. M., Borycki, A. G., Placzek, M. and Wilson, S. A. (2011) 'FatJ acts via the Hippo mediator Yap1 to restrict the size of neural progenitor cell pools', *Development* 138(10): 1893-902.
→ Van Itallie, C. M., Aponte, A., Tietgens, A. J., Gucek, M., Fredriksson, K. and Anderson, J. M. (2013) 'The N and C termini of ZO-1 are surrounded by distinct proteins and functional protein networks', *The Journal of biological chemistry* 288(19): 13775-88.
→ van Reeuwijk, J., Arts, H. H. and Roepman, R. (2011) 'Scrutinizing ciliopathies by unraveling ciliary interaction networks', *Human molecular genetics* 20(R2): R149-57.
→ Varelas, X., Samavarchi-Tehrani, P., Narimatsu, M., Weiss, A., Cockburn, K., Larsen, B. G., Rossant, J. and Wrana, J. L. (2010) 'The Crumbs complex couples cell density sensing to Hippo-dependent control of the TGF-beta-SMAD pathway', *Developmental cell* 19(6): 831-44.
→ Vassilev, A., Kaneko, K. J., Shu, H., Zhao, Y. and DePamphilis, M. L. (2001) 'TEAD/TEF transcription factors utilize the activation domain of YAP65, a Src/Yes-associated protein localized in the cytoplasm', *Genes & development* 15(10): 1229-41.
→ Veeman, M. T., Slusarski, D. C., Kaykas, A., Louie, S. H. and Moon, R. T. (2003) 'Zebrafish prickle, a modulator of noncanonical Wnt/Fz signaling, regulates gastrulation movements', *Current biology : CB* 13(8): 680-5.
→ Verghese, S., Waghmare, I., Kwon, H., Hanes, K. and Kango-Singh, M. (2012) 'Scribble acts in the Drosophila fat-hippo pathway to regulate warts activity', *PloS one* 7(11): e47173.
→ Verhey, K. J. and Gaertig, J. (2007) 'The tubulin code', *Cell cycle* 6(17): 2152-60.
→ Vieira, O. V., Gaus, K., Verkade, P., Fullekrug, J., Vaz, W. L. and Simons, K. (2006) 'FAPP2, cilium formation, and compartmentalization of the apical membrane in polarized Madin-Darby canine kidney (MDCK) cells', *Proceedings of the National Academy of Sciences of the United States of America* 103(49): 18556-61.
→ Viktorinova, I., Konig, T., Schlichting, K. and Dahmann, C. (2009) 'The cadherin Fat2 is required for planar cell polarity in the Drosophila ovary', *Development* 136(24): 4123-32.

→ Viktorinova, I., Pismen, L. M., Aigouy, B. and Dahmann, C. (2011) 'Modelling planar polarity of epithelia: the role of signal relay in collective cell polarization', *Journal of the Royal Society, Interface / the Royal Society* 8(60): 1059-63.
→ Villano, J. L. and Katz, F. N. (1995) 'four-jointed is required for intermediate growth in the proximal-distal axis in Drosophila', *Development* 121(9): 2767-77.
→ Vinson, C. R. and Adler, P. N. (1987) 'Directional non-cell autonomy and the transmission of polarity information by the frizzled gene of Drosophila', *Nature* 329(6139): 549-51.
→ Vinson, C. R., Conover, S. and Adler, P. N. (1989) 'A Drosophila tissue polarity locus encodes a protein containing seven potential transmembrane domains', *Nature* 338(6212): 263-4.
→ Visser-Grieve, S., Hao, Y. and Yang, X. (2012) 'Human homolog of Drosophila expanded, hEx, functions as a putative tumor suppressor in human cancer cell lines independently of the Hippo pathway', *Oncogene* 31(9): 1189-95.
→ Vorobjev, I. A. and Chentsov Yu, S. (1982) 'Centrioles in the cell cycle. I. Epithelial cells', *The Journal of cell biology* 93(3): 938-49.
→ Voronina, V. A., Takemaru, K., Treuting, P., Love, D., Grubb, B. R., Hajjar, A. M., Adams, A., Li, F. Q. and Moon, R. T. (2009) 'Inactivation of Chibby affects function of motile airway cilia', *The Journal of cell biology* 185(2): 225-33.
→ Vrabioiu, A. M. and Struhl, G. (2015) 'Fat/Dachsous Signaling Promotes Drosophila Wing Growth by Regulating the Conformational State of the NDR Kinase Warts', *Developmental cell* 35(6): 737-49.

W - Z

→ Wakida, N. M., Botvinick, E. L., Lin, J. and Berns, M. W. (2010) 'An intact centrosome is required for the maintenance of polarization during directional cell migration', *PloS one* 5(12): e15462.
→ Wallingford, J. B. and Harland, R. M. (2002) 'Neural tube closure requires Dishevelled-dependent convergent extension of the midline', *Development* 129(24): 5815-25.
→ Wallingford, J. B. and Mitchell, B. (2011) 'Strange as it may seem: the many links between Wnt signaling, planar cell polarity, and cilia', *Genes & development* 25(3): 201-13.
→ Wallingford, J. B., Rowning, B. A., Vogeli, K. M., Rothbacher, U., Fraser, S. E. and Harland, R. M. (2000) 'Dishevelled controls cell polarity during Xenopus gastrulation', *Nature* 405(6782): 81-5.
→ Wallingford, J. B., Vogeli, K. M. and Harland, R. M. (2001) 'Regulation of convergent extension in Xenopus by Wnt5a and Frizzled-8 is independent of the canonical Wnt pathway', *The International journal of developmental biology* 45(1): 225-7.
→ Wang, J., Hamblet, N. S., Mark, S., Dickinson, M. E., Brinkman, B. C., Segil, N., Fraser, S. E., Chen, P., Wallingford, J. B. and Wynshaw-Boris, A. (2006a) 'Dishevelled genes mediate a conserved mammalian PCP pathway to regulate convergent extension during neurulation', *Development* 133(9): 1767-78.
→ Wang, J., Mark, S., Zhang, X., Qian, D., Yoo, S. J., Radde-Gallwitz, K., Zhang, Y., Lin, X., Collazo, A., Wynshaw-Boris, A. et al. (2005) 'Regulation of polarized extension and planar cell polarity in the cochlea by the vertebrate PCP pathway', *Nature genetics* 37(9): 980-5.
→ Wang, L., Piao, T., Cao, M., Qin, T., Huang, L., Deng, H., Mao, T. and Pan, J. (2013) 'Flagellar regeneration requires cytoplasmic microtubule depolymerization and kinesin-13', *Journal of cell science* 126(Pt 6): 1531-40.
→ Wang, Y., Guo, N. and Nathans, J. (2006b) 'The role of Frizzled3 and Frizzled6 in neural tube closure and in the planar polarity of inner-ear sensory hair cells', *The Journal of neuroscience : the official journal of the Society for Neuroscience* 26(8): 2147-56.
→ Warming, S., Costantino, N., Court, D. L., Jenkins, N. A. and Copeland, N. G. (2005) 'Simple and highly efficient BAC recombineering using galK selection', *Nucleic acids research* 33(4): e36.
→ Watnick, T. and Germino, G. (2003) 'From cilia to cyst', *Nature genetics* 34(4): 355-6.
→ Wehrli, M. and Tomlinson, A. (1998) 'Independent regulation of anterior/posterior and equatorial/polar polarity in the Drosophila eye; evidence for the involvement of Wnt signaling in the equatorial/polar axis', *Development* 125(8): 1421-32.
→ Wei, X., Shimizu, T. and Lai, Z. C. (2007) 'Mob as tumor suppressor is activated by Hippo kinase for growth inhibition in Drosophila', *The EMBO journal* 26(7): 1772-81.

→ Westermann, S. and Weber, K. (2003) 'Post-translational modifications regulate microtubule function', *Nature reviews. Molecular cell biology* 4(12): 938-47.
→ Westlake, C. J., Baye, L. M., Nachury, M. V., Wright, K. J., Ervin, K. E., Phu, L., Chalouni, C., Beck, J. S., Kirkpatrick, D. S., Slusarski, D. C. et al. (2011) 'Primary cilia membrane assembly is initiated by Rab11 and transport protein particle II (TRAPPII) complex-dependent trafficking of Rabin8 to the centrosome', *Proceedings of the National Academy of Sciences of the United States of America* 108(7): 2759-64.
→ Wharton, K. A., Johansen, K. M., Xu, T. and Artavanis-Tsakonas, S. (1985) 'Nucleotide sequence from the neurogenic locus notch implies a gene product that shares homology with proteins containing EGF-like repeats', *Cell* 43(3 Pt 2): 567-81.
→ Wiese, C. and Zheng, Y. (1999) 'Gamma-tubulin complexes and their interaction with microtubule-organizing centers', *Current opinion in structural biology* 9(2): 250-9.
→ Willecke, M., Hamaratoglu, F., Kango-Singh, M., Udan, R., Chen, C. L., Tao, C., Zhang, X. and Halder, G. (2006) 'The fat cadherin acts through the hippo tumor-suppressor pathway to regulate tissue size', *Current biology : CB* 16(21): 2090-100.
→ Willecke, M., Hamaratoglu, F., Sansores-Garcia, L., Tao, C. and Halder, G. (2008) 'Boundaries of Dachsous Cadherin activity modulate the Hippo signaling pathway to induce cell proliferation', *Proceedings of the National Academy of Sciences of the United States of America* 105(39): 14897-902.
→ Williams, C. L., Li, C., Kida, K., Inglis, P. N., Mohan, S., Semenec, L., Bialas, N. J., Stupay, R. M., Chen, N., Blacque, O. E. et al. (2011) 'MKS and NPHP modules cooperate to establish basal body/transition zone membrane associations and ciliary gate function during ciliogenesis', *The Journal of cell biology* 192(6): 1023-41.
→ Williams, C. L., Masyukova, S. V. and Yoder, B. K. (2010) 'Normal ciliogenesis requires synergy between the cystic kidney disease genes MKS-3 and NPHP-4', *Journal of the American Society of Nephrology : JASN* 21(5): 782-93.
→ Williams, C. L., Winkelbauer, M. E., Schafer, J. C., Michaud, E. J. and Yoder, B. K. (2008) 'Functional redundancy of the B9 proteins and nephrocystins in Caenorhabditis elegans ciliogenesis', *Molecular biology of the cell* 19(5): 2154-68.
→ Winkelbauer, M. E., Schafer, J. C., Haycraft, C. J., Swoboda, P. and Yoder, B. K. (2005) 'The C. elegans homologs of nephrocystin-1 and nephrocystin-4 are cilia transition zone proteins involved in chemosensory perception', *Journal of cell science* 118(Pt 23): 5575-87.
→ Winyard, P. and Jenkins, D. (2011) 'Putative roles of cilia in polycystic kidney disease', *Biochimica et biophysica acta* 1812(10): 1256-62.
→ Wodarz, A. (2000) 'Tumor suppressors: linking cell polarity and growth control', *Current biology : CB* 10(17): R624-6.
→ Wolff, T. and Rubin, G. M. (1998) 'Strabismus, a novel gene that regulates tissue polarity and cell fate decisions in Drosophila', *Development* 125(6): 1149-59.
→ Wong, H. C., Bourdelas, A., Krauss, A., Lee, H. J., Shao, Y., Wu, D., Mlodzik, M., Shi, D. L. and Zheng, J. (2003) 'Direct binding of the PDZ domain of Dishevelled to a conserved internal sequence in the C-terminal region of Frizzled', *Molecular cell* 12(5): 1251-60.
→ Woods, D. F., Hough, C., Peel, D., Callaini, G. and Bryant, P. J. (1996) 'Dlg protein is required for junction structure, cell polarity, and proliferation control in Drosophila epithelia', *The Journal of cell biology* 134(6): 1469-82.
→ Woods, D. F., Wu, J. W. and Bryant, P. J. (1997) 'Localization of proteins to the apico-lateral junctions of Drosophila epithelia', *Developmental genetics* 20(2): 111-8.
→ Wu, J., Roman, A. C., Carvajal-Gonzalez, J. M. and Mlodzik, M. (2013) 'Wg and Wnt4 provide long-range directional input to planar cell polarity orientation in Drosophila', *Nature cell biology* 15(9): 1045-55.
→ Wu, S., Huang, J., Dong, J. and Pan, D. (2003) 'hippo encodes a Ste-20 family protein kinase that restricts cell proliferation and promotes apoptosis in conjunction with salvador and warts', *Cell* 114(4): 445-56.
→ Wu, S., Liu, Y., Zheng, Y., Dong, J. and Pan, D. (2008) 'The TEAD/TEF family protein Scalloped mediates transcriptional output of the Hippo growth-regulatory pathway', *Developmental cell* 14(3): 388-98.
→ Xiao, K., Allison, D. F., Kottke, M. D., Summers, S., Sorescu, G. P., Faundez, V. and Kowalczyk, A. P. (2003) 'Mechanisms of VE-cadherin processing and degradation in microvascular endothelial cells', *The Journal of biological chemistry* 278(21): 19199-208.

→ Xiao, L., Chen, Y., Ji, M. and Dong, J. (2011) 'KIBRA regulates Hippo signaling activity via interactions with large tumor suppressor kinases', *The Journal of biological chemistry* 286(10): 7788-96.

→ Xie, Y., Vessey, J. P., Konecna, A., Dahm, R., Macchi, P. and Kiebler, M. A. (2007) 'The GTP-binding protein Septin 7 is critical for dendrite branching and dendritic-spine morphology', *Current biology : CB* 17(20): 1746-51.

→ Xu, T., Wang, W., Zhang, S., Stewart, R. A. and Yu, W. (1995) 'Identifying tumor suppressors in genetic mosaics: the Drosophila lats gene encodes a putative protein kinase', *Development* 121(4): 1053-63.

→ Yabuta, N., Fujii, T., Copeland, N. G., Gilbert, D. J., Jenkins, N. A., Nishiguchi, H., Endo, Y., Toji, S., Tanaka, H., Nishimune, Y. et al. (2000) 'Structure, expression, and chromosome mapping of LATS2, a mammalian homologue of the Drosophila tumor suppressor gene lats/warts', *Genomics* 63(2): 263-70.

→ Yamamoto, N., Okano, T., Ma, X., Adelstein, R. S. and Kelley, M. W. (2009) 'Myosin II regulates extension, growth and patterning in the mammalian cochlear duct', *Development* 136(12): 1977-86.

→ Yang, C. H., Axelrod, J. D. and Simon, M. A. (2002) 'Regulation of Frizzled by fat-like cadherins during planar polarity signaling in the Drosophila compound eye', *Cell* 108(5): 675-88.

→ Yang, J., Adamian, M. and Li, T. (2006) 'Rootletin interacts with C-Nap1 and may function as a physical linker between the pair of centrioles/basal bodies in cells', *Molecular biology of the cell* 17(2): 1033-40.

→ Yap, A. S., Niessen, C. M. and Gumbiner, B. M. (1998) 'The juxtamembrane region of the cadherin cytoplasmic tail supports lateral clustering, adhesive strengthening, and interaction with p120ctn', *The Journal of cell biology* 141(3): 779-89.

→ Yilmazel, B., Hu, Y., Sigoillot, F., Smith, J. A., Shamu, C. E., Perrimon, N. and Mohr, S. E. (2014) 'Online GESS: prediction of miRNA-like off-target effects in large-scale RNAi screen data by seed region analysis', *BMC bioinformatics* 15: 192.

→ Yin, F., Yu, J., Zheng, Y., Chen, Q., Zhang, N. and Pan, D. (2013) 'Spatial organization of Hippo signaling at the plasma membrane mediated by the tumor suppressor Merlin/NF2', *Cell* 154(6): 1342-55.

→ Yoder, B. K. (2007) 'Role of primary cilia in the pathogenesis of polycystic kidney disease', *Journal of the American Society of Nephrology : JASN* 18(5): 1381-8.

→ Yoder, B. K., Hou, X. and Guay-Woodford, L. M. (2002) 'The polycystic kidney disease proteins, polycystin-1, polycystin-2, polaris, and cystin, are co-localized in renal cilia', *Journal of the American Society of Nephrology : JASN* 13(10): 2508-16.

→ Yoshimura, S., Egerer, J., Fuchs, E., Haas, A. K. and Barr, F. A. (2007) 'Functional dissection of Rab GTPases involved in primary cilium formation', *The Journal of cell biology* 178(3): 363-9.

→ Youn, Y. H., Pramparo, T., Hirotsune, S. and Wynshaw-Boris, A. (2009) 'Distinct dose-dependent cortical neuronal migration and neurite extension defects in Lis1 and Ndel1 mutant mice', *The Journal of neuroscience : the official journal of the Society for Neuroscience* 29(49): 15520-30.

→ Yu, F. X. and Guan, K. L. (2013) 'The Hippo pathway: regulators and regulations', *Genes & development* 27(4): 355-71.

→ Yu, J., Wu, W. K., Li, X., He, J., Li, X. X., Ng, S. S., Yu, C., Gao, Z., Yang, J., Li, M. et al. (2015) 'Novel recurrently mutated genes and a prognostic mutation signature in colorectal cancer', *Gut* 64(4): 636-45.

→ Yu, J., Zheng, Y., Dong, J., Klusza, S., Deng, W. M. and Pan, D. (2010) 'Kibra functions as a tumor suppressor protein that regulates Hippo signaling in conjunction with Merlin and Expanded', *Developmental cell* 18(2): 288-99.

→ Yurchenco, P. D., Sung, U., Ward, M. D., Yamada, Y. and O'Rear, J. J. (1993) 'Recombinant laminin G domain mediates myoblast adhesion and heparin binding', *The Journal of biological chemistry* 268(11): 8356-65.

→ Zakaria, S., Mao, Y., Kuta, A., Ferreira de Sousa, C., Gaufo, G. O., McNeill, H., Hindges, R., Guthrie, S., Irvine, K. D. and Francis-West, P. H. (2014) 'Regulation of neuronal migration by Dchs1-Fat4 planar cell polarity', *Current biology : CB* 24(14): 1620-7.

→ Zang, Z. J., Cutcutache, I., Poon, S. L., Zhang, S. L., McPherson, J. R., Tao, J., Rajasegaran, V., Heng, H. L., Deng, N., Gan, A. et al. (2012) 'Exome sequencing of gastric adenocarcinoma identifies

recurrent somatic mutations in cell adhesion and chromatin remodeling genes', *Nature genetics* 44(5): 570-4.

→ Zhang, H., Li, C., Chen, H., Wei, C., Dai, F., Wu, H., Dui, W., Deng, W. M. and Jiao, R. (2015) 'SCF(Slmb) E3 ligase-mediated degradation of Expanded is inhibited by the Hippo pathway in Drosophila', *Cell research* 25(1): 93-109.

→ Zhang, J., Smolen, G. A. and Haber, D. A. (2008a) 'Negative regulation of YAP by LATS1 underscores evolutionary conservation of the Drosophila Hippo pathway', *Cancer research* 68(8): 2789-94.

→ Zhang, L., Ren, F., Zhang, Q., Chen, Y., Wang, B. and Jiang, J. (2008b) 'The TEAD/TEF family of transcription factor Scalloped mediates Hippo signaling in organ size control', *Developmental cell* 14(3): 377-87.

→ Zhang, N., Bai, H., David, K. K., Dong, J., Zheng, Y., Cai, J., Giovannini, M., Liu, P., Anders, R. A. and Pan, D. (2010) 'The Merlin/NF2 tumor suppressor functions through the YAP oncoprotein to regulate tissue homeostasis in mammals', *Developmental cell* 19(1): 27-38.

→ Zhao, B., Wei, X., Li, W., Udan, R. S., Yang, Q., Kim, J., Xie, J., Ikenoue, T., Yu, J., Li, L. et al. (2007) 'Inactivation of YAP oncoprotein by the Hippo pathway is involved in cell contact inhibition and tissue growth control', *Genes & development* 21(21): 2747-61.

→ Zhao, B., Ye, X., Yu, J., Li, L., Li, W., Li, S., Lin, J. D., Wang, C. Y., Chinnaiyan, A. M., Lai, Z. C. et al. (2008) 'TEAD mediates YAP-dependent gene induction and growth control', *Genes & development* 22(14): 1962-71.

→ Zhao, X., Yang, C. H. and Simon, M. A. (2013) 'The Drosophila Cadherin Fat regulates tissue size and planar cell polarity through different domains', *PloS one* 8(5): e62998.

→ Zheng, Y., Wong, M. L., Alberts, B. and Mitchison, T. (1995) 'Nucleation of microtubule assembly by a gamma-tubulin-containing ring complex', *Nature* 378(6557): 578-83.

→ Zhu, Y., Li, D., Wang, Y., Pei, C., Liu, S., Zhang, L., Yuan, Z. and Zhang, P. (2015) 'Brahma regulates the Hippo pathway activity through forming complex with Yki-Sd and regulating the transcription of Crumbs', *Cellular signalling* 27(3): 606-13.

→ Zilian, O., Frei, E., Burke, R., Brentrup, D., Gutjahr, T., Bryant, P. J. and Noll, M. (1999) 'double-time is identical to discs overgrown, which is required for cell survival, proliferation and growth arrest in Drosophila imaginal discs', *Development* 126(23): 5409-20.

→ Zou, J., Wang, X. and Wei, X. (2012) 'Crb apical polarity proteins maintain zebrafish retinal cone mosaics via intercellular binding of their extracellular domains', *Developmental cell* 22(6): 1261-74.

→ Zullo, A., Iaconis, D., Barra, A., Cantone, A., Messaddeq, N., Capasso, G., Dolle, P., Igarashi, P. and Franco, B. (2010) 'Kidney-specific inactivation of Ofd1 leads to renal cystic disease associated with upregulation of the mTOR pathway', *Human molecular genetics* 19(14): 2792-803.

→ Zuo, X., Guo, W. and Lipschutz, J. H. (2009) 'The exocyst protein Sec10 is necessary for primary ciliogenesis and cystogenesis in vitro', *Molecular biology of the cell* 20(10): 2522-9.